BABAR Analysis Document #130, Version 4.00
July 14, 2001

Vertexing performances and systematic checks with fully reconstructed B events

Vertexing and Composition Tools Group [1]

Abstract

Performances and systematic checks of the *BABAR* Vertexing for fully reconstructed B events, single vertex and Δz, in the Run1 data are described in this document, including extensive comparison between data and simulation.

[1]Direct contributors to this document are: Riccardo Faccini (*Univ. di Roma La Sapienza*), David Kirkby (*Stanford University*), Stephen Levy (*U.C. Santa Barbara*), **Fernando Martinez-Vidal (contact person and editor)** (*INFN-Pisa*), Art Snyder (*SLAC*), Jan Stark (*LPNHE, Univ. Paris 6&7*)

Contents

1 Overview

This document is intended to describe with detail the vertexing performances in fully reconstructed B events, both single vertex and Δz, for the Run1 *BABAR* data, with extensive checks and comparison between the data and Monte Carlo. Detailed systematic checks are also reported. By its nature, this is a quite dynamic document so our goal is to provide in each new version the most up-to-date status of these studies.

If you want to have the most up-to-date version you should check-out the head of CVS:

```
% cvs co BAD/note130
% cd BAD
% cvs co pubboard
% ln -s ../pubboard/ .
% latex paper.tex
% ...
```

Most of the results obtained in this document have been obtained using the *analysis-7* release, with the following vertexing related tags on top:

```
VtxFitter V00-08-48-02
VertexingTools V00-08-44-02
BetaTools V00-10-06-03
FastVtx V03-03-07
```

All the studies performed through this document make use of the data and Monte Carlo samples of fully reconstructed B's into charmonium [4] and open charm [5] modes. The goal was to include also results from $D^{*}l\nu$ events [6], but nothing has been written yet. Reconstructed B events into open charm modes (hereafter called *Breco*) are:

$$\overline{B}^0 \to D^{*+}\pi^-,\ D^{*+}\rho^-,\ D^{*+}a_1^-,\ D^+\pi^-,\ D^+\rho^-,\ D^+a_1^-$$
$$B^- \to D^{*0}\pi^-,\ D^0\pi^-$$

As detailed in [5], the Monte Carlo has been generated with a 'cocktail' of all those modes together.

B events into exclusive charmonium were reconstructed into the following modes:

$$B^0 \to J/\psi\, K^0_S(\pi^+\pi^-,\pi^0\pi^0),\ \psi(2S)K^0_S,\ J/\psi\, K^{*0}(K^+\pi^-)$$

$$B^- \to J/\psi\, K^-,\ J/\psi\, K^{*-}(K^-\pi^0, K^0_S\pi^-),\ \psi(2S)K^-$$

2 Vertexing of fully reconstructed B events

2.1 Hadronic B decays

Hadronic B decays are reconstructed using the default vertexing/kinematic fitting algorithm, `GeoKin` [1]. Apart of the B mode dependent selection, the common vertexing B selection criteria is to require convergence on the B vertex (only geometric constraint) with no cut on the χ^2 probability. As described in detail in [1], `GeoKin` fits the complete decay tree proceeding leaf by leaf, applying by default the non-zero lifetime constraint when resonant states are present in the decay chain.

Techniques for vertexing Breco [5] and charmonium [4] events are essentially the same. For example, to fit the decay tree $B^- \to D^0\pi^-$, $D^0 \to K^-\pi^+$, first a fit of the $K^-\pi^+$ vertex is performed. Then the internal degrees of freedom of the D^0 candidate are frozen and a fit of the $D^0\pi^-$ vertex is performed. Additional constraints are applied in these fits. The masses of D/D^* mesons and J/ψ, $\psi(2S)$ candidates are constrained to the nominal values. This constraint does not improve the vertex resolution, but it improves the ΔE resolution, key ingredient of the B selection [3]. For $D^{*+} \to D^0\pi^+$ selection we constrain the vertex of the D^{*+} candidate to be compatible with the beam spot. In order to account for the flight of the B in the transverse plane we use an enhanced beam spot width of 30 μm as provided by `beamSpotBFlight()` [1]. This constraint improves the Δm (mass difference between the D^* and the D meson) resolution, therefore improving the candidate selection. Beam spot and mass constraints are, however, not applied simultaneously: first, the D^* is selected using the beam spot contraint; second, a mass constrained D^* is used to build the B for selection. Vertexing/kinematic fitting of $J/\psi \to e^+e^-$candidates accounts for the bremstrahlung emission by correcting for the four-momenta of the photon estimated at point of closest approach to the primary vertex of the electron candidate [4].

The decay vertices of short-living resonances (ρ^+, a_1^+, K^{*+}, K^{*0}, D^*'s, J/ψ, $\psi(2S)$) are constrained to be identical to the decay vertex of the B [1]. As already mentioned, the B selection criteria include the requirement that the kinematical fit of the decay tree has converged.

There is an additional complexity derived by the fact that mass constrained D^*'s and J/ψ, $/\psi(2S)$ 'resonant' candidates used for B selection are not the most appropiate for vertex (and therefore Δz) reconstruction:

- $D^{*+} \to D^0\pi^+$ candidates (with mass and no beam spot contraint) have very poor vertex information;
- $D^{*+} \to D^+\pi^0$ and $D^{*0} \to D^0\pi^0/\gamma$ have no position information;
- $J/\psi \to e^+e^-$with bremstrahlung emission can pull the vertex position.

As mass constraints do not help in vertex resolution, then the B candidates used for vertex estimation are those without mass constraints applied to the intermediate 'resonant' states. In this way (as described in [1]) the D^* daughters are attached directly to the B and then the vertex is reconstructed. Similarly, J/ψ and $\psi(2S)$ mass constraints are also removed for vertex and Δz measurements.

The resolution on the vertex of fully reconstructed B depends on the decay mode. Tables 1 and 2 summarise the values obtained from Monte Carlo for some typical decay modes, for the transverse and z components respectively. Two-Gaussian fits were performed on the distributions of the residuals (difference between the reconstructed and the generated vertex coordinates) and the pulls (difference normalized to its measured error). In both instances, the weighed mean of the two widths is quoted. All modes have a constant core resolution in z of the order of 40 μm. However, the fraction of the tail Gaussian depends on the modes, and as consequence the RMS is mode dependent, ranging from 50 μm for the most precise modes (low multiplicity, high momentum) to 80 μm for the less well measured (higher multiplicity and presence of neutrals). Pulls for core Gaussian are consitent with unity, and the overall RMS is of the order of 1.1-1.2. As an ilustration on how the resolution and pull behaves, figure 1 shows the the difference between the reconstructed and true B vertex and its pull for fully reconstructed $B^0 \to J/\psi K^0_S$ events. The fit to two Gaussians to the residual gives a fraction of 77% with resolution 41 μm for the central Gaussian. The overall RMS is 68 μm. A similar fit to the pull distribution gives a fraction of 84% with 0.97 scale for the central Gaussian, with overall RMS of 1.2.

B $\to$	D $\to$	σ_x (μm)	σ_y (μm)	pull$_x$	pull$_y$
$\overline{B}^0$					
$D^+\pi^-$	$K^-\pi^+\pi^+$	54	54		
$D^+\pi^-$	$K^0_S\ \pi^+$	78	95		
B^-					
$D^0\pi^-$	$K^-\pi^+$	56	56		
$D^0\pi^-$	$K^-\pi^+\pi^0$	67	67		
$D^0\pi^-$	$K^-\pi^+\pi^-\pi^+$	54	56		
$D^0\pi^-$	$K^0_S\ \pi^+\pi^-$	61	62		
$J/\psi\ K^-$	e^+e^-	48	48		
$J/\psi\ K^-$	$\mu^+\mu^-$	45	44		

Table 1: Resolutions on the transverse vertex coordinates of the reconstructed B meson and the corresponding pulls, for a few typical modes. Fits to two gaussians are used to estimate the resolutions using the weighed mean of the two widths.

The χ^2 probability distribution for Monte Carlo and data signal B candidates in the whole data sample is shown in figure 2. Figure 3 shows the event-by-event z error position. It can be seen that the charmonium events are significantly more peaked at zero with a significantly more pronounced slope. This is because the χ^2 and $ndof$ of the B vertex account for the internal degrees of freedom of the charmonium vertex, with the mass constraint and the bremsstrahlung recovery applied, being therefore a highly constrained vertex. As a proof of this, figure 4 shows the χ^2 distribution for a small sample of $B^0 \to J/\psi K^0_S$ Monte Carlo when those constraints are removed. A flatter χ^2 probability distribution is obtained. No

Mode	f_{core}	μ_1	σ_1	μ_2	σ_2	RMS
Residual (μm)						
$\overline{B}^0 \to J/\psi\ K^0_S(\pi^+\pi^-)$	0.769 ± 0.023	1.0 ± 0.5	41.4 ± 0.9	2.9 ± 2.4	118 ± 6	68
$\overline{B}^0 \to \psi(2S)\ K^0_S(\pi^+\pi^-)$	0.847 ± 0.017	0.9 ± 0.6	42.6 ± 0.8	-8.3 ± 4.3	133 ± 9	65
$\overline{B}^0 \to D^+\pi^-,\ K^-\pi^+\pi^+$	0.837 ± 0.015	0.2 ± 0.4	39.1 ± 0.6	-0.6 ± 2.3	114 ± 5	58
$\overline{B}^0 \to D^+\pi^-,\ K^0_S\pi^+$	0.728 ± 0.012	2.9 ± 1.0	40.5 ± 1.2	-3.3 ± 6.4	132 ± 4	77
$\overline{B}^0 \to D^{*+}\pi^-,\ K^-\pi^+$	0.832 ± 0.018	-0.9 ± 0.5	39.3 ± 0.8	3.5 ± 5.0	129 ± 9	64
$\overline{B}^0 \to D^{*+}\pi^-,\ K^-\pi^+\pi^0$	0.690 ± 0.029	1.9 ± 1.2	42.4 ± 1.5	-7.5 ± 4.6	130 ± 7	80
$\overline{B}^0 \to D^{*+}\pi^-,\ K^-\pi^+\pi^+\pi^-$	0.922 ± 0.010	-0.6 ± 0.8	45.2 ± 0.8	-13 ± 12	182 ± 27	67
$B^- \to J/\psi\ K^-$	0.801 ± 0.013	1.6 ± 0.3	36.2 ± 0.5	4.2 ± 1.7	97 ± 3	54
$B^- \to D^0\pi^-,\ K^-\pi^+$	0.831 ± 0.007	-0.2 ± 0.3	38.9 ± 0.4	-0.0 ± 2.1	148 ± 5	70
Pull						
$\overline{B}^0 \to J/\psi\ K^0_S(\pi^+\pi^-)$	0.837 ± 0.027	0.014 ± 0.013	0.970 ± 0.018	0.21 ± 0.06	1.96 ± 0.10	1.19
$\overline{B}^0 \to \psi(2S)\ K^0_S(\pi^+\pi^-)$	0.931 ± 0.015	0.005 ± 0.013	1.030 ± 0.016	0.15 ± 0.15	2.67 ± 0.29	1.22
$\overline{B}^0 \to D^+\pi^-,\ K^-\pi^+\pi^+$	0.921 ± 0.018	0.006 ± 0.009	0.972 ± 0.012	-0.05 ± 0.08	2.02 ± 0.13	1.09
$\overline{B}^0 \to D^+\pi^-,\ K^0_S\pi^+$	0.00 ± 0.00	0.000 ± 0.000	0.00 ± 0.00	0.00 ± 0.00	0.00 ± 0.00	0.00
$\overline{B}^0 \to D^{*+}\pi^-,\ K^-\pi^+$	0.00 ± 0.00	0.000 ± 0.000	0.00 ± 0.00	0.00 ± 0.00	0.00 ± 0.00	0.00
$\overline{B}^0 \to D^{*+}\pi^-,\ K^-\pi^+\pi^0$	0.00 ± 0.00	0.000 ± 0.000	0.00 ± 0.00	0.00 ± 0.00	0.00 ± 0.00	0.00
$\overline{B}^0 \to D^{*+}\pi^-,\ K^-\pi^+\pi^+\pi^-$	0.00 ± 0.00	0.000 ± 0.000	0.00 ± 0.00	0.00 ± 0.00	0.00 ± 0.00	0.00
$B^- \to J/\psi\ K^-$	0.923 ± 0.013	0.049 ± 0.009	1.020 ± 0.011	0.12 ± 0.06	2.44 ± 0.16	1.19
$B^- \to D^0\pi^-,\ K^-\pi^+$	0.918 ± 0.011	-0.003 ± 0.007	0.975 ± 0.009	-0.02 ± 0.04	2.20 ± 0.11	1.13

Table 2: z position resolutions of the reconstructed B meson and the corresponding pull, for a few typical modes. Fits to two gaussians are used to estimate the resolutions using the weighed mean of the two widths.

change in the per-event vertex position error is noticeable. It should be stressed that the mass constraint of the charmonium is removed when reconstructing Δz.

2.2 Semileptonic B decays

2.3 Checks

2.3.1 SVT content

Figures 5, 6, 7 and 8 show the data/Monte Carlo comparison for B^0 Breco, B^+ Breco, B^0 charmonium and B^+ charmonium species, respectively, of the available SVT information in tracks used to fit the vertex of the fully reconstructed B event. Top (left/right) distributions show the number of SVT z ($R\phi$) layers per track for tracks used to fit the reco side vertex. Bottom/left plots show the fraction of tracks used in the reco side vertex with at least 2 SVT z layers (after quality cuts, as detailed in section 3.1, altough these cuts affect mainly the tagging side vertex). From all these figures it is concluded than altough it is not explicitely required a minimum number of SVT hits for tracks used for vertex reconstruction, the highly efficient SVT combined with the tracking and vertexing systems, naturally selects tracks with a very large amount of SVT information.

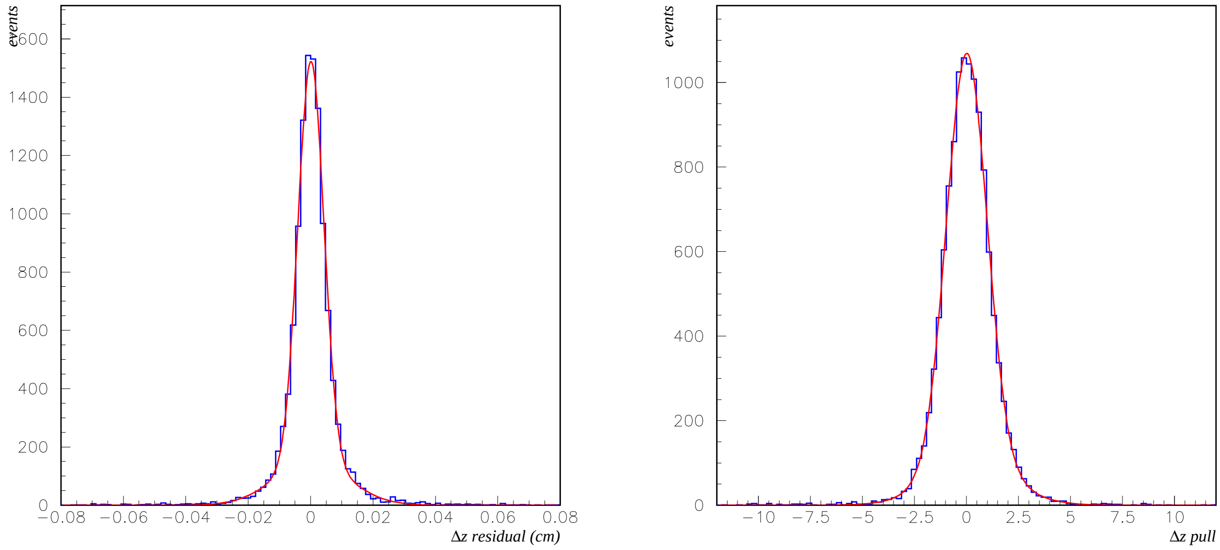

Figure 1: Residual (left) and pull (right) of the $B^0 \rightarrow J/\psi\, K_S^0$ vertex. A two Gaussian fit is superimposed.

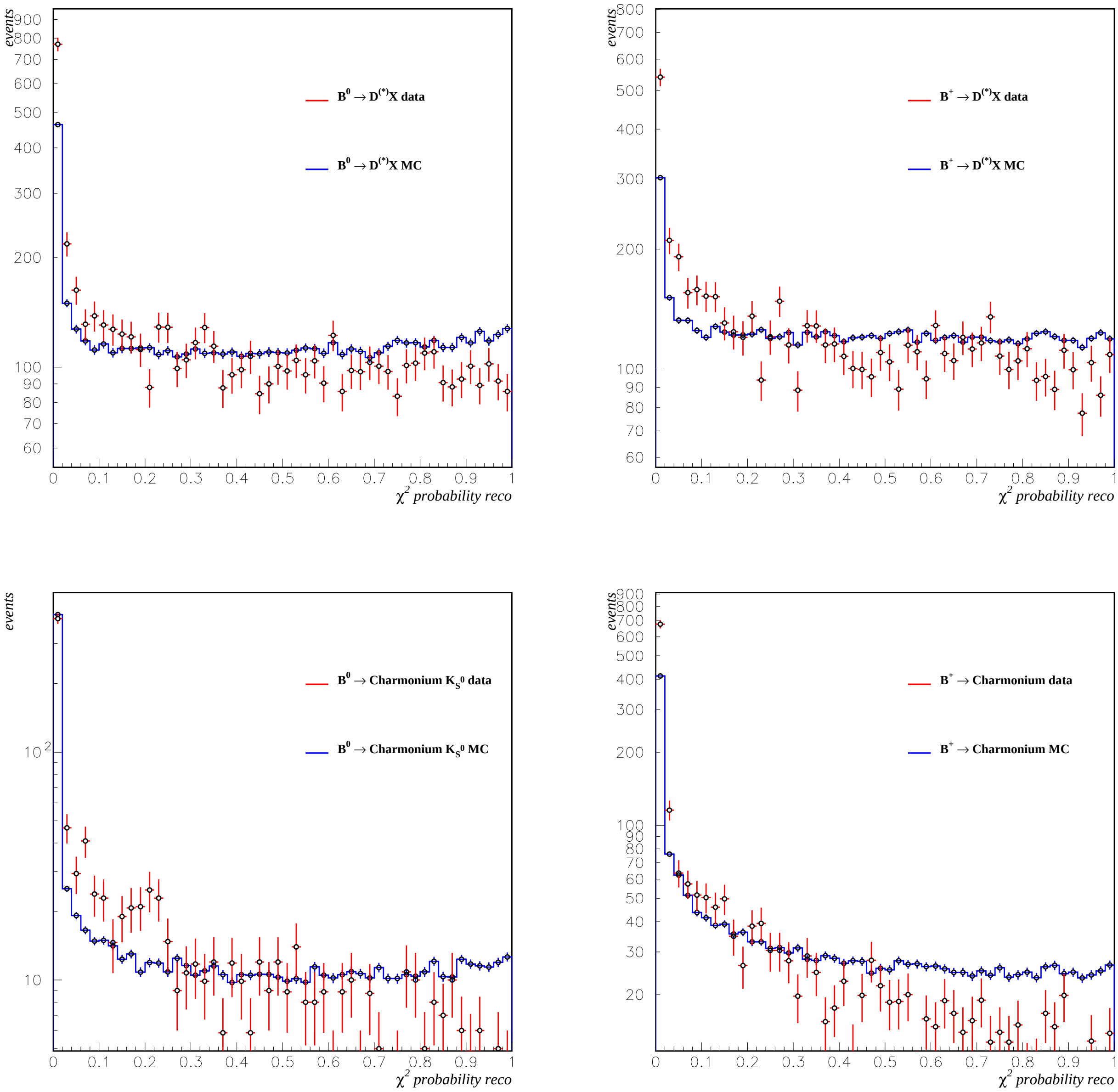

Figure 2: Data/Monte Carlo comparison of χ^2 probability of the fully reco B vertex for B Breco and charmonium events (excluding K_L^0 data): (top/left) B^0 Breco; (top/right) B^+ Breco; (bottom/left) B^0 charmonium; (bottom/right) B^+ charmonium.

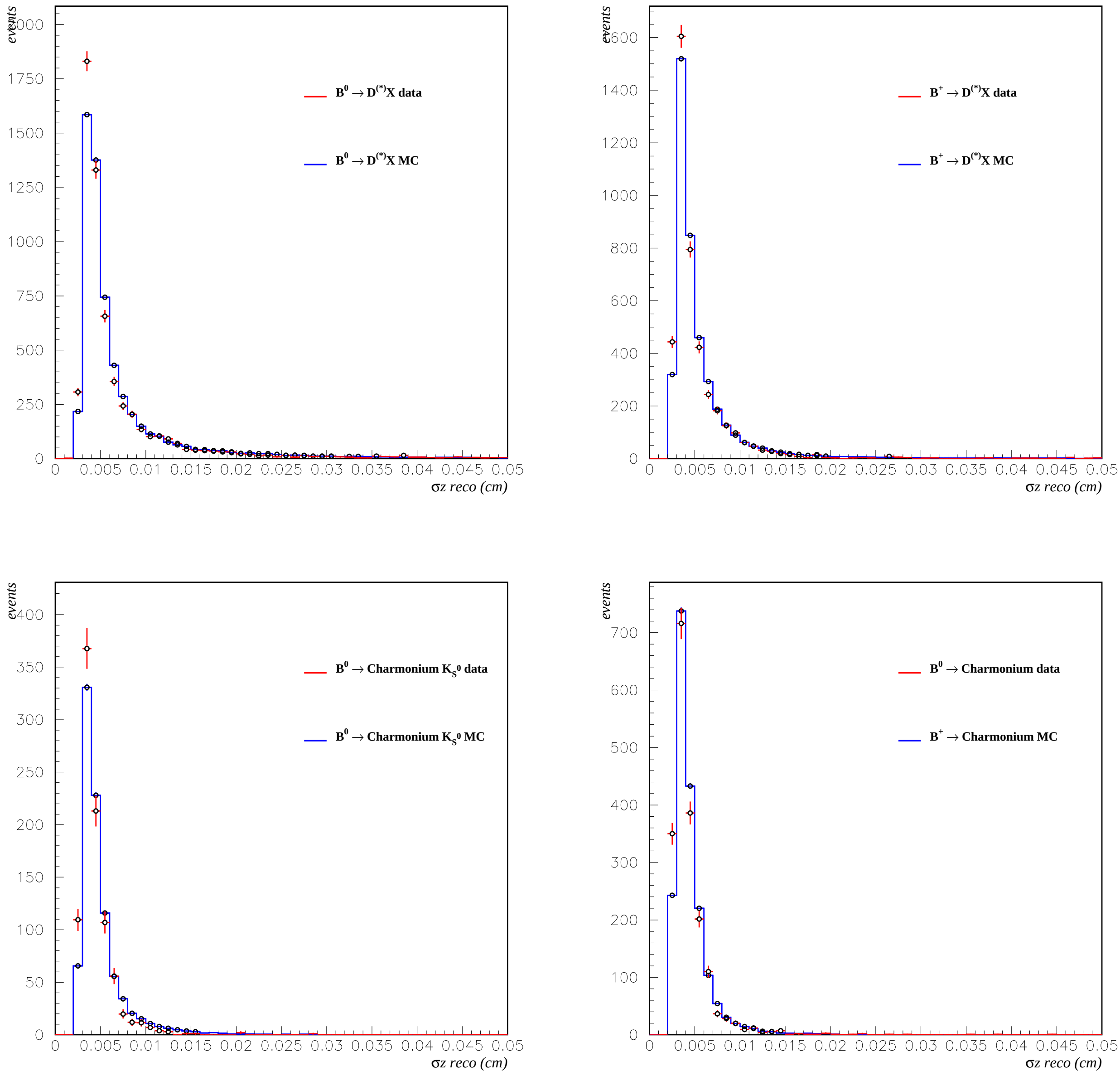

Figure 3: Data/Monte Carlo comparison of event-by-event z error of the fully reco B vertex for B Breco and charmonium events (excluding K_L^0 data): (top/left) B^0 Breco; (top/right) B^+ Breco; (bottom/left) B^0 charmonium; (bottom/right) B^+ charmonium.

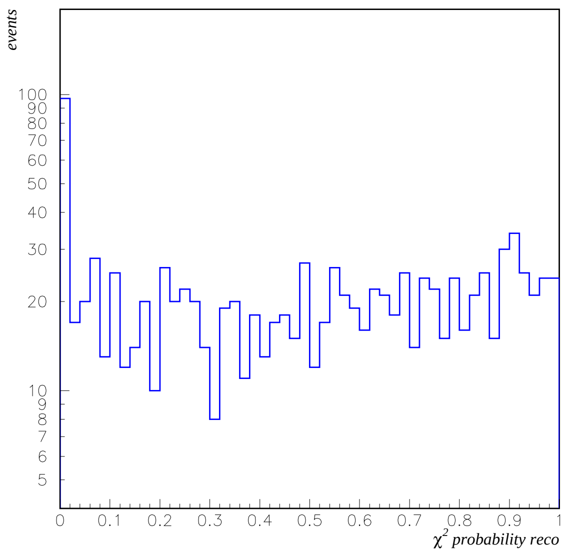

Figure 4: χ^2 probability of the fully reco B ($J/\psi\, K_S^0$) in Monte Carlo after excluding the mass constraint and the bremsstrahlung recovery.

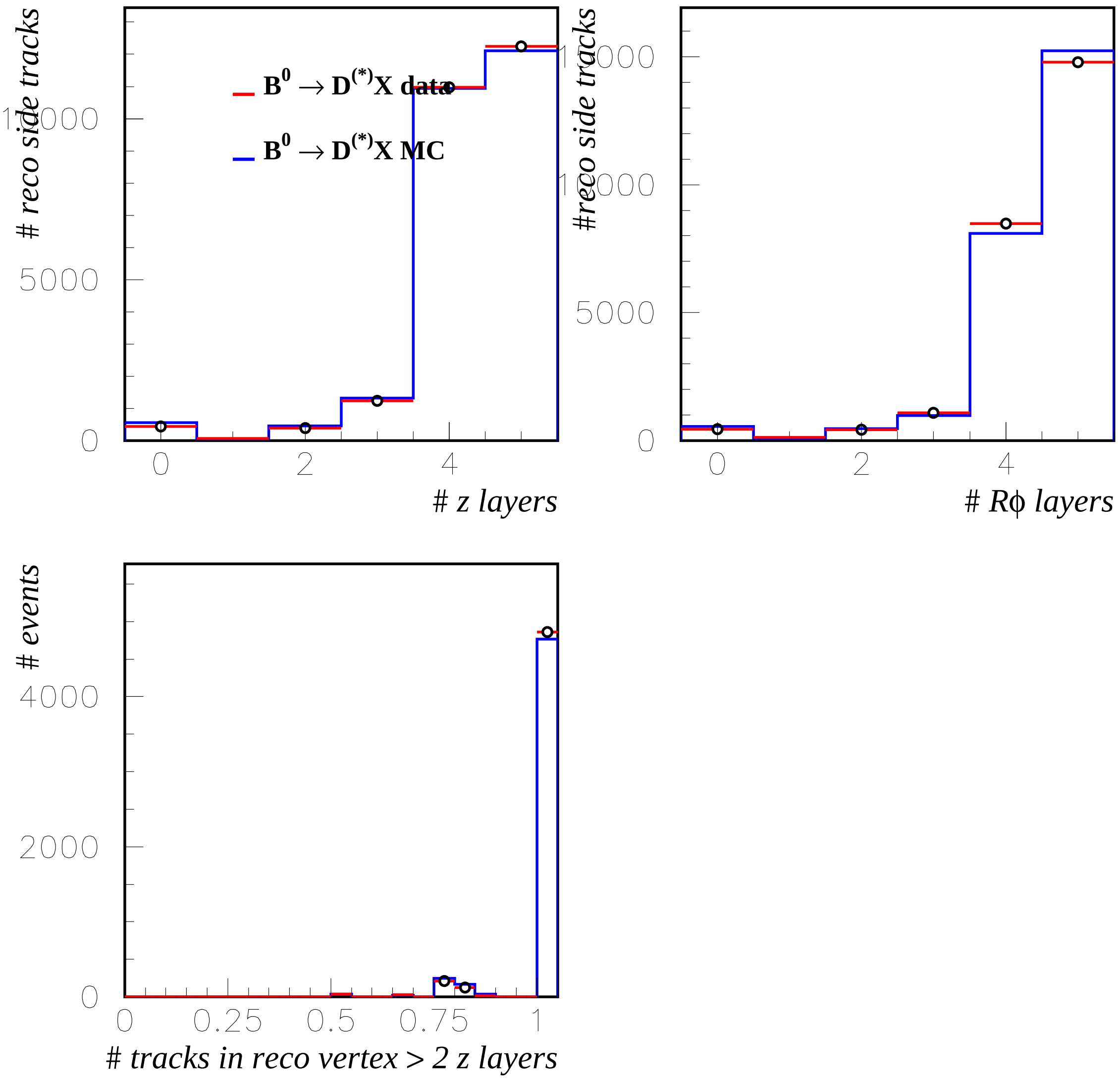

Figure 5: Data/Monte Carlo comparison of SVT information in reconstructed side vertex for B^0 Breco events: (top/left) number of SVT z layers per track for tracks used in the reco vertex; (top/right) same but SVT $R\phi$ layers; (bottom/right) fraction of tracks used in the reco side vertex with at least 2 SVT z layers (after quality cuts). Distributions are normalized to the number of events after quality cuts.

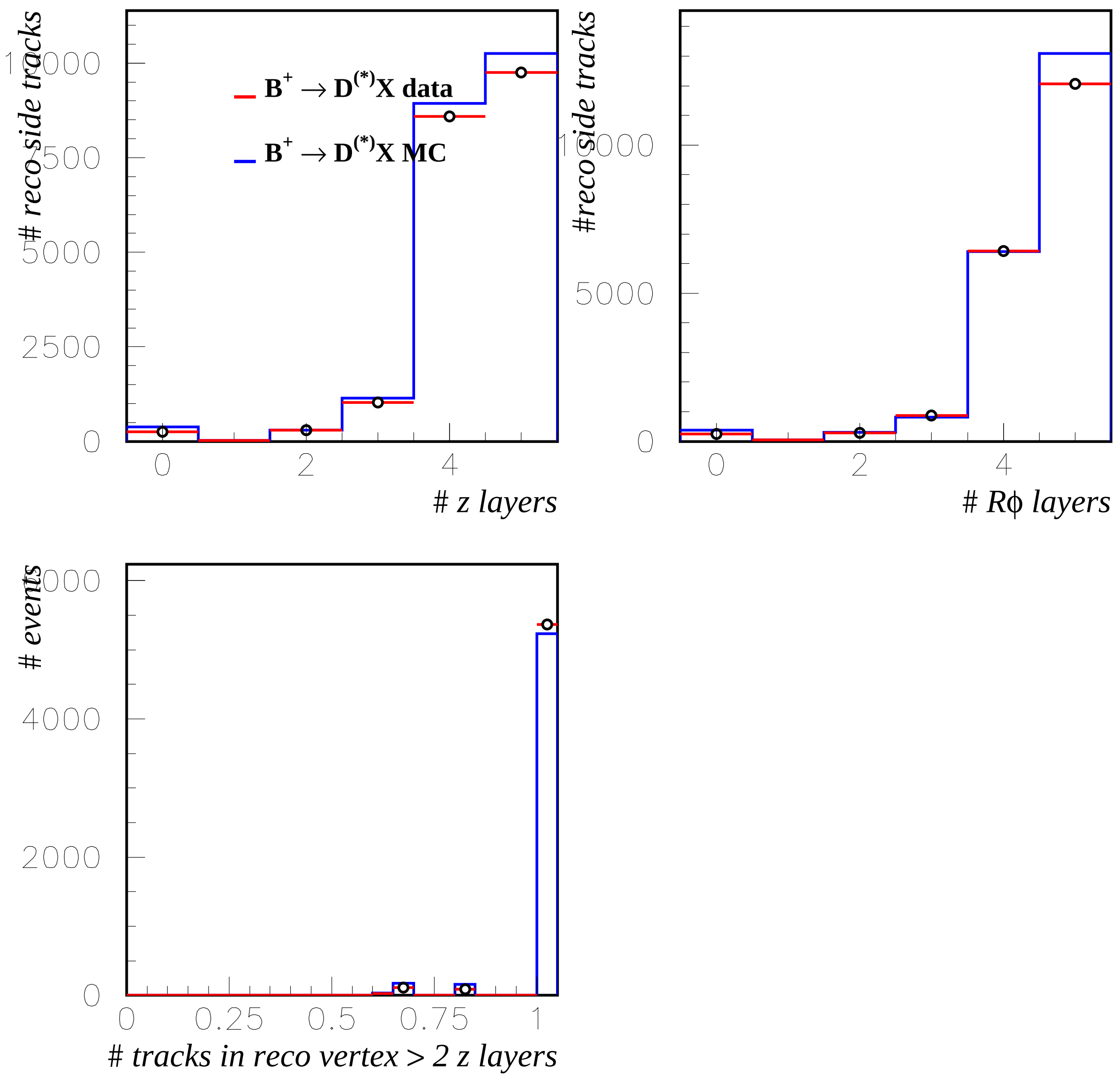

Figure 6: Data/Monte Carlo comparison of SVT information in reconstructed side vertex for B^+ Breco events: (top/left) number of SVT z layers per track for tracks used in the reco vertex; (top/right) same but SVT $R\phi$ layers; (bottom/right) fraction of tracks used in the reco side vertex with at least 2 SVT z layers (after quality cuts). Distributions are normalized to the number of events after quality cuts.

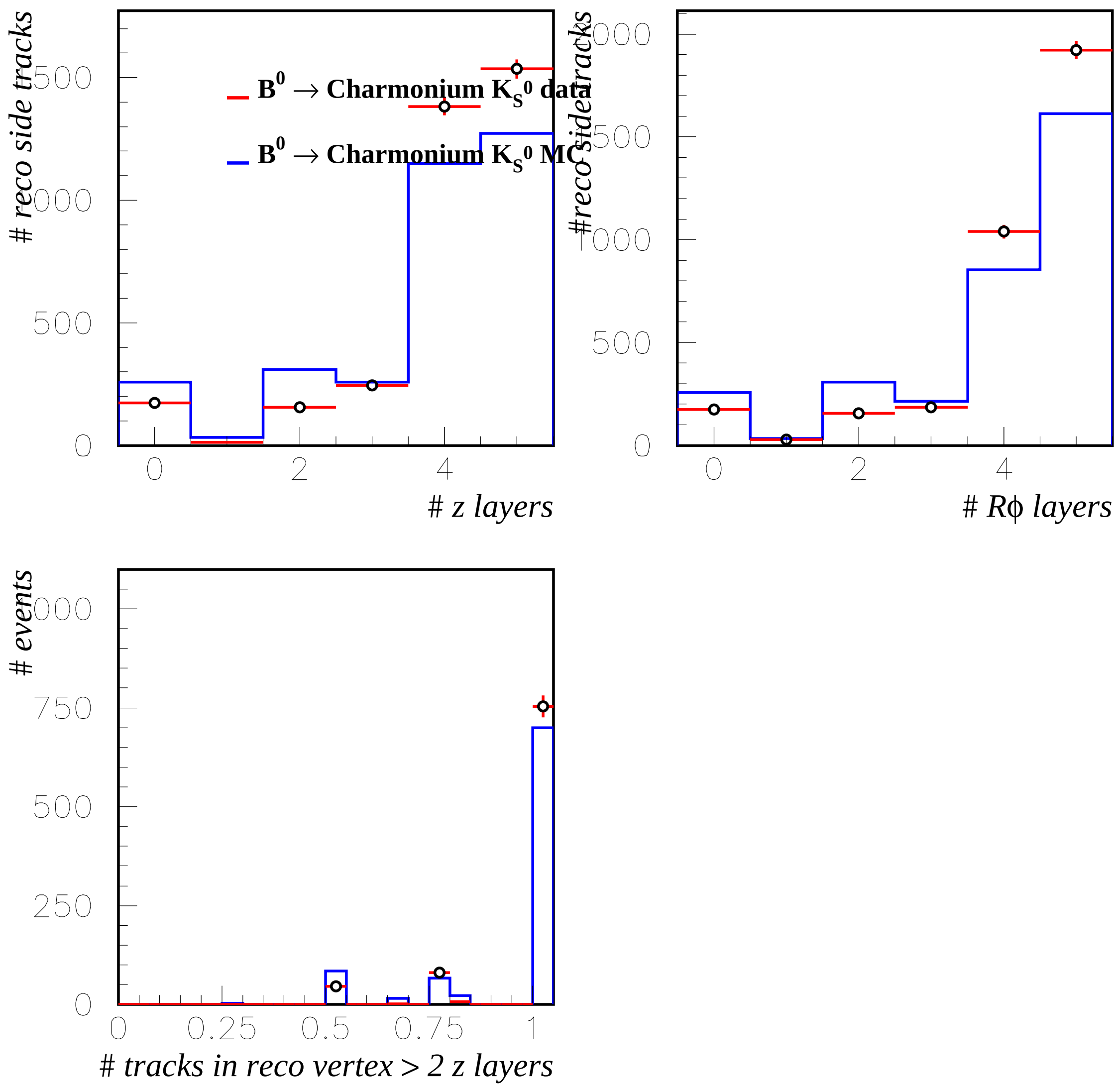

Figure 7: Data/Monte Carlo comparison of SVT information in reconstructed side vertex for B^0 charmonium events: (top/left) number of SVT z layers per track for tracks used in the reco vertex; (top/right) same but SVT $R\phi$ layers; (bottom/right) fraction of tracks used in the reco side vertex with at least 2 SVT z layers (after quality cuts). Distributions are normalized to the number of events after quality cuts.

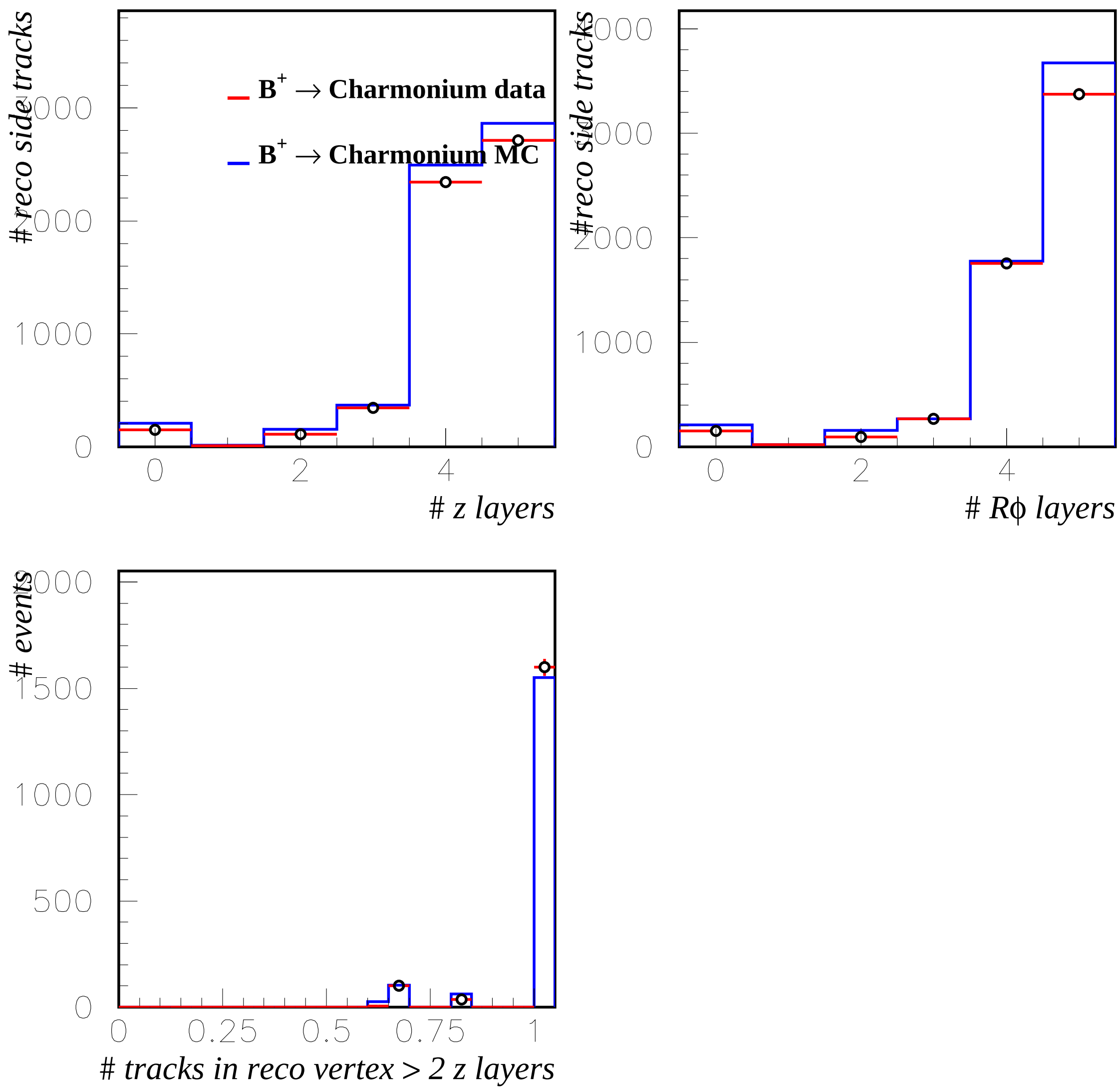

Figure 8: Data/Monte Carlo comparison of SVT information in reconstructed side vertex for B^+ charmonium events: (top/left) number of SVT z layers per track for tracks used in the reco vertex; (top/right) same but SVT $R\phi$ layers; (bottom/right) fraction of tracks used in the reco side vertex with at least 2 SVT z layers (after quality cuts). Distributions are normalized to the number of events after quality cuts.

3 Δz vertexing (with beam constraints)

In this section we discuss the differents aspects of the vertex tag vertexing in *default configuration*, including selection criteria, basic performances, basic description of the resolution function, differences among modes and algorithms and several effects affecting it. Misalignment effects are described in section 6.

In time-dependent measurements that use the Δz technique, it is difficult to disentangle the effects of the B lifetime and the detector resolution. In analyses like D lifetime where both the production and decay points are measured the situation is, in principle, easier. In the latter analyses the true proper decay time is distributed exponentially: events at negative decay time provide a measurement of the detector resolution, events at positive decay time contain the convoluted effect of the resolution and the lifetime. This provides a relatively easy way to distangle between resolution and lifetime. However, for decay length difference Δz analyses, the Δz distribution is symmetric around zero, and all the information about resolution and lifetime is contained in the width (shape) of the distribution. A detailed understanding of the resolution function is therefore crucial for any time-dependent measurement. In addition to some basics about the resolution function described below, section 5 contains much more detailed studies of the relationshio between resolution and B lifetime. To complete the study of the resolution function, reference [2] describes two Δz control samples which allow us to check the reliability of the resolution function extractions as done in the lifetime/mixing analyses as well as direct comparison between data and Monte Carlo.

3.1 Configuration and selection criteria

The vertex tag is reconstructed using the default algorithm, `VtxTagBtaSelFit` in default configuration [1]:

- apply full set of available constraints, i.e. beam constraints [1];
- χ^2 step for track rejection and stopping criteria is 6.0;
- do not require any minimal number of tracks in vertex, i.e. $n = 0$ according with the notation used in the previous reference.

On top of the mode dependent event selection, the following cuts are applied (unless otherwise specified):

- the fit is required to converge, but no global χ^2 cut is applied. The Δz convergence implicitely requires the convergence of the vertex of the fully reconstructed side;
- the error on Δz must be smaller than 400 μm;
- Δz must be smaller than 3 mm in absolute value.

The results related to the detector issues will be discussed in terms of Δz. The conversion factor to Δt is ≈ 0.006 ps μm^{-1}.

3.2 Basic performances

3.2.1 Δz resolution and pulls

The vertex tag reconstruction largely dominates the uncertainty on Δz. Therefore, basic performaces can be investigated using our benchmark mode, $B_0 \to J\Psi K_S$ Monte Carlo. Differences among modes are investigated in section 3.3.

The resolution in Δz, Δz(reconstructed)-Δz(generated), is shown in figure 9(left). The corresponding results of the fit to two Gaussians and one "flat" outliers are shown in table 3. The fraction of outliers is left free in the fit, the width is fixed to 1.3 mm and the bias to 0. The central gaussian contains 65% of the events and its resolution is 92 μm. The fraction of outliers is 2%. The situation is better if the pulls are considered, as shown in figure 9(right): the fraction of outliers becomes 1.4% and the fraction of the core Gaussian is now 84% with width 1.05 and the RMS is 1.25 (without considering outliers).

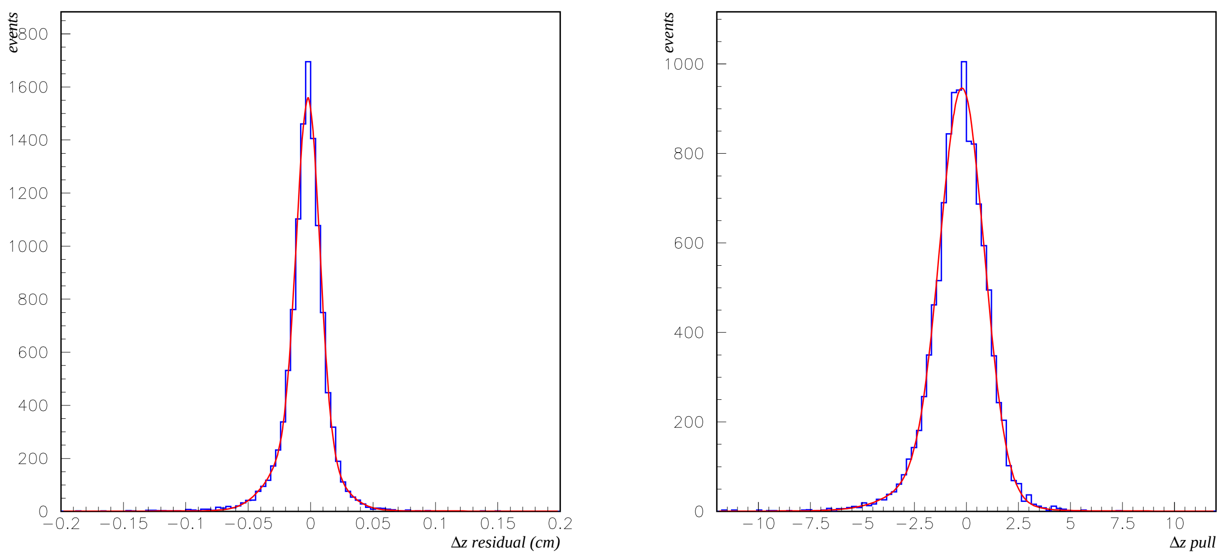

Figure 9: Residual (a) and pull (b) of Δz in $B_0 \to J\Psi K_S$ MC.

f_{core}	f_{out}	μ_1	σ_1	μ_2	σ_2	μ	RMS
Residual (μm)							
0.654 ± 0.024	0.020 ± 0.002	-19.4 ± 1.4	91.9 ± 2.4	-60 ± 6	224 ± 8	-34	151
Pull							
0.842 ± 0.028	0.014 ± 0.003	-0.193 ± 0.017	1.054 ± 0.020	-1.09 ± 0.15	1.97 ± 0.10	-0.33	1.25

Table 3: Results of a fit to double Gaussian plus outliers on the residual and pull of Δz distributions in $B_0 \to J\Psi K_S$ MC. The RMS does not include the outliers component.

The distributions are biased because of the presence of tracks from charm decays in the vertex tag. The vertex tag algorithms try to get ride of these tracks [1] but the short decay length of D mesons compared with the resolution is not enough to separate them efficiently.

As shown in table 3 the bias is about -20 μm and 0.2 in residual and pull, respectively, for the core Gaussian.

3.2.2 Errors and χ^2 distributions

The distribution of the error on Δz for the reference $B_0 \to J\Psi K_S$ MC is shown in figure 10(left). The error distribution can be empirically parameterized by a Landau as well as a Crystall Ball distributions. When using event-by-event Δz errors for maximum likelihood fits, these empirical parameterizations can be used for definining a PDF which accounts properly for the event-by-event distribution [14, 15], otherwise a flat distribution would be used which will not bias the result but will cause a global translation of the likelihood surface [14]. As an example, a Landau fit provides a peak value of about 81 μm and a width of 15. The probability of χ^2 distribution is shown in figure 10(right) and presents 4% of the events with χ^2 less than 1%. The mean value is 0.495.

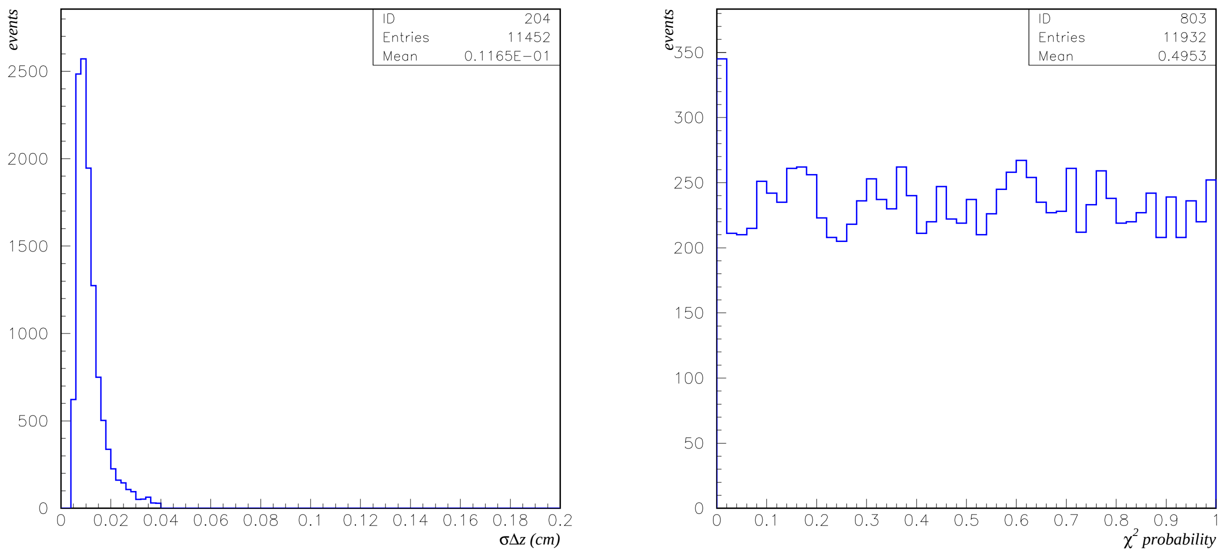

Figure 10: (Left) Error on Δz and (right) χ^2 distribution in $B_0 \to J\Psi K_S$ Monte Carlo. The cut at 400 μm in the Δz error distribution can be observed.

3.2.3 Efficiency

The efficiency for the vertex reconstruction and quality cuts (see section 3.1) is (96.0$\pm$0.2)% $B_0 \to J\Psi K_S$ MC. Figure 11 shows the vertex tag efficiency after quality cuts as a function of the track event multiplicity (`ChargedTracks`) for B^0 breco events. This figure compares also the efficiency with the alternative vertexing algorithm, `FvtClusterer` (see reference [1] for details on the differences among both algorithms).

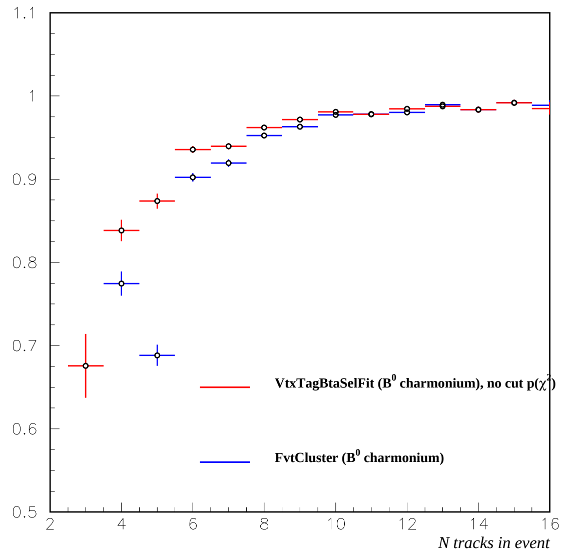

Figure 11: Vertex tag efficiency after quality cuts as a function of the track event multiplicity (`ChargedTracks` for `VtxTagBtaSelFit` and `FvtClusterer` for the B^0 breco signal events.

3.2.4 Resolution models

The shape of the Δz distribution is asymmetric because the reconstruction of z_{opp} (z component of the vertex tag side) is biased. On the other hand, due to presence of wrongly reconstructed tracks and the non-perfect parameterization of the material, the Δz pull distribution is not completely gaussian.

Several parameterisations have been tried. The first parameterization uses two Gaussians with different means and widths, as it has already been used in the previous sections, and it contains five parameters: the fraction f_{core} of events in the narrow Gaussian, the width σ_1 and the bias μ_1 of the narrow gaussian, and the width and bias of the wide gaussian (σ_2,μ_2). An alternative parameterisation uses a Gaussian with variable width and zero bias plus the same Gaussian convoluted with a function that is zero for negative values and decreases exponentially for positive values. This parameterisation $G + G \otimes E$ (known hereafter as *GExp* model) uses three parameters: the fraction f of events in the central gaussian, the width σ of the gaussian and the "lifetime" τ of the exponential. The results of a fit of the *GExp* parameterisation to the Δz pull is shown on figure 12.

The two Gaussian model with different means and widths used in previous sections uses five parameters: the fraction f_{core} of events in the narrow Gaussian, the width σ_1 and the bias μ_1 of the narrow gaussian, and the width and bias of the wide gaussian (σ_2,μ_2).

3.3 Differences among modes

As standard approach in lifetime, mixing and CP analyses we assume a common resolution function for different modes. In particular, for the CP asymmetry extraction we measure

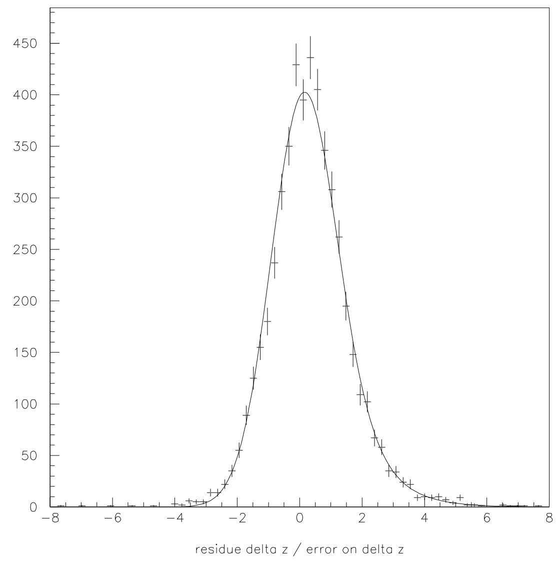

Figure 12: Fit of a Gaussian centred at zero plus the same Gaussian convoluted with an exponential function (*GExp* model) to the Δz pull.

the resolution function from the fully reconstructed hadronic modes (D*lν events are used as cross-check), therefore we need to make sure that the extrapolation to the CP events is correct. Also, several different modes are used for the CP measurement and we need to make sure that the resolutions are equivalent.

A comparison of the χ^2 probability, event-by-event error and number of candidates in vertex tag for several charmonium CP modes, $\mathrm{B_0 \rightarrow J\Psi K_S}(\pi^+\pi^-)$, $\mathrm{B_0 \rightarrow J\Psi K_S}(\pi^0\pi^0)$ and $\mathrm{B_0 \rightarrow \Psi(2S) K_S}$, with the B^0 breco cocktail in Monte Carlo is shown in figure 13. There is no evidence of differences with respect to the Breco events, as expected from the fact that the Δz is dominated by the tagging side, largely independent of the fully reconstructed mode. The agreement among the different charmonium events is also satisfactory. Only for the $\mathrm{B_0 \rightarrow J\Psi K_S}(\pi^0\pi^0)$ mode mode seems to appear a small excess of events (compared with the 'Breco cocktail') at small probability, effect certainly due to the presence of two π^0's in the reco side which can spoil slightly the determination of the B tag direction, giving a small worsening of the χ^2 distribution. The effect is however very small, even more if we take into account that no cut on χ^2 is applied.

The Δz resolution and pull parameters for different B decays to charmonium are shown in Table 4. These parameters are shown for B decays to hadronic D modes in Table 5. Figure 14 ilustrates the differences in resisdual and pull for three different B species. Results of fits of the *GExp* resolution model to the Δz pull obtained for different B modes in the Monte Carlo are summarised in table 6.

Comparisons have been done between the data and Monte Carlo for the Breco and chamonium samples, and for charged and neutral B mesons. Figures 15 and 16 compare the χ^2 probability distributions for B^0 and B^+ Breco and charmonium events, respectively. Figures 17 and 18 show a similar comparison but now for the event-by-event Δz error.

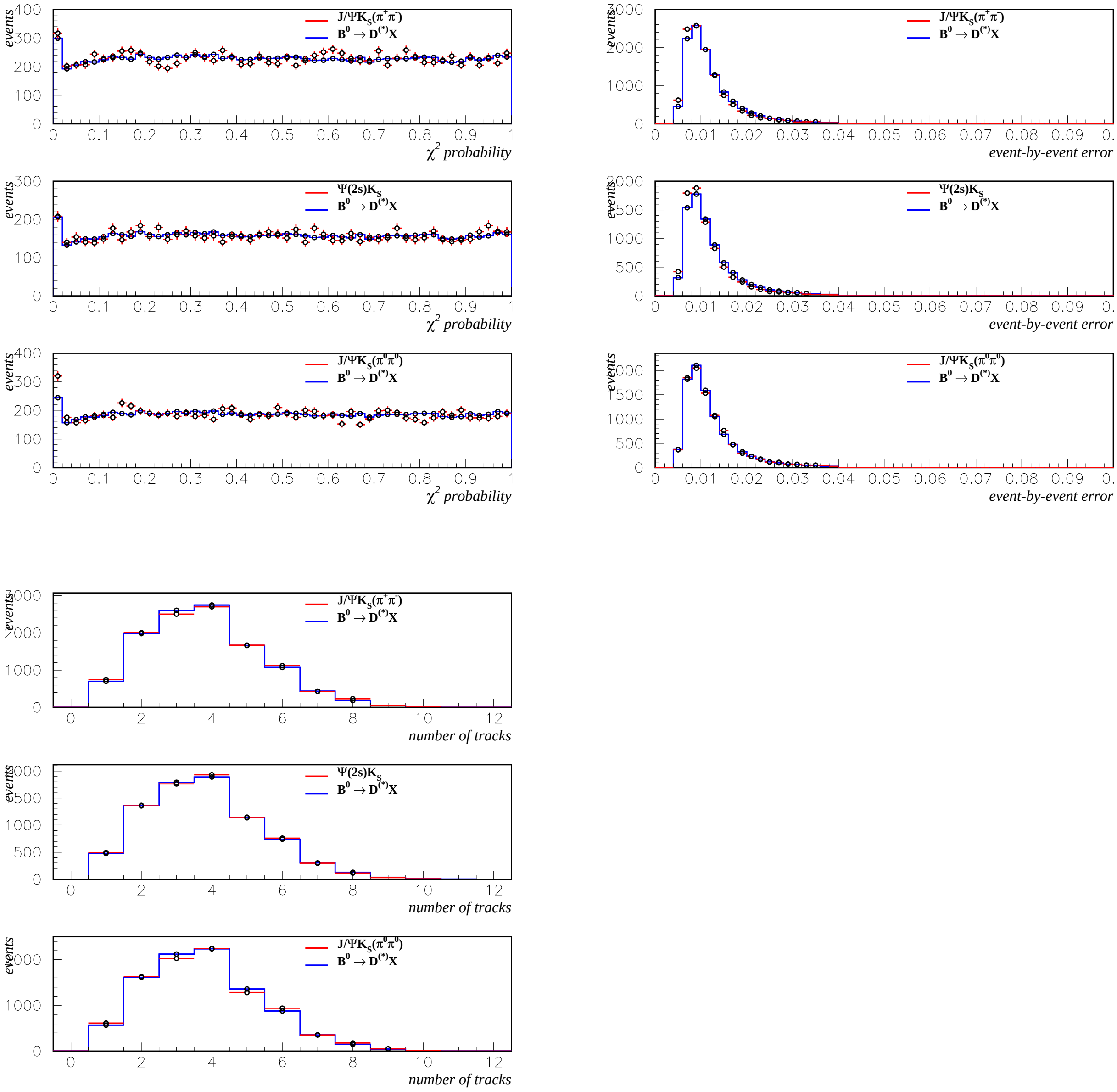

Figure 13: Comparison among the distributions of χ^2 probability (top/left), event-by-event error (top/right) and number of candidates (bottom/left) in vertex tag for several charmonium modes, $B_0 \to J\Psi K_S(\pi^+\pi^-)$, $B_0 \to J\Psi K_S(\pi^0\pi^0)$ and $B_0 \to \Psi(2S) K_S$, with the B^0 Breco cocktail in Monte Carlo.

Δz reso	f_1	σ_1	μ_1	f_{out}	$\frac{\sigma_2}{\sigma_1}$	$\mu_2 - \mu_1$	RMS	RMS(3g)	μ
JpsiKs	66.8	93. $\pm$ 2. μm	-19.$\pm$ 2. μm	2.44	2.44$\pm$ 0.06	-44.$\pm$ 6. μm	149.$\pm$ 3. μm	193.$\pm$ 5. μm	-32. mum
Psi2sKs	69.4	93. $\pm$ 2. μm	-14.$\pm$ 2. μm	1.84	2.52$\pm$ 0.08	-53.$\pm$ 7. μm	149.$\pm$ 3. μm	183.$\pm$ 5. μm	-29. mum
JpsiKs2pi0	70.2	100. $\pm$ 2. μm	-22.$\pm$ 2. μm	2.58	2.53$\pm$ 0.08	-45.$\pm$ 8. μm	159.$\pm$ 4. μm	203.$\pm$ 5. μm	-34. mum
JpsiKstar0Kp	64.7	86. $\pm$ 2. μm	-18.$\pm$ 2. μm	2.90	2.49$\pm$ 0.06	-49.$\pm$ 6. μm	143.$\pm$ 3. μm	196.$\pm$ 5. μm	-33. mum
JpsiKstar0ks	72.2	98. $\pm$ 4. μm	-20.$\pm$ 2. μm	2.34	2.27$\pm$ 0.11	-43.$\pm$ 12. μm	142.$\pm$ 5. μm	186.$\pm$ 7. μm	-30. mum
JpsiKstarpKp	72.9	92. $\pm$ 2. μm	-17.$\pm$ 2. μm	1.48	2.61$\pm$ 0.09	-35.$\pm$ 8. μm	146.$\pm$ 4. μm	175.$\pm$ 6. μm	-26. mum
JpsiKstarpKs	71.8	93. $\pm$ 3. μm	-18.$\pm$ 2. μm	2.42	2.46$\pm$ 0.09	-29.$\pm$ 8. μm	142.$\pm$ 4. μm	188.$\pm$ 6. μm	-25. mum
JpsiK	63.0	82. $\pm$ 2. μm	-16.$\pm$ 1. μm	1.81	2.38$\pm$ 0.04	-33.$\pm$ 4. μm	135.$\pm$ 2. μm	171.$\pm$ 3. μm	-27. mum
Δz pull	f_1	σ_1	μ_1	f_{out}	$\frac{\sigma_2}{\sigma_1}$	$\mu_2 - \mu_1$	RMS	RMS(3g)	μ
JpsiKs	90.3	1.11 $\pm$ 0.01	-0.24$\pm$ 0.01	1.79	2.82$\pm$ 0.10	-1.11$\pm$ 0.14	1.39$\pm$ 0.02	1.74$\pm$ 0.05	-0.33
Psi2sKs	89.5	1.11 $\pm$ 0.01	-0.21$\pm$ 0.02	2.57	2.66$\pm$ 0.11	-1.07$\pm$ 0. 16	1.35$\pm$ 0.02	1.85$\pm$ 0.07	-0.29
JpsiKs2pi0	89.8	1.12 $\pm$ 0.01	-0.24$\pm$ 0.01	2.18	2.83$\pm$ 0.11	-1.18$\pm$ 0.16	1.41$\pm$ 0.02	1.83$\pm$ 0.06	-0.33
JpsiKstar0Kp	88.0	1.10 $\pm$ 0.01	-0.25$\pm$ 0.01	1.99	2.89$\pm$ 0.09	-0.93$\pm$ 0.13	1.46$\pm$ 0.02	1.83$\pm$ 0.05	-0.34
JpsiKstar0Ks	89.5	1.10 $\pm$ 0.02	-0.22$\pm$ 0.02	4.36	2.79$\pm$ 0.16	-1.61$\pm$ 0.29	1.31$\pm$ 0.02	2.11$\pm$ 0.10	-0.31
JpsiKstarpKp	91.2	1.11 $\pm$ 0.01	-0.22$\pm$ 0.02	2.92	2.98$\pm$ 0.15	-0.83$\pm$ 0.20	1.34$\pm$ 0.02	1.90$\pm$ 0.07	-0.26
JpsiKstarpKs	90.0	1.11 $\pm$ 0.01	-0.22$\pm$ 0.02	2.92	3.25$\pm$ 0.15	-0.74$\pm$ 0.19	1.44$\pm$ 0.02	1.97$\pm$ 0.07	-0.26
JpsiK	92.8	1.10 $\pm$ 0.01	-0.23$\pm$ 0.01	1.04	2.79$\pm$ 0.09	-0.91$\pm$ 0.11	1.32$\pm$ 0.01	1.54$\pm$ 0.03	-0.29

Table 4: Δz resolution function parameters for charmonium modes.

Δz reso	f_1	σ_1	μ_1	f_{out}	$\frac{\sigma_2}{\sigma_1}$	$\mu_2 - \mu_1$	RMS	RMS(3g)	μ
BchDstar	68.8	90. $\pm$ 1. μm	-17.$\pm$ 1. μm	1.75	2.53$\pm$ 0.04	-33.$\pm$ 4. μm	146.$\pm$ 2. μm	179.$\pm$ 3. μm	-26. μm
BchD0	68.1	89. $\pm$ 1. μm	-16.$\pm$ 0. μm	1.69	2.43$\pm$ 0.02	-32.$\pm$ 2. μm	141.$\pm$ 1. μm	175.$\pm$ 1. μm	-26. μm
B0Dstar	67.9	91. $\pm$ 1. μm	-16.$\pm$ 0. μm	1.98	2.42$\pm$ 0.02	-35.$\pm$ 2. μm	143.$\pm$ 1. μm	181.$\pm$ 1. μm	-27. μm
B0Dch	67.2	91. $\pm$ 1. μm	-16.$\pm$ 0. μm	2.34	2.42$\pm$ 0.02	-36.$\pm$ 1. μm	145.$\pm$ 1. μm	188.$\pm$ 1. μm	-27. μm
Δz pull	f_1	σ_1	μ_1	f_{out}	$\frac{\sigma_2}{\sigma_1}$	$\mu_2 - \mu_1$	RMS	RMS(3g)	μ
BchDstar	86.3	1.05 $\pm$ 0.01	-0.18$\pm$ 0.01	0.86	1.99$\pm$ 0.07	-0.59$\pm$ 0.08	1.23$\pm$ 0.02	1.43$\pm$ 0.03	-0.25
BchD0	88.7	1.06 $\pm$ 0.01	-0.19$\pm$ 0.00	0.73	2.00$\pm$ 0.04	-0.68$\pm$ 0.04	1.22$\pm$ 0.01	1.39$\pm$ 0.01	-0.26
B0Dstar	87.7	1.06 $\pm$ 0.01	-0.18$\pm$ 0.00	0.93	1.98$\pm$ 0.03	-0.71$\pm$ 0.04	1.22$\pm$ 0.01	1.44$\pm$ 0.01	-0.26
B0Dch	87.2	1.06 $\pm$ 0.00	-0.18$\pm$ 0.00	1.11	2.00$\pm$ 0.03	-0.72$\pm$ 0.03	1.23$\pm$ 0.01	1.49$\pm$ 0.01	-0.26

Table 5: Δz resolution function parameters for Breco modes.

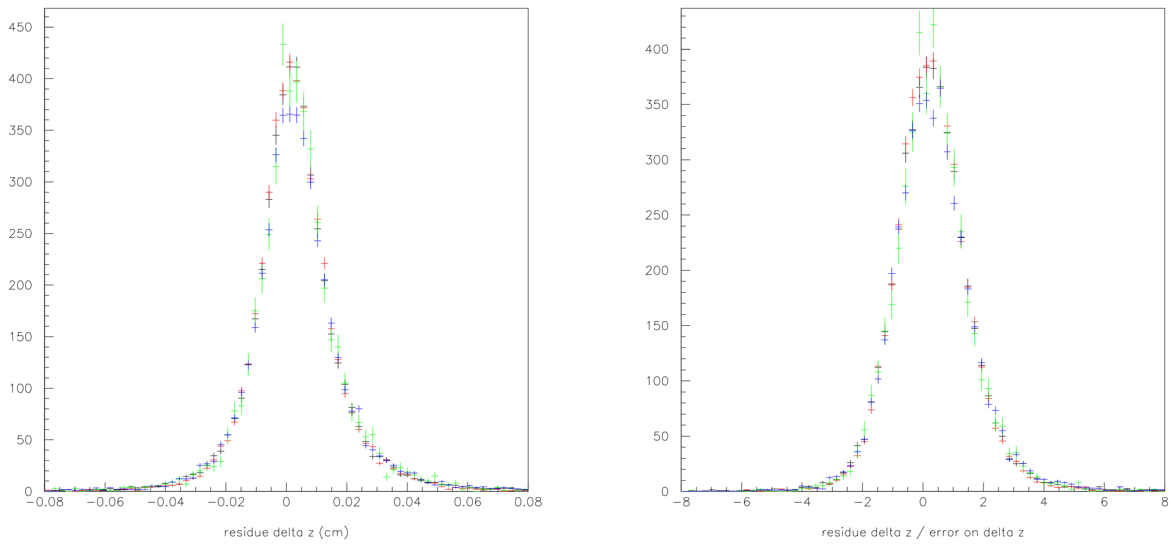

Figure 14: Δz residual (left) and pull (right) for different decay chains of the fully reconstructed B. Black: $B^- \to J/\psi K^-$, red: $B^- \to D^0\pi^-$, green: $\overline{B}^0 \to D^+\pi^-$ and blue: $\overline{B}^0 \to D^{*+}\pi^-$.

Finally, figures 19 and 20 compare the number of candidates (tracks+V^0's) used to make the vertex tag. The agreement in the event-by-event errors and number of tracks is quite satisfactory. The situation is not so good for the χ^2 distributions where data is significantly worse than the simulation. The fact that event-by-event errors agree quite well but it is not so for the χ^2 gives evidence that the Monte Carlo does not include accurate simulation of data. As it is investigated in section 6, this effect can be explained by the misalignment of our data, not accounted for in our detector simulation.

As it has been already mentioned before, as for the CP asymmetry extraction we measure the resolution function using the fully reconstructed Breco events it is very important to compare that for both sets of events (in data) there is good agreement for the relevant variables involved in the vertex tag recontruction. Figures 21, 22 and 23 show the comparison of the χ^2 probability, Δz event-by-event error and the number of candidates (tracks+V^0's) used to make the vertex tag, respectively, for B^0 and B^+ Breco and charmonium data. B^0 Breco and CP events are compared separately. The agreement is very satisfactory. As

B →	D* →	D →	σ	τ	f	RMS
$\overline{B}^0$						
$D^{*+}\pi^-$	$D^0\pi^+$	$K^-\pi^+$	1.06 ± 0.03	0.589 ± 0.099	0.503 ± 0.090	1.30
$D^{*+}\pi^-$	$D^0\pi^+$	$K^-\pi^+\pi^0$	1.07 ± 0.03	1.22 ± 0.22	0.734 ± 0.050	1.41
$D^{*+}\pi^-$	$D^0\pi^+$	$K^-\pi^+\pi^-\pi^+$	1.03 ± 0.02	0.882 ± 0.098	0.600 ± 0.052	1.34
$D^{*+}\pi^-$	$D^+\pi^0$	$K^-\pi^+\pi^+$	1.03 ± 0.02	0.614 ± 0.074	0.484 ± 0.067	1.26
$D^{*+}\rho^-$	$D^0\pi^+$	$K^-\pi^+\pi^0$	1.03 ± 0.03	1.09 ± 0.24	0.657 ± 0.067	1.35
$D^{*+}\rho^-$	$D^0\pi^+$	$K^-\pi^+\pi^-\pi^+$	1.02 ± 0.04	0.524 ± 0.144	0.416 ± 0.166	1.31
$D^{*+}a_1^-$	$D^0\pi^+$	$K^-\pi^+\pi^-\pi^+$	1.04 ± 0.03	0.773 ± 0.184	0.591 ± 0.097	1.28
$D^+\pi^-$		$K^-\pi^+\pi^+$	1.03 ± 0.01	0.967 ± 0.059	0.693 ± 0.024	1.34
$D^+\pi^-$		$K^0_S\ \pi^+$	0.99 ± 0.04	0.774 ± 0.288	0.748 ± 0.099	1.26
$D^+\rho^-$		$K^0_S\ \pi^+$	1.06 ± 0.05	1.34 ± 0.61	0.734 ± 0.085	1.29
$D^+a_1^-$		$K^-\pi^+\pi^+$	0.96 ± 0.02	1.29 ± 0.16	0.741 ± 0.035	1.36
B^-						
$D^0\pi^-$		$K^-\pi^+$	1.01 ± 0.08	0.756 ± 0.029	0.620 ± 0.018	1.25
$D^0\pi^-$		$K^-\pi^+\pi^0$	1.05 ± 0.01	0.719 ± 0.048	0.653 ± 0.029	1.25
$D^0\pi^-$		$K^-\pi^+\pi^-\pi^+$	1.03 ± 0.01	0.800 ± 0.037	0.643 ± 0.020	1.25
$D^{*0}\pi^-$	$D^0\pi^0$	$K^-\pi^+$	1.04 ± 0.02	0.732 ± 0.076	0.659 ± 0.041	1.26
$D^{*0}\pi^-$	$D^0\pi^0$	$K^-\pi^+\pi^0$	1.04 ± 0.02	0.880 ± 0.106	0.712 ± 0.043	1.27
$D^{*0}\pi^-$	$D^0\gamma$	$K^-\pi^+$	1.01 ± 0.02	0.761 ± 0.070	0.662 ± 0.041	1.24
$D^{*0}\pi^-$	$D^0\gamma$	$K^-\pi^+\pi^0$	1.01 ± 0.03	0.515 ± 0.117	0.498 ± 0.119	1.25
	charmonium					
$\overline{B}^0$						
$J/\psi\ \bar{K}^{*0}$	e^+e^-	$\bar{K}^{*0} \rightarrow K^-\pi^+$	1.00 ± 0.03	0.979 ± 0.214	0.703 ± 0.070	1.42
B^-						
$J/\psi\ K^-$	e^+e^-		1.04 ± 0.01	0.810 ± 0.066	0.701 ± 0.031	1.29
$J/\psi\ K^-$	$\mu^+\mu^-$		1.01 ± 0.01	0.791 ± 0.047	0.592 ± 0.029	1.26
$\psi(2S)K^-$	$\pi^+\pi^-\ J/\psi$	$\ell^+\ell^-$	0.95 ± 0.03	0.646 ± 0.157	0.581 ± 0.107	1.26

Table 6: *GExp* parametrization of the pull representation of the Δz resolution function for a variety of exclusively reconstructed hadronic modes. It can be seen that the parameters are stable from mode to mode. Therefore a unique resolution function is used and the modes Δz can safely be summed.

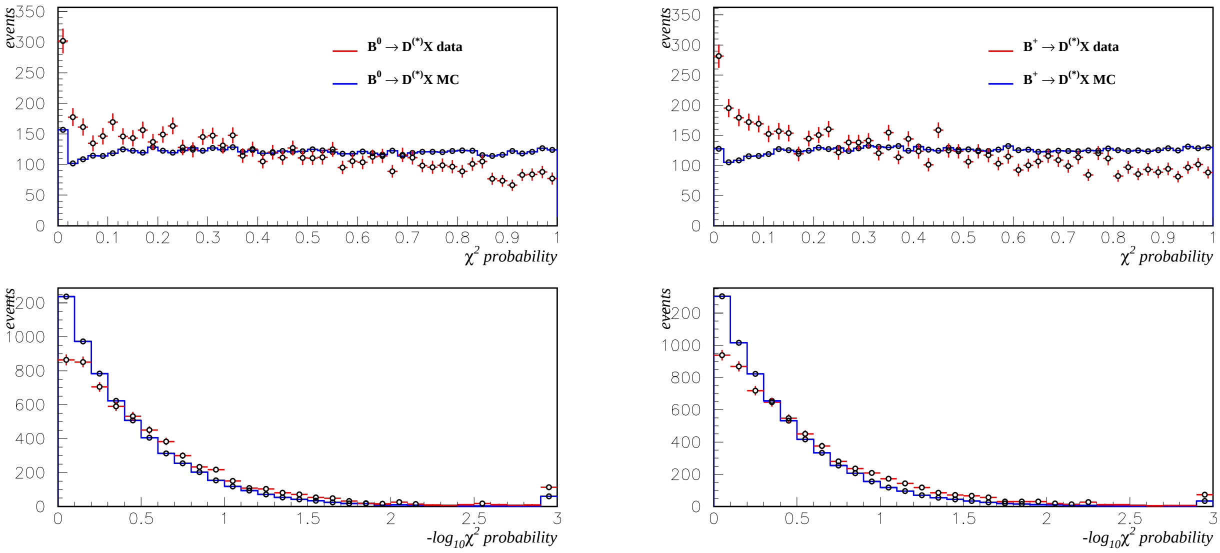

Figure 15: Data/Monte Carlo comparison of the χ^2 vertex tag probability for B Breco events in linear (top) and and logarithm (bottom) scale: (left) B^0 events; (right) B^+ events.

expected, charmonium events have an slightly better event-by-event error, mainly due to differences in the resolution of the fully reconstructed side. which propagates to Δz via the z component of the reco side vertex [2]. This difference in resolution, well reproduced by the reconstructed error, shows that likelihood fits to the data have to be performed on the basis of pulls rather than residuals (resolutions), otherwise the assumption of equivalence of resolution function for Breco and CP events does not apply.

Differences between data and Monte Carlo, and betwwen Breco and charmonium data (especially in χ^2 distributions) can reflect in differences in reconstruction and quality cuts efficiencies. Table 7 summarizes the Δz reconstruction efficiciencies (after quality cuts) for charmonium and Breco modes and data and Monte Carlo, for different configurations and cuts. For comparison with the default configuration it is shown the case when we require as additional stopping criteria two tracks ($n = 2$, as described in [1]) in vertex tag. Figure 24 compares the χ^2 distributions in Breco and charmonium data with this configuration. This figure should be compared with 21. To reduce large tails and outliers this configuration requires a cut on the χ^2 probability (0.1% in this exercise), which induces significant differences between data and Monte Carlo and to a less extend, Breco and charmonium data.

Table 8 shows the number of charmonium and Breco events by mode with a probability of χ^2 less than 1% for data and Monte Carlo with the final configuration ($n = 0$). It should be stressed that the χ^2 cut is not applied in this configuration.

[2]This difference in resolution is induced by the propagation to Δz of the differences in resolution of the reconstructed side, via the z component of the reco side vertex, and not via 'pseudo-track' mechanism. This is investigated with some detail in section 7. The Δz configuration with no beam constraints (here reco and tag side vertices are reconstructed in a completely independent way), as documented in section 4, also show this feature.

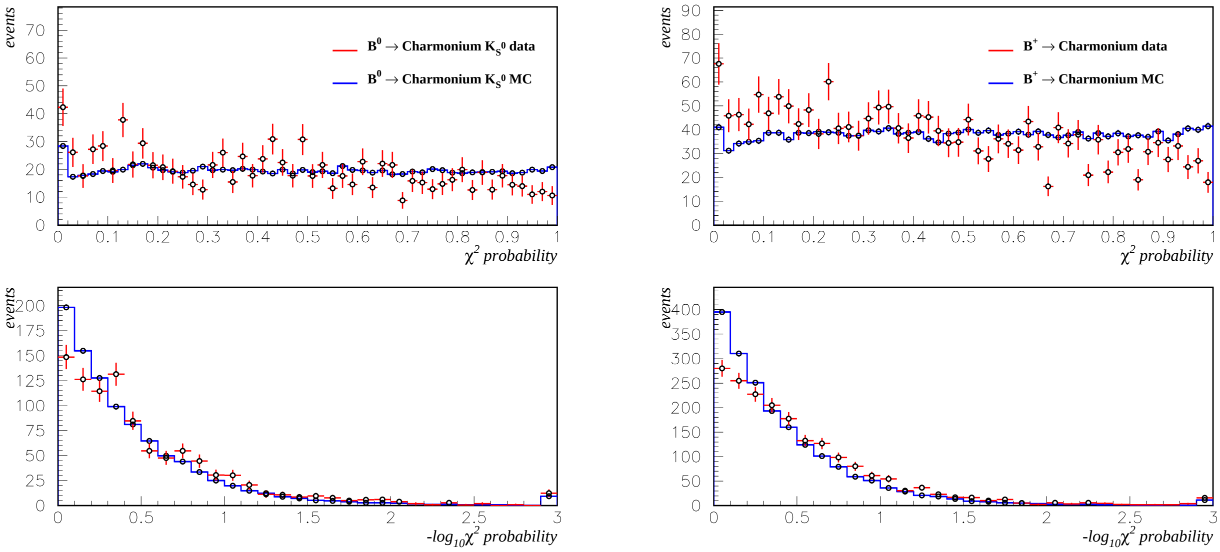

Figure 16: Data/Monte Carlo comparison if the χ^2 vertex tag probability for B charmonium events in linear (top) and logarithm (bottom) scale: (left) B^0 events; (right) B^+ events.

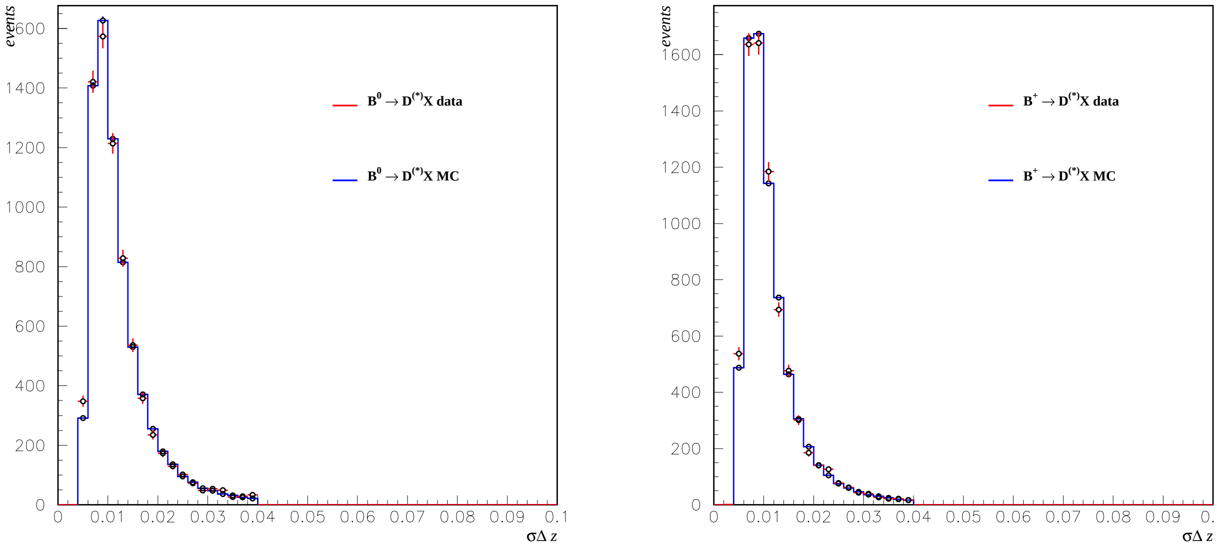

Figure 17: Data/Monte Carlo comparison of the event-by-event Δz error for B Breco events: (left) B^0 events; (right) B^+ events.

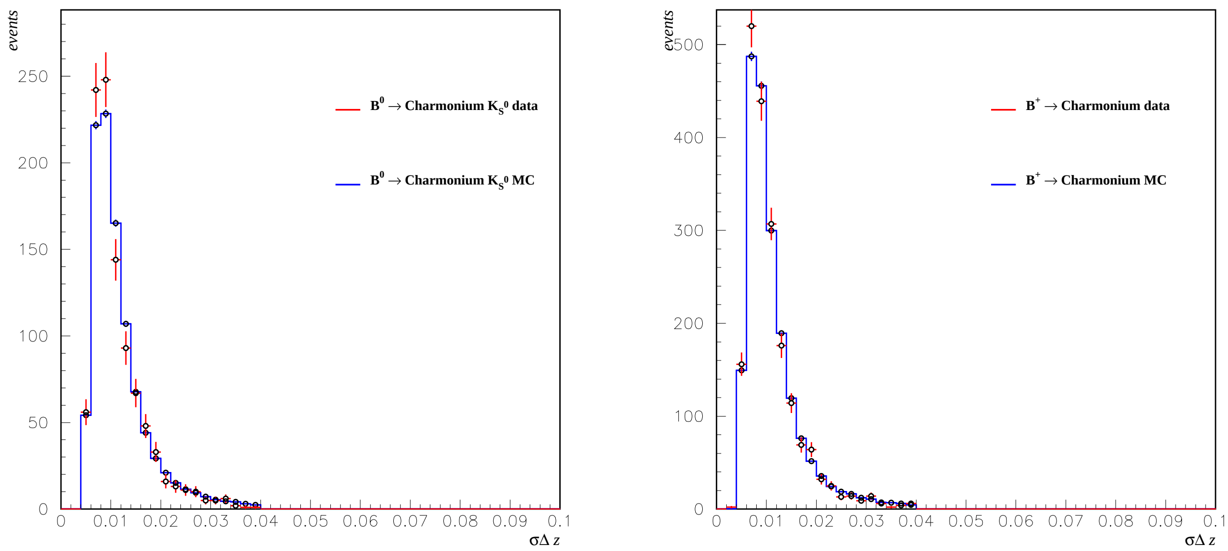

Figure 18: Data/Monte Carlo comparison of the event-by-event Δz error for B charmonium events: (left) B^0 events; (right) B^+ events.

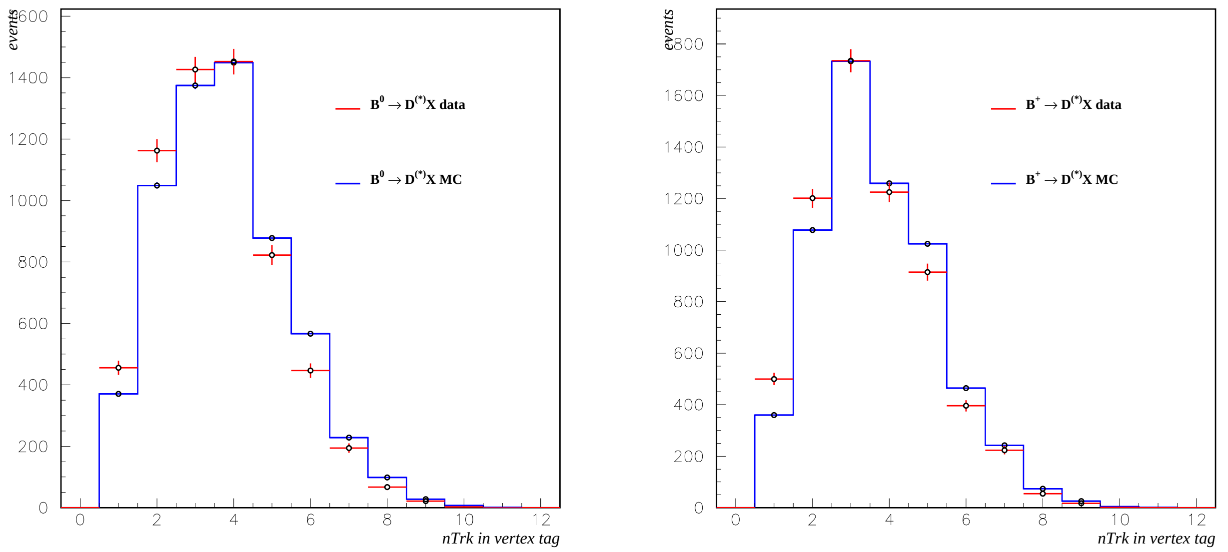

Figure 19: Data/Monte Carlo comparison of the number of candidates (tracks+V^0's) used to make the vertex tag for B breco events: (left) B^0 events; (right) B^+ events.

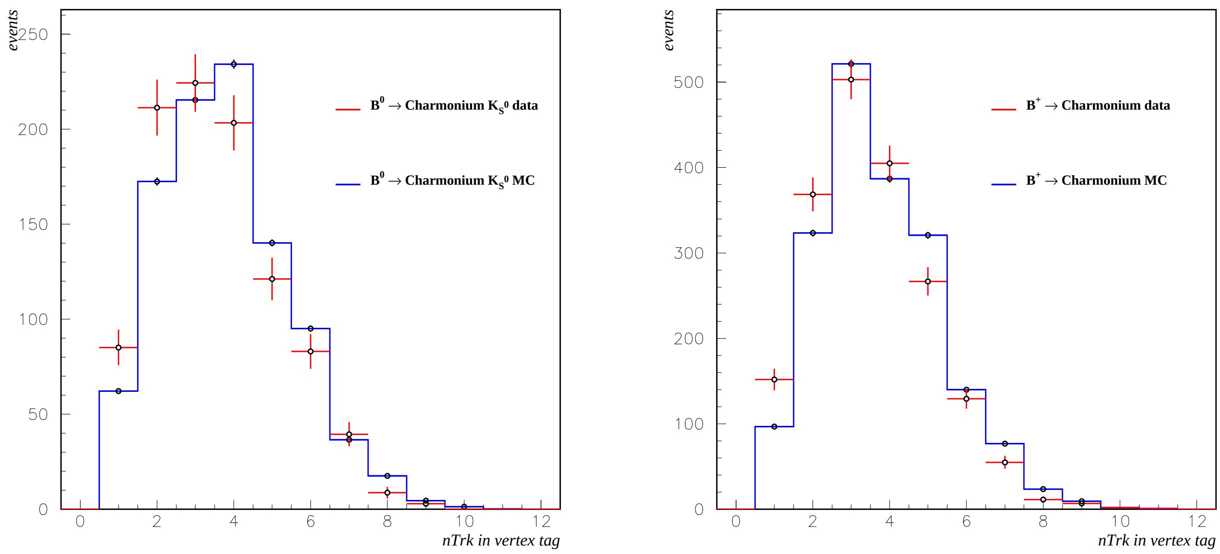

Figure 20: Data/Monte Carlo comparison of the number of candidates (tracks+V^0's) used to make the vertex tag for B charmonium events: (left) B^0 events; (right) B^+ events.

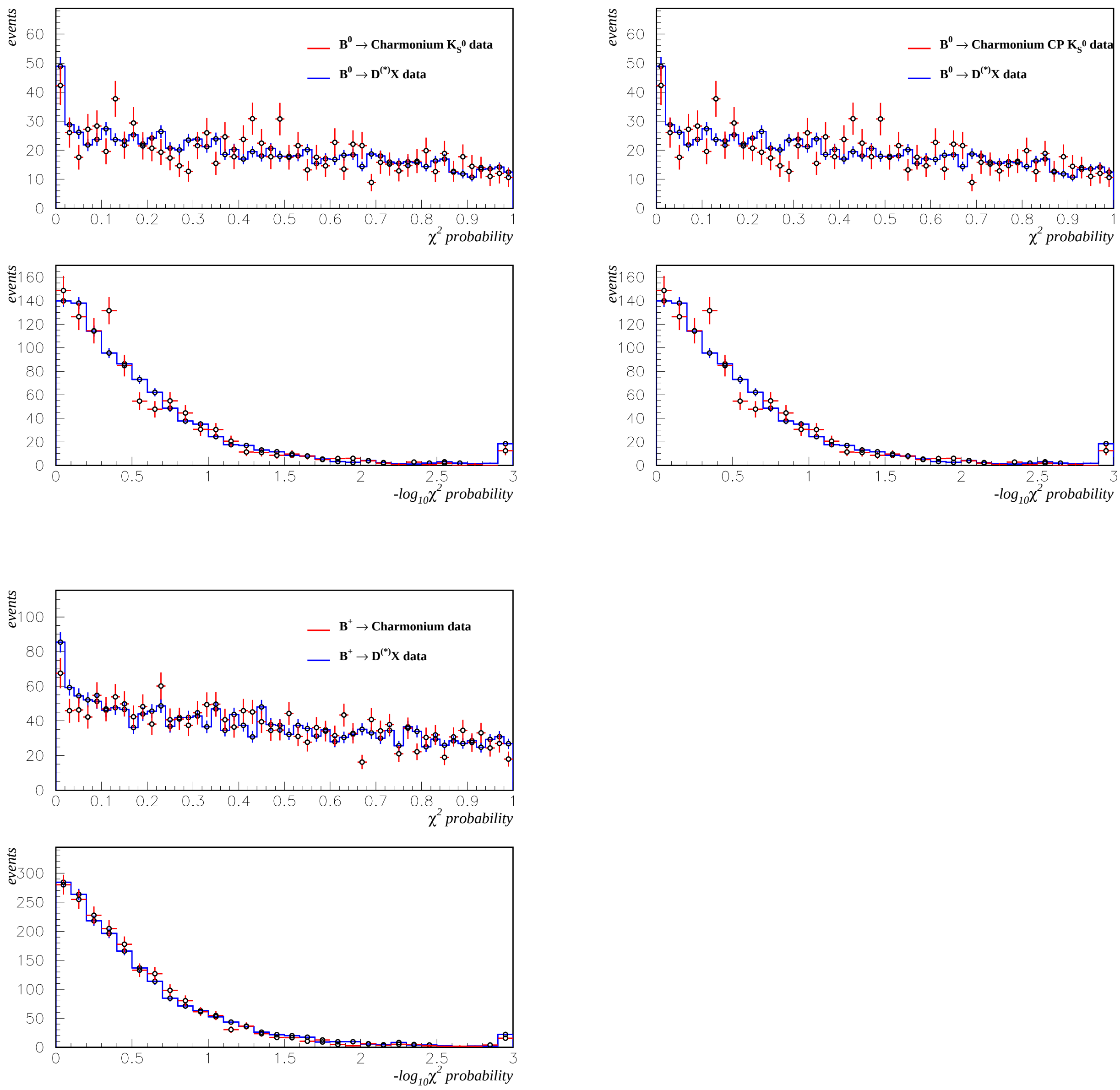

Figure 21: Breco/charmonium (excluding K_L^0 modes) data comparison of the χ^2 vertex tag in linear and logarithm scale: (top/left) B^0 events; (top/right) B^0 Breco and only B^0 charmonium CP events; (bottom/left) B^+ events.

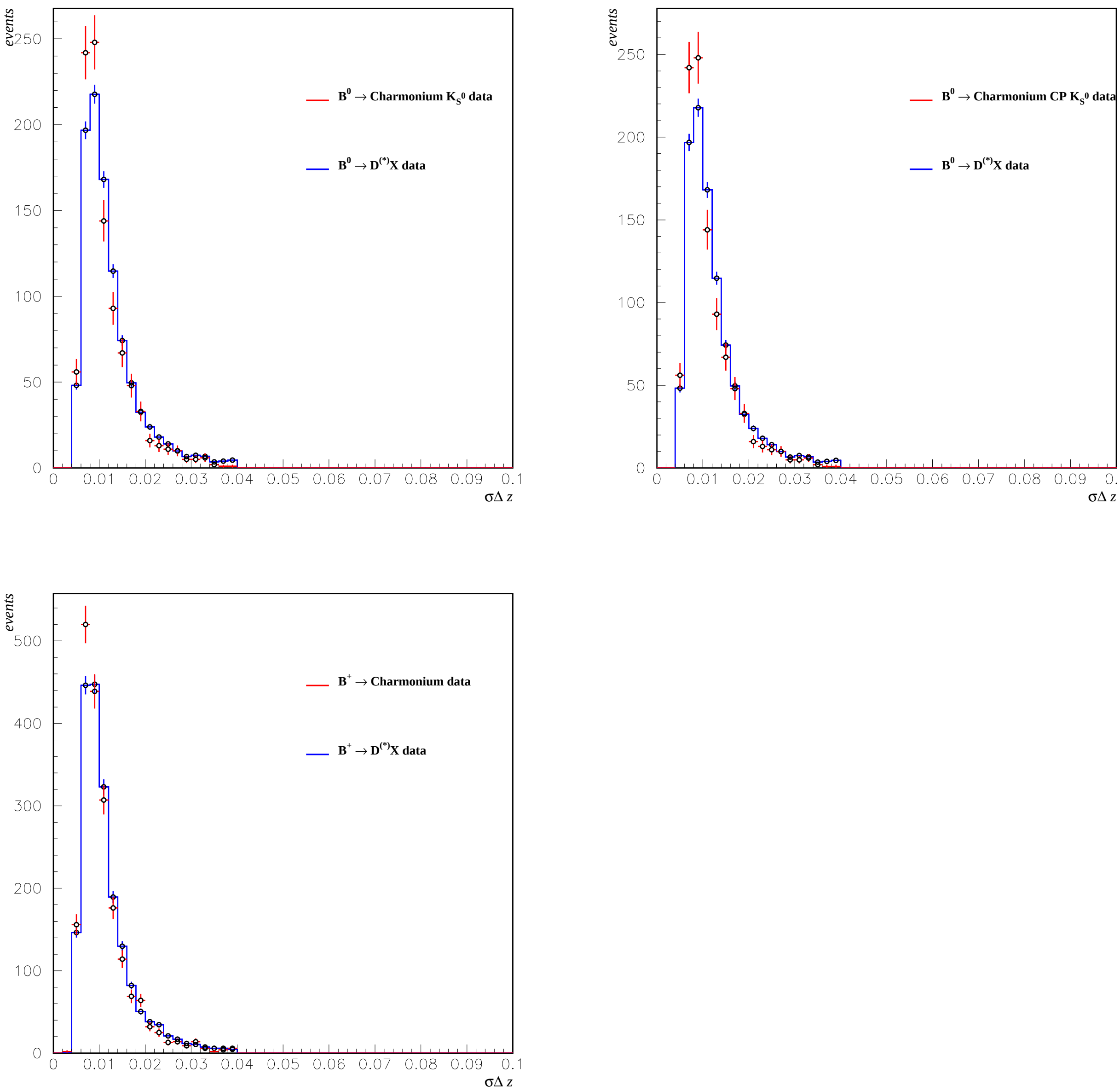

Figure 22: Breco/charmonium (excluding K_L^0 modes) data comparison of the event-by-event Δz error: (top/left) B^0 events; (top/right) B^0 Breco and only B^0 charmonium CP events; (bottom/left) B^+ events.

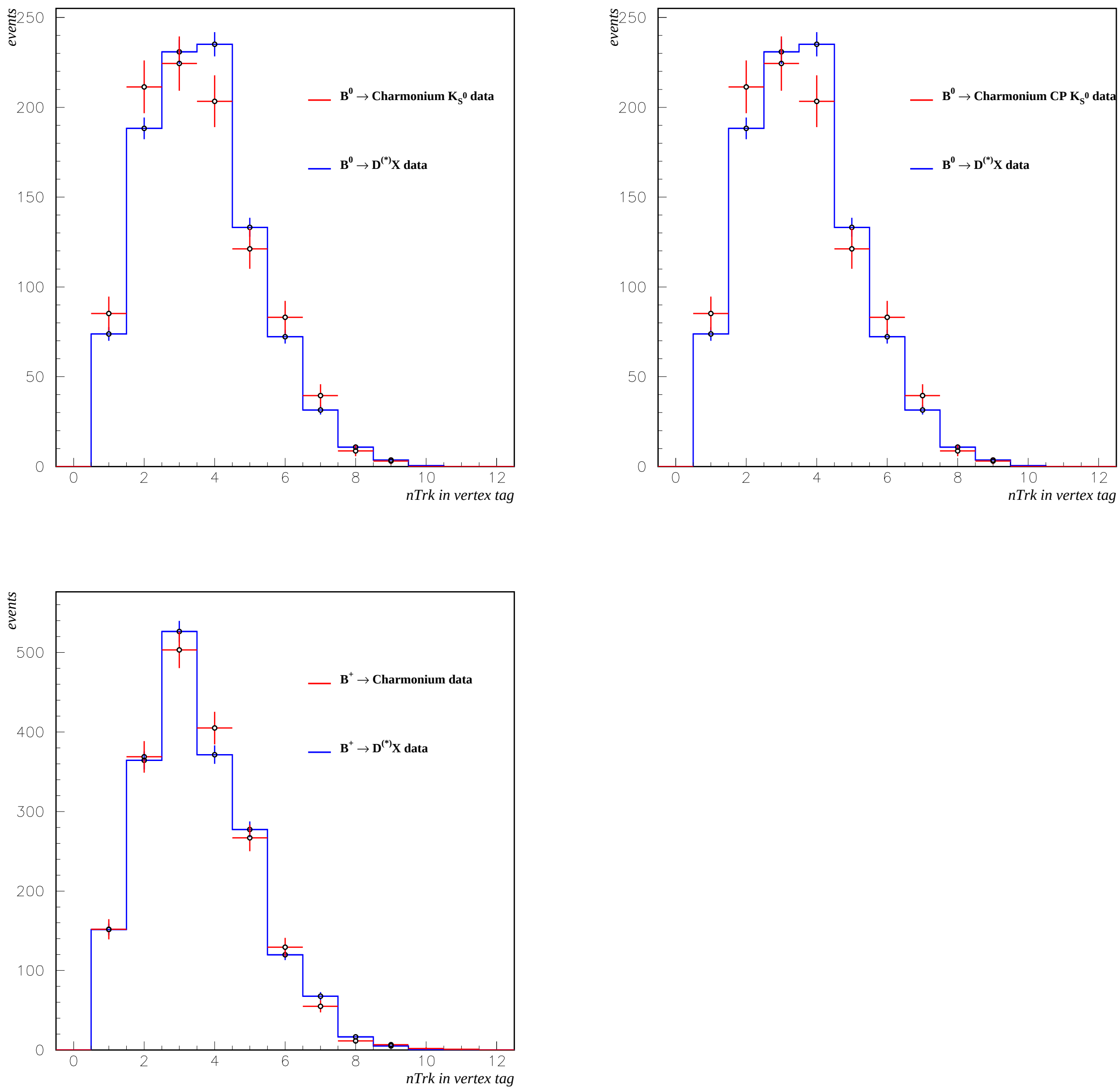

Figure 23: Breco/charmonium (excluding K_L^0 modes) data comparison of the number of candidates (tracks+V^0's) used to make the vertex tag: (top/left) B^0 events; (top/right) B^0 Breco and only B^0 charmonium CP events; (bottom/left) B^+ events.

	$n = 0$, no cut on χ^2	
	Monte Carlo	Data
B^0 Breco	0.958 ± 0.001	0.950 ± 0.003
B^+ Breco	0.966 ± 0.001	0.955 ± 0.003
B^0 Charmonium	0.959 ± 0.001	0.945 ± 0.010
B^0 Charmonium CP	0.959 ± 0.001	0.941 ± 0.011
B^+ Charmonium	0.967 ± 0.001	0.967 ± 0.004
	$n = 2$, no cut on χ^2 probability	
	Monte Carlo	Data
B^0 Breco	0.963 ± 0.001	0.960 ± 0.002
B^+ Breco	0.968 ± 0.001	0.964 ± 0.002
B^0 Charmonium	0.961 ± 0.002	0.968 ± 0.005
B^0 Charmonium CP	0.961 ± 0.002	0.96 ± 0.02
B^+ Charmoniu	0.970 ± 0.002	0.971 ± 0.003
	$n = 2$, probability $\chi^2 > 0.1\%$	
	Monte Carlo	Data
B^0 Breco	0.927 ± 0.002	0.907 ± 0.003
B^+ Breco	0.940 ± 0.001	0.913 ± 0.004
B^0 Charmonium	0.922 ± 0.002	0.898 ± 0.009
B^0 Charmonium CP	0.922 ± 0.002	0.87 ± 0.02
B^+ Charmonium	0.939 ± 0.002	0.924 ± 0.005

Table 7: Δz reconstruction efficiciencies (after quality cuts) for charmonium and Breco modes, data and Monte Carlo, for different configurations and cuts. MC errors are rounded to the 3rd digit.

Mode	Prob $\chi^2 < 0.01$ Data	Prob $\chi^2 < 0.01$ MC
Charmonium		
JpsiKs	3.30	1.75
Psi2sKs	0.66	1.66
JpsiKs2pi0	3.58	2.38
JpsiKstar0Kp	2.57	1.76
JpsiKstar0ks	15.7	1.61
JpsiKstarpKp	2.86	1.40
JpsiKstarpKs	2.69	1.64
JpsiK	2.26	1.38
Breco		
B0Dch	2.97	1.39
B0Dstar	3.86	1.32
BchD0	2.92	1.24
BchDstar	3.03	1.43

Table 8: Probability χ^2 less than 1% for charmonium and Breco data and MC.

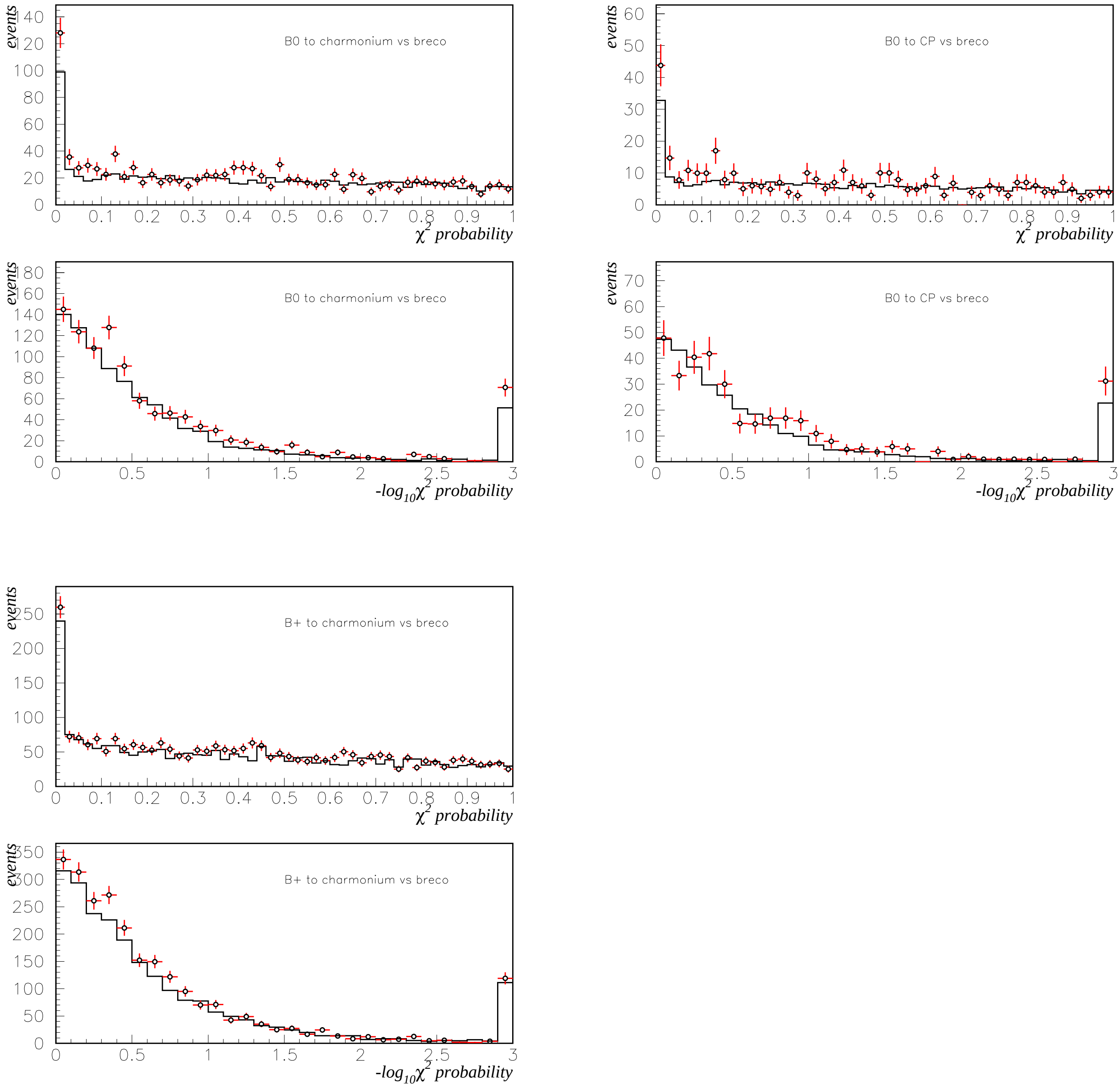

Figure 24: Breco/charmonium (excluding K_L^0 modes) data comparison of the χ^2 vertex tag in linear and logarithm scale when we stop the track rejection in the vertex tag algorithm when only two tracks remain ($n = 2$, see reference [1]): (top/left) B^0 events; (top/right) B^0 Breco and only B^0 charmonium CP events; (bottom/left) B^+ events.

3.4 Information from XY vertices

Very valuable information can be extracted from the vertex components in the plane orthogonal to the z axis to check the agreement between data and Monte Carlo, to resolve in case of disagreement among algorithms and to monitor the beamspot and the vertex reconstruction. There are several quantities of interest:

- The distance between the B reconstruted vertex and the nominal beam spot is a good indicator of the resolution of the vertex. The x component is, however, dominated by the beam spot spread (200 μm), and therefore is less useful. And non-negligible contribution to the y component is the lifetime of the B in the transverse plane (25 μm rms). Figures 25 and 26 show the data/Monte Carlo comparison of these distances and their pulls for Breco and charmonium events, respectively. Breco and charmonium data are directly compared in figure 27. Global bias and RMS from two-Gaussian fits are provided in table 9. No biases are observed and the agreement in resolution between data and Monte Carlo is fair. As expected, charmonium events have an slightly better resolution, ~ 60 μm against $80\,\mu$m, in the line of results obtained in section 2. In pull distribution there is a data/Monte Carlo disagreement of the order of 15%, well in agreement with the scale factors found with other independent control samples, as described in reference [2].

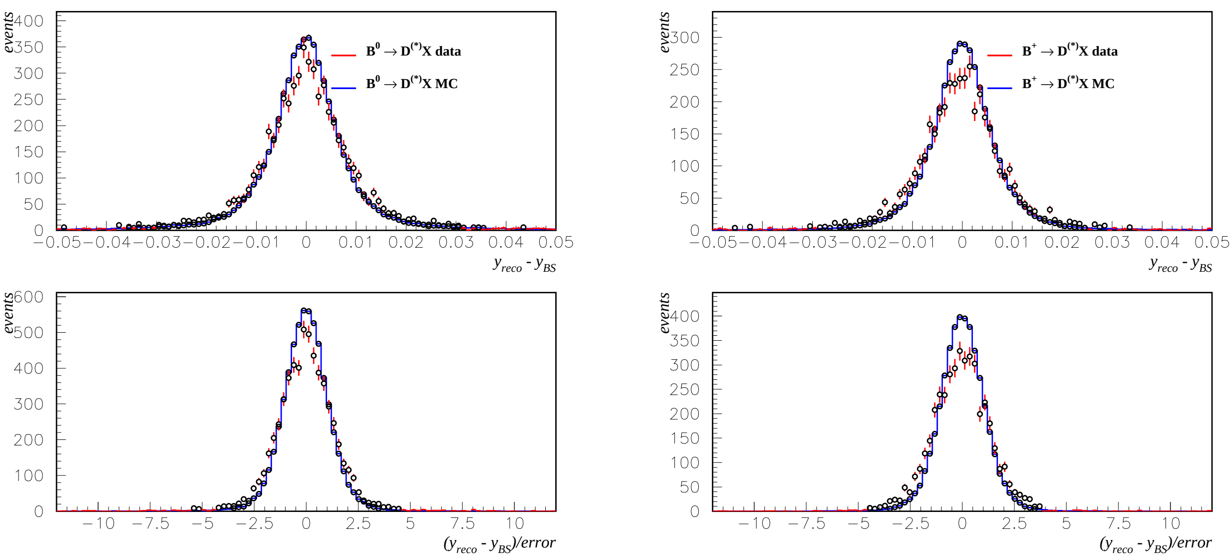

Figure 25: Data/Monte Carlo comparison of the y distance and pull between the fully reconstructed B vertex and the beam spot position for B^0 (left) and B^+ (right) Breco events.

- the distance between the tag vertex and the beam spot can be used to identify problems with the tag vertex reconstruction. The beam spot constraint in this case dominates the distribution, so this tend to be narrower than the corresponding B recontructed

	$y_{CP} - y_{BS}$ residual (μm)		$y_{CP} - y_{BS}$ Pull			
	μ	RMS	μ	RMS	σ_{core}	f_{core}
B^0 Breco signal MC	-0.3 ± 0.3	69.4 ± 1.1	-0.003 ± 0.005	1.05 ± 0.02	0.98 ± 0.02	0.964 ± 0.003
B^0 Breco Data	-0.7 ± 1.8	80.0 ± 6.0	-0.02 ± 0.03	1.24 ± 0.08	1.09 ± 0.08	0.87 ± 0.02
B^0 Charmonium signal MC	-0.5 ± 0.5	62.4 ± 1.4	-0.009 ± 0.009	1.10 ± 0.02	0.97 ± 0.03	0.931 ± 0.006
B^0 Charmonium Data	-0.3 ± 3.3	58.0 ± 6.8	0.03 ± 0.06	1.23 ± 0.07	1.07 ± 0.09	0.80 ± 0.04
	$y_{TAG} - y_{BS}$ residual (μm)		$y_{TAG} - y_{BS}$ Pull			
	μ	RMS	μ	RMS	σ_{core}	f_{core}
B^0 Breco signal MC	0.3 ± 0.2	36.6 ± 0.4				
B^0 Breco Data	0.1 ± 0.6	39.5 ± 1.5				
B^0 Charmonium signal MC	-0.1 ± 0.2	34.2 ± 0.6				
B^0 Charmonium Data	2.1 ± 1.1	30.0 ± 2.3				

Table 9: y residuals and pulls between the reco and tagging B vertices and the beam spot, for charmonium and Breco modes, data and Monte Carlo, with respect to the beam spot position in y. The distributions are fitted to two Gaussians. Pulls for vertex tag side have not been computed since they require the large correlation between the vertex and the beam spot, not available yet in the standard ntuples.

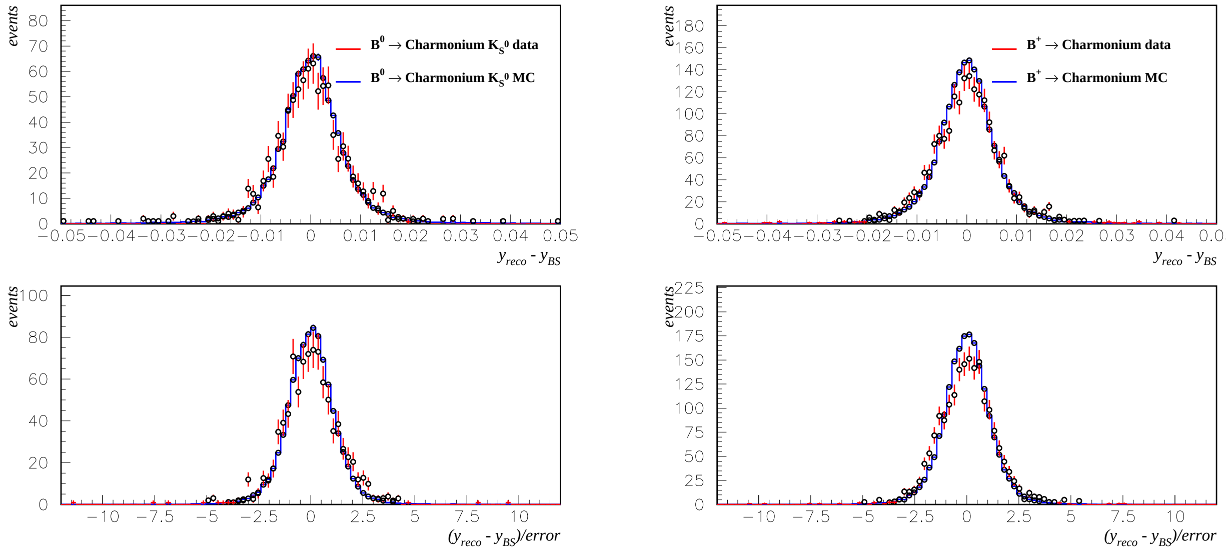

Figure 26: Data/Monte Carlo comparison of the y distance and pull between the fully reconstructed B vertex and the beam spot position for B^0 (left) and B^+ (right) charmonium events.

vertex distributions. It should be mentioned the fact that the beam spot contraint in fully reconstructed B is applied directly to the B production point and not to the decay point. As this check compares positions at the decay point we have an interesting way to monitor not only the beam spot position, but also whether the pseudo-track mechanism is able to correct by the B transverse component. This can be done looking at the RMS is the distribution, which will result from the convoluted effect of the B flight and the intrinsic width of the beam spot (~ 30 μm, see [1]). The check is however less useful in case of partially reconstructed B events when the beam spot constraint is applied directly to the B decay point.

Figures 28 and 29 show the data/Monte Carlo comparison of these distances and their pulls for Breco and charmonium, respectively. Breco and charmonium data are directly compared in figure 30. Global bias and RMS from two-Gaussian fits are provided in table 9. Again, no biases are observed and the agreement in resolution between data and Monte Carlo is good. The effect of the B is clearly visible. RMS of the order of $\sim$ 35 μm in all samples is an indication that no problems are affecting the reconstruction.

- the distance between the reconstructed B and the B tagging vertices in the transverse plane (d_{XY}) could be used to identify badly reconstructed vertices if too pronounced. The correlation of this variable and the pull on Δz has been studied in Monte Carlo. Figure 31(left) shows the distribution of the Δz pull for events with a d_{XY} smaller (top) or larger (bottom) than 300 μm. The correlation is encouraging, but figure 31(right) shows the fraction of non-outliers that is killed versus the fraction of outliers that still survives. 30% of the outliers can be killed at the expence of 5% of signal.

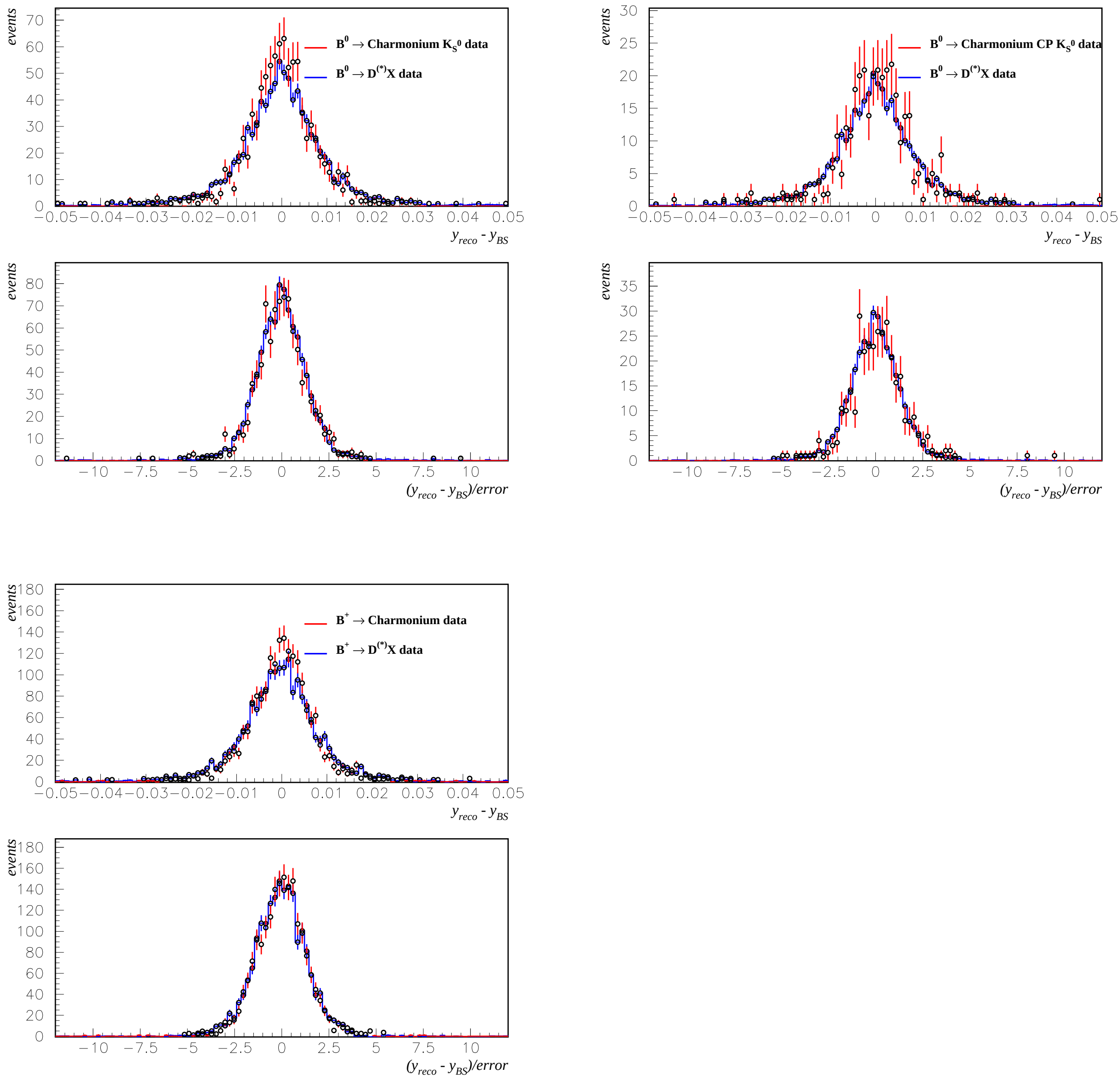

Figure 27: Breco/charmonium data (excluding K_L^0) comparison of the y distance and pull between the fully reconstructed B vertex and the beam spot position for B^0 (top/left), B^0 reco and B^0 CP events (top/right) and B^+ (bottom/left) events.

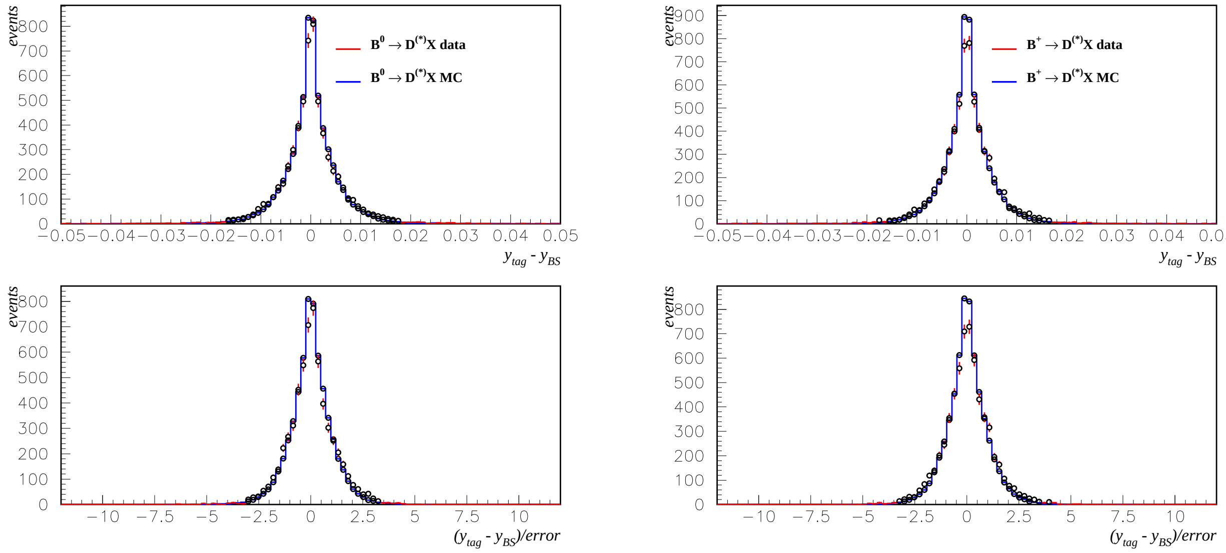

Figure 28: Data/Monte Carlo comparison of the y distance and pull between the B tag vertex and the beam spot position for B^0 (left) and B^+ (right) Breco events.

More likely the most adviceable usage of this variable is to monitor the fraction of outliers, comparing data and simulation. Figure 32 shows the comparison of the distributions. The fraction of events above 300 μm is 5.2% in the data and 4.6% in MC. In the data there is an accumulation of events at 300 μm which is not too significant, but needs to be monitored.

3.5 Effects from PEP-II parameters

3.5.1 Beam spot position, size and xz tilt

The impact of an incorrect determination of the beam spot or of the evaluation of the covariance matrix on it, is estimated. For a given MC generation, several shifts in the assumed beam spot position with respect to the true one are considered: 100, 200, 300 μm in x; 10, 20, 30 μm in y; and 1,2 or 3 mm in z. For each configuration the distribuiton of the resolutions and pulls are considered. Figure 33 shows the distributions for the most extreeme cases in the three coordinates. No significant effect is observed. This statement is quantified in table 10.

Extreme values of the shifts have also been tried: 3 mm in x, 100 μm in y and 3 cm in z. The z displacement has no effect (as expected since the z beam spot information does not enter into the Δz constraints, see reference [1] for details), while the other two components have sizeable effects. In particular the x shift causes a worsening of the RMS of the pull from 1.4 to 1.9 . The mean bias is instead unchanged. A shift of 100 μm in y (with a beam-spot width of 40 μm) causes a degradation of the RMS to 1.5. No additional bias is observed.

The test of changing the y component of the error on the beamspot from 7 to 40 mum

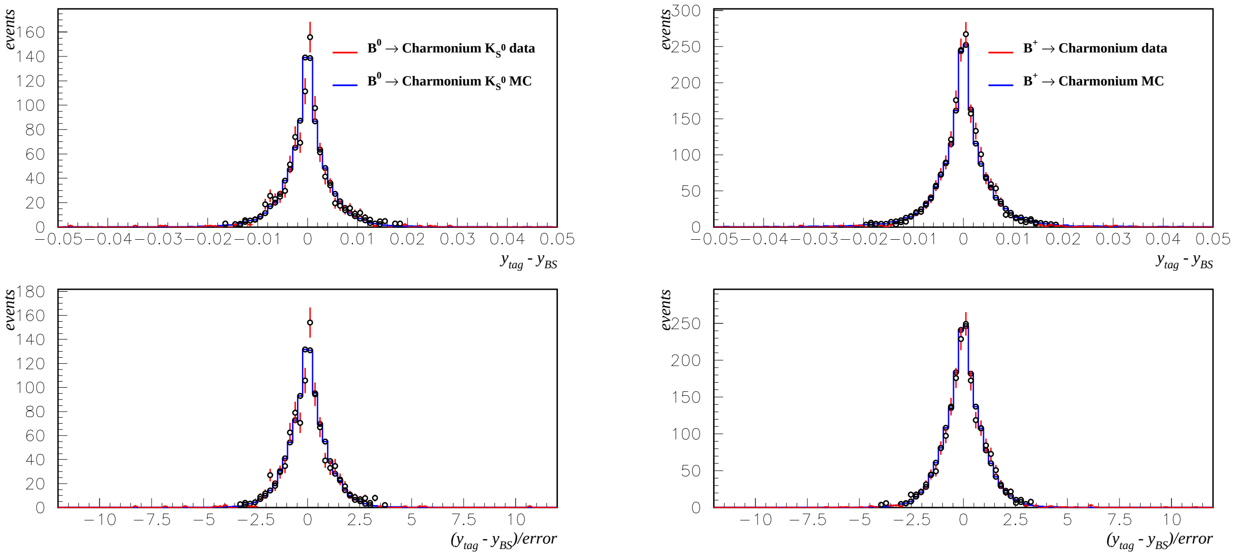

Figure 29: Data/Monte Carlo comparison of the y distance and pull between the B tag vertex and the beam spot position for B^0 (left) and B^+ (right) charmonium events.

has also been performed, but no change was observed if the beam spot estimate is correct. If there are shifts in the beamspot measurement they will be amplified if the error applied to them is smaller. However, beam spot studies have shown that shifts resulting from run-by-run variations as well as variations within a run are at the level of a few microns [17, 1], well below the 10 μm assumed size.

Tables 11 and 12 show the results to fits to the residuals and pulls of a similar and independent study: first the y size of the beam spot was increased 30, 50, 100 and 200 μm; second, a systematic offset of 10, 20, 30, 50, 100 and 200 μm was introduced; finally, randow offsets of 20, 30, 50, 100 and 200 μmwere tried. The only noticeable effect of worsening the beam spot size is a degradation of the width of the pull distribution, and to a less extend of the residual, for the second Gaussian (but the effect is in fact quite marginal). Biases are also slightly more significant, due to the fact that there is less secondary tracks rejection power. The effect of introducing systematic and random offset in the beam spot y position is largely supressed, and even at exterme and unrealistic biases of 200 μmthe increase of Δz bias is of only a few microns, and it is even less significant in terms of pull. This means that a degradation of the resolution and pull in data at 20% level could be explained only by a quite unrealistic shift in the beam spot position of about 100 μm.

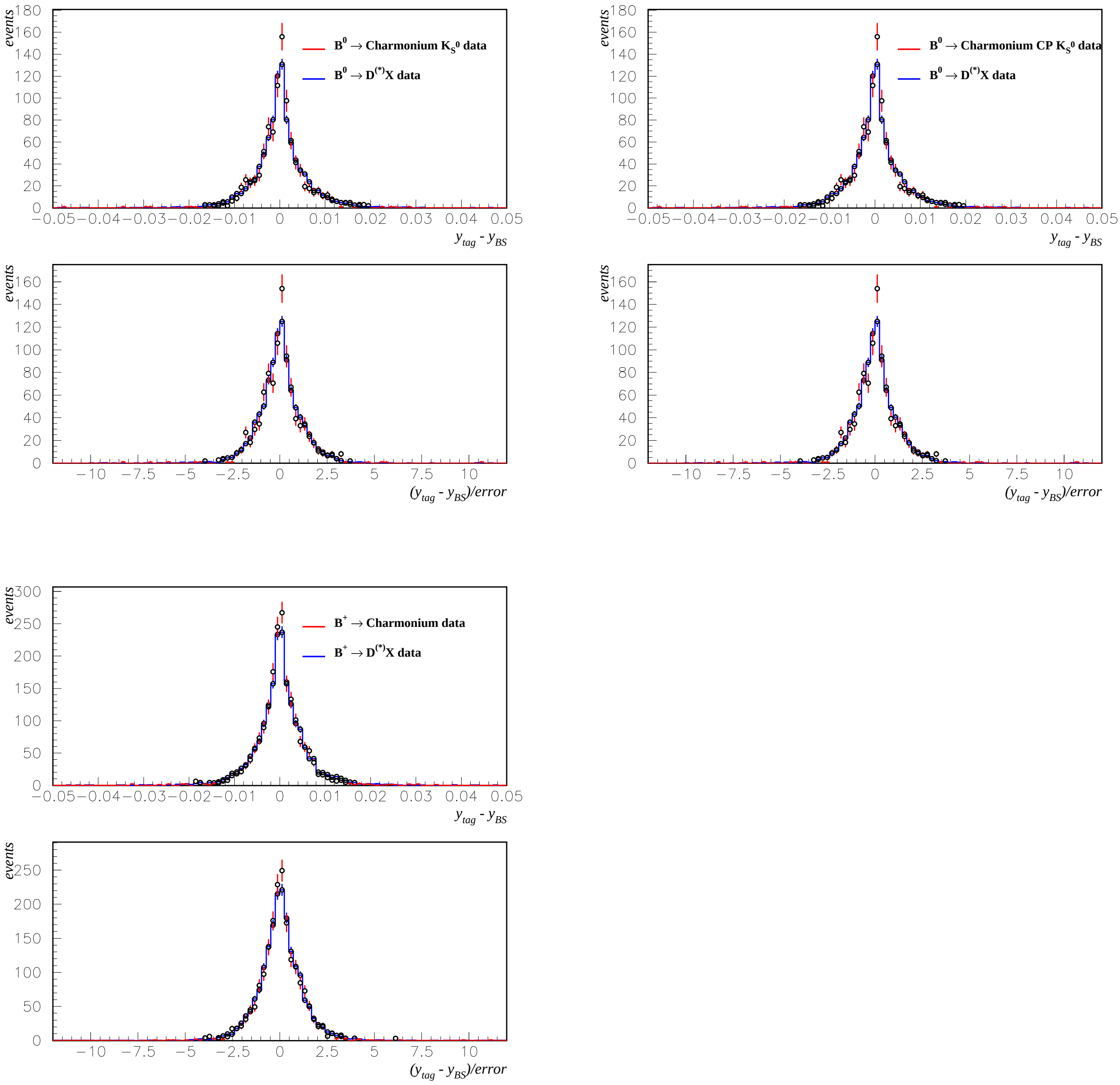

Figure 30: Breco/charmonium data (excluding K_L^0) comparison of the y distance and pull between the B tag vertex and the beam spot position for B^0 (top/left), B^0 reco and B^0 CP events (top/right) and B^+ (bottom/left) events.

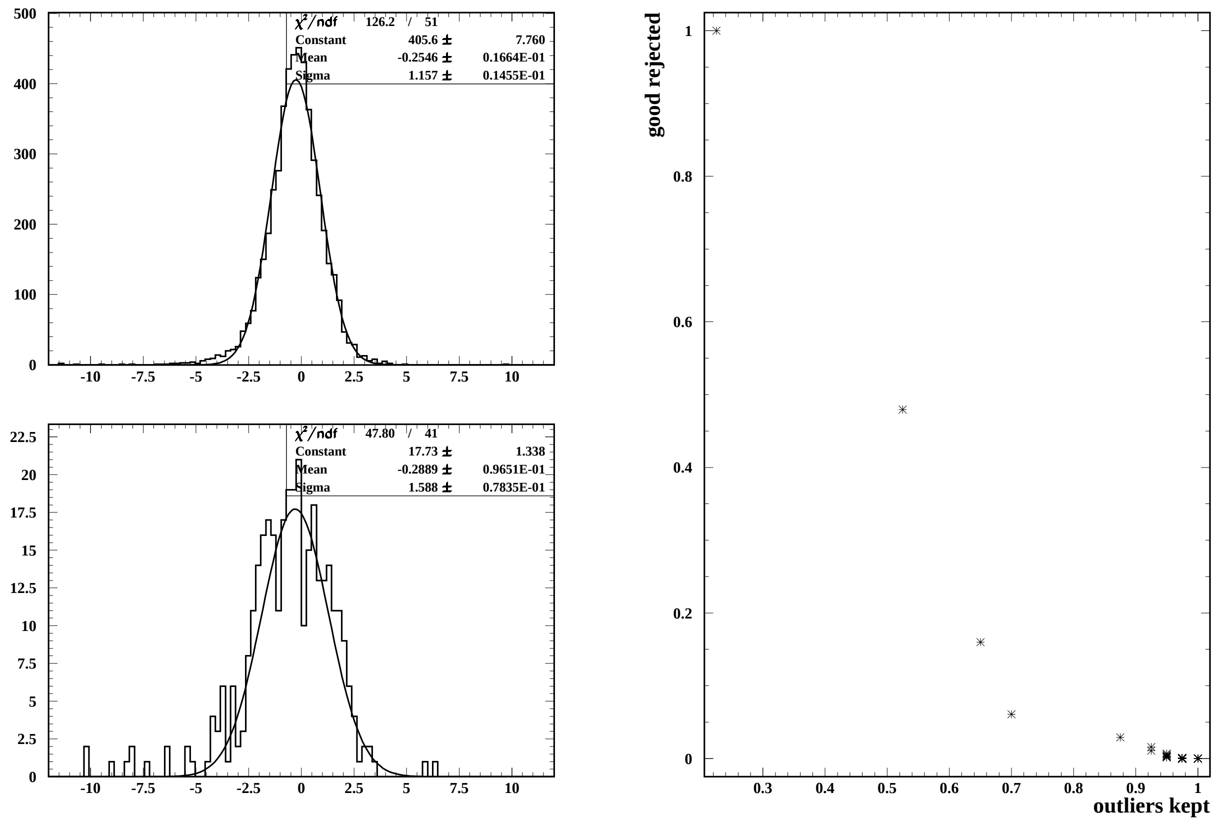

Figure 31: (Left) Distribution of the Δz pull for events with a d_{XY} smaller (top) or larger (bottom) than 300 μm. (Right) Fraction of outliers accepted (here, events above 300 μm) against the fraction of good rejected events in Monte Carlo.

The large insensitivy of biases in Δz to biases in the beam spot position can be explained as follows. As it is detailed in [1], Δz is extracted from the difference between the decay lengths of the fully reconstructed and tag side vertices with respect to the $\Upsilon(4S)$ decay point, L_z^{CP} and L_z^{TAG}. Neglecting the x components and assuming a negligible beam spot size in y, $L_z^{CP} \approx \frac{y_{CP}-y_{\Upsilon}}{p_{y,CP}/p_{z,CP}}$ and $L_z^{TAG} \approx \frac{y_{TAG}-y_{\Upsilon}}{p_{y,TAG}/p_{z,TAG}}$. On average, the ratios $p_{y,CP}/p_{z,CP}$ and $p_{y,TAG}/p_{z,TAG}$ are equivalent, so when estimating Δz as $L_z^{CP} - L_z^{TAG}$, on average, the dependecy on the actual central value of y_{Υ} cancels out, and only the relative vertical displacement between the fully reconstructed and the tag sides matters. Therefore, no significant bias in Δz can be induced by a bias in beam spot position. However, this is not true on a event-by-event basis, what will reflect in a deterioration of the resolution and the quality of the event-by-event estimation of the resolution.

Global Δz biases could, however, be induced by relative artificial vertical biases between the fully reconstructed and the tag side vertices. The difference in Δz pull for events at small and large transverse distance was shown in figure 31(left) using $B^+ \to J/\psi K^+$ Monte Carlo events. Within the difference in statistics no effect is seen when splitting the sample in events at d_{XY} smaller or larger than 300 μm. There is however some evidence for a larger

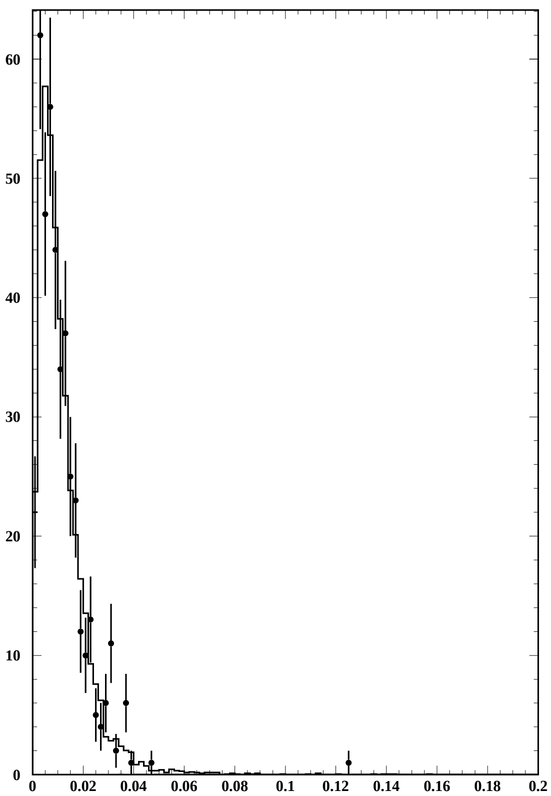

Figure 32: Data/Monte Carlo comparison (in $B^+ \to J/\psi K^+$ events) of the distance between the y component of the reconstructed and the tagging B vertices and the one of the beam spot.

fraction of events at larger negative pull.

Beam spot tilt effects are accounted for using the y and x sizes in the rotated planes. The checks detailed about enhancing the y size therefore include any possible tilt effect. Beam spot sizes in x of 300 μm were also tried, and not noticeable changes were observed in the resolution function.

3.5.2 Beam energies and spread

Recall that the pseudo-track (formed from the fully reconstructed B candidate and a knowledge of the average position of the interaction point and the $\Upsilon(4S)$ four-momentum) is fit to a common vertex with the tracks from the tag-side of the event. The effect that this pseudo-track constraint has on the measurment of Δz using the `VtxTagSelBtaFit` algorithm was investigated for $B_0 \to J\Psi K_S$ MC. The fits that immediately follow show results for when the constraint was not implemented in the analysis. The resolution in Δz and the fit to the pull are shown in Figures 34a and b respectively.

In Table 13, the results of the fit to two gaussians and one "flat" outlier gaussian is

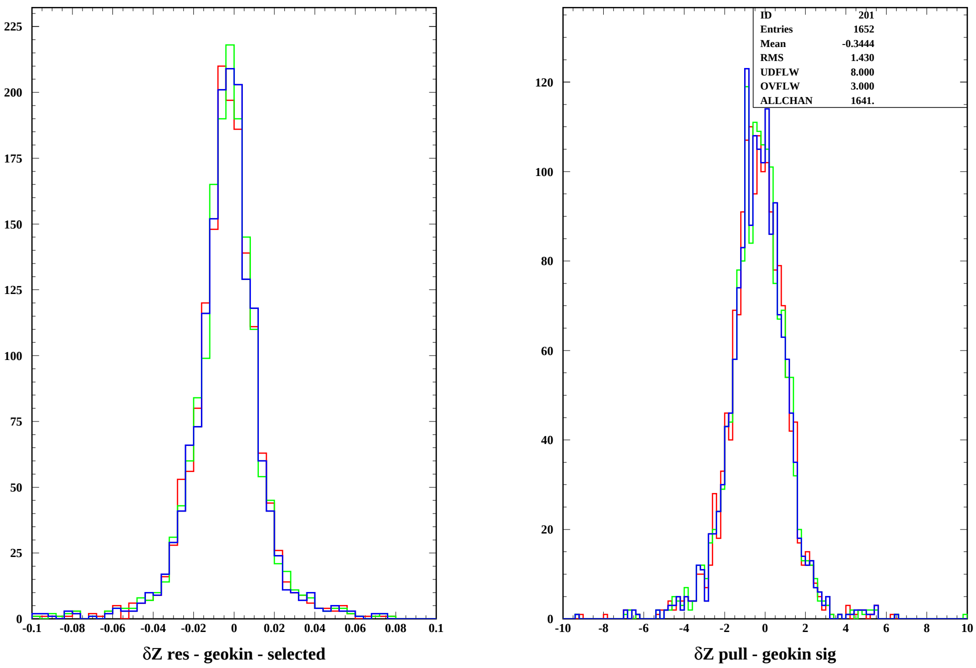

Figure 33: Distribution of the Δz resolution (a) and pull (d) when the beam spot is reconstructed without any shift (black), with a 300 μm shift in x (red), with a 30 μm shift in y (blue) and with a 3 mm shift in z (green).

compared to the standard analysis results which used the pseudo-track constraint. The fraction of outliers and their mean value are left free to float in both fits. The width of the outlier gaussian is fixed to 1.3 mm in the resolution fit and allowed to float in the pull. The fit parameters are nearly identical for the two analyses. The central gaussian of the residual fit is approximately 73% for both analyses with a resolution of 96 μm. The fraction of outliers changes from 1.9% to 1.6% for the standard analysis when comparing the resolution on Δz to the pull. This fraction changes from 1.7% to 1.6% for the analysis which did not use the pseudo-track. Both analyses have a pull RMS of 1.3 when the outliers are excluded.

It is observed that using the pseudo-track constraint effectively removes outliers from the pull distribution of Δz. The effect of the constraint on the probability of the χ^2, the χ^2, and number of degrees of freedom distributions is shown in Figure 35a, b, and c respectively. The histograms in red (blue) plot correspond to using (not using) the constraint. The χ^2 distribution when the constraint is not used is shifted to a lower mean resulting (combined with the one fewer degree of freedom shown) in the difference in the probability of the χ^2 plot for values near zero.

configuration	μ_1	$\mu_2 - \mu_1$	σ_1	$\frac{\sigma_2}{\sigma_1}$	f_{out}
resoltion(mum)					
correct	-31.7± 3.8	-29.4± 25.3	113.1± 4.2	3.0± 0.2	0.17± 0.03
x=+1	-31.3± 3.7	-26.7± 23.7	112.1± 4.2	3.0± 0.2	0.18± 0.03
x=+2	-30.9± 3.8	-27.2± 22.6	110.9± 4.4	3.0± 0.2	0.19± 0.03
x=+3	-30.8± 3.8	-27.1± 22.2	111.6± 4.6	2.9± 0.2	0.20± 0.03
y=+1	-31.6± 3.8	-33.0± 26.2	114.3± 4.3	3.0± 0.2	0.17± 0.03
y=+2	-32.2± 3.7	-35.5± 27.5	116.8± 3.7	3.0± 0.2	0.16± 0.02
y=+3	-32.6± 3.9	-30.2± 25.7	117.4± 4.3	2.9± 0.2	0.16± 0.03
z=+1	-31.7± 3.8	-29.4± 25.3	113.1± 4.2	3.0± 0.2	0.17± 0.03
z=+2	-31.7± 3.8	-29.4± 25.3	113.1± 4.2	3.0± 0.2	0.17± 0.03
z=+3	-31.7± 3.8	-29.4± 25.3	113.1± 4.2	3.0± 0.2	0.17± 0.03
x+30	-28.3± 5.1	-17.6± 26.5	124.7± 6.5	3.3± 0.2	0.28± 0.04
y+10	-34.0± 4.1	-36.0± 28.7	126.2± 4.8	2.9± 0.2	0.17± 0.03
z+30	-30.1± 3.8	-27.1± 20.0	107.3± 4.4	2.8± 0.2	0.21± 0.03
pull					
correct	-0.29± 0.03	-0.38± 0.24	1.10± 0.04	2.5± 0.2	0.13± 0.03
x=+1	-0.29± 0.03	-0.36± 0.23	1.09± 0.04	2.5± 0.2	0.14± 0.03
x=+2	-0.29± 0.04	-0.37± 0.23	1.10± 0.04	2.4± 0.2	0.14± 0.03
x=+3	-0.30± 0.03	-0.38± 0.25	1.12± 0.04	2.6± 0.2	0.12± 0.03
y=+1	-0.29± 0.03	-0.46± 0.24	1.10± 0.04	2.5± 0.2	0.13± 0.03
y=+2	-0.29± 0.03	-0.49± 0.25	1.11± 0.04	2.5± 0.2	0.13± 0.03
y=+3	-0.29± 0.03	-0.57± 0.26	1.11± 0.03	2.5± 0.2	0.12± 0.03
z=+1	-0.29± 0.03	-0.38± 0.24	1.10± 0.04	2.5± 0.2	0.13± 0.03
z=+2	-0.29± 0.03	-0.38± 0.24	1.10± 0.04	2.5± 0.2	0.13± 0.03
z=+3	-0.29± 0.03	-0.38± 0.24	1.10± 0.04	2.5± 0.2	0.13± 0.03
x+30	-0.27± 0.05	-0.14± 0.21	1.32± 0.07	2.4± 0.1	0.25± 0.05
y+10	-0.32± 0.03	-0.51± 0.25	1.22± 0.04	2.7± 0.2	0.09± 0.03
z+30	-0.29± 0.03	-0.46± 0.25	1.11± 0.04	2.5± 0.2	0.12± 0.03

Table 10: Results of a fit to two gaussians of the distribution of the resolutions and pulls for several beam spot configurations. The shifts are in units of 100 μm for the x component, 10 μm for the y component and 1 mm for the z component (x=+1 means that the x component has been shifted by 100 μm).

3.6 Effects from B_{rec} selection

3.7 Δz dependent effects

The dependency of the Δz reconstruction effienciency as a function of the true Δz has been also investigated. As this tests requires a high statistics, all available charmonium and Breco signal Monte Carlo has been used. Figure 36 shows the dependence. By fitting to a straigh line, the observed dependence is 0.020 ± 0.024 ps^{-1}, therefore no dependence is observed with the available statistics.

The dependency of the Δz pull on the true value of Δz has also been checked using $B^0 \rightarrow J/\psi K^0_S$ Monte Carlo events. Four bins between 0 and 1 of the cumulative of the lifetime ($G(\Delta z) = exp(-\Delta z/250\mu m)$) have been studied separately. Figure 37 shows no significant effect.

3.8 Dependency on tagging category

The algorithm used so far does not make use of tagging information but the performances do nevertheless depend on the tagging category: in the case of the leptonic tags the leading particle does actually come from the primary vertex, while in the case of the kaon tags it is likely that the bias is going to be bigger. Table 14 shows the resolution function parameters

Configuration	f_{core}	$f_{outliers}$	μ_1	σ_1	μ_2	σ_2	μ_3
Residual (μm)							
correct	0.65 ± 0.03	0.025 ± 0.004	-15.3 ± 1.8	86.4 ± 2.6	-47 ± 6	199 ± 8	-319 ± 260
$\sigma_y = 30$ μm	0.66 ± 0.03	0.023 ± 0.003	-15.4 ± 1.8	87.2 ± 2.7	-48 ± 6	203 ± 9	-148 ± 250
$\sigma_y = 50$ μm	0.68 ± 0.03	0.022 ± 0.003	-16.1 ± 1.8	88.4 ± 2.5	-47 ± 6	210 ± 9	-77 ± 260
$\sigma_y = 100$ μm	0.67 ± 0.03	0.022 ± 0.003	-16.5 ± 1.8	88.4 ± 2.7	-44 ± 6	211 ± 10	27 ± 250
$\sigma_y = 200$ μm	0.66 ± 0.03	0.022 ± 0.003	-16.5 ± 1.8	88.7 ± 2.6	-46 ± 6	213 ± 9	-59 ± 240
syst offset $y = +10$ μm	0.65 ± 0.03	0.024 ± 0.004	-16.5 ± 1.8	86.2 ± 2.7	-43 ± 5	200 ± 8	-259 ± 250
syst offset $y = +20$ μm	0.62 ± 0.03	0.024 ± 0.004	-16.6 ± 1.8	84.0 ± 2.6	-43 ± 5	196 ± 7	-67 ± 250
syst offset $y = +30$ μm	0.63 ± 0.03	0.023 ± 0.003	-16.8 ± 1.9	85.8 ± 2.7	-43 ± 5	197 ± 7	-63 ± 250
syst offset $y = +50$ μm	0.64 ± 0.03	0.021 ± 0.003	-18.1 ± 2.0	89.5 ± 2.8	-43 ± 6	207 ± 8	-132 ± 270
syst offset $y = +100$ μm	0.55 ± 0.04	0.027 ± 0.004	-20.1 ± 2.5	97.1 ± 3.7	-40 ± 5	221 ± 8	90 ± 221
syst offset $y = +200$ μm	0.46 ± 0.06	0.037 ± 0.006	-24.5 ± 5.2	152 ± 9	-49 ± 8	320 ± 14	-131 ± 200
random offset $y = 20$ μm	0.63 ± 0.03	0.025 ± 0.004	-14.1 ± 1.9	86.4 ± 2.5	-50 ± 6	190 ± 7	-333 ± 250
random offset $y = 30$ μm	0.67 ± 0.03	0.021 ± 0.003	-15.4 ± 1.9	90.2 ± 2.6	-54 ± 7	206 ± 9	-138 ± 274
random offset $y = 50$ μm	0.65 ± 0.03	0.023 ± 0.004	-15.6 ± 1.9	90.8 ± 2.7	-51 ± 6	212 ± 8	-155 ± 260
random offset $y = 100$ μm	0.61 ± 0.03	0.027 ± 0.003	-16.7 ± 2.0	95.6 ± 2.8	-42 ± 6	240 ± 9	-216 ± 220
random offset $y = 200$ μm	0.48 ± 0.03	0.047 ± 0.005	-17.2 ± 2.4	97.4 ± 4.0	-33 ± 6	291 ± 11	-171 ± 130

Table 11: Results of a fit to three Gaussians of the distribution of the resolutions and pulls for several beam spot configurations. The width of the third Gaussian has been fixed to 1.3 mm and 8.0 for the residual abd pull distributions respectively. The nominal configuration used 10 μm and ~ 200 μm beam spot width for y and x respectively.

for each of the categories as evaluated in MC. The lepton tags have a significantly better resolution and a smaller bias. While the resolution is properly accounted for by the error, the difference in bias is not. The worst case is the kaon one.

From the distribution of M_{ES} in the four categories is data for the four charmonium modes considered here ($B_0 \rightarrow J\Psi K_S$,$B_0 \rightarrow \Psi(2S) K_S$,$B_0 \rightarrow J\Psi K^{*0}$,$B^+ \rightarrow J\Psi K^+$), the background level is estimated to be 1.7% for leptons, 5.9% for kaons, 3.0% for NT1 and 8.0% (NT2). From these observations, the possible improvents are:

- use only the lepton track in the case of a lepton tag. Presently the use of the tagging track is not enforced. Nevertheless it turns out that they are used in 95.4±0.4% of the cases in MC. On data, with sideband subtraction, the fraction turns out to be 93.2±1.8%. The properties of the events where the lepton has not been used for the tag vertex have been studies. The mistag rate in MC is 19±4 % as opposed to 9.6±0.6%. Their Δt resolution (see figure 38a) shows a clear tail with high negative bias due to the incorrect tags. Their p* distribution (see figure 38b) shows no clear bias. Figure 38c shows that in a big majority of the cases there is at least another track used in addition to the lepton in making the vertex;
- discard the tagging kaon in the case of a kaon tag;
- use only the n "best" tracks that would have made the vertex, where n is a parameter to be tuned.

The first thing to check is the loss of efficiency due to the changes in the algorithm. The numbers are shown in table 15 where the efficiency are reported for three different algorithms: the standard one, the one where only the lepton is used and the kaons are removed and the one where only the three most energetic tracks are passed to the vertex finder.

Configuration	f_{core}	$f_{outliers}$	μ_1	σ_1	μ_2	σ_2	μ_3
			Pull				
correct	0.85 ± 0.06	0.017 ± 0.003	-0.16 ± 0.03	1.06 ± 0.03	-0.9 ± 0.3	1.68 ± 0.14	-1.1 ± 1.5
$\sigma_y = 30\ \mu$m	0.86 ± 0.06	0.019 ± 0.003	-0.16 ± 0.03	1.06 ± 0.03	-0.9 ± 0.3	1.65 ± 0.15	-1.3 ± 1.4
$\sigma_y = 50\ \mu$m	0.80 ± 0.08	0.020 ± 0.003	-0.15 ± 0.03	1.03 ± 0.04	-0.7 ± 0.2	1.63 ± 0.16	-0.8 ± 1.3
$\sigma_y = 100\ \mu$m	0.87 ± 0.04	0.016 ± 0.003	-0.18 ± 0.02	1.06 ± 0.03	-0.9 ± 0.2	1.95 ± 0.19	-1.2 ± 1.6
$\sigma_y = 200\ \mu$m	0.88 ± 0.03	0.017 ± 0.004	-0.18 ± 0.02	1.06 ± 0.02	-0.9 ± 0.2	2.07 ± 0.20	-1.3 ± 1.6
syst offset $y = +10\ \mu$m	0.82 ± 0.06	0.017 ± 0.003	-0.16 ± 0.03	1.05 ± 0.03	-0.8 ± 0.2	1.68 ± 0.12	-0.1 ± 1.7
syst offset $y = +20\ \mu$m	0.81 ± 0.07	0.016 ± 0.003	-0.16 ± 0.03	1.06 ± 0.03	-0.7 ± 0.2	1.67 ± 0.13	-1.4 ± 1.6
syst offset $y = +30\ \mu$m	0.80 ± 0.08	0.015 ± 0.003	-0.17 ± 0.03	1.06 ± 0.04	-0.6 ± 0.2	1.68 ± 0.14	-1.5 ± 1.5
syst offset $y = +50\ \mu$m	0.76 ± 0.10	0.017 ± 0.003	-0.19 ± 0.03	1.08 ± 0.05	-0.55 ± 0.14	1.67 ± 0.16	-0.5 ± 1.4
syst offset $y = +100\ \mu$m	0.73 ± 0.20	0.019 ± 0.004	-0.19 ± 0.06	1.23 ± 0.08	-0.5 ± 0.2	1.77 ± 0.23	-1.5 ± 1.5
syst offset $y = +200\ \mu$m	0.95 ± 0.02	0.024 ± 0.006	-0.21 ± 0.05	1.85 ± 0.04	-4.1 ± 0.5	1.18 ± 0.21	0.1 ± 1.9
random offset $y = 20\ \mu$m	0.86 ± 0.05	0.016 ± 0.003	-0.18 ± 0.02	1.08 ± 0.03	-0.8 ± 0.3	1.8 ± 0.16	-0.9 ± 1.6
random offset $y = 30\ \mu$m	0.82 ± 0.05	0.016 ± 0.003	-0.17 ± 0.03	1.07 ± 0.03	-0.7 ± 0.2	1.7 ± 0.12	0.9 ± 1.7
random offset $y = 50\ \mu$m	0.80 ± 0.06	0.016 ± 0.003	-0.16 ± 0.03	1.09 ± 0.03	-0.70 ± 0.14	1.76 ± 0.12	0.9 ± 1.7
random offset $y = 100\ \mu$m	0.76 ± 0.06	0.018 ± 0.003	-0.20 ± 0.03	1.16 ± 0.04	-0.44 ± 0.10	2.09 ± 0.16	-2.0 ± 1.8
random offset $y = 200\ \mu$m	0.55 ± 0.08	0.030 ± 0.005	-0.17 ± 0.03	1.15 ± 0.08	-0.33 ± 0.06	2.30 ± 0.16	0.77 ± 1.1

Table 12: Results of a fit to three Gaussians of the distribution of the resolutions and pulls for several beam spot configurations. The width of the third Gaussian has been fixed to 1.3 mm and 8.0 for the residual abd pull distributions respectively. The nominal configuration used 10 μm and $\sim$ 200 μm beam spot width for y and x respectively.

Δzreso	f_1	σ_1	μ_1	f_2	$\frac{\sigma_2}{\sigma_1}$	$\mu_2 - \mu_1$	RMS
Pseudo Used	73.7	96 $\pm$ 2 μm	-16 $\pm$ 2 μm	24.3	2.66 $\pm$0.08	-49 $\pm$8 μm	155 μm
Pseudo Not Used	72.7	97 $\pm$ 2 μm	-15 $\pm$ 2 μm	25.6	2.77 $\pm$0.08	-45 $\pm$8 μm	165 μm
Δzpull	f_1	σ_1	μ_1	f_2	$\frac{\sigma_2}{\sigma_1}$	$\mu_2 - \mu_1$	RMS
Pseudo Used	79.3	1.03 $\pm$ 0.03	-0.12 $\pm$ 0.02	19.1	1.79 $\pm$0.09	-0.65 $\pm$0.14	1.25
Pseudo Not Used	80.9	1.03 $\pm$ 0.03	-0.12 $\pm$ 0.02	17.5	1.94 $\pm$0.09	-0.67 $\pm$0.13	1.27

Table 13: Results of a fit to double gaussian on the residual and pull of the Δz measurement comparing analyses that did and did not use the pseudo-track constraint for $B_0 \to J\Psi K_S$ MC. The RMS does not include the outliers compononent.

There are significant efficiency losses, in particular in the algorithm that keeps only the lepton and removes the kaon. It is relevant to check if these losses are in the right or wrong tags. Figure 39 shows how the mistag rate changes before and after the algorithm is applied. A part from the case of the Kaons for the algorithm removing candidates the mistag fraction is reduced by using a smarter algorithm: the loss of efficiency affect mainly wrong tags. The resolutions and the pulls for the three algorithms are reported in table 16. A few obsevations:

- all the proposed changes reduce the bias, but it is typically quite a marginal improvement. In particular the lepton category is completely bias free, but it was already small enough at the beginning;
- the RMS of the pull for the lepton category is stable, the net effect of using only the tagging lepton is a reduction of the bias to being negligible;
- resolutions in the kaon and NT categories tend to worsen, although the pull are stable: the reduction of the number of tracks used hurt.

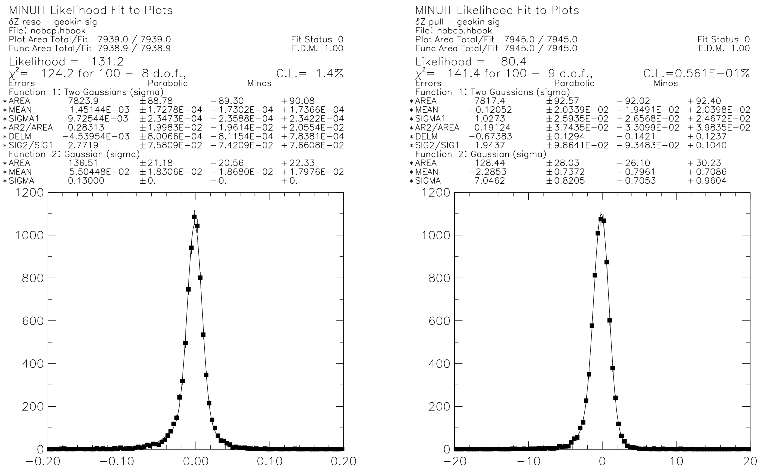

Figure 34: Residual (a) and pull (b) of Δz in $B_0 \rightarrow J\Psi K_S$ MC when the pseudo-track constraint was not used.

Δt reso	f_1	σ_1	μ_1	f_{out}	$\frac{\sigma_2}{\sigma_1}$	$\mu_2 - \mu_1$	RMS	μ
leptons	74.6	0.48 ± 0.02 ps	-0.05±0.01 ps	2.2	2.71±0.17	-0.28 ±0.08 ps	0.77ps	-0.15 ps
kaons	65.8	0.56 ± 0.02 ps	-0.11±0.01 ps	1.9	2.50±0.07	-0.23 ±0.04 ps	0.94ps	-0.19 ps
NT1	62.5	0.51 ± 0.03 ps	-0.07±0.02 ps	1.3	2.55±0.17	-0.20 ±0.06 ps	0.89ps	-0.15 ps
NT2	63.3	0.59 ± 0.03 ps	-0.07±0.02 ps	2.3	2.71±0.17	-0.36 ±0.07 ps	1.08ps	-0.20 ps
Δt pull	f_1	σ_1	μ_1	f_{out}	$\frac{\sigma_2}{\sigma_1}$	$\mu_2 - \mu_1$	RMS	μ
leptons	81.3	1.00 ± 0.04	-0.10±0.03	2.6	2.0±0.2	-0.5 ±0.2	1.25	-0.19
kaons	88.9	1.15 ± 0.02	-0.23±0.02	1.5	2.0±0.2	-1.1 ±0.2	1.32	-0.35
NT1	80.4	1.03 ± 0.04	-0.13±0.03	0.8	2.0±0.1	-0.7 ±0.2	1.30	-0.27
NT2	84.5	1.09 ± 0.04	-0.13±0.04	2.3	2.0±0.2	-1.1 ±0.3	1.08	-0.30

Table 14: Results of a fit to double gaussian plus outliers (8 ps gaussian with 0 mean)on the Δt residual and pull of the four tagging categories in $B_0 \rightarrow J\Psi K_S$ MC. The RMS does not include the outliers component.

Pulls have also been checked for the right and wrong tags both before and after applying the new suggested algorithm. The results are in table 17. One can see that:

- there is no significant difference in resolution between right and wrong tag fractions for the NT categories.
- with the standard algorithm, the difference is particularly significant for the lepton category and small but significant for the kaon category.
- using exclusively the lepton from the tag vertex reconstruction enhances these differences.
- removing the tagging kaons from the tag vertex reconstruction reduces the asymmetry in the kaon tags.

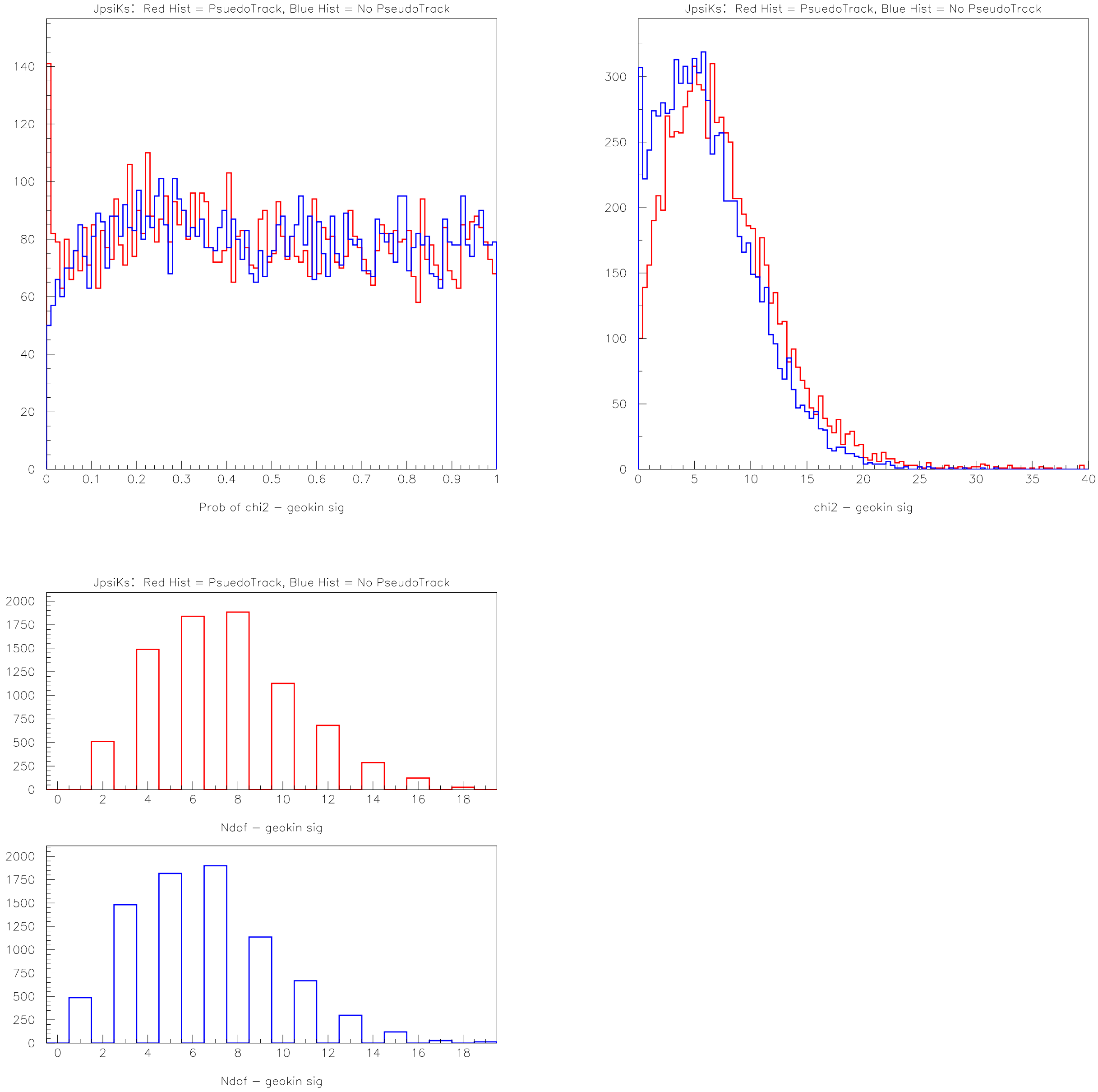

Figure 35: Comparison among the distributions of (a) the probability of χ^2 , (b) the χ^2 , and (c) the number of degrees of freedom with the analysis using (not using) the constraint show in red (blue).

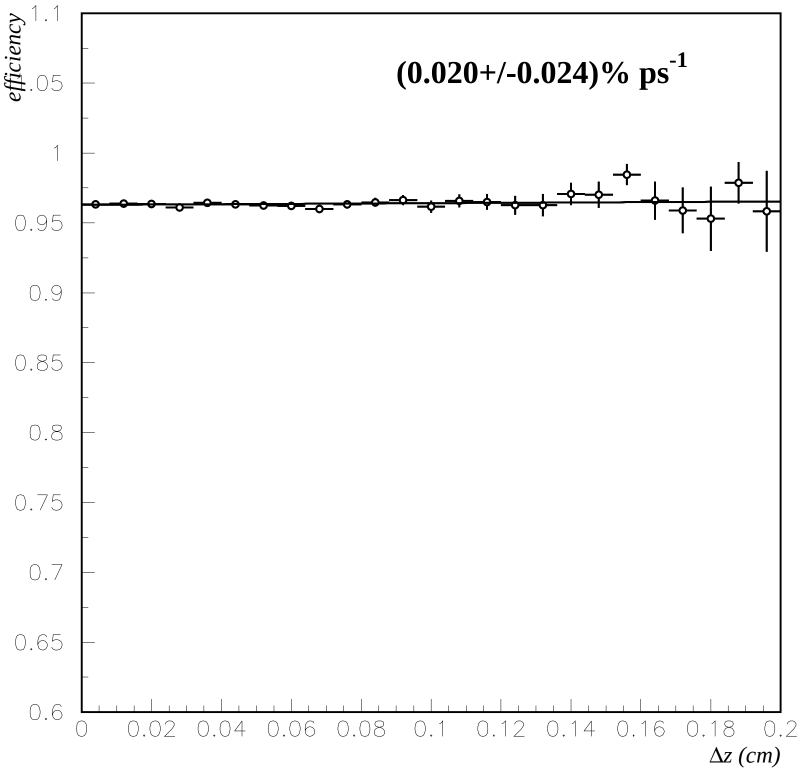

Figure 36: Dependence of the Δz reconstruction efficiency with the true value of Δz, for charmonium and Breco signal Monte Carlo events.

3.9 Check of Δt distributions

Figures 40 and 41 show the data/Monte Carlo comparison of the Δt distributions for signal events (after background subtraction) for B Breco and charmonium events, respectively, regardless tagging. CP events are shown separately. Figure 42 compares directly Breco and charmonium events in data. Figures 43, 44 and 45 are the equivalent distributions but after tagging. Good agreement is observed in all distributions. There seems to be a small excess of CP events in data over simulation at small Δt after tagging. The fact that this effect is not seen in the other events (Breco and charged charmonium B's), combined with the observation that the effect is significantly less significant -if any- before tagging (with a significantly larger statistics), gives support to the statistical fluctuation hypothesis. Nevertheless, this effect deserves some investigation, which is the main motivation of all the studies reported in section 7.

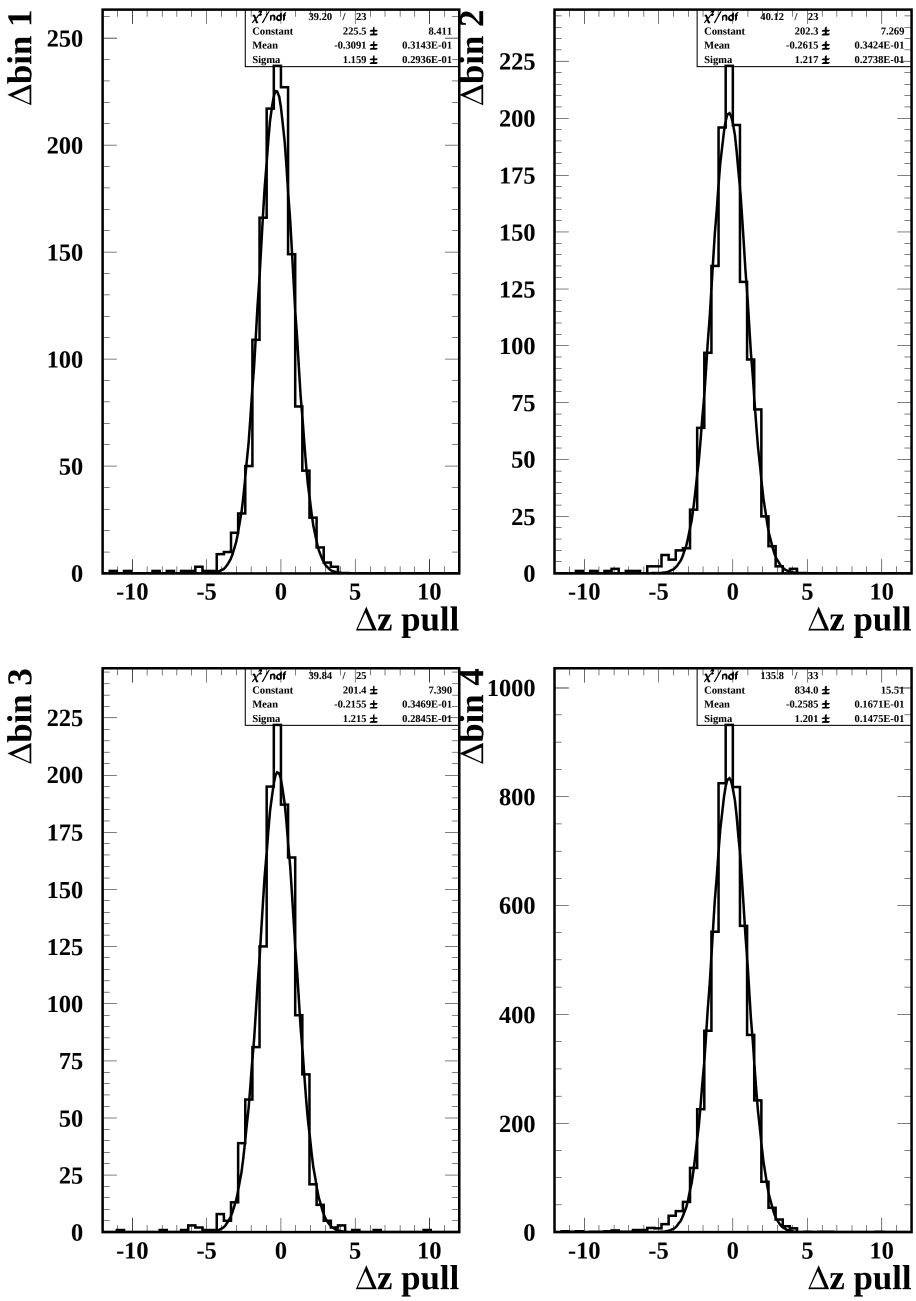

Figure 37: Pull distributions for four different bins between 0 and 1 of the cumulative lifetime $G(\Delta z) = exp(-\Delta z/250\mu m)$ for $B^0 \rightarrow J/\psi\, K_s^0$ Monte Carlo events.

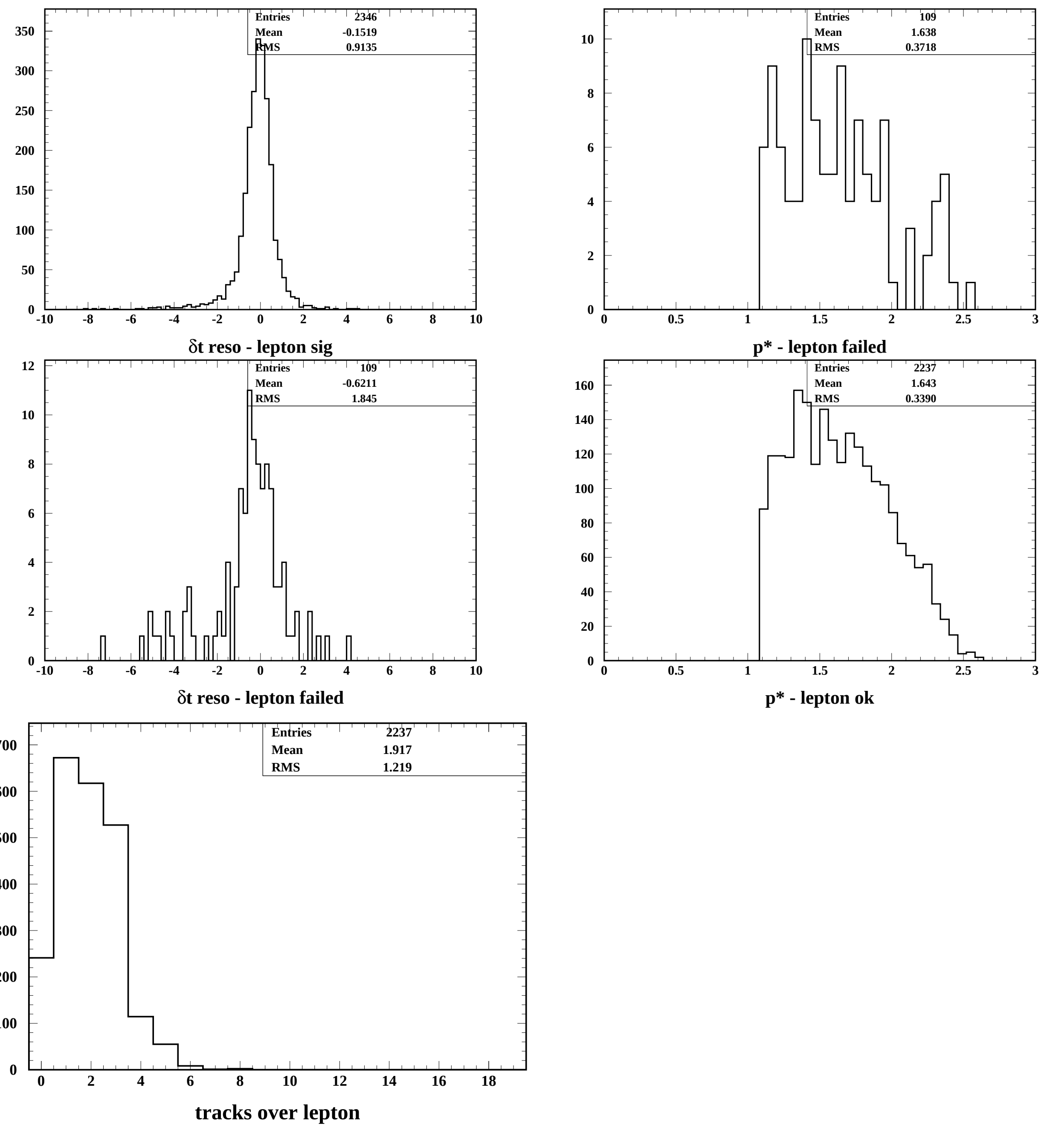

Figure 38: Distribution on MC of the Δt resolution (a) and the p* (b) for lepton tags where the lepton has not been used for the vertex (top) and for all the lepton tags (bottom) and (c) distribution of the number of tracks other than the lepton used in the tag vertex reconstruction.

configuration	leptons	kaons	NT1	NT2
Standard algo	97.2	98.4	96.6	94.2
Lepton/Kaon	95.1	92.6	“	“
Only 3 tracks	97.8	94.6	96.5	91.1

Table 15: Efficiency (in %) of the vertexing tags for the three different possible algorithms.

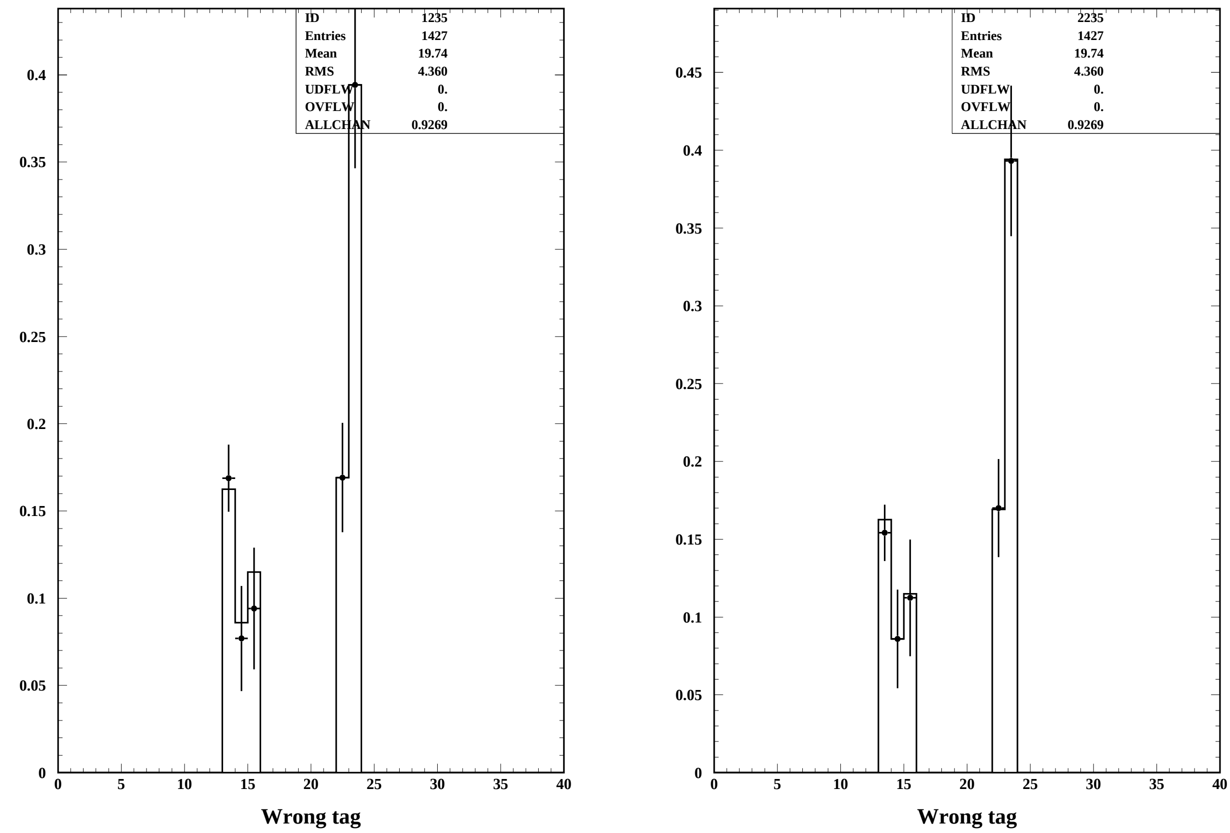

Figure 39: mistag rates before (histogram) and after (dots) applying the kaon/lepton correlation algorithm (a) and the restriction to the three most energetic tracks (b).

configuration	μ_1	$\mu_2 - \mu_1$	σ_1	$\frac{\sigma_2}{\sigma_1}$	f_{out}
resolution(ps)-leptons					
standard	-0.06± 0.01	-0.47± 0.10	0.51± 0.01	3.7± 0.1	0.15± 0.01
kaon/lepton	0.00± 0.01	-0.32± 0.08	0.54± 0.02	3.7± 0.1	0.23± 0.02
only 3 tracks	-0.04± 0.04	-0.9± 1.2	0.55± 0.03	6.3± 1.8	0.06± 0.02
resolution(ps)-kaons					
standard	-0.15± 0.01	-0.44± 0.08	0.66± 0.01	3.4± 0.1	0.14± 0.01
kaon/lepton	-0.14± 0.01	-0.33± 0.07	0.71± 0.01	3.3± 0.1	0.18± 0.01
only 3 tracks	-0.22± 0.04	-0.7± 0.3	0.77± 0.04	3.5± 0.3	0.16± 0.03
resolution(ps)-NT1					
standard	-0.14± 0.05	1.3± 0.7	0.62± 0.05	3.8± 0.7	0.11± 0.05
only 3 tracks	-0.13± 0.05	1.0± 0.6	0.60± 0.05	4.1± 0.6	0.14± 0.05
resolution(ps)-NT2					
standard	-0.25± 0.06	-1.1± 0.9	0.81± 0.06	4.2± 1.0	0.08± 0.04
only 3 tracks	-0.25± 0.07	-0.7± 0.7	0.82± 0.07	4.1± 0.8	0.12± 0.05
pull-leptons					
standard	-0.14± 0.02	-0.98± 0.26	1.07± 0.02	3.0± 0.2	0.09± 0.01
kaon/lepton	-0.03± 0.02	-0.95± 0.29	1.05± 0.02	3.1± 0.2	0.07± 0.01
only 3 tracks	-0.09± 0.08	-	1.13± 0.06	0.0± 0.2	0.01± 0.02
pull-kaons					
standard	-0.27± 0.01	-0.85± 0.14	1.15± 0.02	2.6± 0.1	0.10± 0.01
kaon/lepton	-0.21± 0.01	-0.75± 0.12	1.07± 0.01	2.7± 0.1	0.11± 0.01
only 3 tracks	-0.34± 0.07	-0.6± 0.3	1.13± 0.07	2.7± 0.3	0.19± 0.06
pull-NT1					
standard	-0.20± 0.08	0.0± 0.9	1.03± 0.06	2.8± 0.8	0.08± 0.05
only 3 tracks	-0.16± 0.08	0.1± 0.4	1.00± 0.07	2.8± 0.7	0.08± 0.06
pull-NT2					
standard	-0.33± 0.10	-0.4± 0.4	0.96± 0.11	2.4± 0.3	0.23± 0.11
only 3 tracks	-0.29± 0.09	-0.3± 0.5	0.95± 0.09	2.8± 0.4	0.22± 0.08

Table 16: Results of a fit to two gaussians of the distribution of the resolutions and pulls for the three algorithm for vertex reconstruction, given the tagging output.

configuration	μ_1	$\mu_2 - \mu_1$	σ_1	$\frac{\sigma_2}{\sigma_1}$	f_{out}
resolution(ps)-leptons					
standard - right	-0.06± 0.01	-0.45± 0.11	0.51± 0.01	3.6± 0.2	0.14± 0.02
standard - wrong	-0.10± 0.04	-0.51± 0.26	0.52± 0.05	4.0± 0.4	0.28± 0.05
kaon/lepton - right	0.00± 0.01	-0.22± 0.09	0.53± 0.02	3.6± 0.1	0.21± 0.02
kaon/lepton - wrong	-0.08± 0.07	-0.80± 0.28	0.68± 0.10	3.3± 0.4	0.38± 0.08
resolution(ps)-kaons					
standard - right	-0.14± 0.01	-0.44± 0.08	0.65± 0.01	3.4± 0.1	0.14± 0.01
standard - wrong	-0.20± 0.02	-0.45± 0.17	0.69± 0.03	3.3± 0.2	0.17± 0.03
kaon/lepton - right	-0.13± 0.01	-0.30± 0.07	0.69± 0.01	3.3± 0.1	0.19± 0.01
kaon/lepton - wrong	-0.17± 0.03	-0.52± 0.20	0.76± 0.03	3.6± 0.2	0.16± 0.02
resolution(ps)-NT1					
standard - right	-0.11± 0.02	-0.41± 0.12	0.62± 0.02	3.2± 0.1	0.16± 0.02
standard - wrong	-0.16± 0.04	-0.51± 0.37	0.72± 0.04	3.4± 0.4	0.10± 0.03
resolution(ps)-NT2					
standard - right	-0.12± 0.02	-0.67± 0.14	0.68± 0.02	3.7± 0.2	0.16± 0.02
standard - wrong	-0.09± 0.03	-0.55± 0.15	0.69± 0.03	3.2± 0.2	0.22± 0.03
pull-leptons					
standard - right	-0.13± 0.02	-1.03± 0.26	1.06± 0.02	2.9± 0.2	0.07± 0.01
standard - wrong	-0.23± 0.09	-0.83± 0.64	1.18± 0.10	3.2± 0.5	0.19± 0.06
kaon/lepton - right	0.00± 0.02	-0.69± 0.28	1.03± 0.02	2.8± 0.2	0.06± 0.01
kaon/lepton - wrong	-0.34± 0.10	-1.49± 0.95	1.30± 0.09	3.5± 0.7	0.18± 0.05
pull-kaons					
standard - right	-0.25± 0.02	-0.85± 0.14	1.14± 0.02	2.6± 0.1	0.10± 0.01
standard - wrong	-0.34± 0.04	-0.88± 0.37	1.17± 0.04	2.6± 0.3	0.09± 0.03
kaon/lepton - right	-0.20± 0.01	-0.73± 0.14	1.07± 0.02	2.7± 0.1	0.10± 0.01
kaon/lepton - wrong	-0.23± 0.03	-0.79± 0.25	1.05± 0.04	2.7± 0.2	0.14± 0.03
pull-NT1					
standard - right	-0.19± 0.03	-0.76± 0.22	1.10± 0.03	2.3± 0.1	0.12± 0.03
standard - wrong	-0.19± 0.06	-0.63± 0.28	1.00± 0.07	2.4± 0.2	0.23± 0.07
pull-NT2					
standard - right	-0.18± 0.02	-1.01± 0.21	1.07± 0.02	2.8± 0.2	0.12± 0.02
standard - wrong	-0.14± 0.03	-0.95± 0.25	1.11± 0.04	2.5± 0.2	0.14± 0.03

Table 17: Results of a fit to two gaussians of the distribution of the pulls for the standard algorithm for vertex reconstruction and the one with special treatment of leptons and kaons, separately for the right and wrong tags.

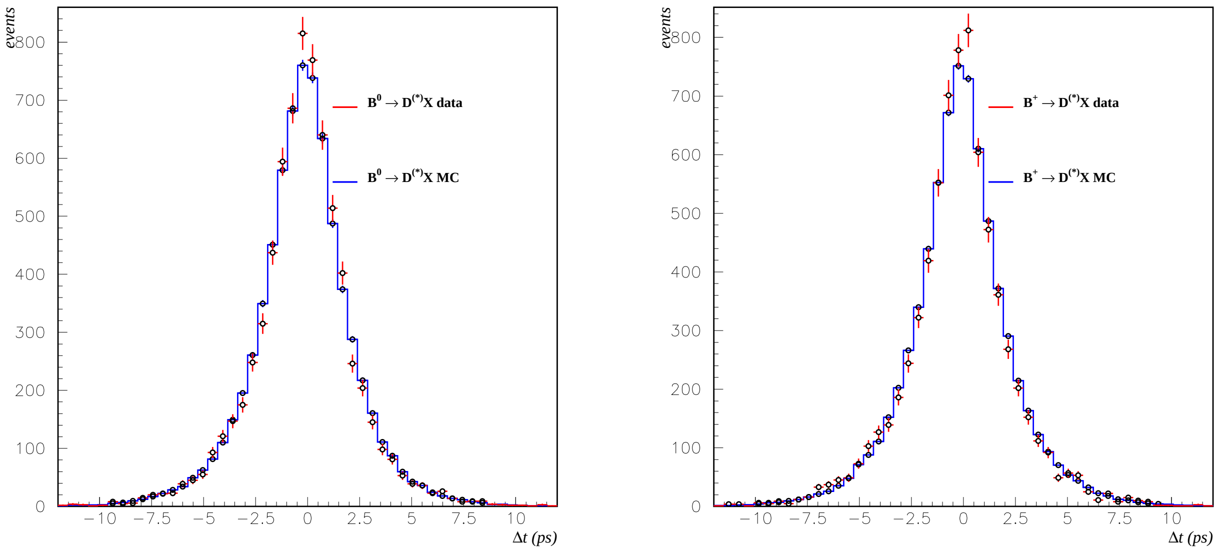

Figure 40: Data/Monte Carlo comparison the Δt distributions for signal (after background subtraction and before tagging) for B Breco events: (left) B^0 (right) B^+.

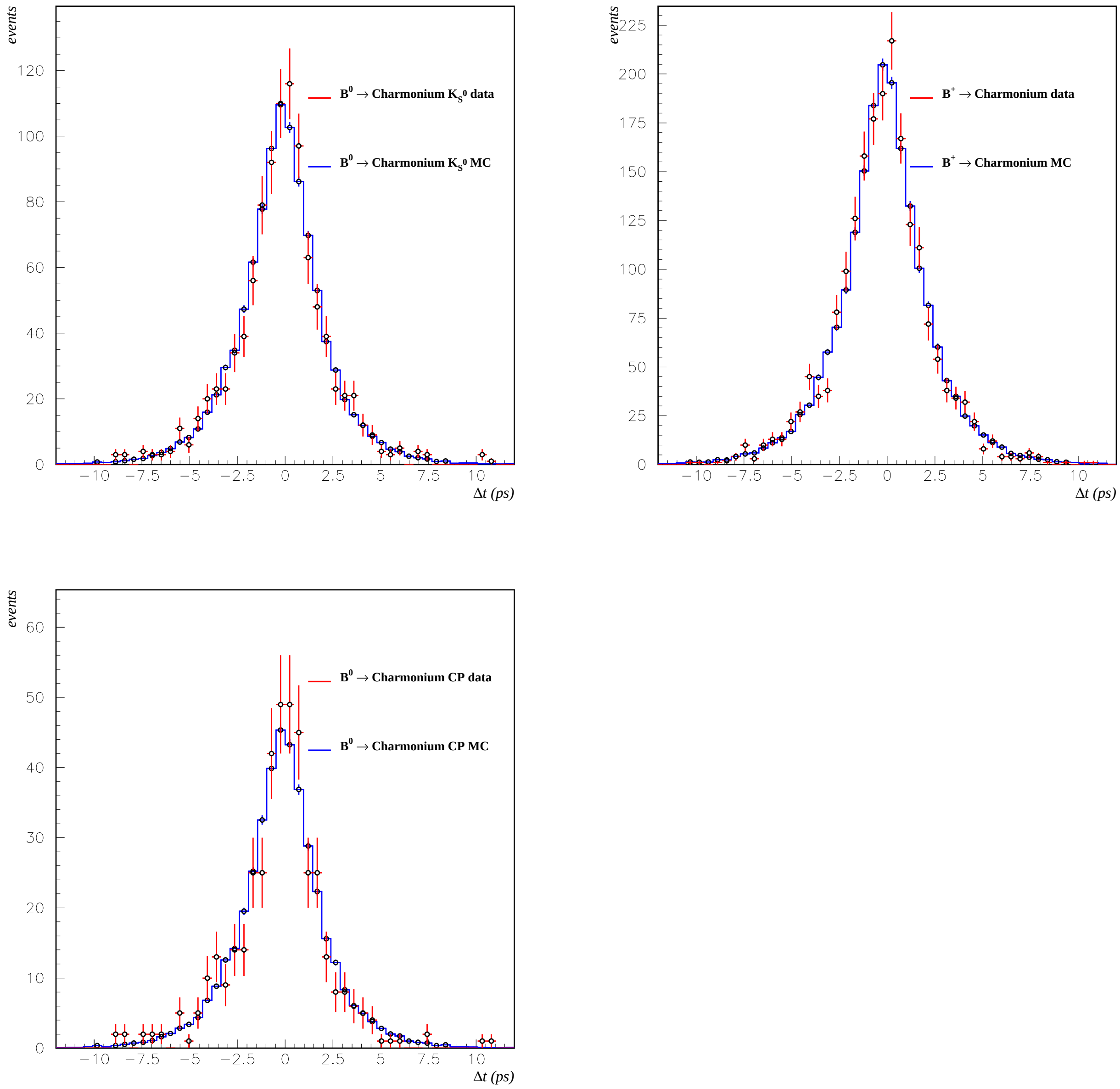

Figure 41: Data/Monte Carlo comparison the Δt distributions for signal (after background subtraction and before tagging) for B charmonium events: (top/left) B^0 (top/right) B^0 for only CP modes, (bottom/left) B^+.

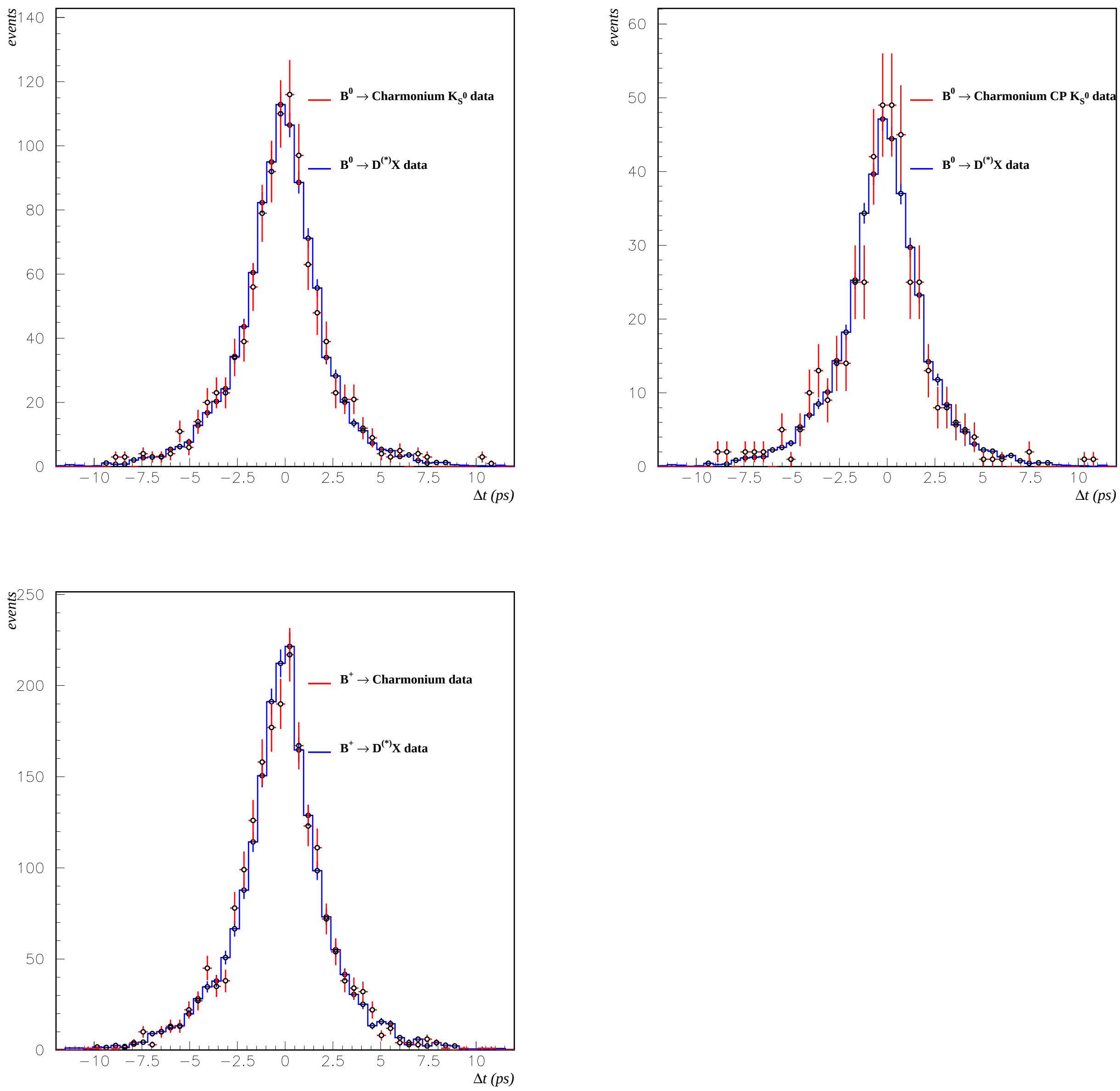

Figure 42: Breco/charmonium data (excluding K_L^0) comparison of the Δt distributions for signal (after background subtraction and before tagging): (top/left) B^0 (top/left) B^0 Breco and B^0 CP events, (bottom/left) B^+ events.

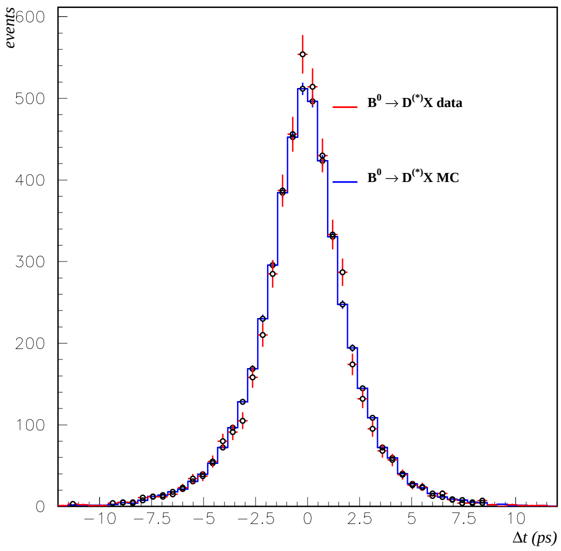

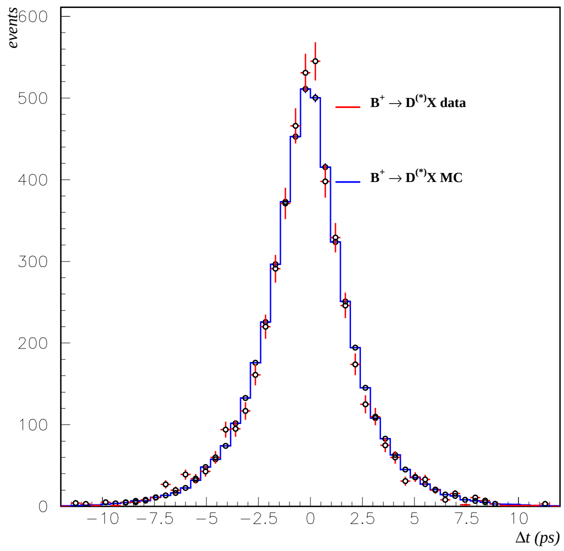

Figure 43: Data/Monte Carlo comparison the Δt distributions for signal (after background subtraction and after tagging) for B Breco events: (left) B^0 (right) B^+.

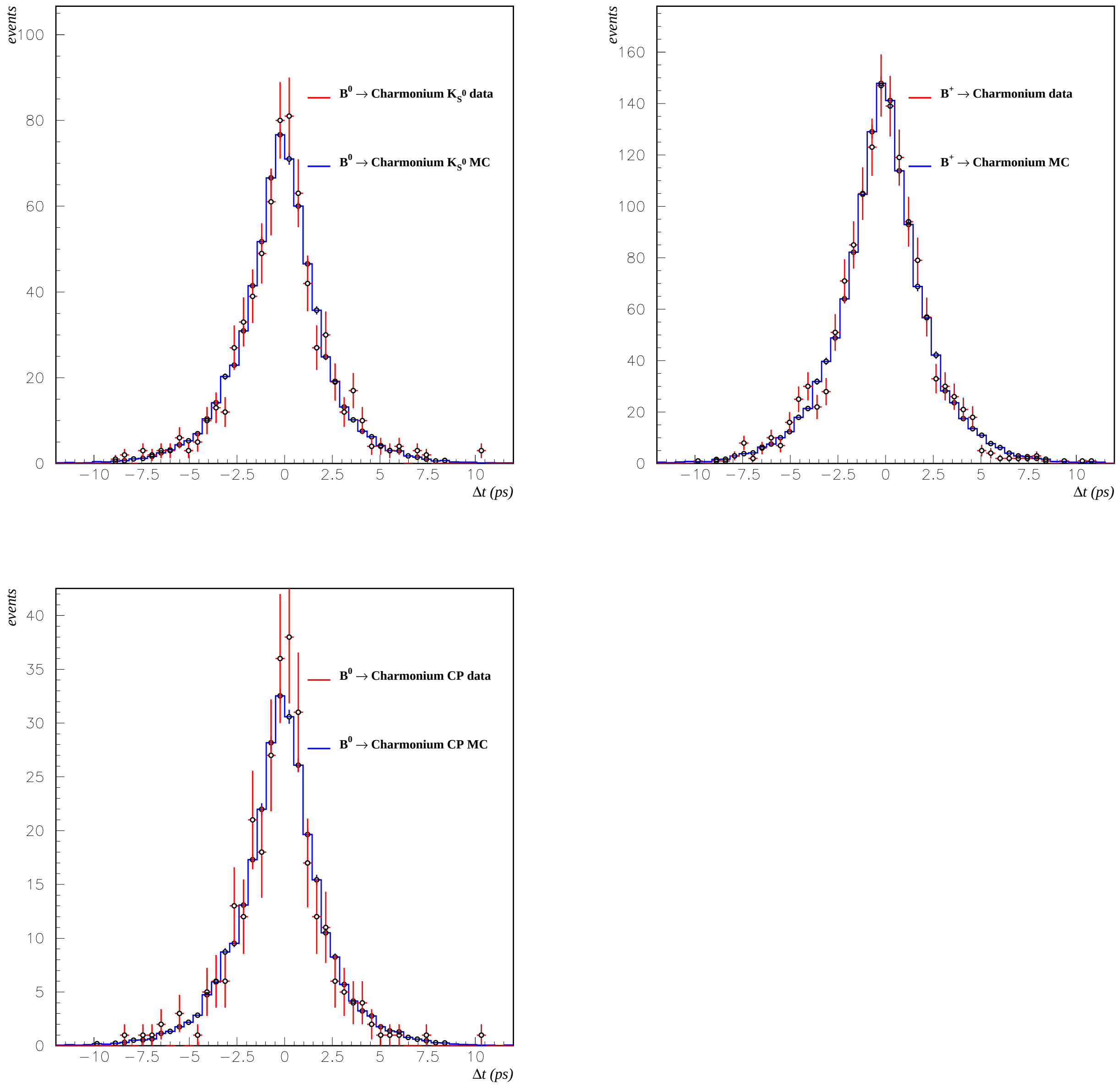

Figure 44: Data/Monte Carlo comparison the Δt distributions for signal (after background subtraction and after tagging) for B charmonium events: (top/left) B^0 (top/right) B^0 for only CP modes, (bottom/left) B^+.

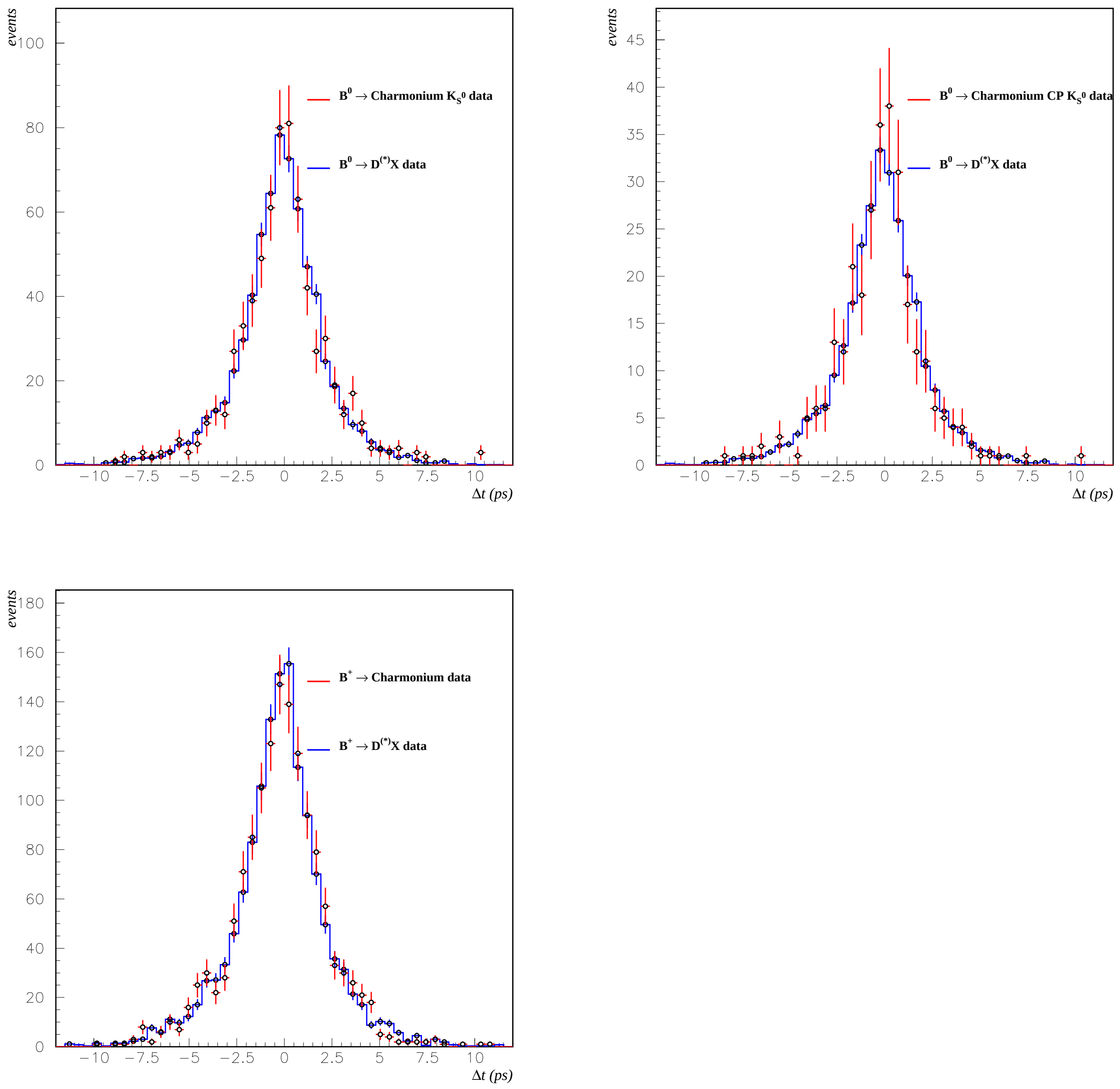

Figure 45: Breco/charmonium data (excluding K_L^0) comparison of the Δt distributions for signal (after background subtraction and after tagging): (top/left) B^0 (top/left) B^0 breco and B^0 CP events, (bottom/left) B^+ events.

3.10 Other checks

Several cross-checks can be done with the tracks accepted for fitting the vertex tag. Here we include two of them, but certainly several others could be done. The third check in the list below has been applied to the reco side in charmonium (K_S^0) events.

3.10.1 SVT content

Figures 46, 47, 48 and 49 show a data/Monte Carlo comparison for B^0 Breco, B^+ Breco, B^0 charmonium and B^+ charmonium species, respectively, of the available SVT information in tracks used to fit the vertex tag. Top/left (top/right) distributions give the number of SVT z ($R\phi$) layers per track for tagging vertex tracks. Bottom/left (bottom/right) distributions show the number of tag vertex tracks with at least 2 z SVT layers before (after) quality cuts. We can see that before quality cuts there is already an extremelly small number of with no z SVT tracks. In the charmonium sample these residual events are completely eliminated by the cuts, and in the Breco sample, only 0.06% of the B^0 candidates survived them. Table 18 gives the fraction of events in data and Monte Carlo for the different B species with none or only 1 track in vertex tag with z SVT information (at least 2 z layers).

	Monte Carlo		Data	
	$f_0(\%)$	$f_1(\%)$	$f_0(\%)$	$f_1(\%)$
B^0 Breco	0.06 ± 0.03	6.7 ± 0.3	0.13 ± 0.05	7.9 ± 0.3
B^+ Breco	0.06 ± 0.03	6.4 ± 0.3	0.13 ± 0.04	8.4 ± 0.4
B^0 Charmonium	0.00 ± 0.00	7.0 ± 0.8	0.00 ± 0.00	9.1 ± 0.9
B^0 Charmonium CP	0.00 ± 0.00	7.2 ± 1.3	0.00 ± 0.00	9.0 ± 1.4
B^+ Charmonium	0.00 ± 0.00	5.7 ± 0.5	0.05 ± 0.05	8.5 ± 0.6

Table 18: Fraction of events in data and Monte Carlo for the different B species with none or only 1 track in vertex tag with z SVT information (at least two z layers), after quality cuts.

3.10.2 Tagging content

Figure 50 compares the fraction of tagging leptons used in the vertex tag as a function of the lepton momentum in the center-of-mass frame for data and Monte Carlo and for the different B species, after background subtraction. Table 19 gives the average efficiencies: for all data samples, 96% of the tagging leptons are used in the vertex. In the case of the charmonium B^+ events the average is about two sigma below with respect to what we observe in the Breco events, as well as the B^0 charmonium. The effect is dominated by tagging leptons with a momentum in center-of-mass of about 1.4 GeV/c. This effect has been investigatived and no problems have been found, concluding that it is just an statistical fluctuation.

Figure 51 compares the fraction of tagging kaons used in the vertex tag as a function of the kaon momentum in the center-of-mass frame for data and Monte Carlo and for the different B species. Table 28 gives the average efficiencies: in Monte Carlo, on average 84%

	Monte Carlo	Data
B^0 Breco	0.961 ± 0.002	0.953 ± 0.008
B^+ Breco	0.967 ± 0.002	0.955 ± 0.007
B^0 Charmonium	0.957 ± 0.003	0.982 ± 0.013
B^0 Charmonium CP	0.956 ± 0.003	0.981 ± 0.022
B^+ Charmonium	0.965 ± 0.003	0.902 ± 0.020

Table 19: Average fraction of tagging leptons used in the vertex tag for the different data and Monte Carlo sets.

of the kaons are used in the vertex, and in data the average fraction is slightly smaller, about 81%.

	Monte Carlo	Data
B^0 Breco	0.839 ± 0.002	0.812 ± 0.008
B^+ Breco	0.855 ± 0.002	0.816 ± 0.007
B^0 Charmonium	0.833 ± 0.003	0.768 ± 0.021
B^0 Charmonium CP	0.834 ± 0.004	0.762 ± 0.031
B^+ Charmonium	0.857 ± 0.003	0.809 ± 0.013

Table 20: Average fraction of tagging kaons used in the vertex tag for the different data and Monte Carlo sets.

3.10.3 Use of the K_S^0 in the reconstruction of the CP vertex

The B vertex in CP events makes use of the charmonium vertex as well as the vertex and the direction of flight of the K_S^0 candidate. The impact on the resolution function of using the K_S^0 candidate information is expected to be very small. Using Monte Carlo events we have evaluated the change in Δz resolution by using the vertex of the charmonium candidate instead of the one of the B. Figure 52 shows the change in the Δt pulls. Although the parameters change slightly, the RMS of the core and tail Gaussians is the same within 1%.

More checks should be done...

Document here the studies performed on the impact on the B momentum direction. Data/MC comparison of the angle between the line-of-flight of the K_S^0 and the line joining the charmonium and K_S^0 vertices...

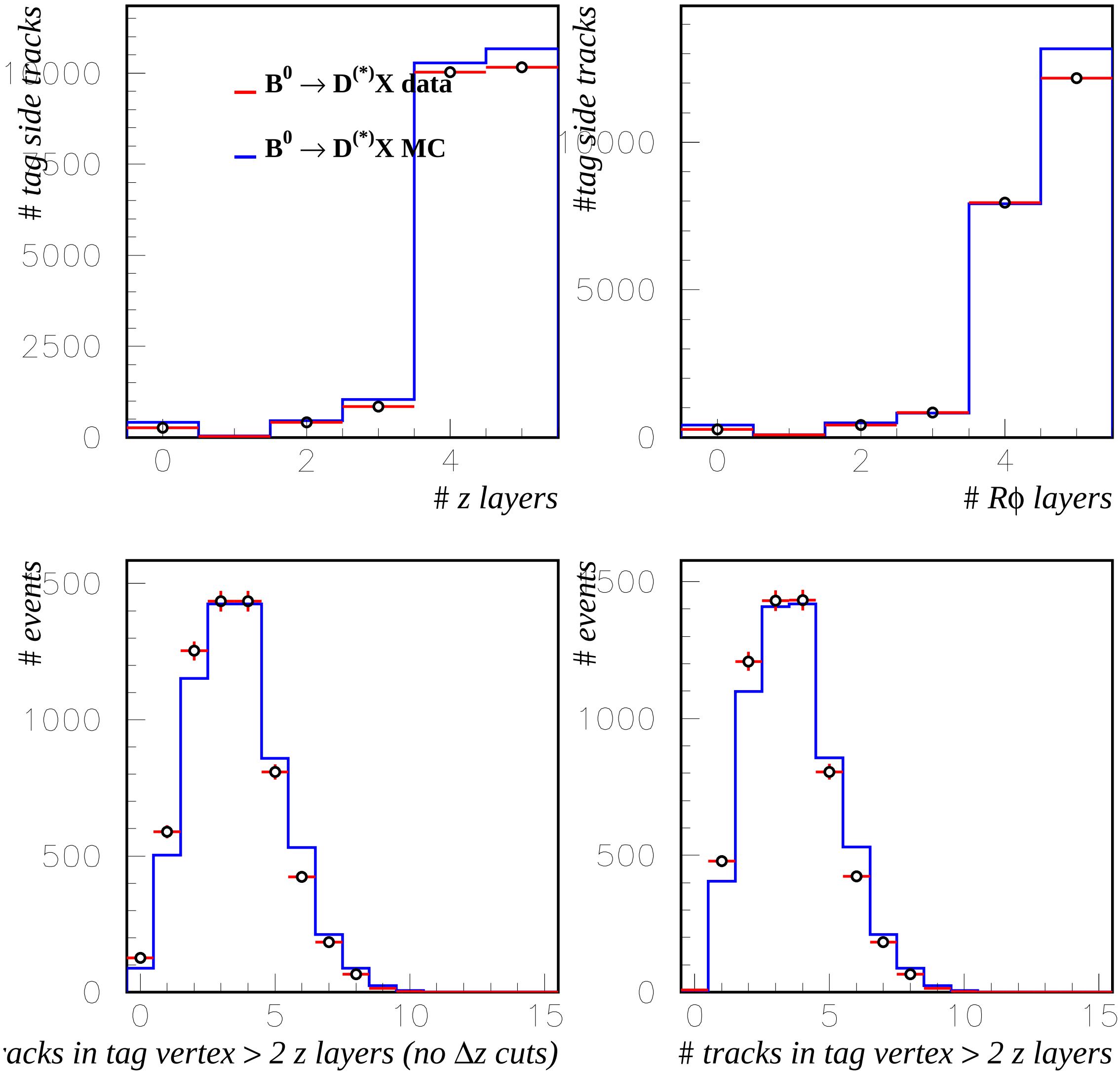

Figure 46: Data/Monte Carlo comparison of SVT information in vertex tag for B^0 Breco events: (top/left) number of SVT z layers per track for tagging vertex tracks; (top/right) same but SVT $R\phi$ layers; (bottom/left) number of tracks used in vertex tag with at least 2 SVT z layers before vertex quality cuts; (bottom/right) number of tracks used in vertex tag with at least 2 SVT z layers after vertex quality cuts. Distributions are normalized to the number of events after quality cuts.

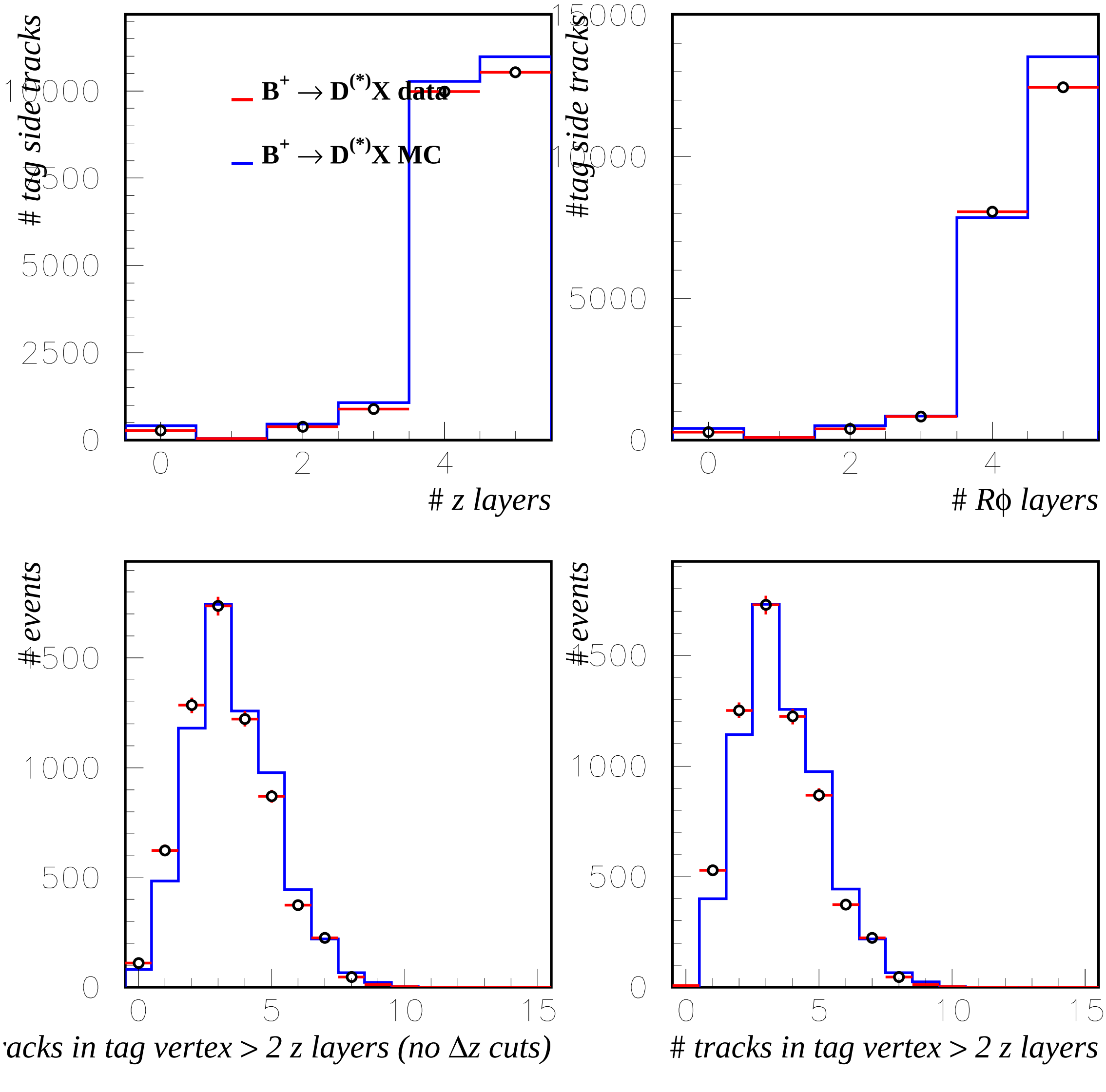

Figure 47: Data/Monte Carlo comparison of SVT information in vertex tag for B^+ Breco events: (top/left) number of SVT z layers per track for tagging vertex tracks; (top/right) same but SVT $R\phi$ layers; (bottom/left) number of tracks used in vertex tag with at least 2 SVT z layers before vertex quality cuts; (bottom/right) number of tracks used in vertex tag with at least 2 SVT z layers after vertex quality cuts. Distributions are normalized to the number of events after quality cuts.

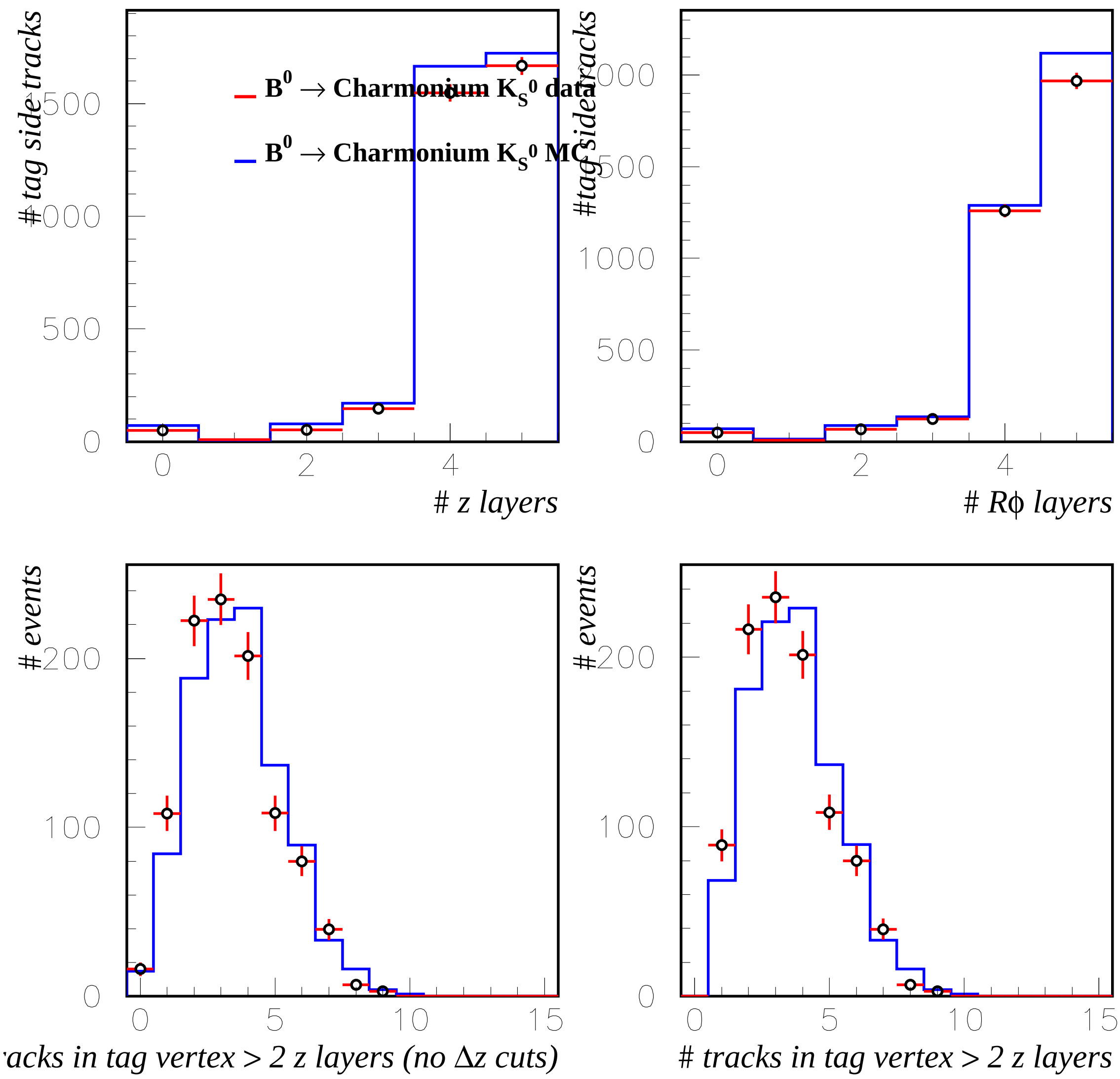

Figure 48: Data/Monte Carlo comparison of SVT information in vertex tag for B^0 charmonium events: (top/left) number of SVT z layers per track for tagging vertex tracks; (top/right) same but SVT $R\phi$ layers; (bottom/left) number of tracks used in vertex tag with at least 2 SVT z layers before vertex quality cuts; (bottom/right) number of tracks used in vertex tag with at least 2 SVT z layers after vertex quality cuts. Distributions are normalized to the number of events after quality cuts.

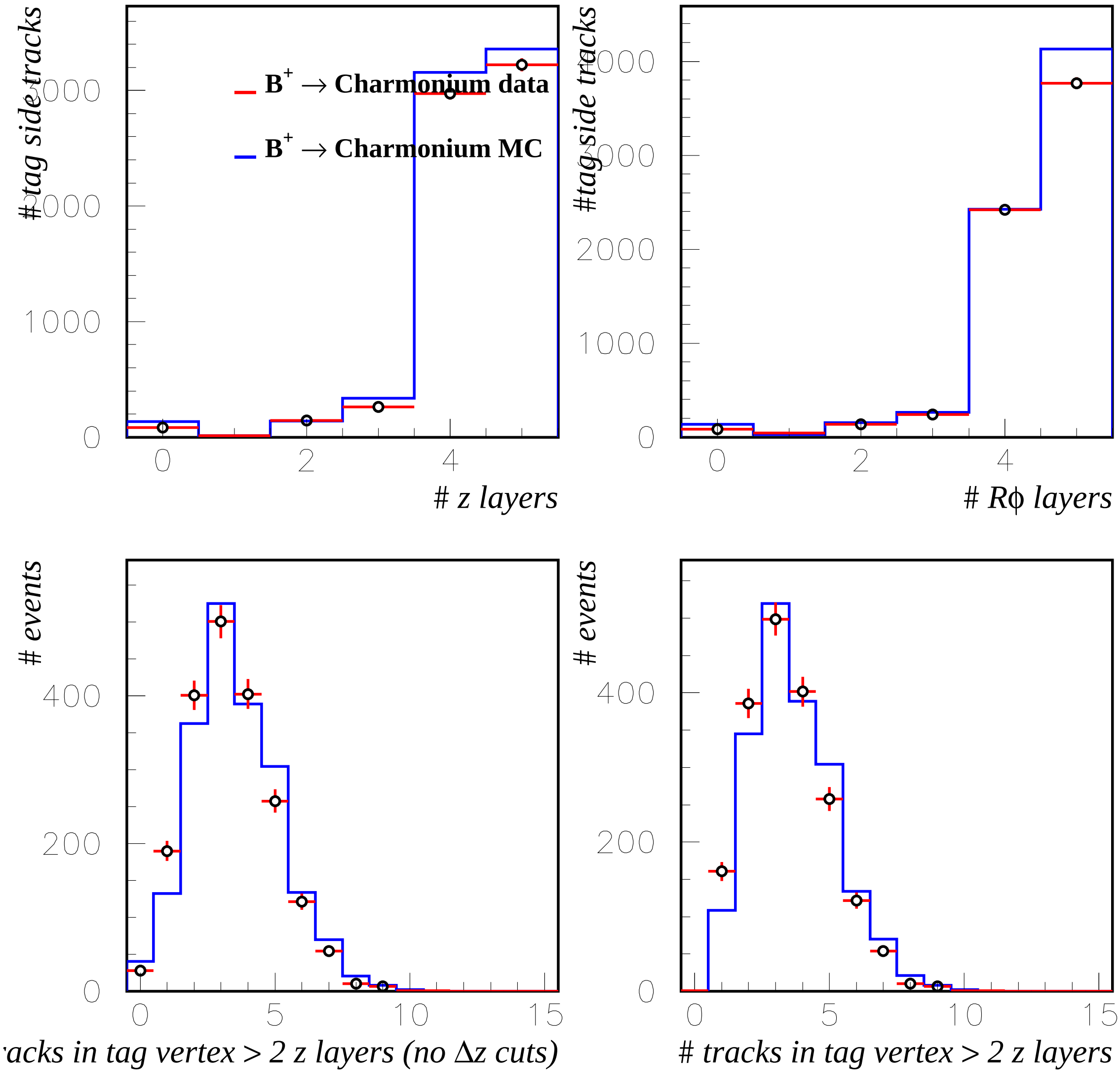

Figure 49: Data/Monte Carlo comparison of SVT information in vertex tag for B^+ charmonium events: (top/left) number of SVT z layers per track for tagging vertex tracks; (top/right) same but SVT $R\phi$ layers; (bottom/left) number of tracks used in vertex tag with at least 2 SVT z layers before vertex quality cuts; (bottom/right) number of tracks used in vertex tag with at least 2 SVT z layers after vertex quality cuts. Distributions are normalized to the number of events after quality cuts.

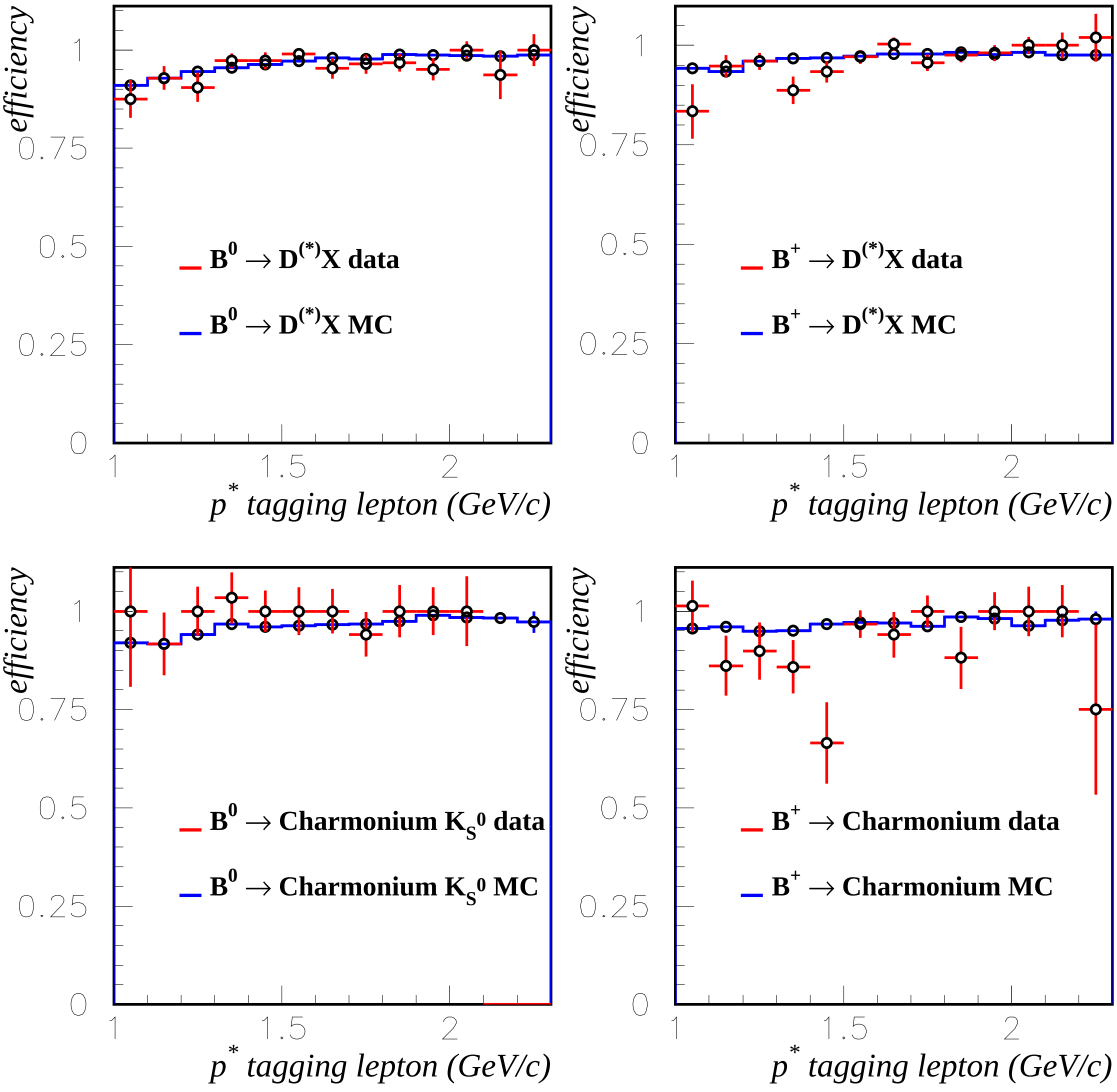

Figure 50: Fraction of tagging leptons used in the vertex tag as a function of the lepton momentum in the center-of-mass frame for data and Monte Carlo and for the different B species.

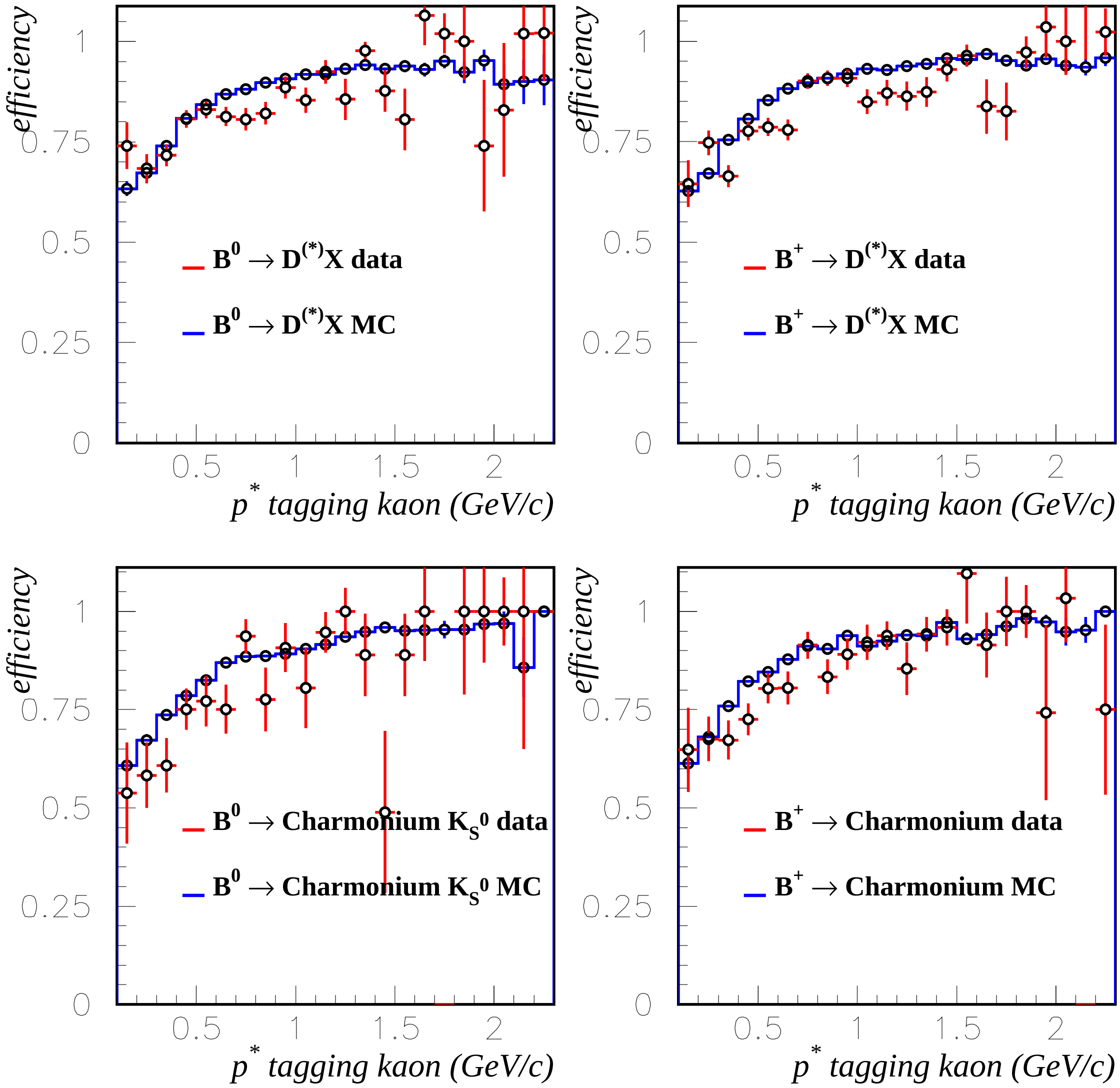

Figure 51: Fraction of tagging kaons used in the vertex tag as a function of the kaon momentum in the center-of-mass frame for data and Monte Carlo and for the different B species.

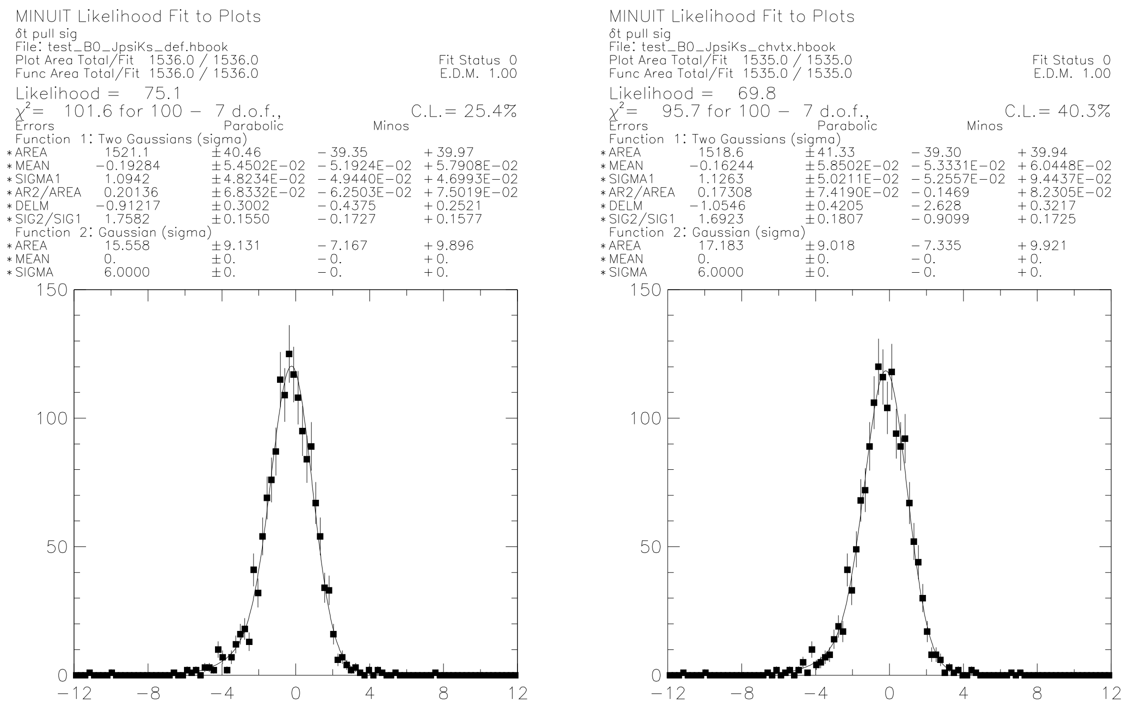

Figure 52: Distribution of Δt pulls when including (left) or excluding (right) the K_s^0 from the charmonium vertex .

4 Δz vertexing without beam constraints

In this section we redo most of the checks presented in section 3 but now removing all the beam constraints (both "pseudo-track" and beam spot) in the reconstruction of the B tagging vertex, i.e. the simplest of all possible configurations. Apart of removing those constraints, the `VtxTagBtaSelFit` configuration remains the same, as well as the quality cuts applied and described in previous section.

4.1 Differences among modes

A comparison of the χ^2 probability, event-by-event error and number of candidates in vertex tag for several charmonium modes ($\mathrm{B_0}\rightarrow\mathrm{J\Psi K_S}(\pi^+\pi^-)$, $\mathrm{B_0}\rightarrow\mathrm{J\Psi K_S}(\pi^0\pi^0)$ and $\mathrm{B_0}\rightarrow\Psi\mathrm{(2S)K_S}$) to the B^0 breco cocktail in Monte Carlo is shown in figure 53. No significant differences with respect to the Breco events are observed, as expected from the fact that the Δz is dominated by the tagging side, largely independent of the fully reconstructed mode. The agreement among the different charmonium events is also satisfactory.

The Δz resolution and pull parameters for different B decays to charmonium are given in Table 21. These parameters are given for B decays to hadronic D modes in Table 22.

Comparisons are made between the data and Monte Carlo for the Breco and chamonium samples, and for charged and neutral B mesons. Figures 54 and 55 compare the χ^2 probability for B^0 and B^+ breco and charmonium events, respectively. Figures 56 and 57 show a similar comparison but now for the event-by-event Δz error. Finally, figures 59 and 59 compare the number of candidates (tracks+V^0's) used to make the vertex tag. As in the case of the configuration with beam constraints, the agreement in the event-by-event errors and number of tracks is quite satisfactory. The agreement now for the χ^2 distributions is slightly better (the algorithm now is much less constrained) but still some discrepancies in the slop of the distrution is seen, more likely due to misalignment effects (see section 6).

Figures 60, 61 and 62 show the comparison of the χ^2 probability, Δz event-by-event error and the number of candidates (tracks+V^0's) used to make the vertex tag, respectively, for B^0 and B^+ Breco and charmonium data. B^0 Breco and CP events are compared separately. As in the default configuration, the agreement is very satisfactory, and charmonium events have an slightly better event-by-event error estimate.

Table 23 summarizes the Δz reconstruction efficiciencies (after quality cuts) for charmonium and Breco modes and data and Monte Carlo. Table 24 shows the number of charmonium and breco events by mode with a probability of χ^2 less than 1% for data and Monte Carlo with the final configuration ($n = 0$). It should be stressed that the χ^2 cut is not applied for the final selection.

4.2 Information from XY vertices

The distance between the tag vertex and the beam spot can be used to identify problems with the tag vertex reconstruction.

As now no beam constraints are applied, the resolution in y will be dominated by the y vertex tag resolution, with some contribution from the B lifetime. Therefore, the y distance resolution in this case will be very similar to that of the z component. Figures 63 and 64

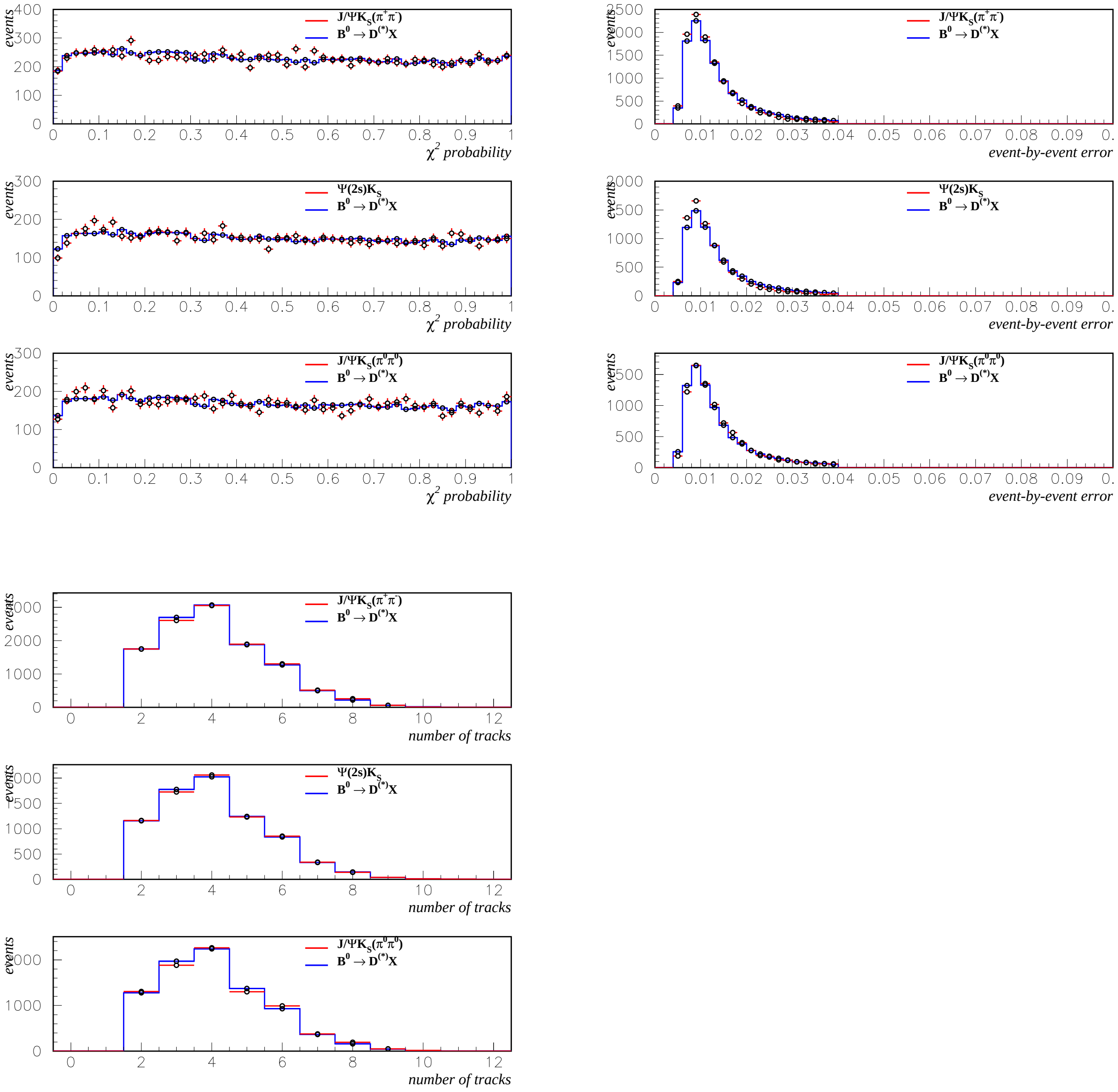

Figure 53: No beam configuration. Comparison among the distributions of χ^2 probability (top/left), event-by-event error (top/right) and number of candidates (bottom/left) in vertex tag for several charmonium modes ($B_0 \to J\Psi K_S(\pi^+\pi^-)$, $B_0 \to J\Psi K_S(\pi^0\pi^0)$ and $B_0 \to \Psi(2S)K_S$) to the B^0 Breco cocktail in Monte Carlo.

Δz reso	f_1	σ_1	μ_1	f_{out}	$\frac{\sigma_2}{\sigma_1}$	$\mu_2 - \mu_1$	RMS	RMS(3g)	μ
JpsiKs	65.1	101. ± 3. μm	-22.± 2. μm	4.15	2.58± 0.07	-46.± 7. μm	169.± 4. μm	232.± 5. μm	-36. μm
Psi2sKs	48.3	84. ± 4. μm	-16.± 2. μm	4.68	2.38± 0.08	-33.± 6. μm	152.± 6. μm	228.± 6. μm	-30. μm
JpsiKs2pi0	62.9	106. ± 4. μm	-20.± 2. μm	5.57	2.37± 0.08	-51.± 9. μm	170.± 5. μm	251.± 6. μm	-35. μm
JpsiKstar0Kp	57.1	91. ± 3. μm	-19.± 2. μm	4.38	2.44± 0.06	-36.± 6. μm	157.± 4. μm	227.± 5. μm	-32. μm
JpsiKstar0Ks	88.3	129. ± 2. μm	-26.± 2. μm	NA	4.13± 0.17	-119.± 27. μm	219.± 6. μm	NA	-40. μm
JpsiKstarpKp	58.9	90. ± 3. μm	-17.± 2. μm	3.58	2.41± 0.07	-32.± 6. μm	153.± 4. μm	213.± 6. μm	-29. μm
JpsiKstarpKs	59.5	91. ± 4. μm	-16.± 2. μm	4.01	2.33± 0.07	-31.± 7. μm	149.± 4. μm	217.± 6. μm	-27. μm
JpsiK	62.7	89. ± 2. μm	-18.± 1. μm	3.38	2.50± 0.05	-34.± 4. μm	150.± 2. μm	208.± 4. μm	-29. μm
Psi2sKp	68.5	93. ± 3. μm	-17.± 2. μm	3.34	2.53± 0.10	-41.± 9. μm	150.± 4. μm	208.± 7. μm	-28. μm
Δz pull	f_1	σ_1	μ_1	f_{out}	$\frac{\sigma_2}{\sigma_1}$	$\mu_2 - \mu_1$	RMS	RMS(3g)	μ
JpsiKs	78.7	1.04 ± 0.02	-0.21± 0.02	2.16	2.05± 0.12	-0.60± 0.08 μm	1.33± 0.04	1.70± 0.08	-0.32
Psi2sKs	80.4	1.05 ± 0.03	-0.18± 0.02	1.99	1.99± 0.15	-0.71± 0.14 μm	1.30± 0.04	1.61± 0.09	-0.30
JpsiKs2pi0	82.0	1.07 ± 0.02	-0.21± 0.02	2.08	2.07± 0.16	-0.67± 0.13 μm	1.33± 0.04	1.77± 0.09	-0.31
JpsiKstar0Kp	77.2	1.06 ± 0.02	-0.18± 0.02	2.56	1.93± 0.08	-0.75± 0.12 μm	1.32± 0.03	1.83± 0.06	-0.32
JpsiKstar0Ks	88.3	1.09 ± 0.02	-0.21± 0.02	0.93	2.40± 0.21	-1.06± 0.22 μm	1.34± 0.04	1.54± 0.09	-0.32
JpsiKstarpKp	89.6	1.10 ± 0.02	-0.21± 0.02	1.42	2.37± 0.22	-0.75± 0.19 μm	1.31± 0.04	1.62± 0.07	-0.28
JpsiKstarpKs	83.3	1.07 ± 0.02	-0.16± 0.02	2.17	2.03± 0.12	-0.80± 0.16 μm	1.29± 0.03	1.74± 0.07	-0.28
JpsiK	53.8	0.92 ± 0.04	-0.13± 0.02	3.51	1.61± 0.04	-0.30± 0.04 μm	1.19± 0.03	1.47± 0.04	-0.26
Psi2sKp	61.0	0.94 ± 0.06	-0.12± 0.04	3.28	1.61± 0.08	-0.38± 0.10 μm	1.18± 0.05	1.47± 0.06	-0.26

Table 21: No beam configuration. Δz resolution function parameters for charmonium modes.

Δz reso	f_1	σ_1	μ_1	f_{out}	$\frac{\sigma_2}{\sigma_1}$	$\mu_2 - \mu_1$	RMS	RMS(3g)	μ
BchDstar									
BchD0									
B0Dstar	61.8	102. ± 6. μm	-22.± 4. μm	4.42	2.45± 0.13	-44.± 15. μm	169.± 8. μm	236.± 10. μm	-36. μm
B0Dch	61.7	99. ± 5. μm	-21.± 3. μm	4.56	2.55± 0.12	-56.± 13. μm	171.± 7. μm	239.± 10. μm	-39. μm
Δz pull	f_1	σ_1	μ_1	f_{out}	$\frac{\sigma_2}{\sigma_1}$	$\mu_2 - \mu_1$	RMS	RMS(3g)	μ
BchDstar									
BchD0									
B0Dstar	84.9	1.08 ± 0.04	-0.22± 0.04	1.62	2.11± 0.27	-0.83± 0.24	1.31± 0.06	1.65± 0.13	-0.33
B0Dch	88.6	1.08 ± 0.03	-0.26± 0.02	0.87	2.49± 0.23	-0.76± 0.23	1.35± 0.05	1.54± 0.09	-0.34

Table 22: No beam configuration. Δz resolution function parameters for Breco modes.

	no beam constraints applied (PRL configuration)	
	Monte Carlo	Data
B^0 Breco	0.840 ± 0.001	0.834 ± 0.004
B^+ Breco	0.875 ± 0.001	0.857 ± 0.004
B^0 Charmonium	0.864 ± 0.002	0.869 ± 0.011
B^0 Charmonium CP	0.864 ± 0.002	0.881 ± 0.010
B^+ Charmonium	0.893 ± 0.002	0.854 ± 0.017

Table 23: No beam configuration. Δz reconstruction efficiciencies (after quality cuts) for charmonium and Breco modes, data and Monte Carlo.

show the data/Monte Carlo comparison of these distances and their pulls for Breco and charmonium, respectively. Breco and charmonium data are directly compared in figure 65. Global bias and RMS from two-Gaussian fits are provided in table 25. Again, no biases are observed and the agreement in resolution between data and Monte Carlo is fair.

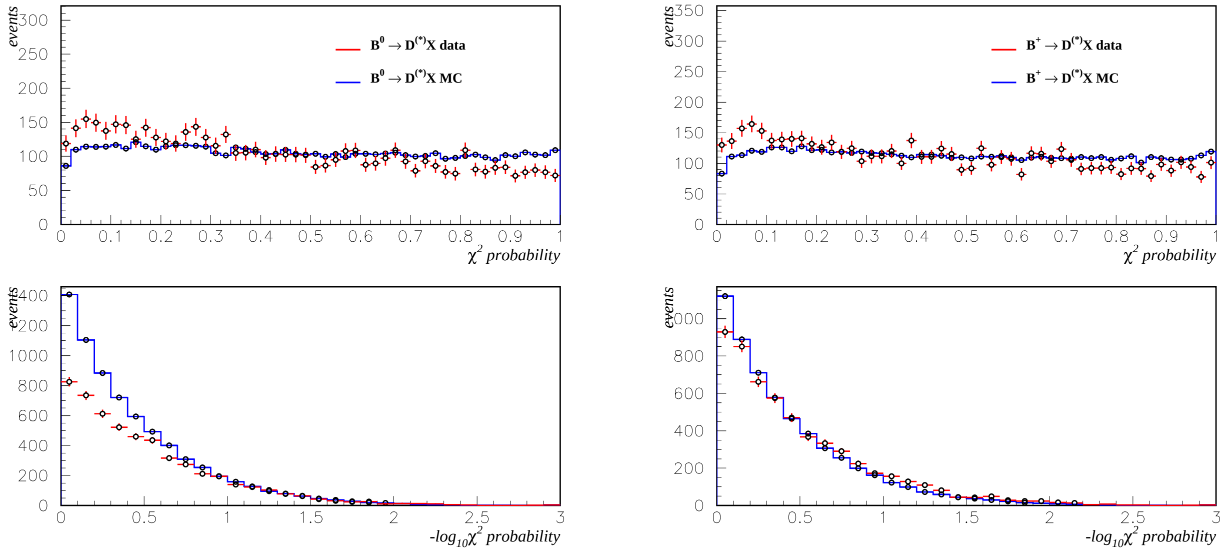

Figure 54: No beam configuration. Data/Monte Carlo comparison of the χ^2 vertex tag probability for B Breco events in linear (top) and and logarithm (bottom) scale: (left) B^0 events; (right) B^+ events.

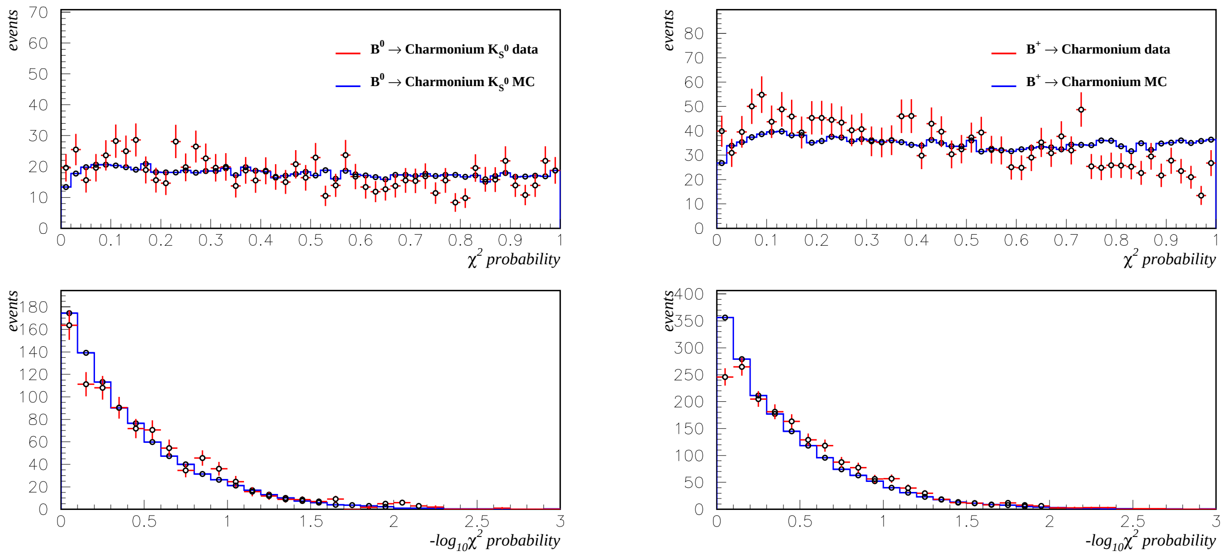

Figure 55: No beam configuration. Data/Monte Carlo comparison if the χ^2 vertex tag probability for B charmonium events in linear (top) and logarithm (bottom) scale: (left) B^0 events; (right) B^+ events.

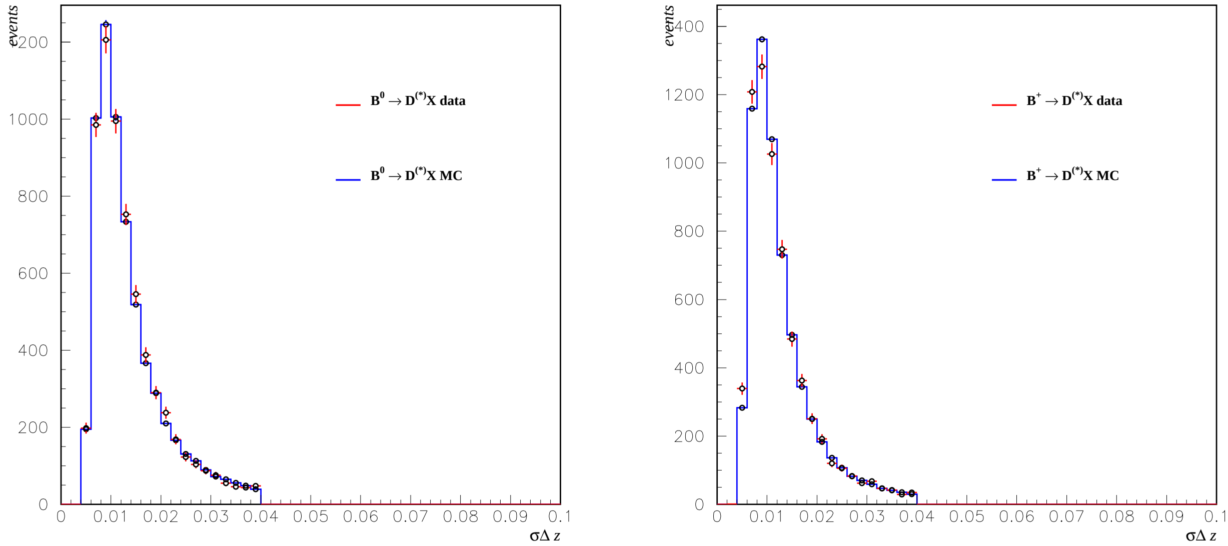

Figure 56: No beam configuration. Data/Monte Carlo comparison of the event-by-event Δz error for B Breco events: (left) B^0 events; (right) B^+ events.

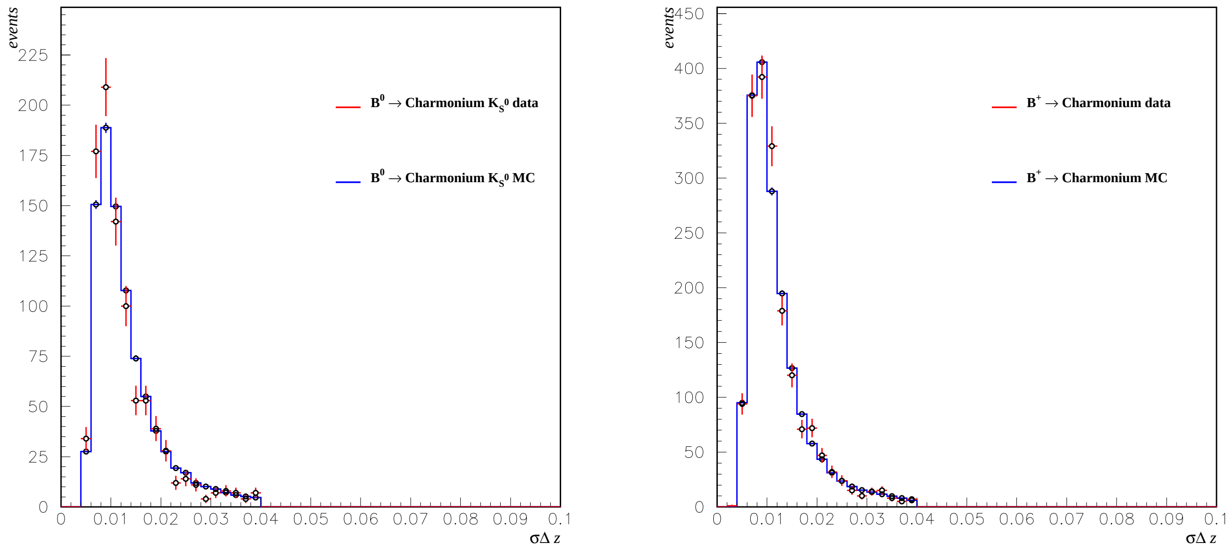

Figure 57: No beam configuration. Data/Monte Carlo comparison of the event-by-event Δz error for B charmonium events: (left) B^0 events; (right) B^+ events.

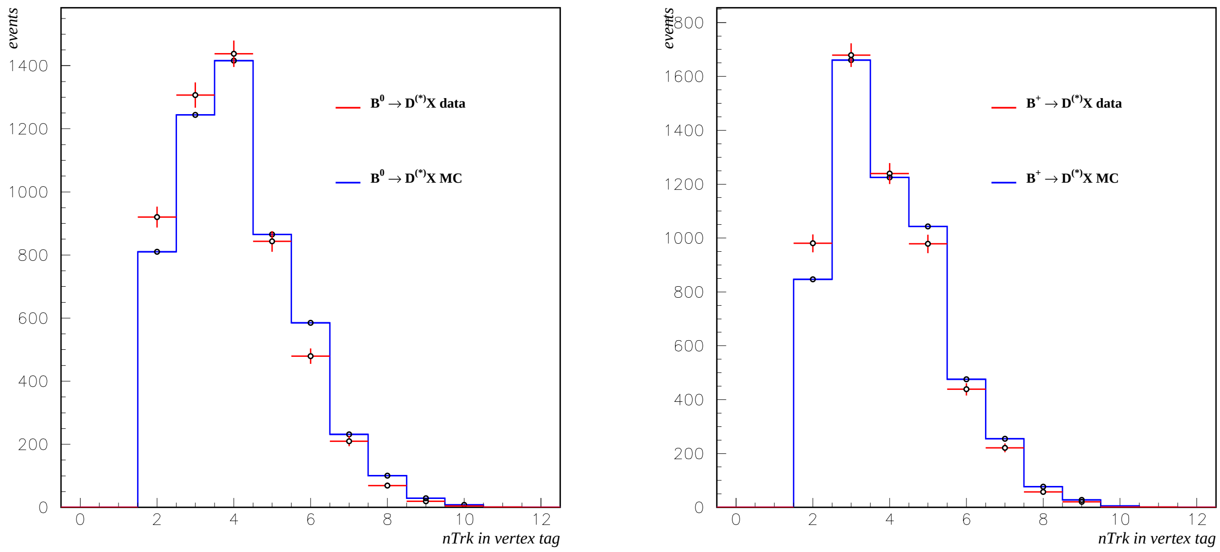

Figure 58: No beam configuration. Data/Monte Carlo comparison of the number of candidates (tracks+V^0's) used to make the vertex tag for B Breco events: (left) B^0 events; (right) B^+ events.

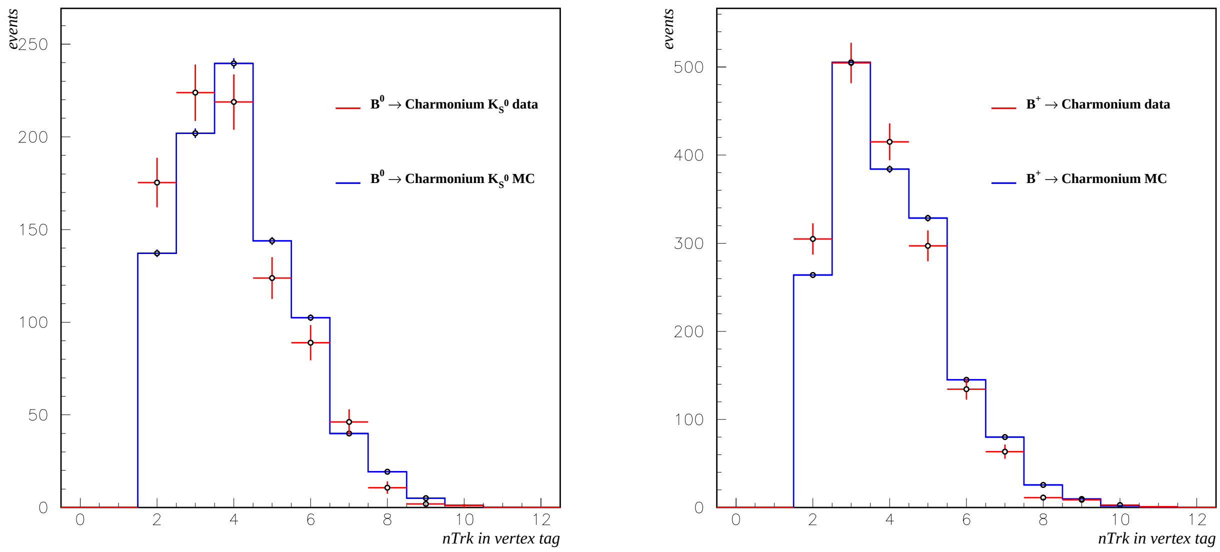

Figure 59: No beam configuration. Data/Monte Carlo comparison of the number of candidates (tracks+V^0's) used to make the vertex tag for B charmonium events: (left) B^0 events; (right) B^+ events.

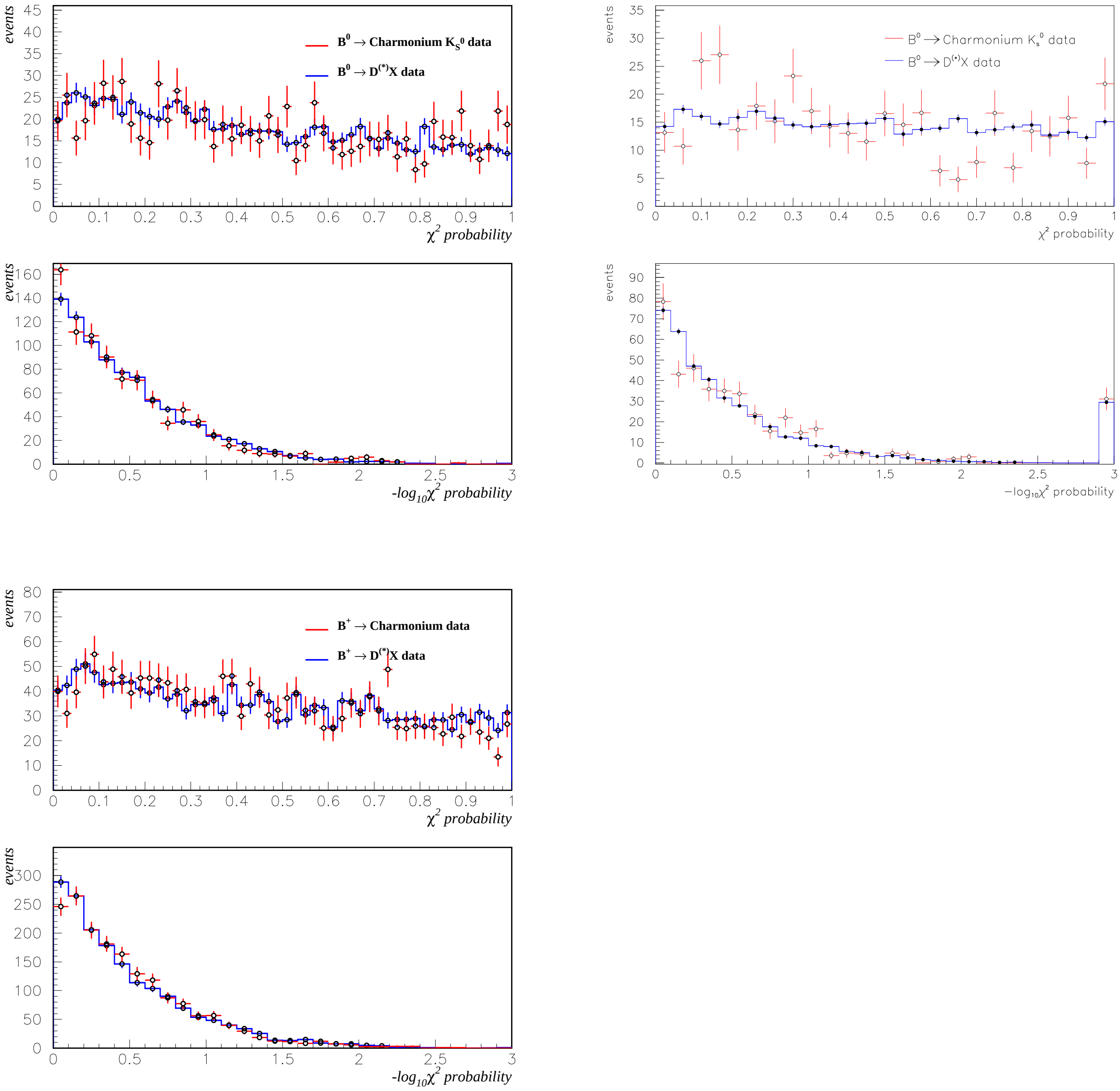

Figure 60: No beam configuration. Breco/charmonium (excluding K_L^0 modes) data comparison of the χ^2 vertex tag in linear and logarithm scale: (top/left) B^0 events; (top/right) B^0 Breco and only B^0 charmonium CP events; (bottom/left) B^+ events.

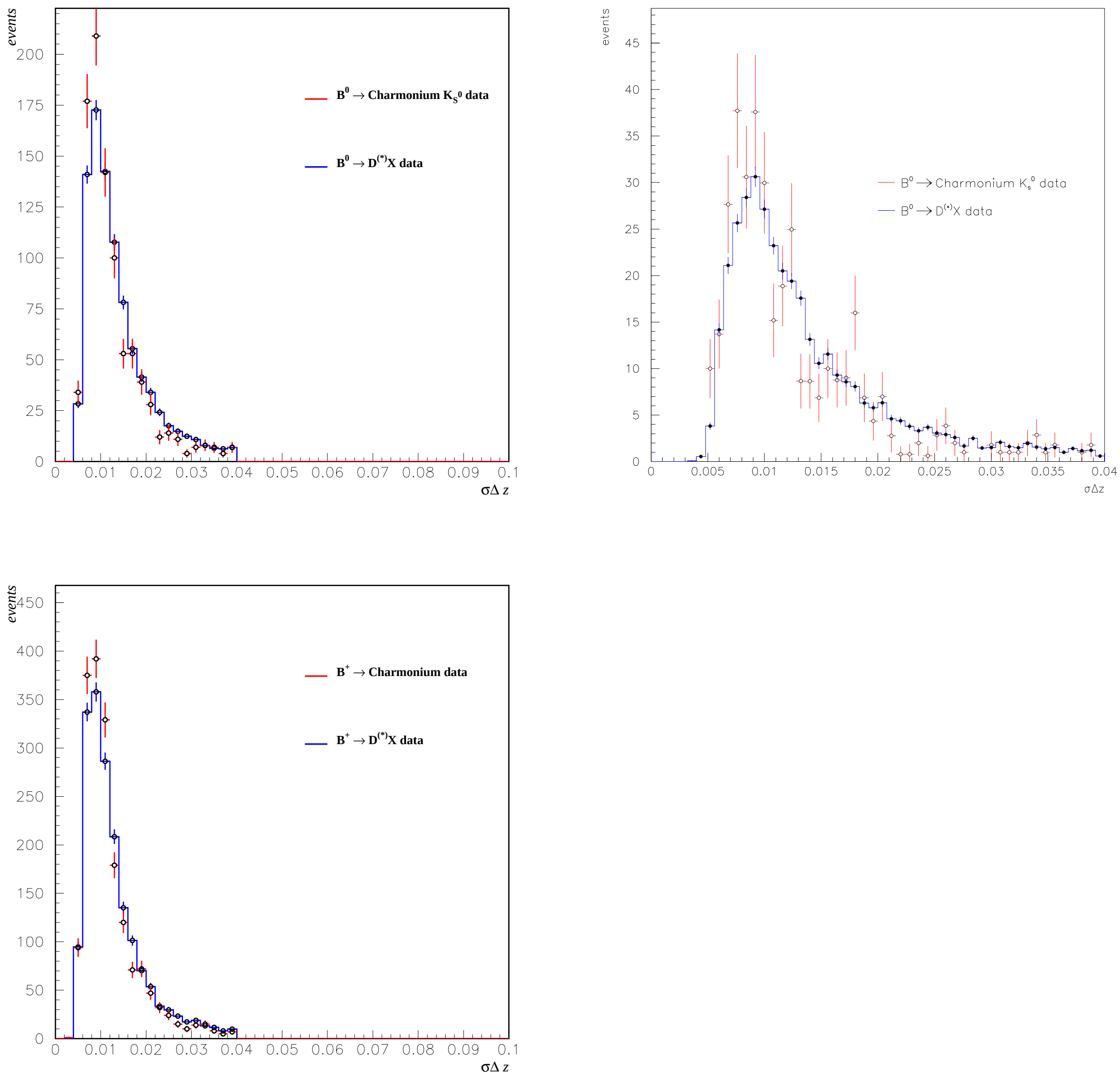

Figure 61: No beam configuration. Breco/charmonium (excluding K_L^0 modes) data comparison of the event-by-event Δz error: (top/left) B^0 events; (top/right) B^0 Breco and only B^0 charmonium CP events; (bottom/left) B^+ events.

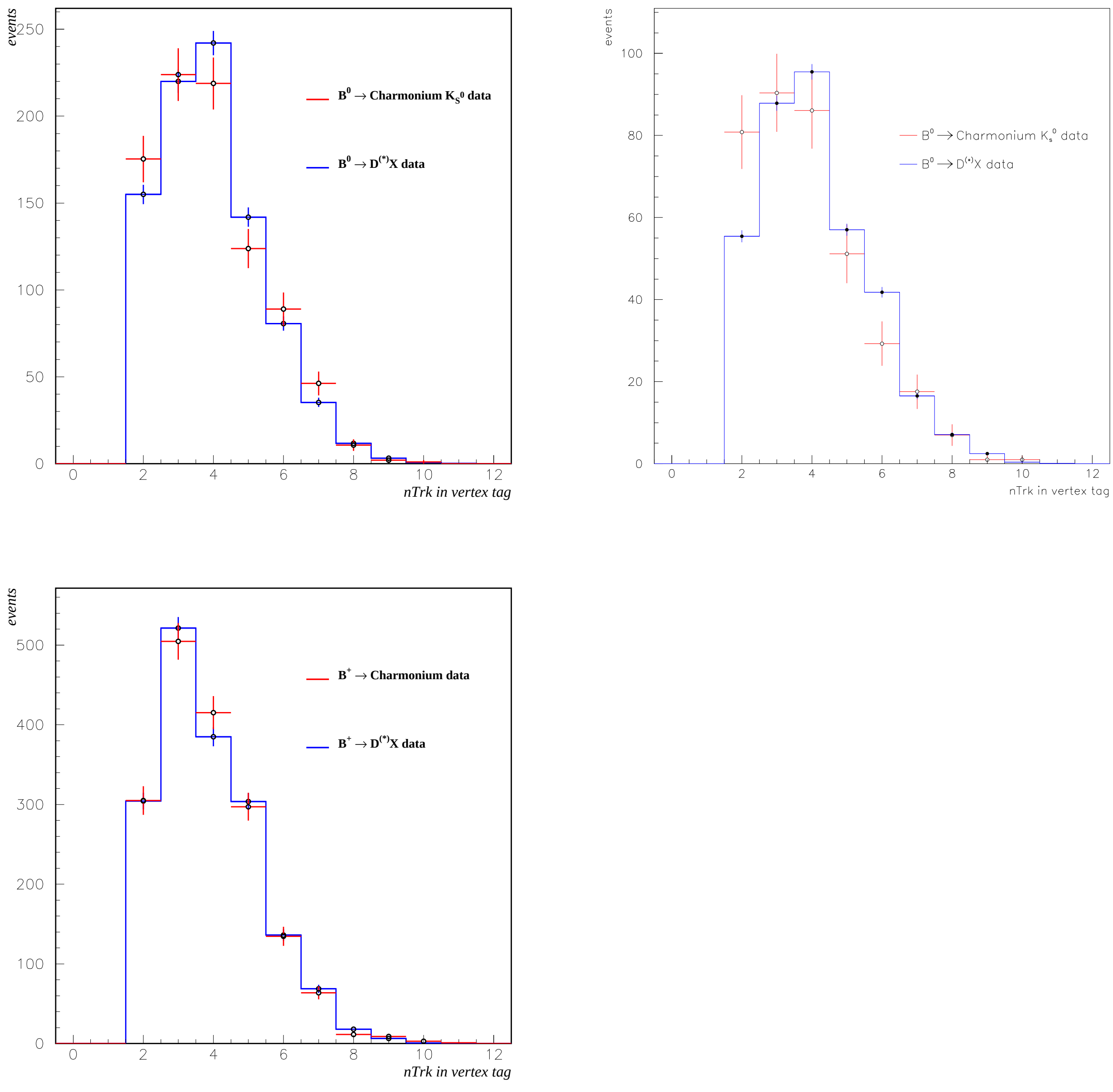

Figure 62: No beam configuration. Breco/charmonium (excluding K_L^0 modes) data comparison of the number of candidates (tracks+V^0's) used to make the vertex tag: (top/left) B^0 events; (top/right) B^0 Breco and only B^0 charmonium CP events; (bottom/left) B^+ events.

Mode	Prob $\chi^2 < 0.01$ Data	Prob $\chi^2 < 0.01$ MC
Charmonium		
JpsiKs	2.61	3.59
Psi2sKs	4.96	3.23
JpsiKs2pi0	7.18	3.67
JpsiKstar0Kp	6.09	?
JpsiKstar0ks	1.54	?
JpsiKstarpKp	3.24	?
JpsiKstarpKs	2.52	?
JpsiK	4.45	3.53
Psi2sKp	3.32	3.45
Breco		
B0Dch	5.13	4.26
B0Dstar	4.91	3.36
BchD0	4.82	?
BchDstar	4.73	?

Table 24: No beam configuration. Probability χ^2 less than one percent for charmonium and breco data and MC.

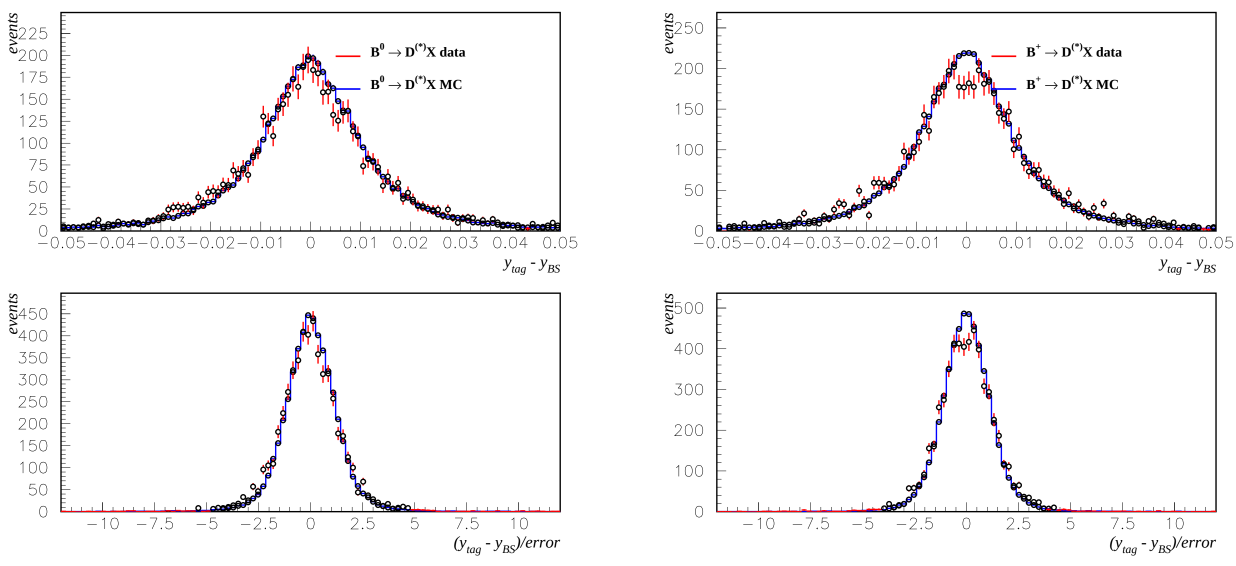

Figure 63: No beam configuration. Data/Monte Carlo comparison of the y distance and pull between the B tag vertex and the beam spot position for B^0 (left) and B^+ (right) Breco events.

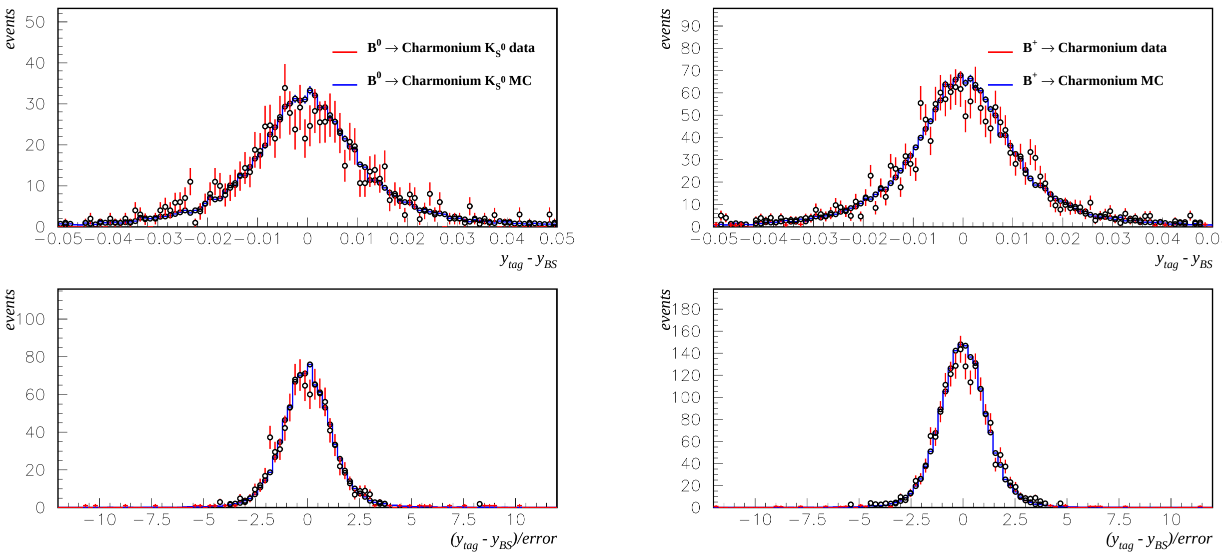

Figure 64: No beam configuration. Data/Monte Carlo comparison of the y distance and pull between the B tag vertex and the beam spot position for B^0 (left) and B^+ (right) charmonium events.

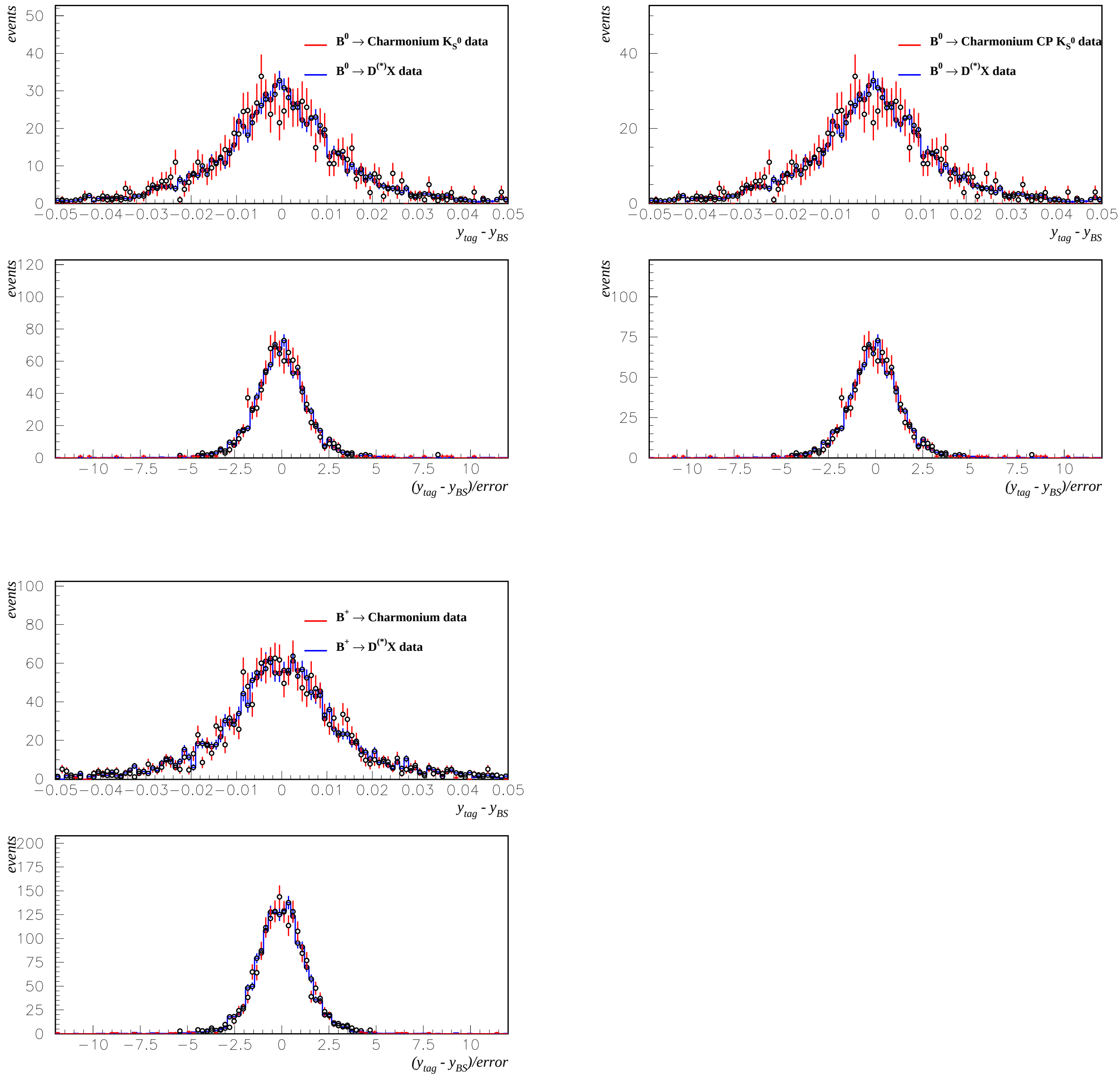

Figure 65: No beam configuration. Breco/charmonium data (excluding K_L^0) comparison of the y distance and pull between the B tag vertex and the beam spot position for B^0 (top/left), B^0 reco and B^0 CP events (top/right) and B^+ (bottom/left) events.

	$y_{TAG} - y_{BS}$ residual (μm)		$y_{TAG} - y_{BS}$ Pull			
	μ	RMS	μ	RMS	σ_{core}	f_{core}
B^0 Breco signal MC	0.6 ± 0.6	120 ± 6	0.005 ± 0.005	1.21 ± 0.01	1.08 ± 0.07	0.954 ± 0.003
B^0 Breco Data	-4.1 ± 2.6	127 ± 8	-0.06 ± 0.03	1.27 ± 0.04	0.99 ± 0.05	0.73 ± 0.03
B^0 Charmonium signal MC	-1.4 ± 1.1	119 ± 10	-0.015 ± 0.011	1.20 ± 0.04	1.07 ± 0.04	0.936 ± 0.006
B^0 Charmonium Data	-6.3 ± 7.6	115 ± 30	-0.07 ± 0.08	1.20 ± 0.14	1.05 ± 0.10	0.76 ± 0.06

Table 25: No beam configuration. y tag side residuals and pulls for charmonium and Breco modes, data and Monte Carlo, with respect to the beam spot position in y. The distributions are fitted to two Gaussians.

4.3 Check of Δt distributions

Figures 66 and 67 show the data/Monte Carlo comparison of the Δt distributions for signal events (after background subtraction) for B breco and charmonium events, respectively, regardless tagging. CP events are shown separately. Similarly figure 42 compares Breco and charmonium events in data. Figures 69, 70 and 71 are the equivalent distributions but after tagging. Agreement in all cases is good.

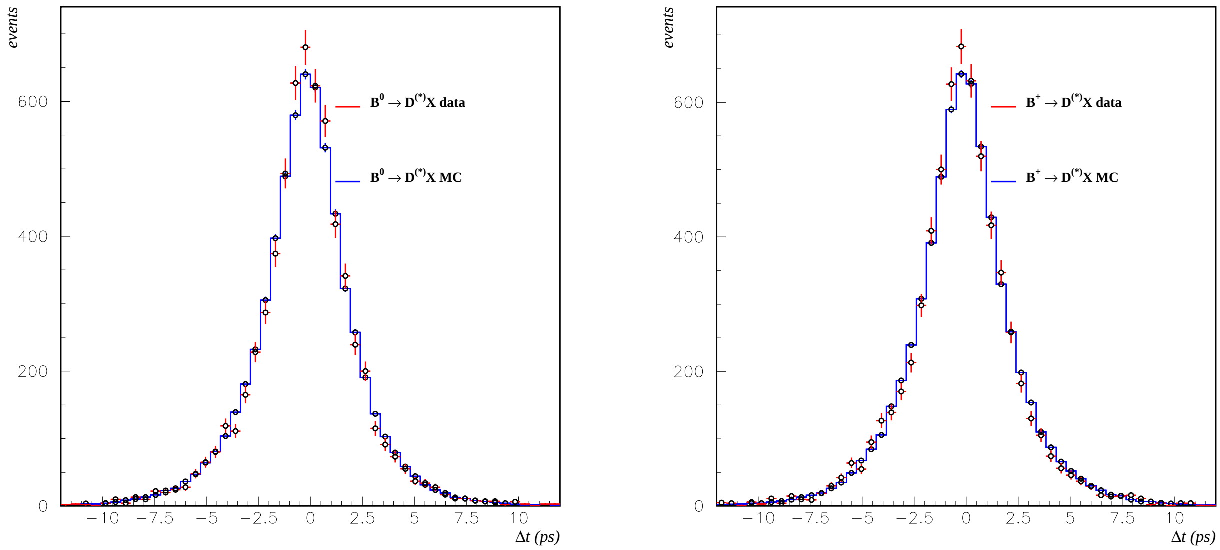

Figure 66: No beam configuration. Data/Monte Carlo comparison the Δt distributions for signal (after background subtraction and before tagging) for B breco events: (left) B^0 (right) B^+.

4.4 Other checks

4.4.1 SVT content

Figures 72, 73, 74 and 75 show a data/Monte Carlo comparison for B^0 Breco, B^+ Breco, B^0 charmonium and B^+ charmonium species, respectively, of the available SVT information in tracks used to fit the vertex tag. Top/left (top/right) distributions give the number of SVT z ($R\phi$) layers per track for tagging vertex tracks. Bottom/left (bottom/right) distributions show the number of tag vertex tracks with at least 2 z SVT layers before (after) quality cuts. We can see that before quality cuts there is a significant fraction of events with very poor SVT information (none or only 1 track with at least two z layers). It should be reminded that in the default configuration with beam constraints this fraction was already very small. The situation becomes much better after quality cuts: here, basically all events with no tracks or only 1 track with hits in two z layers are removed. Table 26 summarizes the fraction of events in data and Monte Carlo for the different B species with none, only 1 track and 2 tracks in vertex tag with z SVT information (hits in at least two z layers).

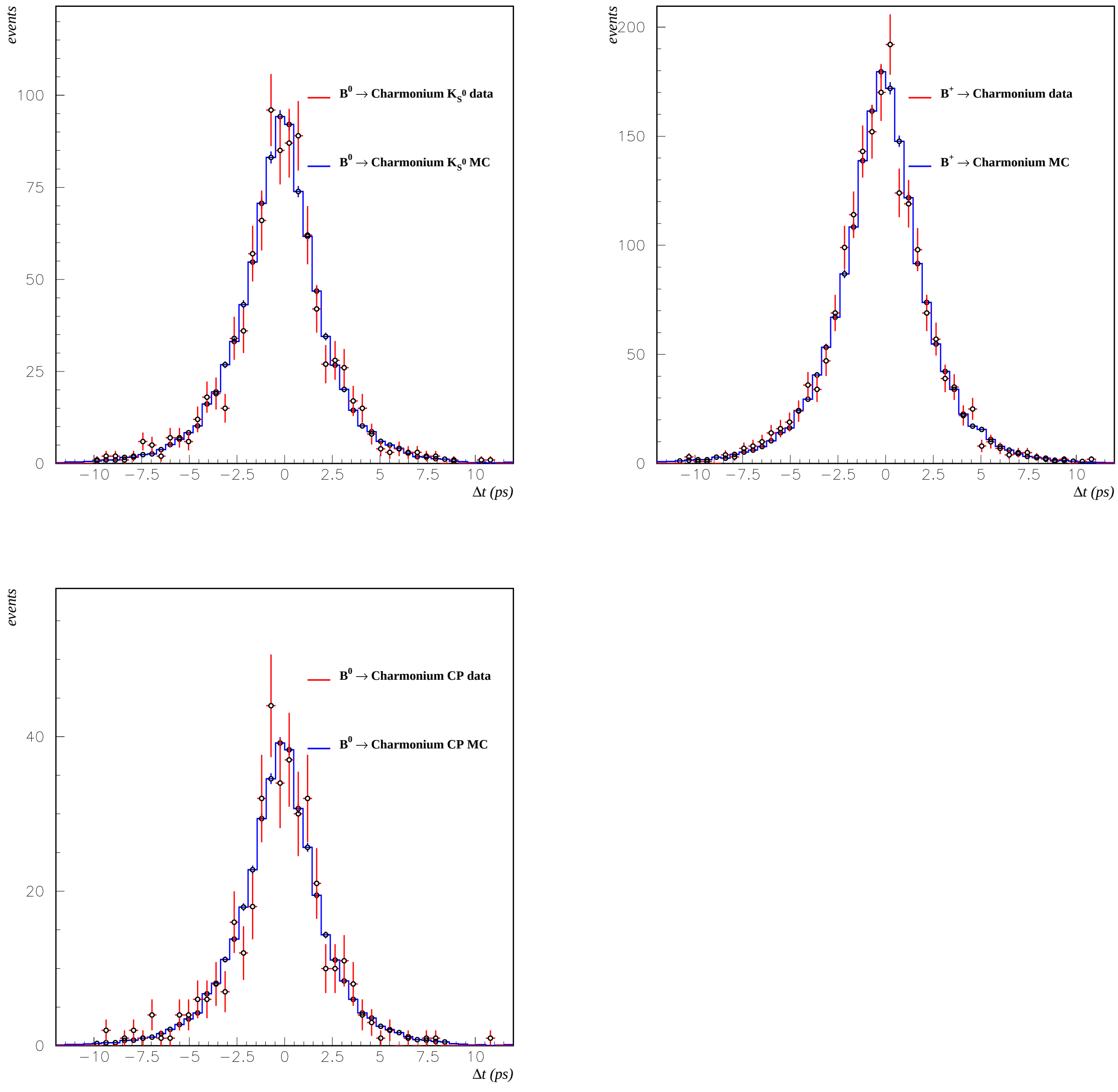

Figure 67: No beam configuration. Data/Monte Carlo comparison the Δt distributions for signal (after background subtraction and before tagging) for B charmonium events: (top/left) B^0 (top/right) B^0 for only CP modes, (bottom/left) B^+.

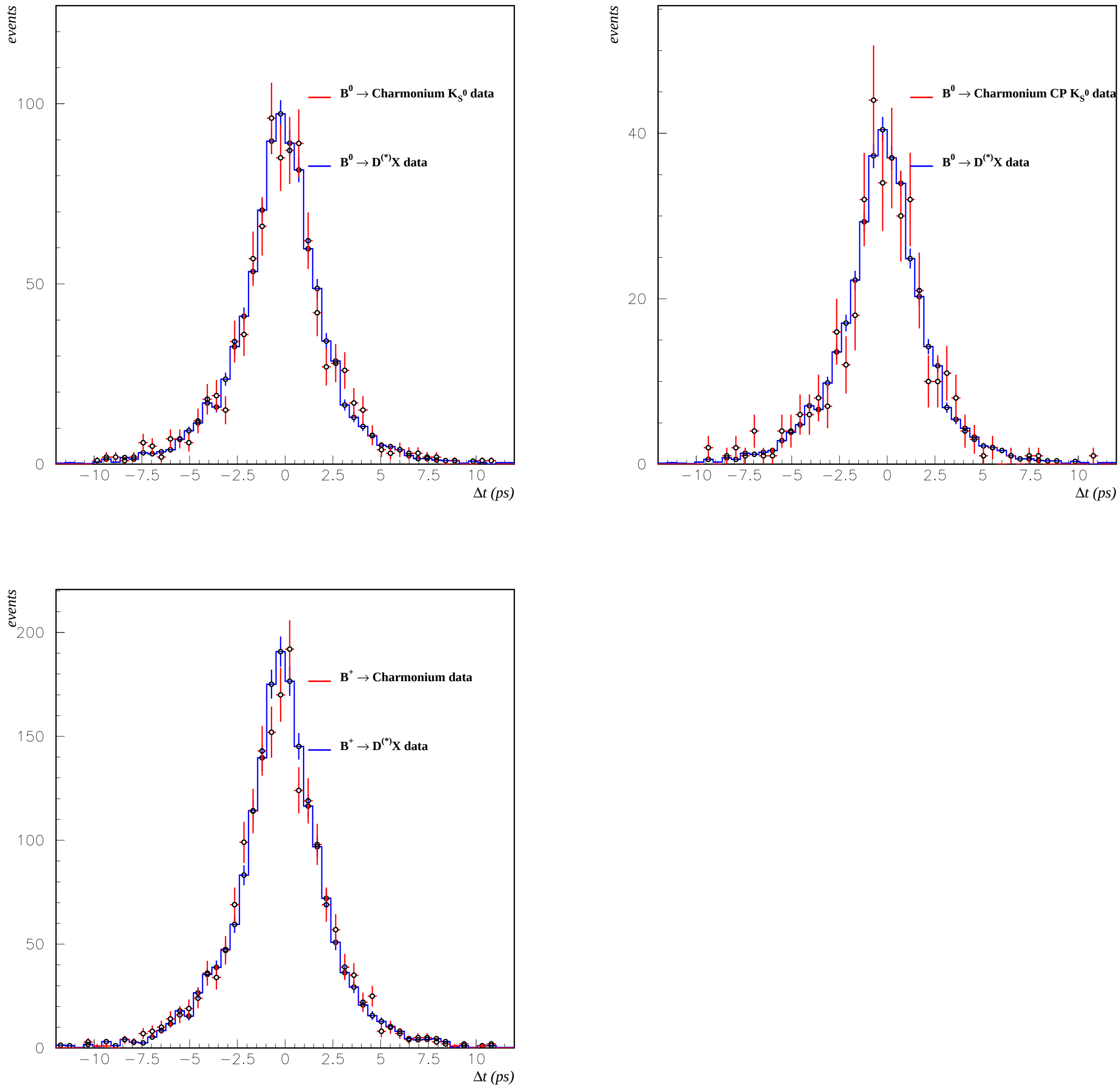

Figure 68: No beam configuration. Breco/charmonium data (excluding K_L^0) comparison of the Δt distributions for signal (after background subtraction and before tagging): (top/left) B^0 (top/left) B^0 breco and B^0 CP events, (bottom/left) B^+ events.

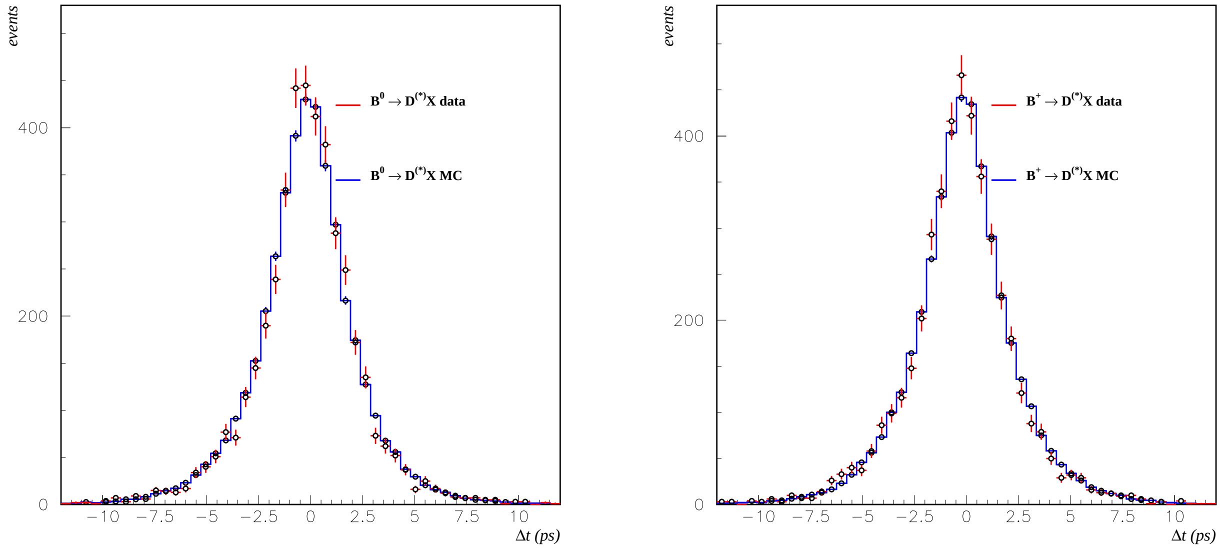

Figure 69: No beam configuration. Data/Monte Carlo comparison the Δt distributions for signal (after background subtraction and after tagging) for B breco events: (left) B^0 (right) B^+.

4.4.2 Tagging content

Figure 50 compares the fraction of tagging leptons used in the vertex tag as a function of the momentum on the center-of-mass frame for data and Monte Carlo and for the different B species, after background subtraction. Table 19 gives the average efficiencies: for all data samples, 98% of the tagging leptons are used in the vertex.

Similarly, figure 51 compares the fraction of tagging kaons used in the vertex tag as a function of the momentum on the center-of-mass frame for data and Monte Carlo and for the different B species. Table 28 gives the average efficiencies: in Monte Carlo, on average 88% of the kaons are used in the vertex, and in data the average fraction is slightly smaller,

	Monte Carlo			Data		
	$f_0(\%)$	$f_1(\%)$	$f_2(\%)$	$f_0(\%)$	$f_1(\%)$	$f_2(\%)$
B^0 Breco	0.06 ± 0.03	0.36 ± 0.08	16.3 ± 0.5	0.15 ± 0.05	0.52 ± 0.10	18.1 ± 0.5
B^+ Breco	0.06 ± 0.03	0.37 ± 0.08	16.4 ± 0.5	0.17 ± 0.06	0.52 ± 0.10	18.2 ± 0.5
B^0 Charmonium	0.00 ± 0.00	0.39 ± 0.21	16.5 ± 1.2	0.00 ± 0.00	0.45 ± 0.22	20.6 ± 1.4
B^0 Charmonium CP	0.00 ± 0.00	0.40 ± 0.33	16.7 ± 2.0	0.00 ± 0.00	0.54 ± 0.40	22.7 ± 2.2
B^+ Charmonium	0.00 ± 0.00	0.35 ± 0.15	16.6 ± 0.9	0.00 ± 0.00	0.39 ± 0.15	18.5 ± 0.9

Table 26: Fraction of events in data and Monte Carlo for the different B species with none, only 1 track and 2 tracks in vertex tag with z SVT information (at least two z layers), after quality cuts.

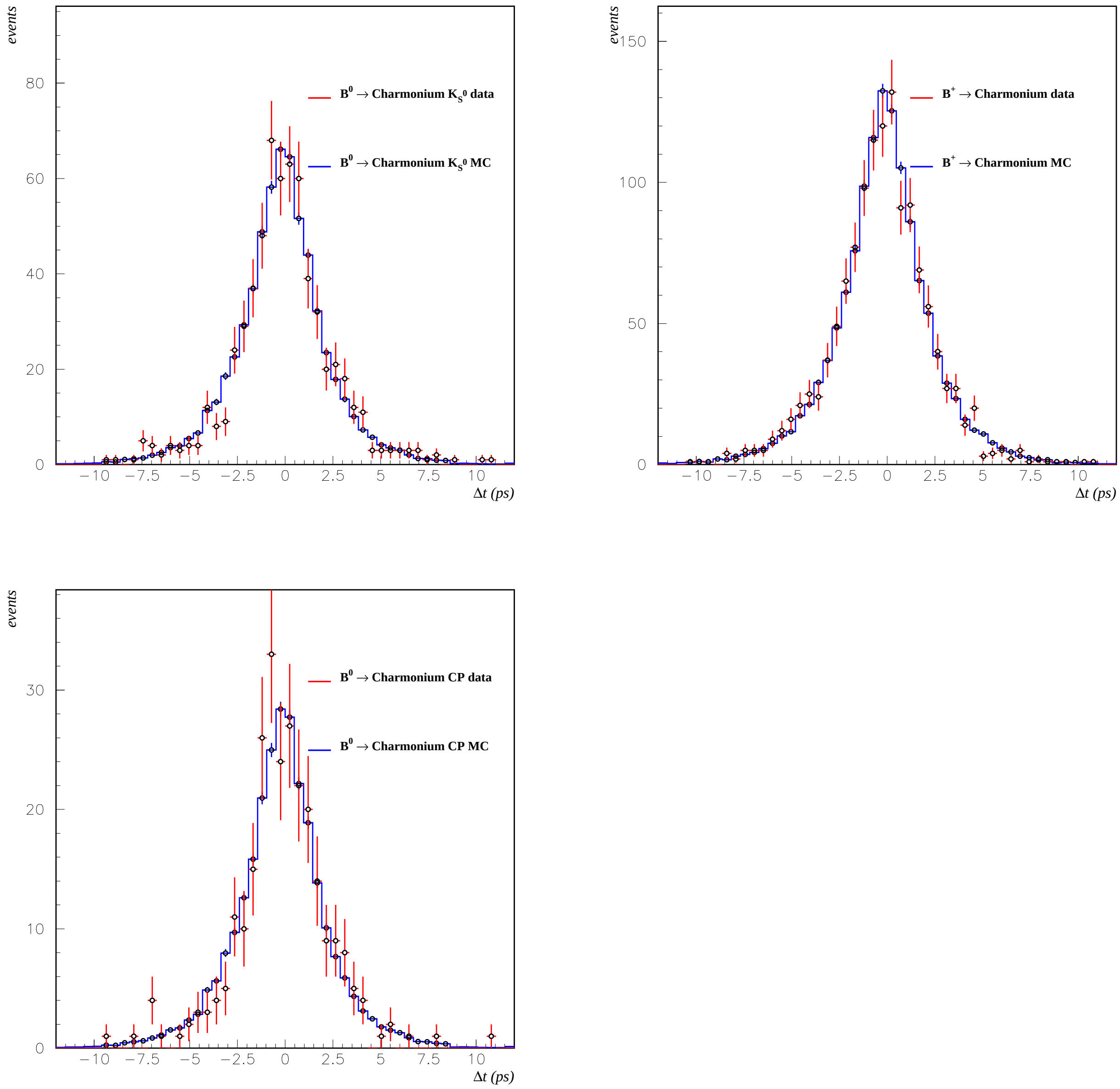

Figure 70: No beam configuration. Data/Monte Carlo comparison the Δt distributions for signal (after background subtraction and after tagging) for B charmonium events: (top/left) B^0 (top/right) B^0 for only CP modes, (bottom/left) B^+.

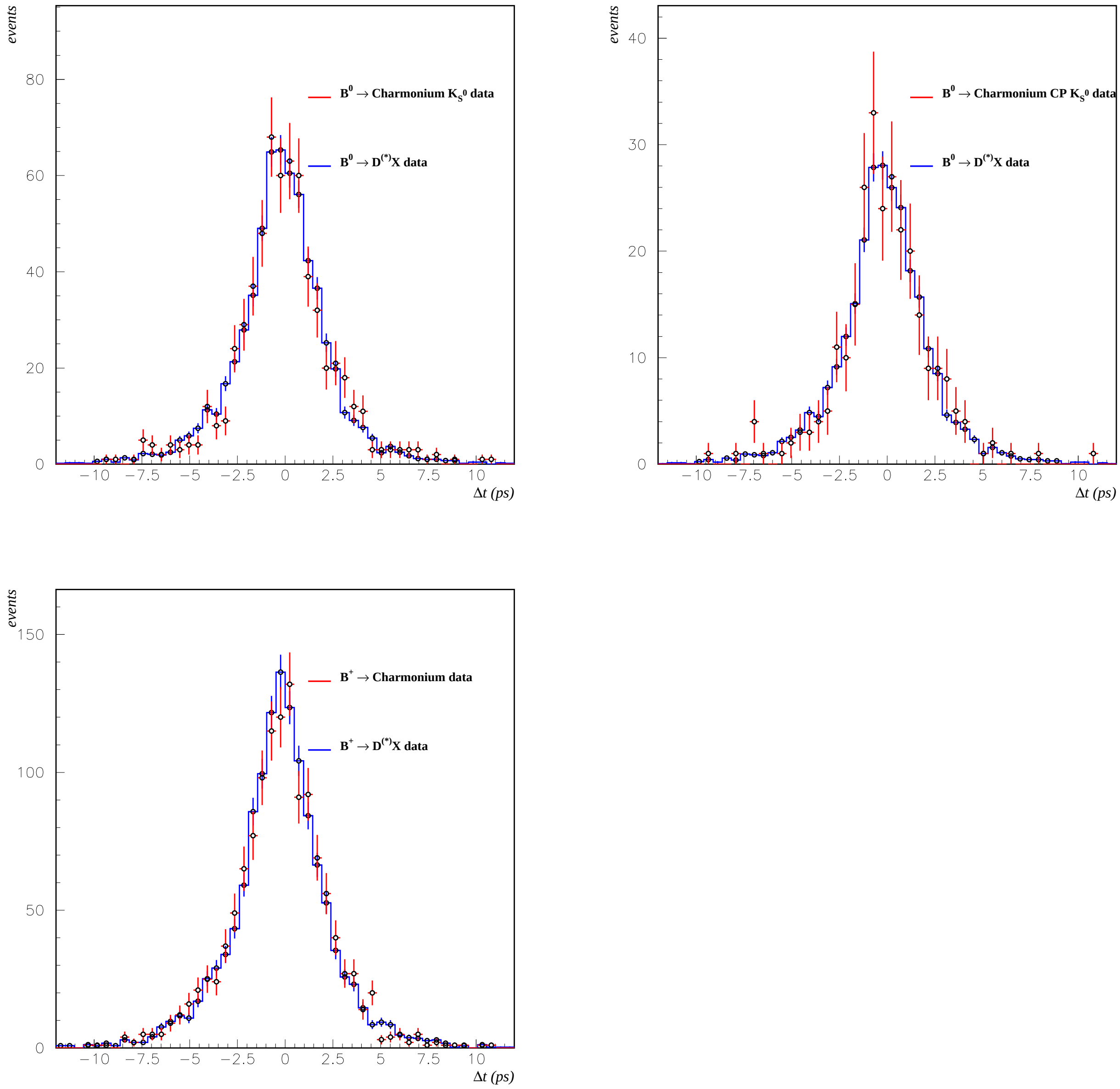

Figure 71: No beam configuration. Breco/charmonium data (excluding K_L^0) comparison of the Δt distributions for signal (after background subtraction and after tagging): (top/left) B^0 (top/left) B^0 breco and B^0 CP events, (bottom/left) B^+ events.

	Monte Carlo	Data
B^0 Breco	0.981 ± 0.001	0.984 ± 0.005
B^+ Breco	0.985 ± 0.001	0.990 ± 0.004
B^0 Charmonium	0.982 ± 0.002	0.978 ± 0.016
B^0 Charmonium CP	0.982 ± 0.002	0.972 ± 0.029
B^+ Charmonium	0.988 ± 0.002	0.975 ± 0.012

Table 27: No beam configuration. Average fraction of tagging leptons used in the vertex tag for the different data and Monte Carlo sets.

about 86%.

	Monte Carlo	Data
B^0 Breco	0.884 ± 0.002	0.857 ± 0.008
B^+ Breco	0.896 ± 0.002	0.873 ± 0.007
B^0 Charmonium	0.880 ± 0.003	0.835 ± 0.018
B^0 Charmonium CP	0.880 ± 0.003	0.844 ± 0.027
B^+ Charmonium	0.898 ± 0.002	0.864 ± 0.012

Table 28: No beam configuration. Average fraction of tagging kaons used in the vertex tag for the different data and Monte Carlo sets.

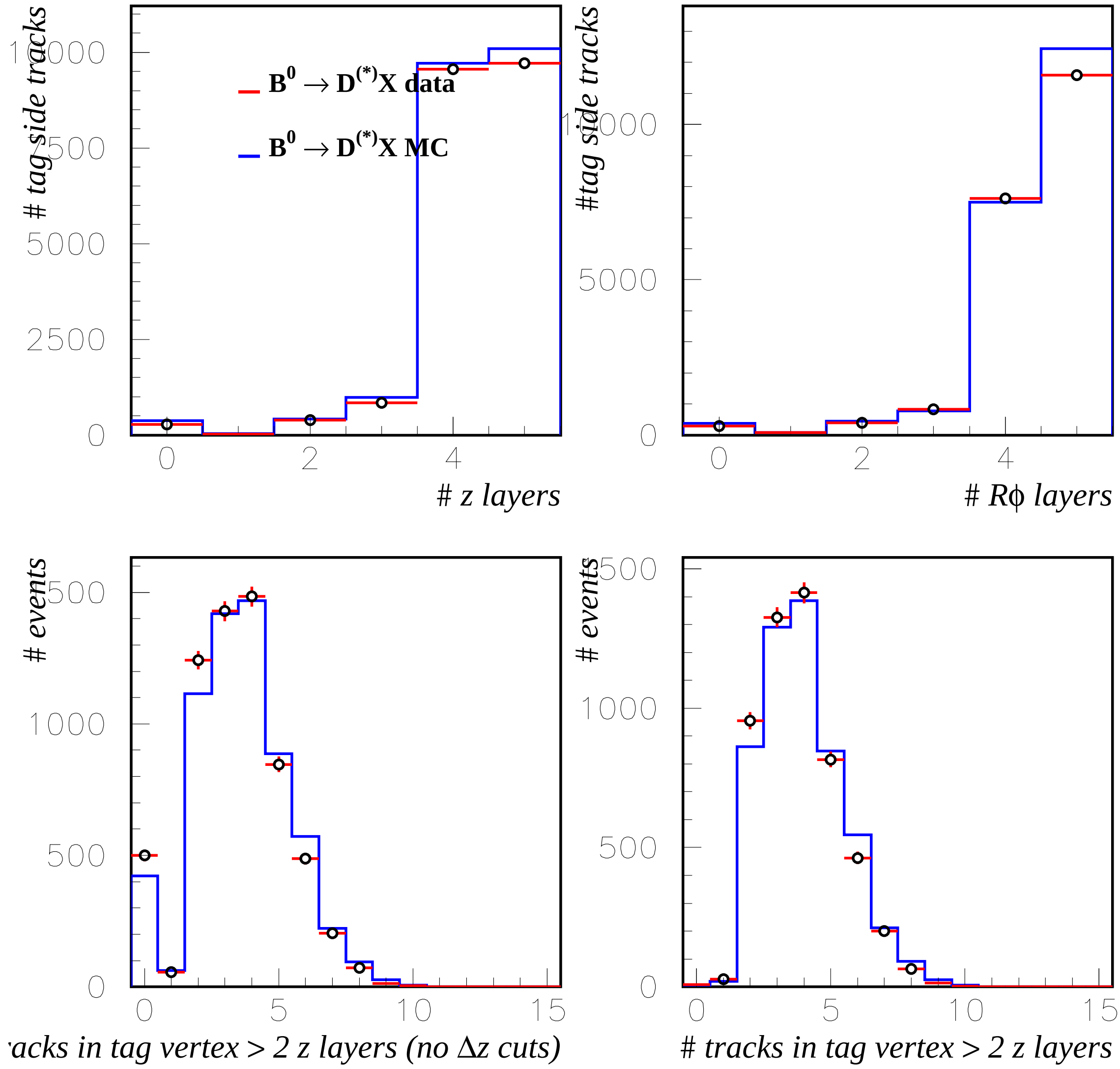

Figure 72: No beam configuration. Data/Monte Carlo comparison of SVT information in vertex tag for B^0 Breco events: (top/left) number of SVT z layers per track for tagging vertex tracks; (top/right) same but SVT $R\phi$ layers; (bottom/left) number of tracks used in vertex tag with at least 2 SVT z layers before vertex quality cuts; (bottom/right) number of tracks used in vertex tag with at least 2 SVT z layers after vertex quality cuts. Distributions are normalized to the number of events after quality cuts.

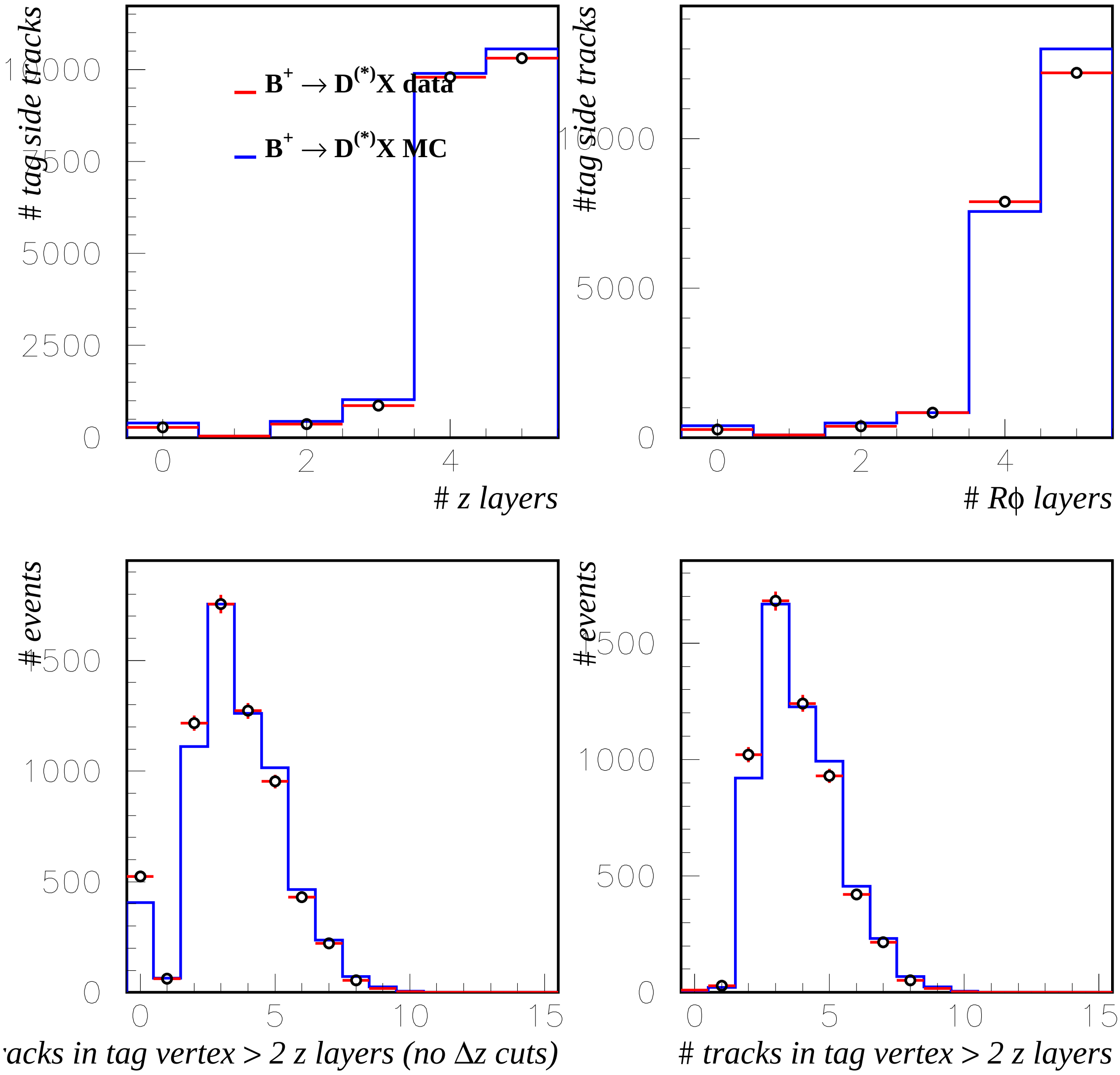

Figure 73: No beam configuration. Data/Monte Carlo comparison of SVT information in vertex tag for B^+ Breco events: (top/left) number of SVT z layers per track for tagging vertex tracks; (top/right) same but SVT $R\phi$ layers; (bottom/left) number of tracks used in vertex tag with at least 2 SVT z layers before vertex quality cuts; (bottom/right) number of tracks used in vertex tag with at least 2 SVT z layers after vertex quality cuts. Distributions are normalized to the number of events after quality cuts.

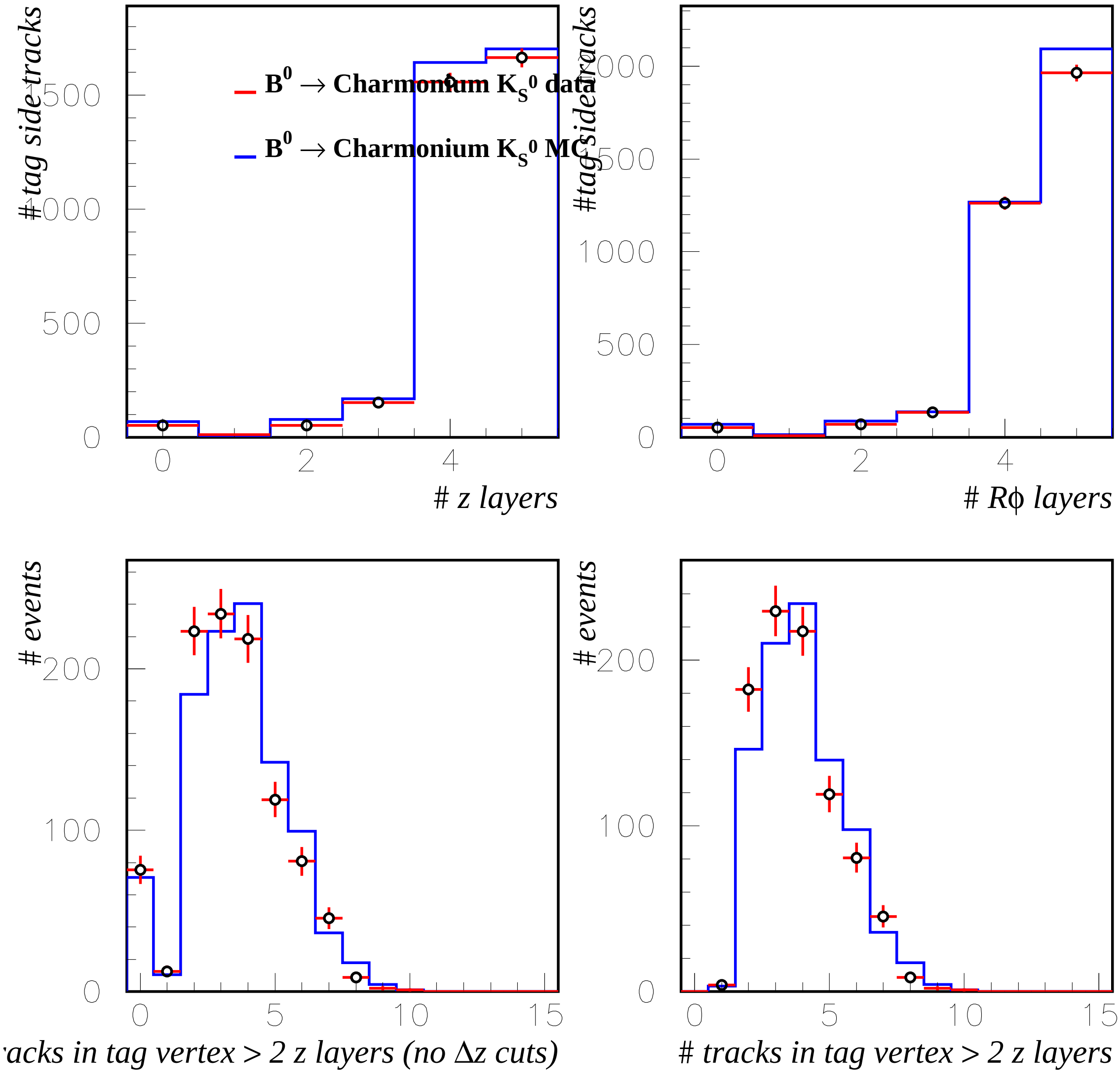

Figure 74: No beam configuration. Data/Monte Carlo comparison of SVT information in vertex tag for B^0 charmonium events: (top/left) number of SVT z layers per track for tagging vertex tracks; (top/right) same but SVT $R\phi$ layers; (bottom/left) number of tracks used in vertex tag with at least 2 SVT z layers before vertex quality cuts; (bottom/right) number of tracks used in vertex tag with at least 2 SVT z layers after vertex quality cuts. Distributions are normalized to the number of events after quality cuts.

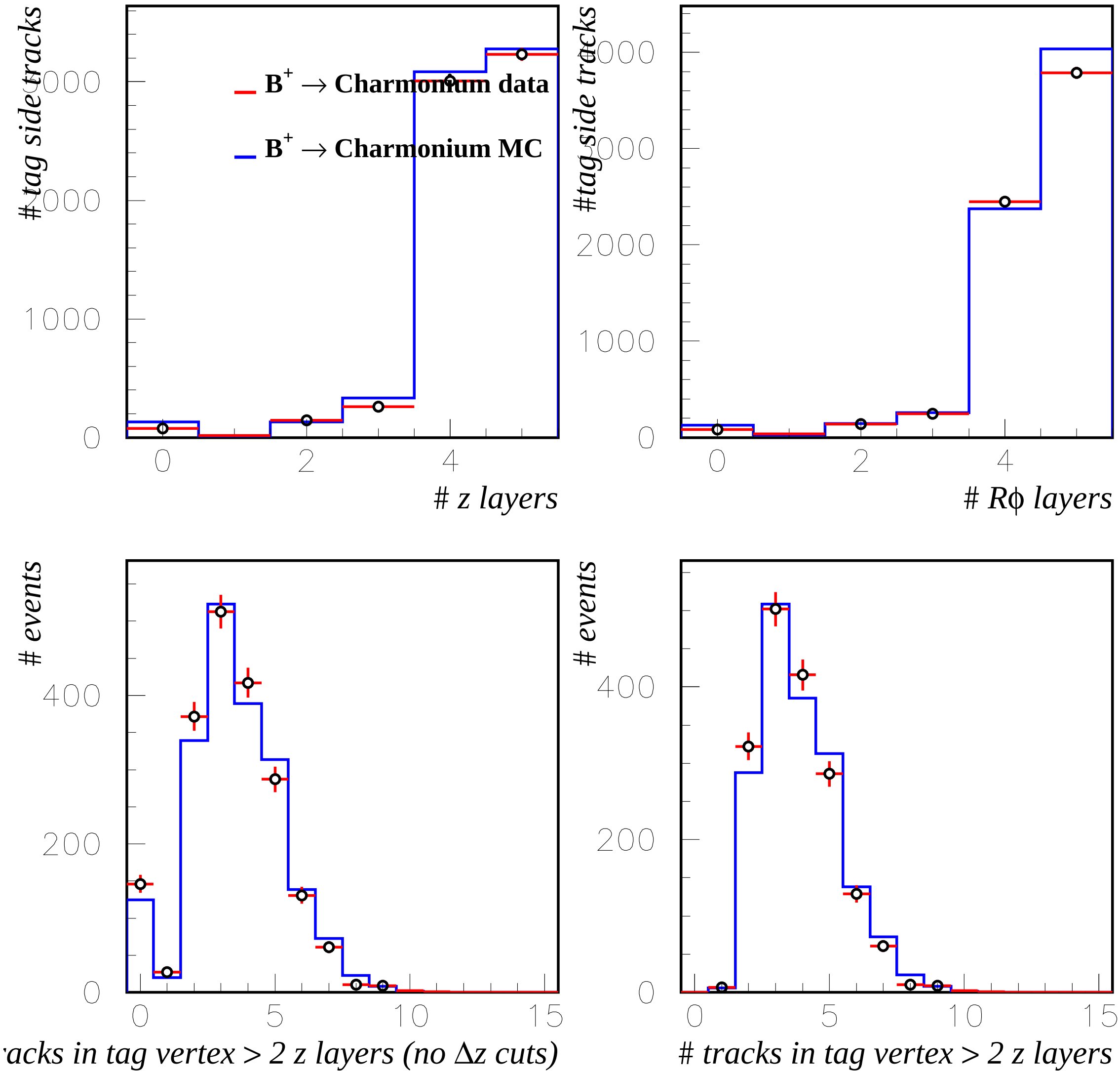

Figure 75: No beam configuration. Data/Monte Carlo comparison of SVT information in vertex tag for B^+ charmonium events: (top/left) number of SVT z layers per track for tagging vertex tracks; (top/right) same but SVT $R\phi$ layers; (bottom/left) number of tracks used in vertex tag with at least 2 SVT z layers before vertex quality cuts; (bottom/right) number of tracks used in vertex tag with at least 2 SVT z layers after vertex quality cuts. Distributions are normalized to the number of events after quality cuts.

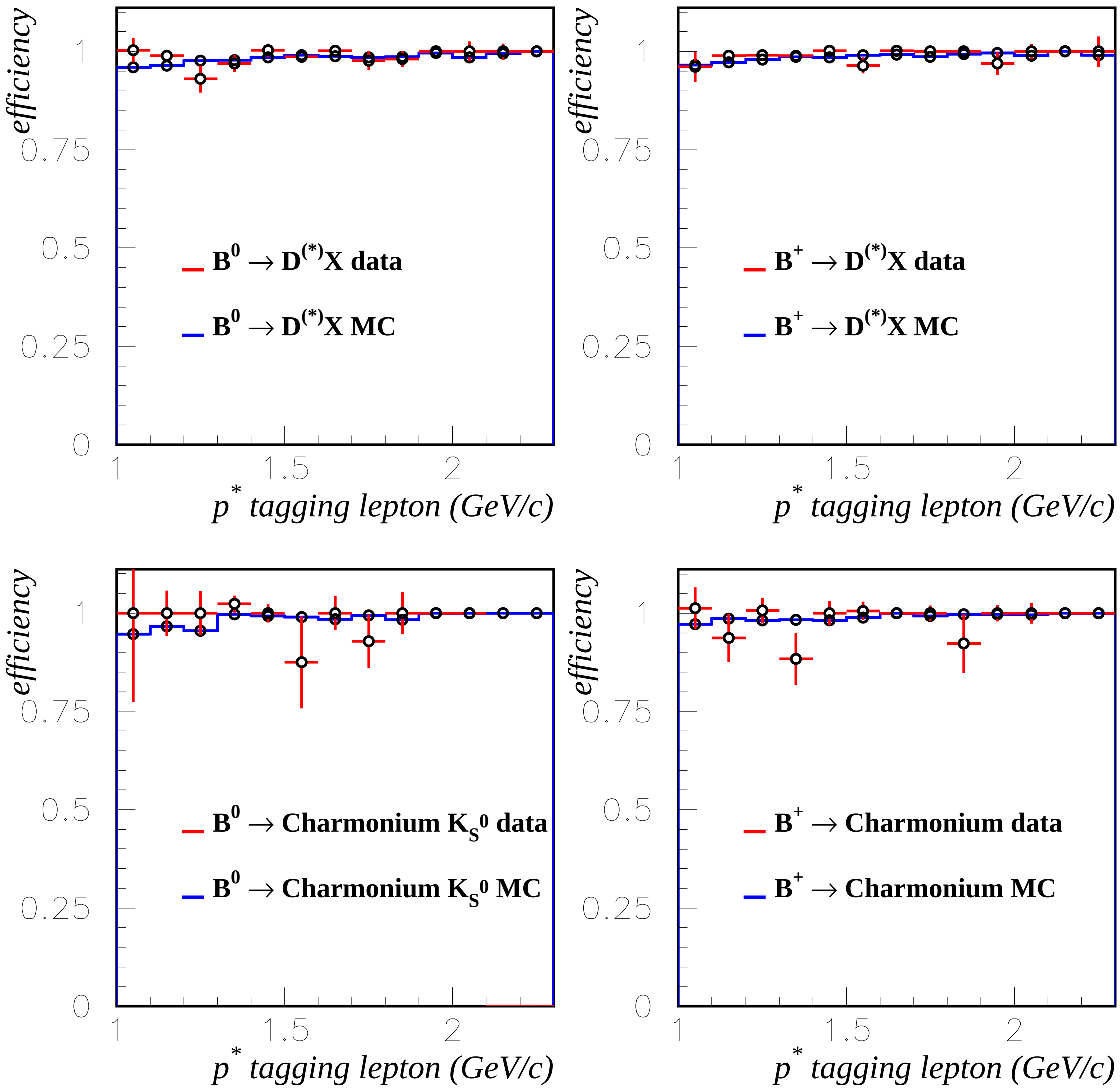

Figure 76: No beam configuration. Fraction of tagging leptons used in the vertex tag as a function of the momentum on the center-of-mass frame for data and Monte Carlo and for the different B species.

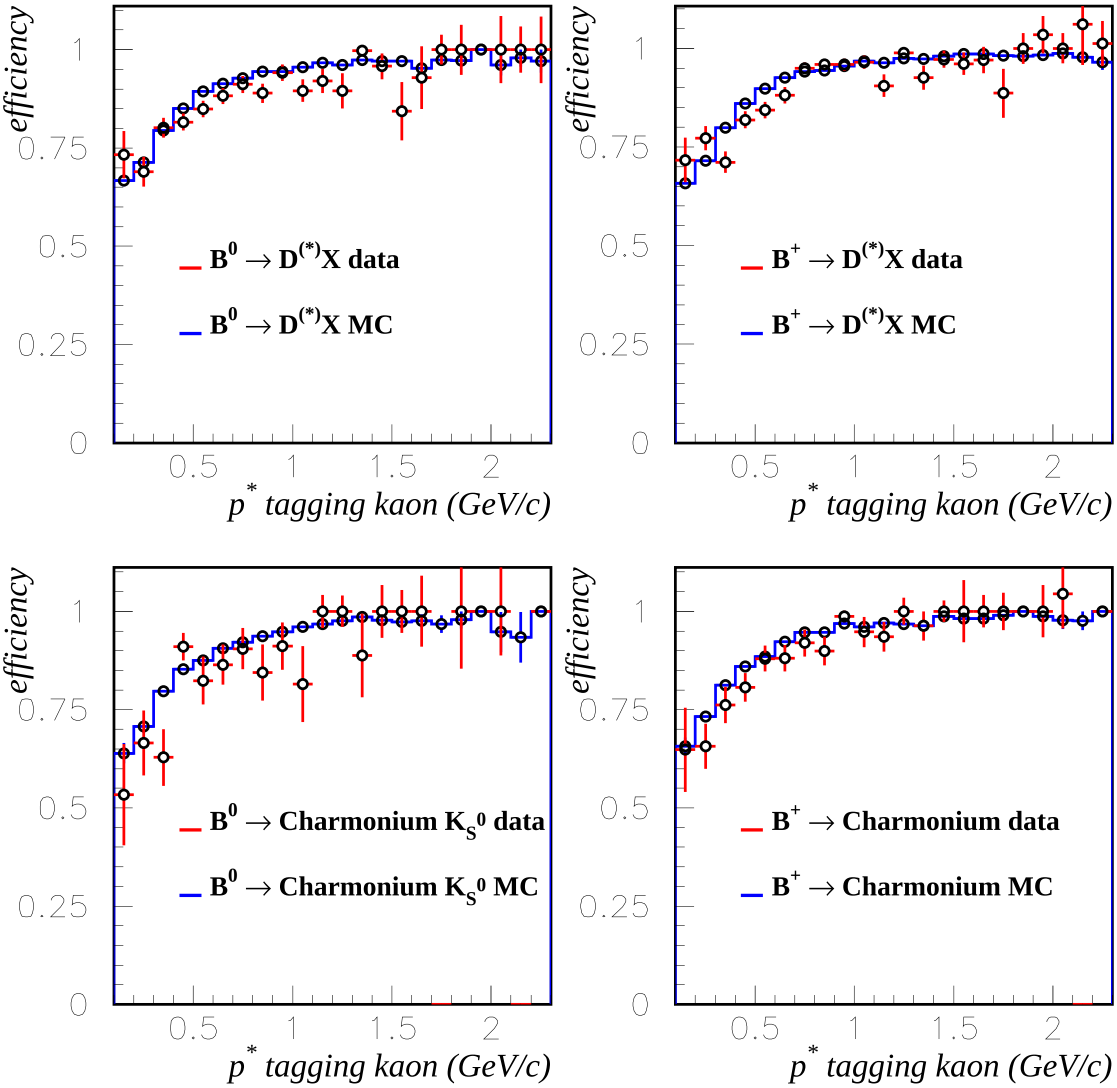

Figure 77: No beam configuration. Fraction of tagging kaons used in the vertex tag as a function of the momentum on the center-of-mass frame for data and Monte Carlo and for the different B species.

5 Resolution and lifetime fits to semileptonic and hadronic signal Monte Carlo

5.1 Description of the Fits

The fits are performed using the RooFitTools macros:

```
BBDecays/Semilep/signalMC.cc
BBDecays/Exclusive/signalMC.cc
```

with the following tags:

```
RooFitTools   V00-02-27
RooFitMacros  V00-00-17
```

These macros read the appropriate signal MC ASCII files and then perform a standard sequence of fits consisting of:

- fit the MC-truth Δt and Δz distributions for the lifetime,
- fit the distribution of MC-truth residuals, $\delta(\Delta t)$, and calculated uncertainty on Δt, $\sigma_{\Delta t}$, to obtain the parameters of 2 different resolution models, and
- fit the reconstructed Δt distribution to obtain the lifetime, using 2 different resolution models, and with the resolution parameters either fixed (to values obtained in the previous step) or else floating in the fit.

The two resolution models are referred to as the G+G+G and G$\otimes$(δ+E)+G models. The G+G+G model consists of 3 Gaussians, each with an absolute bias (measured in ps) and a scale factor which multiplies the per-event error. The bias of the third Gaussian is fixed at zero, but the remaining seven parameters are free. This G+G+G model is similar to the "Osaka" resolution model, except that the scale factor of its widest Gaussian multiplies the per-event error and is a free parameter, rather than having a fixed 8 ps width. The reason for floating the outlier width in the fit is to avoid a systematic bias from choosing a fixed value (this was the largest source of systematic error in the Osaka hadronic B lifetime measurement.) The reason for modeling the outliers with a scale factor parameter, rather than a fixed width, is to reduce the correlation between this parameter and the lifetime. An outlier contribution parameterized in terms of pulls also corresponds more closely to what we mean by "outliers" and appears to provide a more stable fit (a fit to the hadronic signal MC using a fixed width fails to converge – see Table 37).

The G$\otimes$(δ+E)+G model is "Jan's Model", which is similar to what was used for the Osaka hadronic lifetime analysis, but with an additional Gaussian contribution for outliers. The scale factor for this third Gaussian multiplies the per-event errors and so has the same definition as in the G+G+G model.

5.2 Semileptonic Signal MC Samples

The semileptonic signal MC sample is analyzed with analysis-7 using the final vertexing and tagging configuration. The resulting ASCII files are in the directory:

`/nfs/farm/babar/AWG2/Breco/production/Dstarlnu/ascii/MCprod-7-3/`

The events used for these fits are required to be correctly reconstructed, according to the digi associator, in order to minimize the effects of the small backgrounds in these signal samples. Table 29 provides some key figures of merit for the resolution in the semileptonic signal MC. The first row represents the full sample, and subsequent groups of rows provide different breakdowns of this full sample. The equivalent luminosities of these samples, by D^0decay mode, are ?? fb^{-1} (K π), etc. The contributions broken down by D^0decay mode total slightly less than the full sample since they do not include events in which a candidate is correctly reconstructed from the decay of the "other B". The quantity $< \sigma^2_{\Delta t} >$ given in these tables is the appropriate number for multiplying the scale factors in the resolution model to convert them into an RMS for the weighted sample.

Table 29 shows some systematic trends in resolution of different subsamples (see the left-hand plots in Figures 78 and 79):

- the bias and RMS depend most strongly on the tagging category,
- the bias and RMS depend on the D^0decay mode and the tagging category,
- there is a smaller but significant dependence of the mean on the tag flavor, and of the RMS on the reconstructed flavor,
- the average per-event error correlates with the RMS, i.e., the calculated error is sensitive to changes in the RMS resolution,
- the resolution of tagged events is better than that of untagged events, and
- the fraction of events with pulls of 5 or more is about 1%.

5.3 Hadronic Signal MC Samples

The hadronic B^0cocktail signal MC sample is analyzed using the same final vertexing and tagging configuration as the semileptonic samples. The resulting ASCII files are in the directory:

`/nfs/farm/babar/AWG2/sin2b/mc_run1/Breco/anal7c/ASCII/`

All events within 5.27 GeV $\leq m(B)_{SE} \leq$ 5.29 GeV are assumed to be correctly reconstructed signal, and there is no special treatment of the small backgrounds in these signal samples. Table 30 provides summary statistics for the hadronic signal MC samples analyzed here. The first row represents the full sample, and subsequent groups of rows provide different breakdowns of this full sample. The equivalent luminosity of this sample is ?? fb^{-1}.

Table 30 shows similar systematic trends in the resolution of different subsamples which are similar to those seen in the semileptonic samples (see Figures 84 and 85):

Sample	Events	Mean $\delta(\Delta t)$ (ps)	RMS $\delta(\Delta t)$ (ps)	$< \sigma^2_{\Delta t} >$ (ps)	$f(\lvert\text{pull}\rvert > 5)$ (%)
All Combined	10103	-0.2269 ± 0.0023	1.2516 ± 0.0088	0.882	0.911 ± 0.095
Electrons	5156	-0.2187 ± 0.0030	1.246 ± 0.012	0.884	0.80 ± 0.12
Muons	4947	-0.2355 ± 0.0033	1.258 ± 0.013	0.881	1.03 ± 0.14
SVT only	8154	-0.2267 ± 0.0025	1.2614 ± 0.0099	0.892	0.88 ± 0.10
SVT+DCH	1949	-0.2281 ± 0.0052	1.210 ± 0.019	0.840	1.03 ± 0.23
$D^0 \to$ Kπ	5301	-0.2454 ± 0.0034	1.211 ± 0.012	0.876	0.72 ± 0.12
$D^0 \to$ K3π	2735	-0.2187 ± 0.0042	1.241 ± 0.017	0.858	1.24 ± 0.21
$D^0 \to$ K$\pi\pi^0$	1737	-0.2018 ± 0.0048	1.417 ± 0.024	0.947	1.04 ± 0.24
$D^0 \to K^0_s\pi\pi$	198	-0.167 ± 0.012	1.016 ± 0.051	0.861	0.51 ± 0.50
Reco'd B^0	5138	-0.2263 ± 0.0032	1.288 ± 0.013	0.882	1.11 ± 0.15
Reco'd $\overline{B}$	4965	-0.2276 ± 0.0032	1.213 ± 0.012	0.883	0.70 ± 0.12
B^0Tag	3538	-0.2313 ± 0.0039	1.215 ± 0.014	0.828	1.10 ± 0.18
$\overline{B}$Tag	3579	-0.1772 ± 0.0030	1.227 ± 0.014	0.839	0.84 ± 0.15
Lepton Tag	1370	-0.1369 ± 0.0037	1.038 ± 0.020	0.767	1.09 ± 0.28
Kaon Tag	3328	-0.2357 ± 0.0041	1.183 ± 0.015	0.829	0.60 ± 0.13
NT1 Tag	875	-0.1599 ± 0.0054	1.207 ± 0.029	0.795	1.03 ± 0.34
NT2 Tag	1544	-0.2208 ± 0.0056	1.438 ± 0.026	0.916	1.62 ± 0.32
No Tag	2986	-0.2814 ± 0.0051	1.320 ± 0.017	0.990	0.77 ± 0.16

Table 29: Statistics of the semileptonic signal Monte Carlo sample.

- the bias and RMS depend on whether the decay involves a π, ρ, or a_1, and to a smaller extent, whether the decay involves a $D^{*\pm}$ or a $D^{\pm}$,
- any effects due to the flavor of the reconstructed or tagged $B$are small,
- the resolution of tagged events is better than that of untagged events,
- the average per-event error is somewhat smaller in the hadronic sample (0.82 ps) than in the semileptonic sample (0.88 ps), although the RMS values are similar (1.244 ps and 1.252 ps),
- the fraction of events with pulls greater than 5 is about 1%.

5.4 Semileptonic Fit Results

Table 31 lists the parameters of a G+G+G resolution model, obtained from fits to the full sample and the different subsamples. These fits are made simultaneously to the MC truth residuals and the calculated per-event errors, and so represent our best possible knowledge of the resolution in signal MC, and are consistent with how we model the resolution in a lifetime fit. The solid curves in the middle-left and bottom-left plots of Figure 81 show the fit to the full semileptonic sample using linear and log scales.

The mean and RMS values in Table 31 are calculated from the fitted parameter values and take account of the actual distribution of per-event errors in the different samples.

Sample	Events	Mean $\delta(\Delta t)$ (ps)	RMS $\delta(\Delta t)$ (ps)	$\sqrt{<\sigma^2_{\Delta t}>}$ (ps)	$f(\lvert\text{pull}\rvert > 5)$ (%)
All Combined	54697	-0.20486 ± 0.00088	1.2441 ± 0.0038	0.818	1.104 ± 0.045
π Modes	27398	-0.2040 ± 0.0012	1.1806 ± 0.0050	0.773	1.168 ± 0.065
ρ Modes	16994	-0.2062 ± 0.0016	1.2966 ± 0.0070	0.863	0.994 ± 0.076
a_1 Modes	10305	-0.2051 ± 0.0020	1.3180 ± 0.0092	0.861	1.12 ± 0.10
$D^{*\pm}$ Modes	24891	-0.2104 ± 0.0013	1.2286 ± 0.0055	0.813	1.065 ± 0.065
$D^{\pm}$Modes	29806	-0.2003 ± 0.0012	1.2568 ± 0.0051	0.823	1.137 ± 0.061
Reco'd B^0	27488	-0.2019 ± 0.0012	1.2446 ± 0.0053	0.820	1.150 ± 0.064
Reco'd $\overline{B}$	27209	-0.2078 ± 0.0013	1.2435 ± 0.0053	0.817	1.058 ± 0.062
B^0Tag	19284	-0.1792 ± 0.0013	1.1429 ± 0.0058	0.762	1.001 ± 0.072
$\overline{B}$Tag	18785	-0.1739 ± 0.0013	1.1587 ± 0.0060	0.761	1.022 ± 0.073
Lepton Tag	6815	-0.1102 ± 0.0013	1.0029 ± 0.0086	0.696	0.88 ± 0.11
Kaon Tag	18555	-0.1956 ± 0.0014	1.1897 ± 0.0062	0.764	1.013 ± 0.074
NT1 Tag	4636	-0.1535 ± 0.0023	1.107 ± 0.011	0.719	1.12 ± 0.15
NT2 Tag	8063	-0.2021 ± 0.0023	1.1981 ± 0.0094	0.832	1.05 ± 0.11
No Tag	16628	-0.2696 ± 0.0021	1.4330 ± 0.0079	0.935	1.317 ± 0.088

Table 30: Statistics of the hadronic B^0signal Monte Carlo sample.

Figures 78 and 79 compare these values obtained from the fit with those calculated directly from the residuals. The fit systematically underestimates the mean bias and overestimates the RMS resolution. There are several possible explanations for this:

- The fit mean and RMS are integrated over $(-\infty, +\infty)$ while the residuals in data are truncated by the $|\Delta z| < 3$ mm cut. This should have litte effect on the mean but will increase the RMS calculated for the fit.

- The fit weights each event according to its calculated Δt error, but the statistics calculated directly on the data are unweighted.

- The fit assumes an equal number of events at large positive and negative residual since the outlier component is unbiased. Figure 81 actually shows an excess of events at large negative residual, as compared with the fit.

Table 32 lists the parameters of a G$\otimes$(δ+E)+G resolution model, obtained from fits to the full sample and the different subsamples. These fits are also made to the MC truth residuals. The dashed curves in the middle-left and bottom-left plots of Figure 81 show the fit to the full sample on linear and log scales. A comparison of the chi-square probabilities between Tables 31 and 32 shows that the G$\otimes$(δ+E)+G model provides a better description of most samples, although the G+G+G probabilities are generally reasonable. Note that these chi-square values are calculated using only events with residuals of 5 ps or less, and so reflect goodness of fit to the core region only. The G$\otimes$(δ+E)+G model prefers a larger outlier fraction (1.8%) than the G+G+G model (0.8%). The lower-left plot of Figure 81 shows that the G$\otimes$(δ+E)+G model (dashed curve) does a slightly better job of accounting for the excess of events at large negative residual.

Table 33 shows the results of different lifetime fits to the semileptonic sample. The results are quoted as offsets from the generated lifetime ($\tau = 1.548$ ps). The first 2 columns give the results of fits to true Δt and Δz distributions. The true Δt fit reveals any bias introduced by the event selection. With the present MC statistics, there is no evidence of an event selection bias. The Δz fit also includes any bias due to the boost approximation, although the difference between these fits is probably an overestimate of the boost effects since some of these will be absorbed into the resolution model. Figure 80 shows these fits on log scales.

The remaining columns of Table 33 show the results of lifetime fits to the reconstructed Δt distributions. The first pair of columns show results of fits using the G+G+G model, and the second pair uses the G$\otimes$(δ+E)+G model. The first column of each pair is the result of a fit to the lifetime only, with the resolution model parameters fixed at the values given in Table 31 and 32. The second column is a fit to the same data but with the resolution parameters floating. The outlier scale is a free parameter in the fits to the full sample, but was fixed to the value obtained from MC truth in the fits to the subsamples: $S_3 = 8.8$ for the G+G+G model, and 6.1 for the G$\otimes$(δ+E)+G model. Figure 82 shows these fits to the full sample on linear (left-hand plots) and log scales (right-hand plots). The solid curves are the G+G+G fits and the dashed curves are G$\otimes$(δ+E)+G fits. The upper two plots are fits to the lifetime only, and the bottom two plots are the full fits to lifetime and the resolution parameters.

Figure 83 compares the results of the full fits using the two resolution models. There is good agreement in the changes to the lifetime observed using different subsamples, although the G+G+G results are systematically lower by about 50 fs, and have larger errors. Using these results, we could conservatively estimate a systematic error due to the choice of resolution model of $\pm 25fs$, which would be comparable to the expected statistical error for the Run-1 semileptonic sample. Otherwise, we could argue that the G$\otimes$(δ+E)+G model is intrinsically better (which is supported by toy MC studies) and calculate a smaller systematic.

Sample	prob(χ^2)	Mean(ps)	RMS(ps)	Δ_1 (ps)	S_1	Δ_2 (ps)	S_2	S_3	F_1	F_3
All Combined	0.3%	-0.1683	1.391	-0.112	1.118	-0.65	2.34	8.8	0.887	0.0078
				±0.011	±0.020	±0.11	±0.19	±1.3	±0.024	±0.0022
Electrons	1.0%	-0.1568	1.411	-0.100	1.108	-0.53	2.08	9.7	0.860	0.0075
				±0.017	±0.033	±0.13	±0.20	±1.9	±0.046	±0.0022
Muons	0.4%	-0.1844	1.363	-0.123	1.128	-0.84	2.72	8.2	0.907	0.0062
				±0.014	±0.028	±0.22	±0.39	±2.0	±0.027	±0.0042
SVT only	0.7%	-0.1769	1.38	-0.123	1.139	-0.78	2.62	10.5	0.913	0.0044
				±0.011	±0.021	±0.16	±0.27	±2.6	±0.021	±0.0020
SVT+DCH	64.3%	-0.1447	1.448	-0.055	1.046	-0.48	1.74	7.0	0.765	0.0207
				±0.035	±0.058	±0.19	±0.21	±1.2	±0.100	±0.0070
$D^0 \rightarrow$ Kπ	1.1×10^{-5}	-0.1678	1.301	-0.107	1.120	-0.58	2.03	6.6	0.861	0.0100
				±0.019	±0.032	±0.14	±0.22	±1.1	±0.049	±0.0040
$D^0 \rightarrow$ K3π	59.5%	-0.1896	1.747	-0.132	1.164	-1.20	3.50	23.000	0.943	0.0030
				±0.016	±0.023	±0.27	±0.34	*at limit*	±0.012	±0.0018
$D^0 \rightarrow$ K$\pi\pi^0$	85.7%	-0.1618	1.517	-0.092	0.995	-0.39	2.12	9.0	0.758	0.0082
				±0.026	±0.055	±0.11	±0.22	±3.1	±0.069	±0.0049
$D^0 \rightarrow K^0_S\pi\pi$	65.4%	-0.08123	1.008	0.087	0.875	-0.89	1.13	3.2	0.80	0.026
				±0.081	±0.080	±0.39	±0.34	±1.7	±0.12	±0.042
Reco'd B^0	3.3%	-0.185	1.459	-0.123	1.156	-1.23	3.17	12.6	0.939	0.0040
				±0.013	±0.019	±0.24	±0.42	±4.9	±0.013	±0.0027
Reco'd $\overline{B}$	17.3%	-0.1625	1.315	-0.113	1.089	-0.428	2.10	7.7	0.833	0.0067
				±0.016	±0.032	±0.094	±0.18	±1.6	±0.045	±0.0029
B^0Tag	4.8%	-0.1781	1.33	-0.118	1.188	-1.56	3.80	10.8	0.9550	0.0029
				±0.013	±0.021	±0.38	±0.43	±4.2	±0.0094	±0.0024
$\overline{B}$Tag	45.6%	-0.1464	1.399	-0.079	1.114	-0.51	2.11	9.7	0.836	0.0075
				±0.023	±0.049	±0.15	±0.29	±2.5	±0.070	±0.0036
Lepton Tag	10.7%	-0.07173	1.349	-0.03	1.101	-0.9	1.12	6.3	0.92	0.027
				±0.12	±0.080	±1.1	±0.44	±1.2	±0.19	±0.010
Kaon Tag	54.7%	-0.1799	1.288	-0.089	0.96	-0.302	1.62	6.7	0.56	0.0113
				±0.040	±0.12	±0.077	±0.17	±1.2	±0.20	±0.0043
NT1 Tag					*fit failed*					
NT2 Tag	4.2%	-0.189	2.148	-0.119	1.203	-1.16	3.52	23.00	0.928	0.0051
				±0.024	±0.033	±0.35	±0.47	*at limit*	±0.019	±0.0036
No Tag	11.0%	-0.2247	1.334	-0.139	1.051	-0.79	1.91	4.9	0.853	0.0136
				±0.030	±0.037	±0.22	±0.30	±1.1	±0.054	±0.0099

Table 31: Results of fitting a G+G+G hybrid resolution model to the semileptonic signal MC samples.

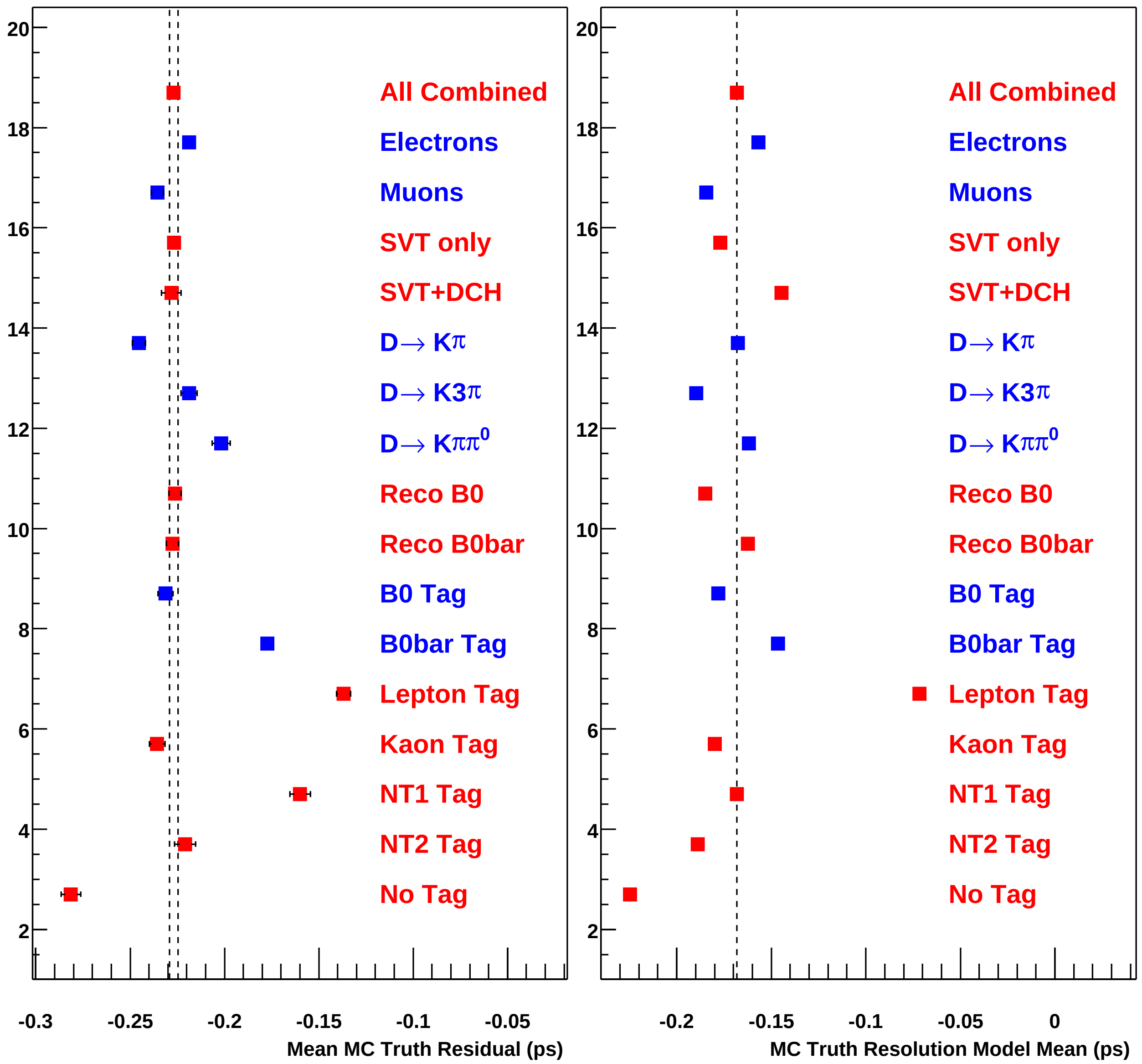

Figure 78: Comparison of mean residuals in the semileptonic signal MC sample, calculated directly from MC truth (left-hand side) or calculated from models fit to MC truth (right-hand side).

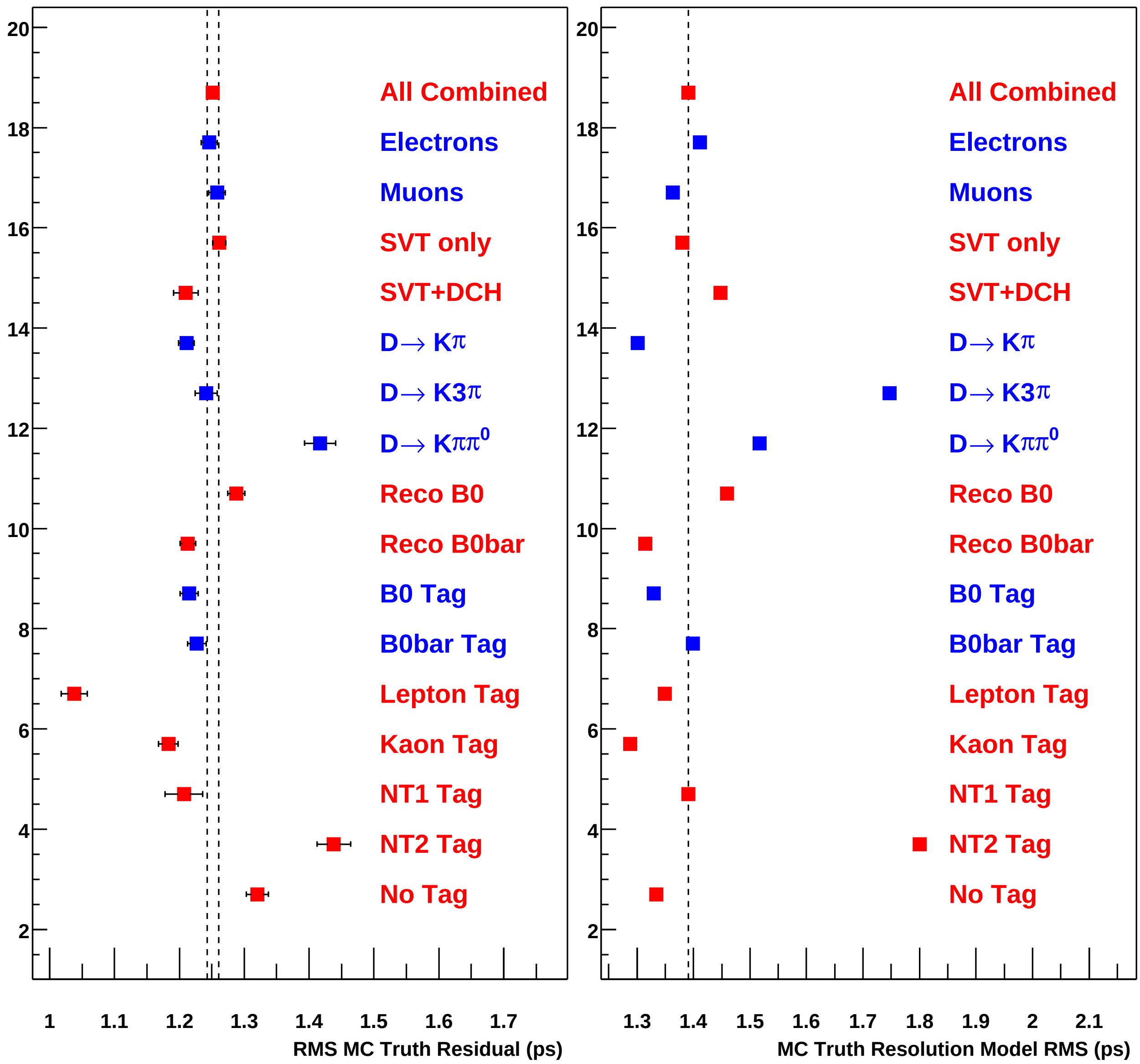

Figure 79: Comparison of RMS of residuals in the semileptonic signal MC sample, calculated directly from MC truth (left-hand side) or calculated from models fit to MC truth (right-hand side).

Sample	prob(χ^2)	Scale	Fraction	τ_{eff}	Outlier Scale	Outlier Fraction
All Combined	18.4%	1.093	0.688	0.915	6.13	0.0178
		±0.011	±0.025	±0.064	±0.46	±0.0031
Electrons	22.5%	1.109	0.696	0.892	7.45	0.0115
		±0.016	±0.034	±0.079	±0.93	±0.0029
Muons	1.7%	1.073	0.674	0.926	5.20	0.0266
		±0.017	±0.038	±0.099	±0.46	±0.0059
SVT only	20.8%	1.097	0.694	0.934	6.14	0.0155
		±0.013	±0.028	±0.073	±0.57	±0.0034
SVT+DCH	83.9%	1.079	0.681	0.89	6.29	0.0247
		±0.026	±0.054	±0.13	±0.85	±0.0067
$D^0 \to$ Kπ	1.5%	1.097	0.630	0.808	5.10	0.0198
		±0.017	±0.039	±0.076	±0.53	±0.0049
$D^0 \to$ K3π	71.7%	1.088	0.702	0.96	7.6	0.0179
		±0.021	±0.052	±0.16	±1.0	±0.0055
$D^0 \to$ K$\pi\pi^0$	92.7%	1.093	0.752	1.11	5.46	0.025
		±0.032	±0.048	±0.17	±0.97	±0.011
$D^0 \to K^0_S\pi\pi$	70.8%	0.68	0.32	1.45	1.11	0.54
		±0.21	±0.38	±0.48	±0.22	±0.38
Reco'd B^0	33.9%	1.081	0.724	1.05	7.13	0.0154
		±0.015	±0.031	±0.10	±0.78	±0.0038
Reco'd $\overline{B}$	63.5%	1.101	0.645	0.802	4.91	0.0222
		±0.018	±0.041	±0.080	±0.53	±0.0059
B^0Tag	24.6%	1.104	0.661	0.80	6.20	0.0247
		±0.020	±0.057	±0.12	±0.68	±0.0061
$\overline{B}$Tag	67.8%	1.140	0.738	1.00	7.1	0.0136
		±0.020	±0.038	±0.12	±1.0	±0.0044
Lepton Tag	20.8%	1.093	0.77	0.62	6.2	0.0275
		±0.029	±0.12	±0.30	±1.0	±0.0092
Kaon Tag	71.6%	1.119	0.614	0.836	5.66	0.0157
		±0.022	±0.048	±0.089	±0.82	±0.0053
NT1 Tag	72.3%	1.109	0.65	0.58	3.92	0.057
		±0.048	±0.18	±0.34	±0.62	±0.022
NT2 Tag	7.8%	1.150	0.779	1.32	9.5	0.0141
		±0.029	±0.049	±0.25	±1.9	±0.0059
No Tag	15.3%	1.022	0.641	0.918	4.38	0.0174
		±0.020	±0.041	±0.089	±0.66	±0.0064

Table 32: Results of fitting a G⊗(δ+E)+G resolution model to the semileptonic signal MC samples.

Sample	True Δt Fit	True Δz Fit	G+G+G τ Only	G+G+G τ+Resln	G$\otimes$(δ+E)+G τ Only	G$\otimes$(δ+E)+G τ+Resln
All Combined	-0.013 ± 0.015	-0.004 ± 0.015	-0.022 ± 0.018	-0.057 ± 0.036	-0.026 ± 0.018	-0.007 ± 0.029
Electrons	-0.014 ± 0.021	-0.006 ± 0.021	-0.025 ± 0.026	-0.059 ± 0.044	-0.027 ± 0.026	-0.019 ± 0.038
Muons	-0.012 ± 0.022	-0.002 ± 0.022	-0.018 ± 0.027	-0.032 ± 0.048	-0.023 ± 0.026	0.015 ± 0.044
SVT only	-0.021 ± 0.017	-0.013 ± 0.017	-0.025 ± 0.021	-0.031 ± 0.035	-0.030 ± 0.020	0.000 ± 0.034
SVT+DCH	0.020 ± 0.036	0.034 ± 0.036	-0.011 ± 0.042	0.000 ± 0.073	-0.011 ± 0.042	0.018 ± 0.072
$D^0 \to$ Kπ	0.004 ± 0.021	0.014 ± 0.021	0.005 ± 0.026	-0.043 ± 0.043	0.000 ± 0.026	-0.017 ± 0.041
$D^0 \to$ K3π	-0.049 ± 0.029	-0.043 ± 0.029	-0.067 ± 0.035	-0.016 ± 0.063	-0.065 ± 0.035	0.019 ± 0.044
$D^0 \to$ K$\pi\pi^0$	0.012 ± 0.037	0.025 ± 0.038	0.005 ± 0.046	0.058 ± 0.072	0.002 ± 0.046	0.065 ± 0.060
$D^0 \to K_S^0\pi\pi$	-0.11 ± 0.10	-0.12 ± 0.10	-0.22 ± 0.11	-0.48 ± 0.14	-0.24 ± 0.11	-0.25 ± 0.16
Reco'd B^0	-0.027 ± 0.021	-0.019 ± 0.021	-0.035 ± 0.026	-0.102 ± 0.049	-0.031 ± 0.026	-0.030 ± 0.042
Reco'd $\overline{B}$	0.001 ± 0.022	0.011 ± 0.022	-0.013 ± 0.026	0.023 ± 0.044	-0.021 ± 0.026	0.030 ± 0.041
B^0Tag	-0.008 ± 0.026	0.005 ± 0.026	-0.032 ± 0.031	-0.112 ± 0.050	-0.027 ± 0.031	-0.042 ± 0.046
$\overline{B}$Tag	-0.022 ± 0.026	-0.018 ± 0.026	-0.016 ± 0.031	-0.047 ± 0.057	-0.021 ± 0.031	-0.007 ± 0.056
Lepton Tag	-0.056 ± 0.040	-0.054 ± 0.040	-0.078 ± 0.047	-0.057 ± 0.083	-0.082 ± 0.047	-0.041 ± 0.077
Kaon Tag	0.027 ± 0.027	0.036 ± 0.027	0.022 ± 0.032	0.008 ± 0.061	0.019 ± 0.032	0.014 ± 0.058
NT1 Tag	-0.076 ± 0.050	-0.078 ± 0.050	-0.089 ± 0.059	*fit failed*	-0.090 ± 0.059	-0.071 ± 0.078
NT2 Tag	-0.036 ± 0.038	-0.017 ± 0.039	-0.038 ± 0.049	-0.084 ± 0.095	-0.030 ± 0.049	0.032 ± 0.063
No Tag	-0.008 ± 0.028	0.002 ± 0.028	-0.020 ± 0.035	-0.025 ± 0.059	-0.021 ± 0.034	0.017 ± 0.055

Table 33: Results of lifetime fits to semileptonic signal MC samples.

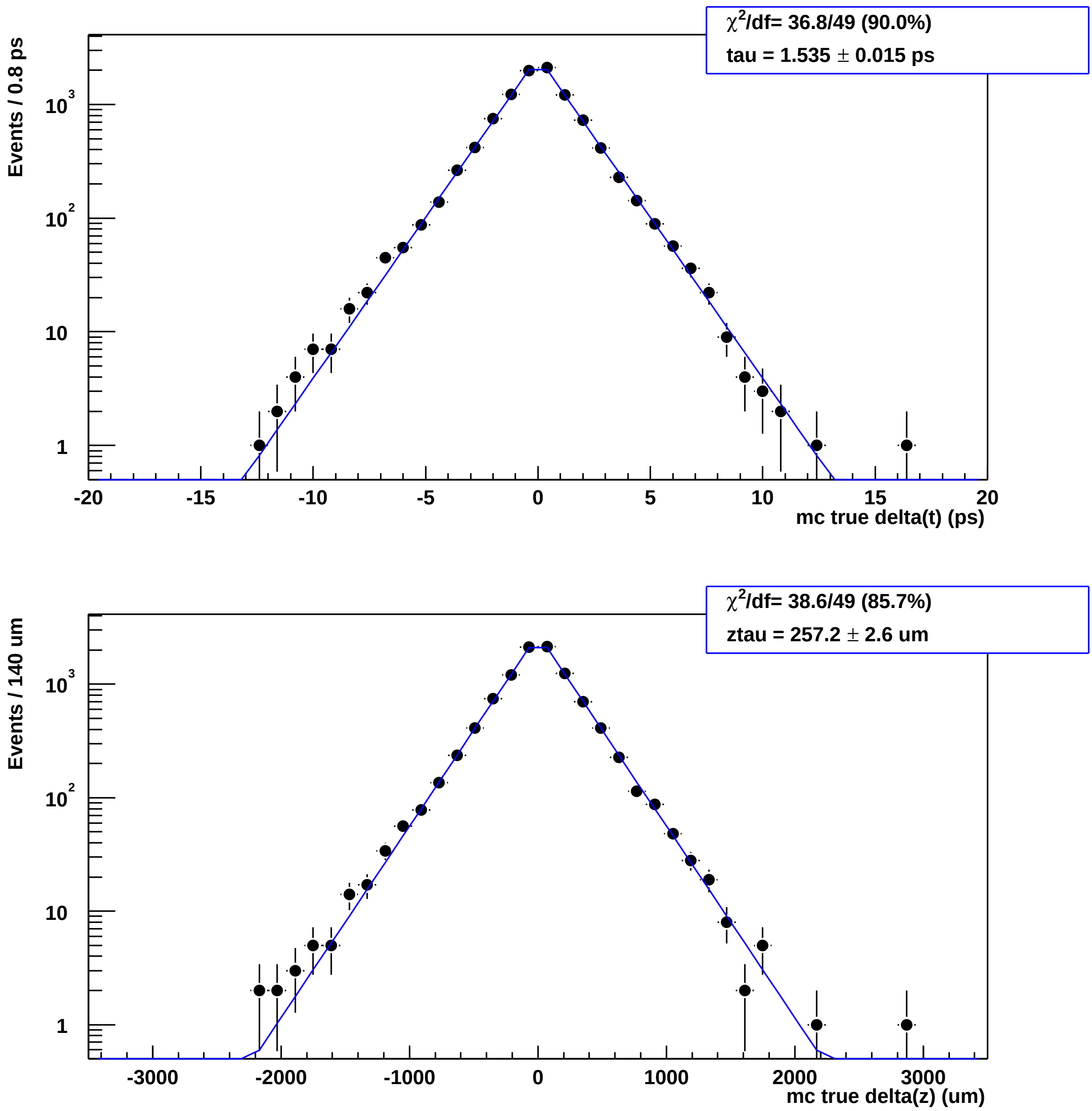

Figure 80: Fits to semileptonic sample MC truth Δt and Δz. See the text for details.

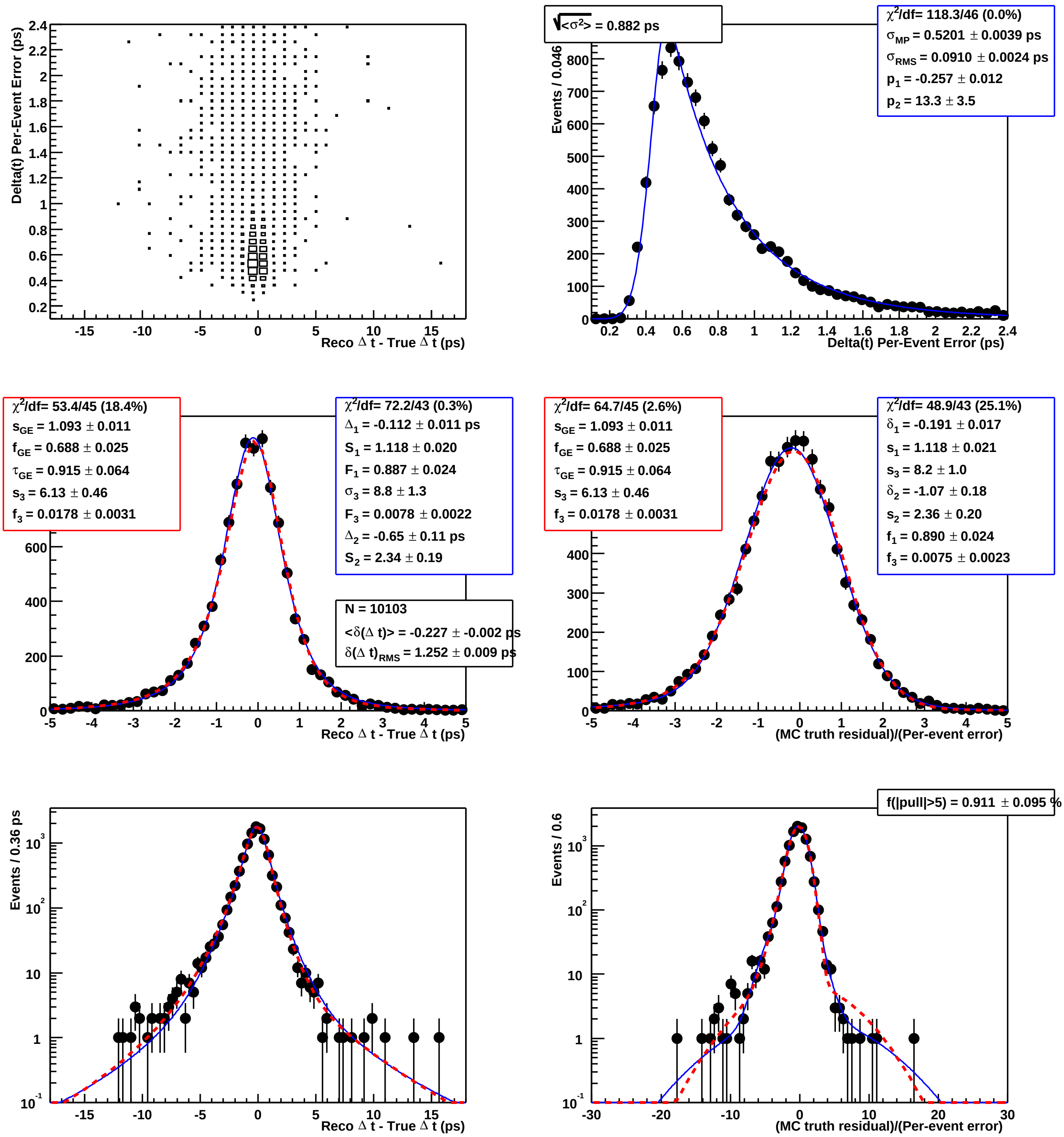

Figure 81: Fits to MC truth resolution in semileptonic signal MC. See the text for details.

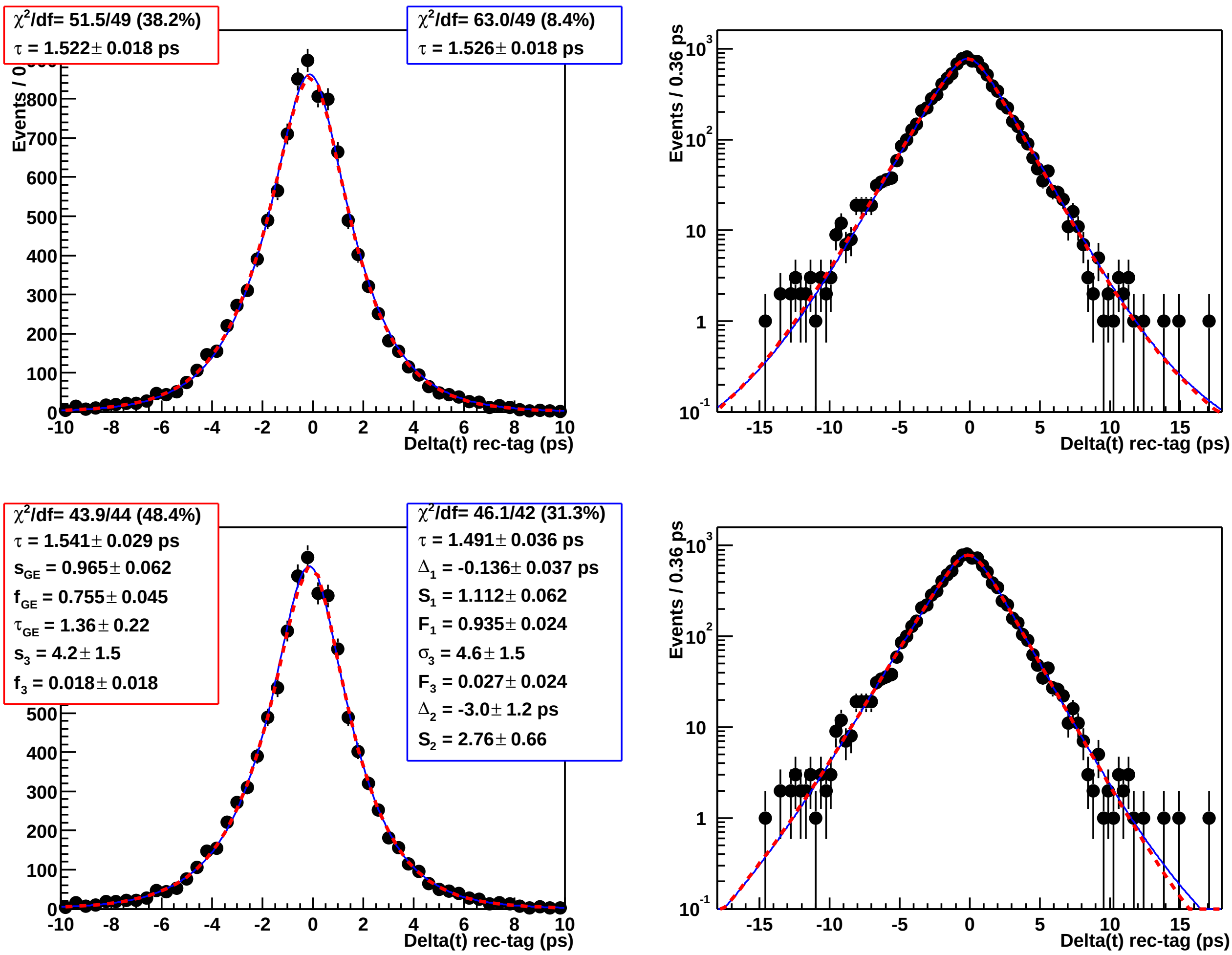

Figure 82: Lifetime Fits to Reconstructed Δt in semileptonic signal MC. See the text for details.

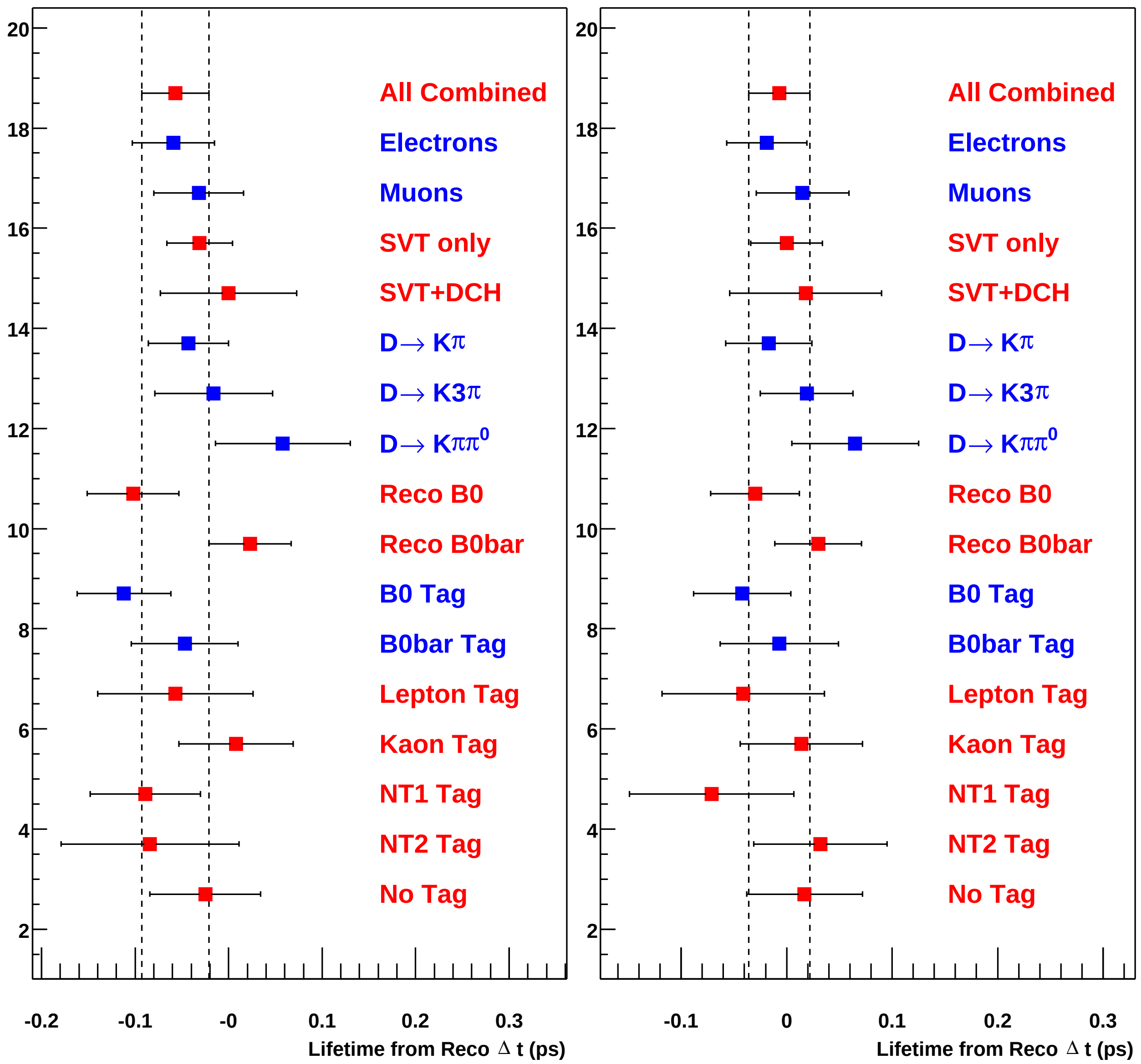

Figure 83: Comparison of lifetimes fitted using either the G+G+G (left-hand side) or G⊗(δ+E)+G (right-hand side) resolution model. Both the lifetime and the resolution model parameters are free in the fit.

5.5 Hadronic Fit Results

The fits to the hadronic sample show many of the same features as the fits to the semileptonic sample. The main features to note are:

- The χ^2 probabilities are generally very small for these fits, presumably due to the large statistics. The G$\otimes$(δ+E)+G model again gives larger probabilities, although still small.
- The mean and RMS calculated from the fits show similar systematic effects to those seen in the semileptonic sample.
- The outlier fraction obtained using either resolution model is slightly higher than in the semileptonic sample, in agreement with the larger fraction of events with pulls > 5.
- There is no evidence for an event selection bias (at the 1.2σ level).

5.6 Summary

Table 37 compares the results of G+G+G fits to different samples and with different outlier models. The first row quotes the resolution parameters used for the Osaka mixing analysis. The next 4 rows are fits to the semileptonic sample: the first pair of rows are fits using an absolute outlier width (as in the Osaka model), and the second pair uses a scaled outlier width (as in the fits used here). The first fit of each pair repeats the resolution parameters obtained on the full sample from a fit to MC truth residuals, and (in the first column) the lifetime (relative to the generated value) obtained from a fit to reconstructed Δt with the resolution parameters fixed to these values. The second fit of each pair gives the results of a full fit to the same data to the lifetime and resolution parameters. The last four rows give results of the same fits to the full hadronic sample.

A comparison of the default (scaled outliers) fits to the semileptonic and hadronic samples shows good agreement for each parameter for both types of fit, but also systematic shifts in the resolution parameters between the two types of fit.

Both types of fits (to MC-truth residuals and a full lifetime fit to reconstructed Δt) give results that are in good statistical agreement between the semileptonic and hadronic samples, but there are systematic shifts in the parameter values between the fits. The solid curves in Figures 82 (semileptonic) and 88 (hadronic) show the different G+G+G resolution models convoluted with the lifetime.

Table 38 compares a similar set of fits (always used a scaled outlier component) with the G$\otimes$(δ+E)+G model. Again, there is good agreement between the semileptonic and hadronic samples. The dashed curves in Figures 82 (semileptonic) and 88 (hadronic) show the different G$\otimes$(δ+E)+G resolution models convoluted with the lifetime.

Sample	prob(χ^2)	Mean(ps)	RMS(ps)	Δ_1 (ps)	S_1	Δ_2 (ps)	S_2	S_3	F_1	F_3
All Combined	4.3×10^{-19}	-0.1555	1.379	-0.1010	1.0752	-0.559	2.305	8.69	0.8686	0.0103
				±0.0040	±0.0082	±0.035	±0.074	±0.45	±0.0098	±0.0011
π Modes	2.4×10^{-11}	-0.1496	1.37	-0.0966	1.075	-0.555	2.39	9.60	0.873	0.0092
				±0.0052	±0.011	±0.047	±0.10	±0.74	±0.012	±0.0014
ρ Modes	3.8×10^{-4}	-0.1597	1.386	-0.092	1.043	-0.486	1.91	7.12	0.809	0.0151
				±0.010	±0.020	±0.059	±0.12	±0.53	±0.034	±0.0024
a_1 Modes	7.3%	-0.164	1.392	-0.1156	1.093	-0.585	2.52	8.7	0.886	0.0085
				±0.0088	±0.017	±0.087	±0.20	±1.3	±0.018	±0.0027
$D^{*\pm}$ Modes	4.6×10^{-9}	-0.157	1.369	-0.0993	1.070	-0.537	2.17	8.33	0.854	0.0113
				±0.0066	±0.013	±0.050	±0.11	±0.60	±0.018	±0.0017
$D^{\pm}$Modes	5.4×10^{-7}	-0.1541	1.388	-0.1013	1.077	-0.573	2.41	9.00	0.877	0.0095
				±0.0051	±0.010	±0.049	±0.10	±0.67	±0.011	±0.0014
Reco'd B^0	3.3×10^{-7}	-0.1496	1.384	-0.0946	1.052	-0.488	2.206	8.11	0.845	0.0122
				±0.0057	±0.012	±0.042	±0.089	±0.53	±0.015	±0.0016
Reco'd $\overline{B}$	7.8×10^{-10}	-0.1616	1.376	-0.1081	1.097	-0.646	2.43	9.50	0.890	0.0083
				±0.0055	±0.010	±0.056	±0.11	±0.80	±0.011	±0.0014
B^0Tag	1.2×10^{-5}	-0.1411	1.259	-0.0862	1.061	-0.440	2.047	7.21	0.829	0.0123
				±0.0072	±0.017	±0.048	±0.099	±0.53	±0.024	±0.0020
$\overline{B}$Tag	1.3×10^{-4}	-0.1411	1.29	-0.0946	1.089	-0.532	2.49	9.6	0.885	0.0070
				±0.0060	±0.013	±0.059	±0.14	±1.1	±0.014	±0.0016
Lepton Tag	25.5%	-0.07986	1.144	-0.058	0.996	-0.181	1.82	6.01	0.79	0.0172
				±0.012	±0.054	±0.065	±0.32	±0.77	±0.11	±0.0060
Kaon Tag	2.6×10^{-5}	-0.1703	1.27	-0.1165	1.121	-0.599	2.38	8.98	0.880	0.0071
				±0.0067	±0.014	±0.061	±0.12	±0.95	±0.015	±0.0015
NT1 Tag	43.0%	-0.1044	1.398	-0.050	0.953	-0.253	1.76	7.82	0.707	0.0192
				±0.015	±0.042	±0.050	±0.14	±0.86	±0.070	±0.0039
NT2 Tag	15.4%	-0.1577	1.336	-0.083	1.043	-0.582	2.02	7.44	0.836	0.0125
				±0.011	±0.020	±0.082	±0.11	±0.83	±0.026	±0.0027
No Tag	0.2%	-0.2058	1.615	-0.1345	1.070	-0.828	2.42	9.84	0.883	0.0118
				±0.0081	±0.013	±0.086	±0.14	±0.97	±0.013	±0.0020

Table 34: Results of fitting a G+G+G hybrid resolution model to the hadronic signal MC samples.

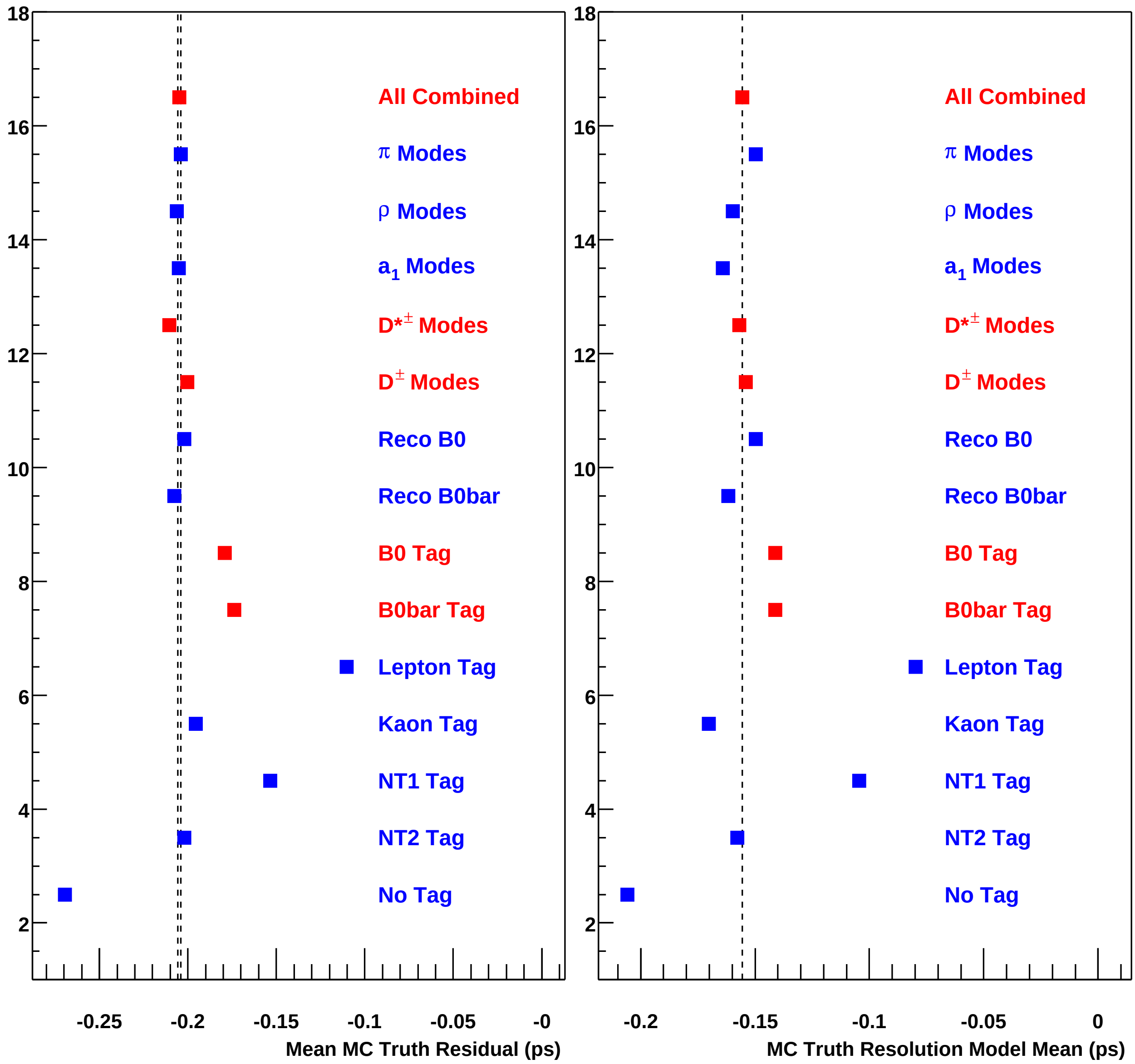

Figure 84: Comparison of mean residuals in the hadronic signal MC sample, calculated directly from MC truth (left-hand side) or calculated from models fit to MC truth (right-hand side).

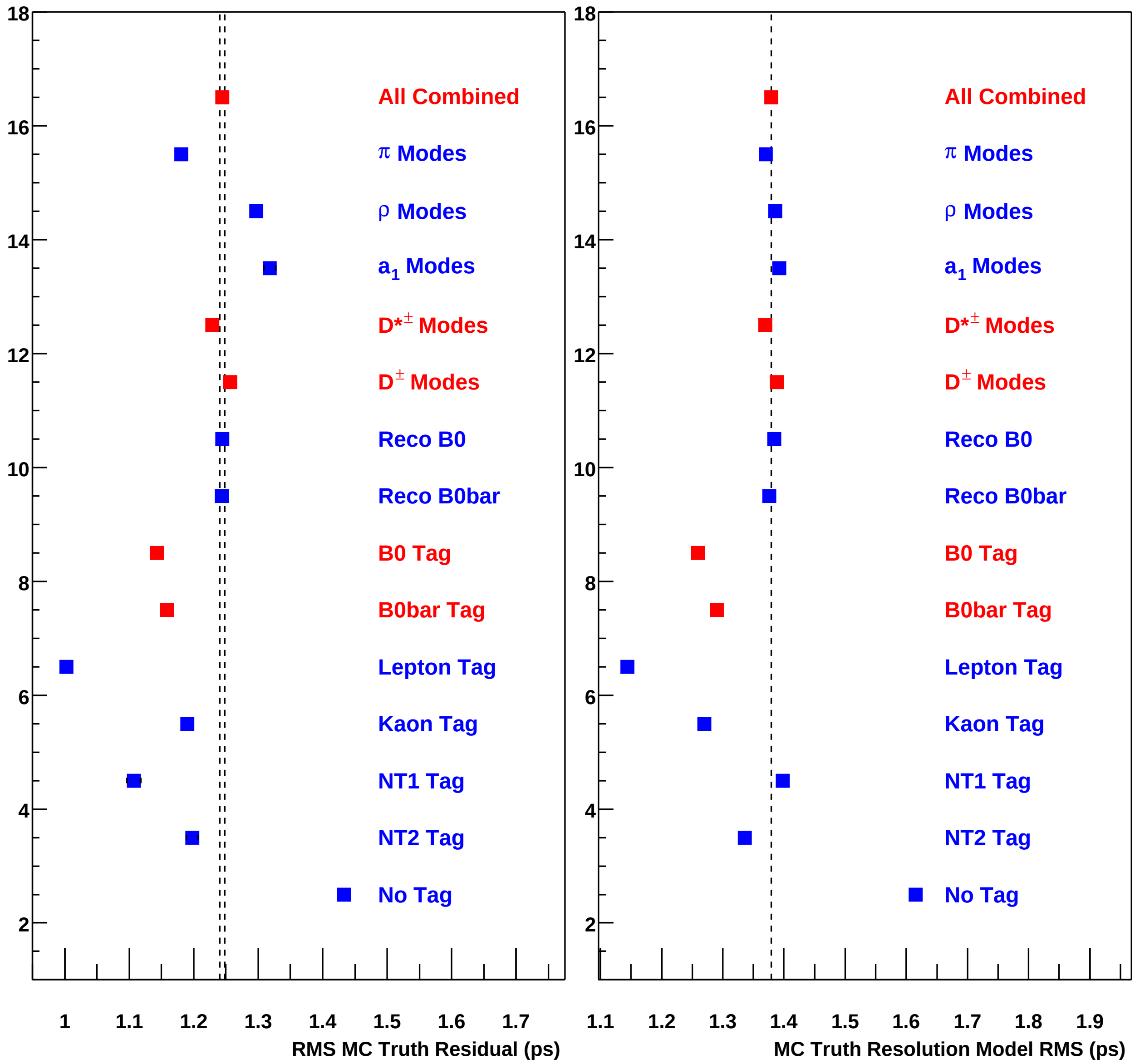

Figure 85: Comparison of RMS of residuals in the hadronic signal MC sample, calculated directly from MC truth (left-hand side) or calculated from models fit to MC truth (right-hand side).

Sample	prob(χ^2)	Scale	Fraction	τ_{eff}	Outlier Scale	Outlier Fraction
All Combined	7.4×10^{-7}	1.0617	0.6995	0.973	6.45	0.0201
		$\pm$0.0048	$\pm$0.0096	$\pm$0.026	$\pm$0.19	$\pm$0.0013
π Modes	2.1×10^{-4}	1.0582	0.709	1.025	6.96	0.0186
		$\pm$0.0068	$\pm$0.013	$\pm$0.037	$\pm$0.30	$\pm$0.0017
ρ Modes	12.2%	1.0592	0.680	0.907	5.98	0.0214
		$\pm$0.0087	$\pm$0.018	$\pm$0.044	$\pm$0.31	$\pm$0.0024
a_1 Modes	4.4%	1.074	0.701	0.941	5.80	0.0235
		$\pm$0.012	$\pm$0.024	$\pm$0.066	$\pm$0.39	$\pm$0.0037
$D^{*\pm}$ Modes	1.1%	1.0635	0.690	0.959	6.53	0.0191
		$\pm$0.0072	$\pm$0.014	$\pm$0.038	$\pm$0.30	$\pm$0.0019
$D^{\pm}$Modes	3.8×10^{-4}	1.0603	0.708	0.986	6.38	0.0210
		$\pm$0.0065	$\pm$0.013	$\pm$0.037	$\pm$0.25	$\pm$0.0018
Reco'd B^0	8.6×10^{-4}	1.0557	0.705	0.980	6.14	0.0229
		$\pm$0.0070	$\pm$0.013	$\pm$0.038	$\pm$0.25	$\pm$0.0020
Reco'd $\overline{B}$	0.4%	1.0667	0.693	0.966	6.77	0.0178
		$\pm$0.0067	$\pm$0.014	$\pm$0.037	$\pm$0.30	$\pm$0.0017
B^0Tag	1.2×10^{-4}	1.0752	0.703	0.950	5.81	0.0206
		$\pm$0.0084	$\pm$0.017	$\pm$0.045	$\pm$0.30	$\pm$0.0024
$\overline{B}$Tag	3.4%	1.0716	0.705	0.937	6.18	0.0212
		$\pm$0.0084	$\pm$0.017	$\pm$0.047	$\pm$0.31	$\pm$0.0024
Lepton Tag	31.4%	1.046	0.741	0.748	4.77	0.0328
		$\pm$0.014	$\pm$0.036	$\pm$0.097	$\pm$0.34	$\pm$0.0054
Kaon Tag	2.3×10^{-4}	1.0978	0.668	0.939	6.23	0.0176
		$\pm$0.0086	$\pm$0.018	$\pm$0.042	$\pm$0.35	$\pm$0.0022
NT1 Tag	14.7%	1.048	0.721	0.916	6.46	0.0285
		$\pm$0.017	$\pm$0.033	$\pm$0.094	$\pm$0.54	$\pm$0.0049
NT2 Tag	29.3%	1.054	0.726	1.054	6.31	0.0169
		$\pm$0.012	$\pm$0.022	$\pm$0.070	$\pm$0.53	$\pm$0.0031
No Tag	7.6%	1.0334	0.685	1.029	7.29	0.0194
		$\pm$0.0083	$\pm$0.016	$\pm$0.045	$\pm$0.38	$\pm$0.0020

Table 35: Results of fitting a G$\otimes$(δ+E)+G resolution model to the hadronic signal MC samples.

			G+G+G		G⊗(δ+E)+G	
Sample	True Δt Fit	True Δz Fit	τ Only	τ+Resln	τ Only	τ+Resln
All Combined	-0.0079 ± 0.0066	-0.0007 ± 0.0066	-0.0186 ± 0.0078	-0.025 ± 0.013	-0.0206 ± 0.0078	0.006 ± 0.012
π Modes	0.0038 ± 0.0094	0.0121 ± 0.0094	0.001 ± 0.011	-0.018 ± 0.019	-0.000 ± 0.011	0.022 ± 0.017
ρ Modes	-0.014 ± 0.012	-0.010 ± 0.012	-0.033 ± 0.014	-0.026 ± 0.024	-0.035 ± 0.014	-0.007 ± 0.021
a_1 Modes	-0.029 ± 0.015	-0.021 ± 0.015	-0.053 ± 0.018	-0.076 ± 0.029	-0.055 ± 0.018	-0.056 ± 0.027
$D^{*\pm}$ Modes	-0.0070 ± 0.0098	0.0009 ± 0.0098	-0.020 ± 0.012	-0.013 ± 0.019	-0.023 ± 0.012	0.010 ± 0.017
$D^{\pm}$Modes	-0.0087 ± 0.0089	-0.0021 ± 0.0090	-0.017 ± 0.011	-0.036 ± 0.018	-0.018 ± 0.011	-0.001 ± 0.016
Reco'd B^0	-0.0090 ± 0.0093	-0.0033 ± 0.0093	-0.023 ± 0.011	-0.038 ± 0.019	-0.025 ± 0.011	-0.004 ± 0.017
Reco'd $\overline{B}$	-0.0069 ± 0.0093	0.0018 ± 0.0094	-0.014 ± 0.011	-0.014 ± 0.020	-0.016 ± 0.011	0.016 ± 0.016
B^0Tag	-0.002 ± 0.011	0.005 ± 0.011	-0.018 ± 0.013	-0.066 ± 0.027	-0.020 ± 0.013	-0.019 ± 0.020
$\overline{B}$Tag	0.004 ± 0.011	0.011 ± 0.011	-0.008 ± 0.013	-0.001 ± 0.021	-0.010 ± 0.013	0.018 ± 0.019
Lepton Tag	0.051 ± 0.019	0.059 ± 0.019	0.039 ± 0.022	0.015 ± 0.031	0.037 ± 0.022	0.036 ± 0.031
Kaon Tag	-0.023 ± 0.011	-0.016 ± 0.011	-0.035 ± 0.013	-0.063 ± 0.024	-0.037 ± 0.013	-0.039 ± 0.021
NT1 Tag	-0.021 ± 0.022	-0.014 ± 0.023	-0.054 ± 0.026	-0.045 ± 0.044	-0.056 ± 0.026	-0.019 ± 0.040
NT2 Tag	0.025 ± 0.018	0.034 ± 0.018	0.015 ± 0.021	0.017 ± 0.035	0.011 ± 0.020	0.048 ± 0.027
No Tag	-0.028 ± 0.012	-0.021 ± 0.012	-0.034 ± 0.015	-0.049 ± 0.027	-0.035 ± 0.015	0.017 ± 0.023

Table 36: Results of lifetime fits to hadronic signal MC samples.

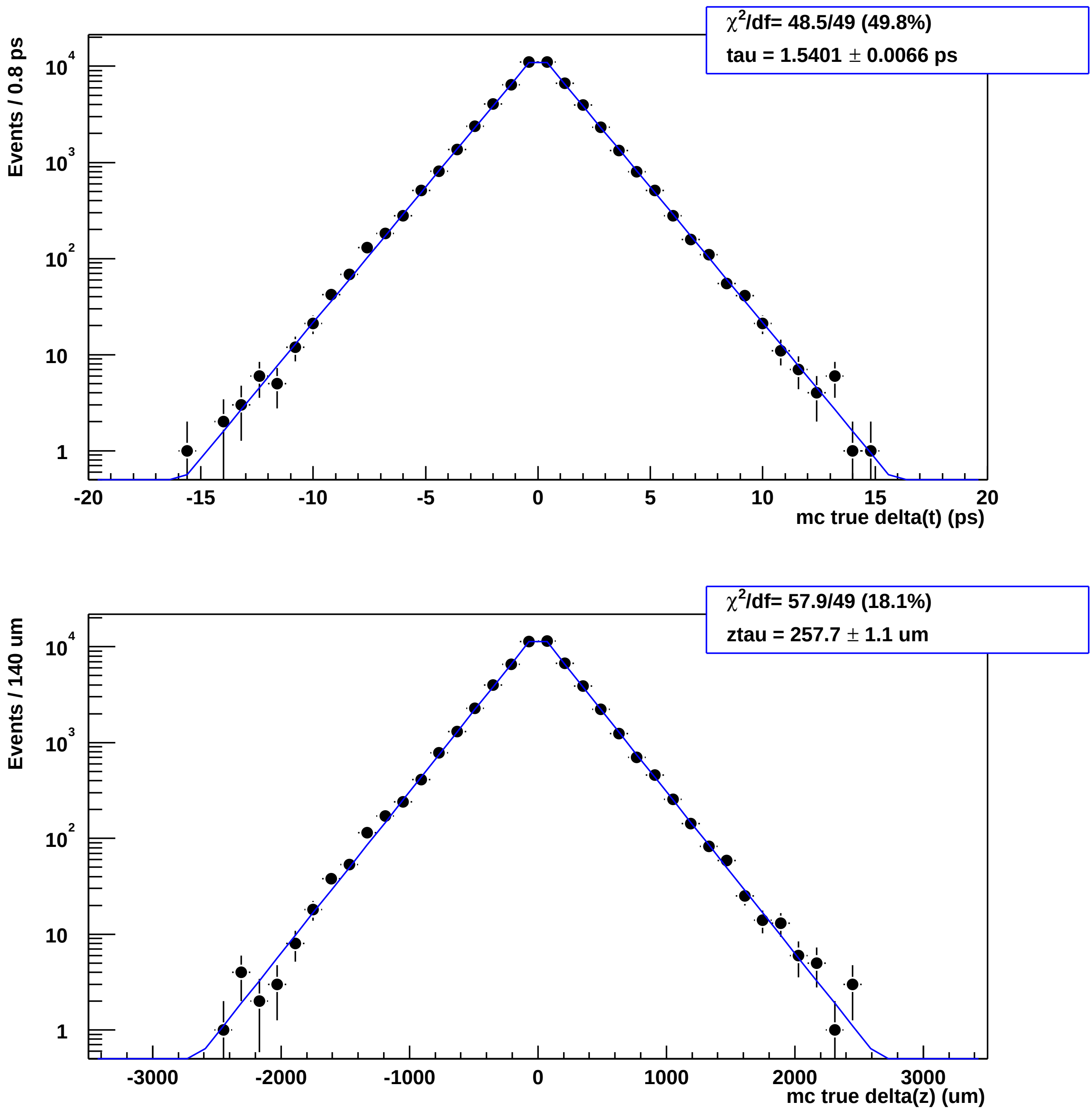

Figure 86: Fits to hadronic sample MC truth Δt and Δz. See the text for details.

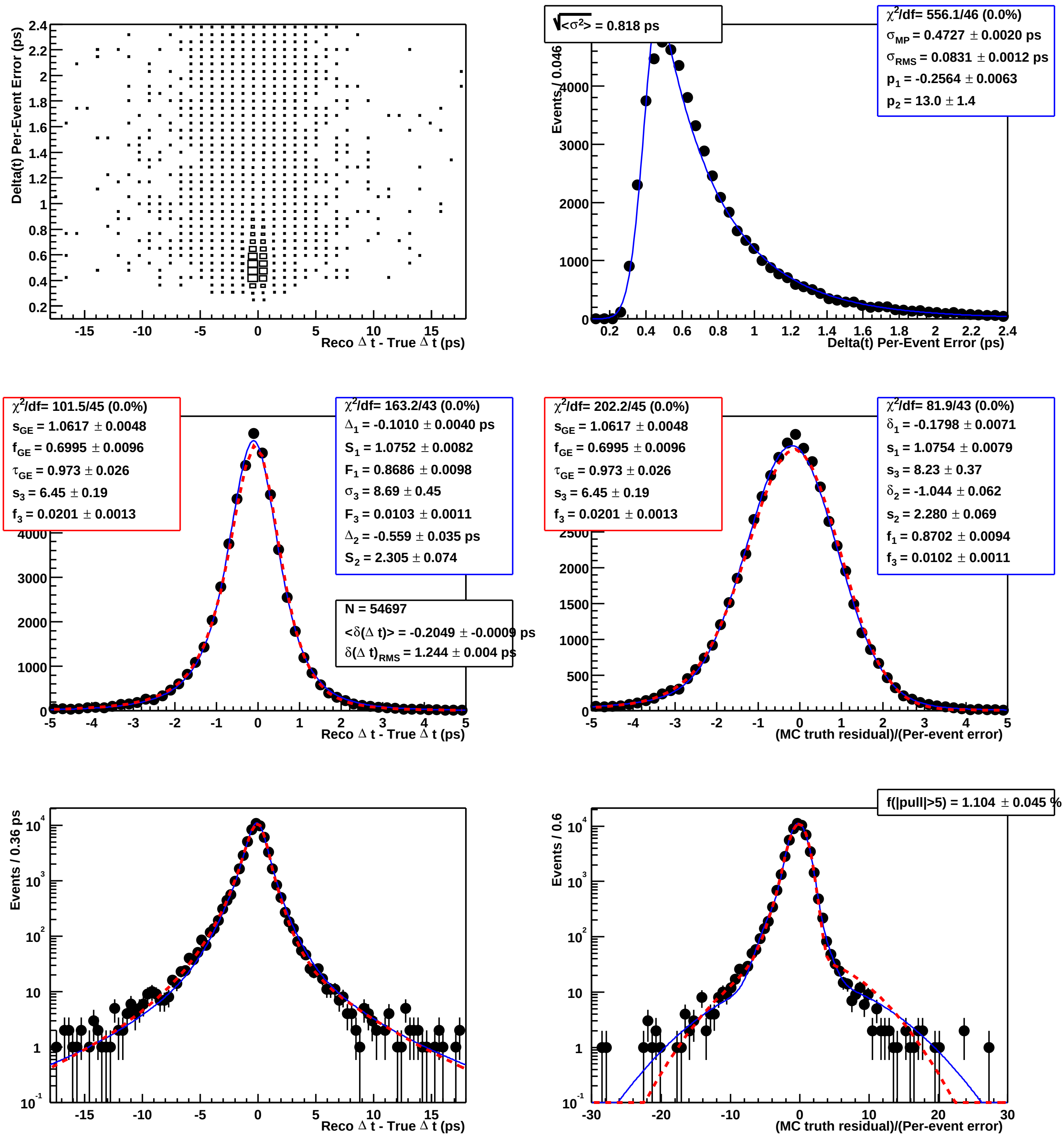

Figure 87: Fits to MC truth resolution in hadronic signal MC. See the text for details.

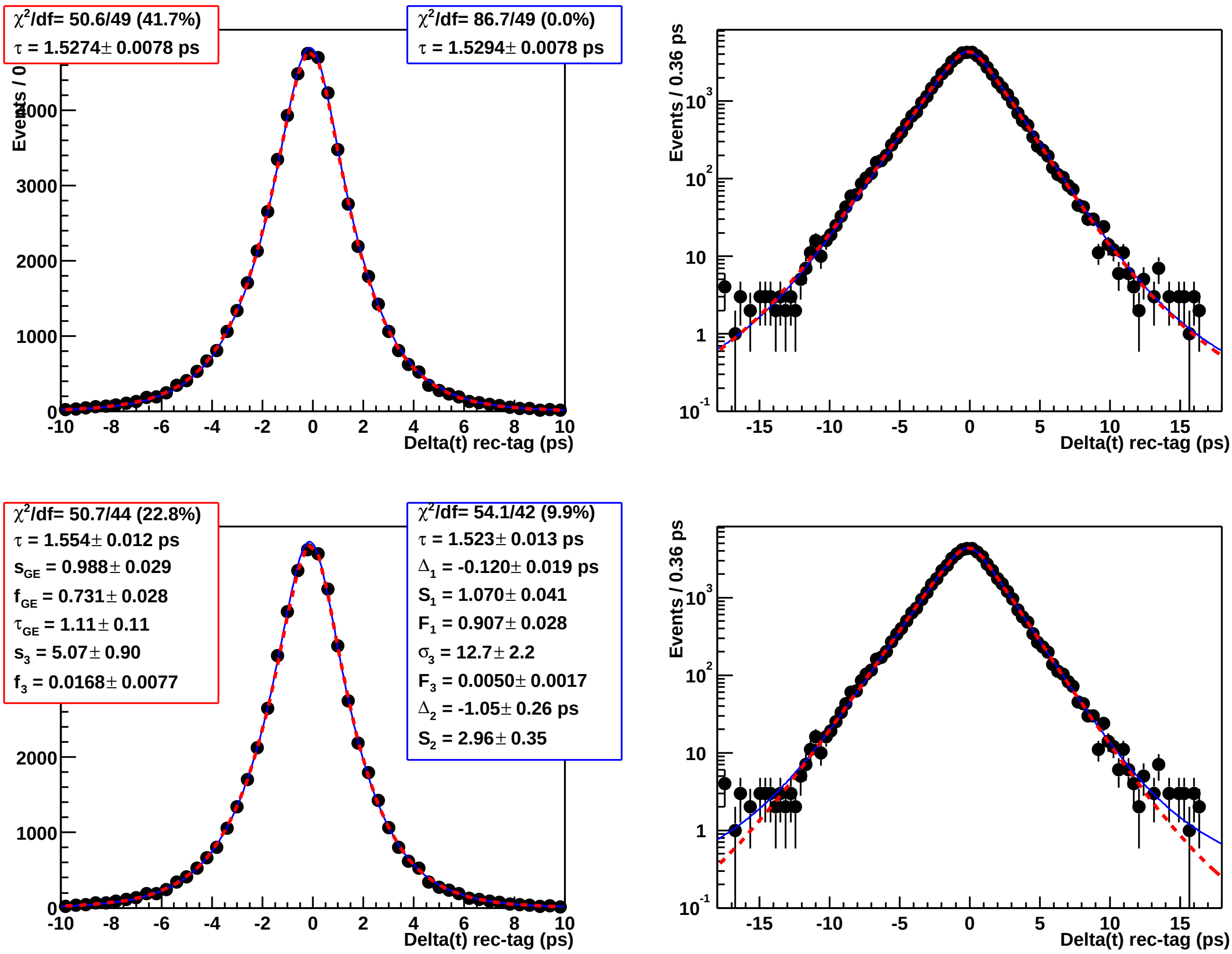

Figure 88: Lifetime Fits to Reconstructed Δt in hadronic signal MC. See the text for details.

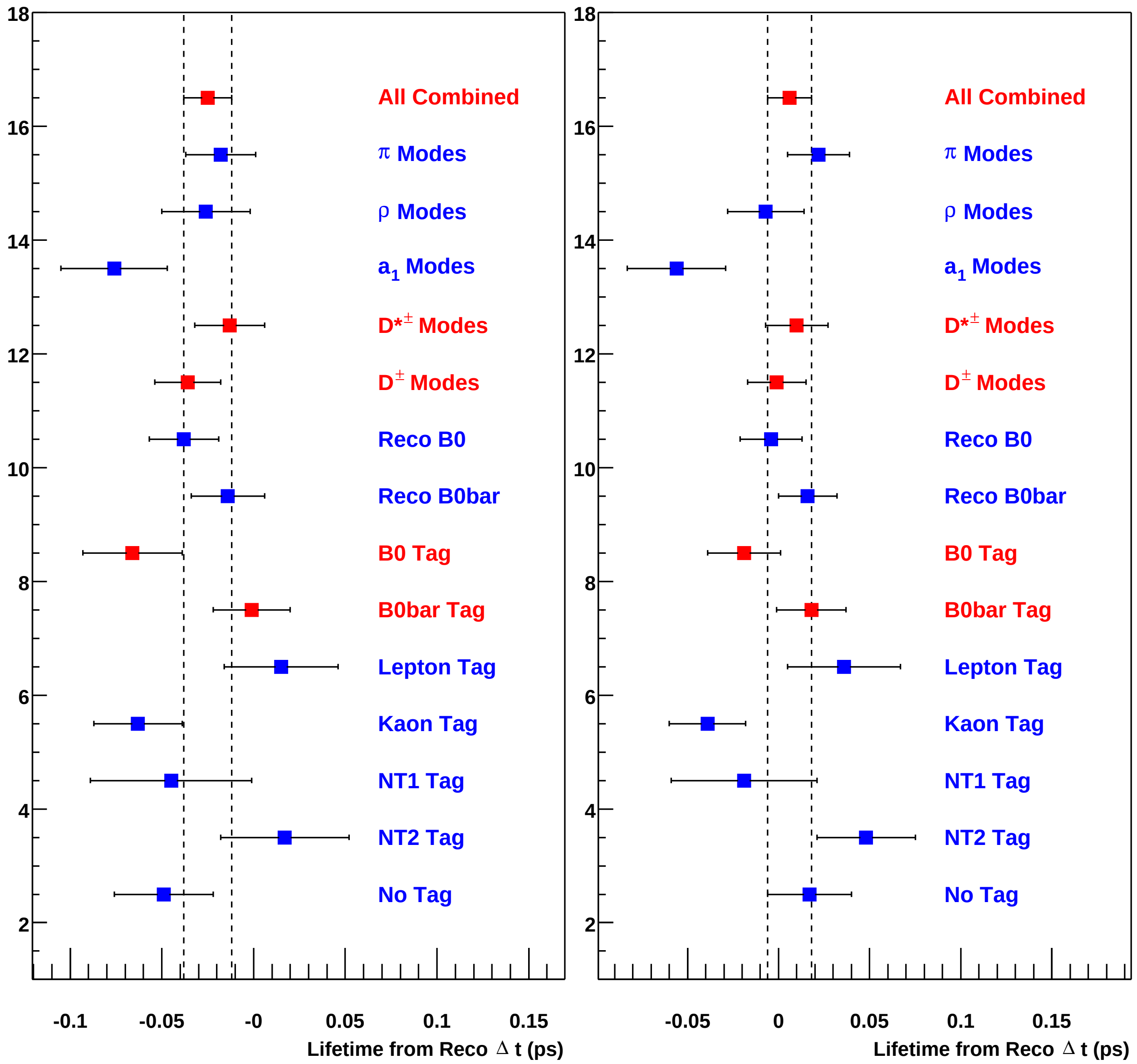

Figure 89: Comparison of lifetimes fitted using either the G+G+G (left-hand side) or G⊗(δ+E)+G (right-hand side) resolution model. Both the lifetime and the resolution model parameters are free in the fit.

Sample	$\delta\tau$ (ps)	Δ_1 (ps)	S_1	Δ_2 (ps)	S_2	S_3	F_1	F_3
Osaka Mixing Paper		-0.2	1.33	0	2.1	8 ps	0.75	?
Semileptonic Residuals Fit	-0.023	-0.113	1.122	-0.68	2.40	5.68 ps	0.892	0.0076
(fixed-width outliers)	±0.019	±0.010	±0.020	±0.12	±0.20	±0.68 ps	±0.023	±0.0021
Semileptonic Lifetime Fit	-0.096	-0.113	1.115	-1.89	3.04	4.8 ps	0.905	0.021
(fixed-width outliers)	±0.079	±0.037	±0.075	±0.77	±0.48	±1.5 ps	±0.048	±0.030
Semileptonic Residuals Fit	-0.022	-0.112	1.118	-0.65	2.34	8.8	0.887	0.0078
(scaled outliers)	±0.018	±0.011	±0.020	±0.11	±0.19	±1.3	±0.024	±0.0022
Semileptonic Lifetime Fit	-0.057	-0.136	1.112	-3.0	2.76	4.6	0.935	0.027
(scaled outliers)	±0.036	±0.037	±0.062	±1.2	±0.66	±1.5	±0.024	±0.024
Hadronic Residuals Fit	-0.0214	-0.1073	1.0911	-0.615	2.587	7.52 ps	0.8917	0.00649
(fixed-width outliers)	±0.0078	±0.0037	±0.0075	±0.038	±0.085	±0.52	±0.0075	±0.00077
Hadronic Lifetime Fit				*fit does not converge*				
(fixed-width outliers)								
Hadronic Residuals Fit	-0.0186	-0.1010	1.0752	-0.559	2.305	8.69	0.8686	0.0103
(scaled outliers)	±0.0078	±0.0040	±0.0082	±0.035	±0.074	±0.45	±0.0098	±0.0011
Hadronic Lifetime Fit	-0.025	-0.120	1.070	-1.05	2.96	12.7	0.907	0.0050
(scaled outliers)	±0.013	±0.019	±0.041	±0.26	±0.35	±2.2	±0.028	±0.0017

Table 37: Comparison between different sets of G+G+G resolution model parameters.

Sample	$\delta\tau$ (ps)	Scale	Fraction	τ_{eff}	Outlier Scale	Outlier Fraction
Osaka Lifetime Paper		1.012	0.643	0.936		
		±0.016	±0.029	±0.062		
Semileptonic Residuals Fit	-0.026	1.093	0.688	0.915	6.13	0.0178
	±0.018	±0.011	±0.025	±0.064	±0.46	±0.0031
Semileptonic Lifetime Fit	-0.007	0.965	0.755	1.36	4.2	0.018
	±0.029	±0.062	±0.045	±0.22	±1.5	±0.018
Hadronic Residuals Fit	-0.0206	1.0617	0.6995	0.973	6.45	0.0201
	±0.0078	±0.0048	±0.0096	±0.026	±0.19	±0.0013
Hadronic Lifetime Fit	0.006	0.988	0.731	1.11	5.07	0.0168
	±0.012	±0.012	±0.028	±0.11	±0.90	±0.0077

Table 38: Comparison between different sets of G⊗(δ+E)+G resolution model parameters.

6 Misalignment effects

In this section we discuss studies of the impact of residual misalignments on the reconstruction of vertices and decay-lengths in the $r\phi$-plane or in the z-direction.
One way of studying such effects is to investigate what would happen if the detector was misaligned in a given hypothetical way. The hypothetical misalignment can be introduced into simulated events and its impact on the reconstruction can be investigated. To connect such studies to the real world, one has to estimate which magnitude of the given type of misalignment is to be expected. For example, the SVT as a whole can move over time with respect to the DCH. The relative drift between two subsequent calibrations gives us an idea of the size of such displacements.
Another approach is to use tracking observables from a pure sample of events of a given type, and to use these observables to construct variables that are sensitive to detector misalignments. The values of these variables can then be monitored in data. The Monte Carlo techniques described above can be used to study the sensitivity of a given variable to a given type of misalignment.

In section 6.1 we describe briefly how misalignments can be introduced into *BABAR* Monte Carlo. Studies of the sensitivity of the beam spot reconstruction to misalignments are described in section **??**. Section **??** describes a control sample based on τ events that can be used to monitor certain alignment effects on data. The impact of various misalignments on the Δz reconstruction is discussed in section 6.2.

6.1 Introducing misalignments into *BABAR* Monte Carlo

BABAR Monte Carlo events are simulated with perfect alignment. A set of alignment constants that describe this perfect alignment are stored in the conditions database. These constants are then used for the official SP3 reconstruction. Users can rerun the reconstruction software and tell it to ignore the constants in the database and use user-supplied constants instead.
In the 9.x.x releases, one can talk to the module `SvtBuildEnv` and supply the constants that describe a displacement and a rotation of the SVT as a whole with respect to its nominal position. In addition, the name of an ASCII file that contains a local SVT alignment, i.e. a set of translations and rotations of each of the individual wafers, can be supplied [10].
In the 8.x.x releases, the same functionality is provided by the module `TrkCombo/ReadAlignments`. By default, this module is not linked into the `Bear` executable. In a private test release it should be inserted into the `SvtReco/SvtPreTrackSequence`, directly after the module `SvtBuildEnv` [11].

6.2 Δz reconstruction

The same sample of 10k $B^- \to D^0\pi^-$, $D^0 \to K^-\pi^+$; $B^+ \to X$ SP3 Monte Carlo events has been reconstructed several times with different misalignments as well as with perfect alignment. The following alignment sets where studied:

- <u>Perfect alignment</u> ("Zero")

- Global shifts of the SVT w.r.t. the DCH: 50 μm along one of the three axes x, y and z ("ShiftX005, ShiftY005, ShiftZ005").
- Global rotations of the SVT: 0.005 rad around one of the three axes x, y and z ("RotateX005, RotateY005, RotateZ005").
- Systematic deformations of the SVT: ($\epsilon = 0.0005$)

"Dip0005":	$y \Rightarrow y + \epsilon\|z\|$	
"Ellips0005":	$x = R\cos\phi \Rightarrow x = R\cos\left[(1+\epsilon\cos(2\phi))\phi\right]$	
	$y = R\sin\phi \Rightarrow y = R\sin\left[(1+\epsilon\cos(2\phi))\phi\right]$	
"ExpandR0005"	$x \Rightarrow (1+\epsilon)x$	(increase SVT radius by 75 μm)
	$y \Rightarrow (1+\epsilon)y$	
"ExpandZ0005"	$z \Rightarrow (1+\epsilon)z$	
"TwistZ0005"	$x = R\cos\phi \Rightarrow x = R\cos(\phi + \epsilon z)$	
	$y = R\sin\phi \Rightarrow y = R\sin(\phi + \epsilon z)$	

- Shifts of the outer two layers w.r.t. the inner layers: 50 μm along y or z ("OuterShiftY005, OuterShiftZ005").
- Uncorrelated random translations of all SVT wafers:
  - "LA101025": The translations in u (parallel to beam axis) and v (in the wafer plane, orthogonal to u) are normally distributed with $\sigma = 10$ μm. The translations in w are normally distributed with $\sigma = 25$ μm.
  - "LA202050": As above, but with $\sigma = 20$ μm in u and v, and $\sigma = 50$ μm in w.

Most of the corresponding alignment files come from a group of people who work on the SVT local alignment [12], who use them to study the SVT alignment procedure. The preliminary results of their studies [10] indicate that the alignment procedure significantly reduces the systematic deformations listed above, at least after several iterations.

`VtxTagBtaSelFit`, the algorithm used in this study to reconstruct Δz, uses an estimate of the beam spot position and size to constrain the common production point of the two B mesons. The effective position of the beam spot, as seen by the detector, could be different from the generated position; especially in the case of global translations of the SVT. The beam spot parameters used in this study were estimated from the distribution of reconstructed decay points of the fully reconstructed B mesons. The effect of the B flight in x and z is negligible compared to the beam spot size. In y we always use a fixed estimate of the width and only the position was extracted from the fit to the decay point distribution.

The results obtained with these different alignment sets are summarized in table 39. The second and third column contain the efficiency for the reconstruction of the fully reconstructed $B_{\rm rec}$, and the efficiency for the reconstruction of the opposite vertex in the events with a successfully reconstructed $B_{\rm rec}$. The Δz resolutions listed in column four were estimated from a fit of two gaussians to the distributions of residuals. The remaining columns contain the result of a fit of the "$G\otimes(1+E)$" function (see section 3.2) to the pull distribution, as well as the corresponding χ^2.

Alignment	$\epsilon(B_{\text{rec}})$	ϵ(opp.vtx.)	$\sigma(\Delta z)$	f	τ	σ	χ^2
Zero	44.95 %	90.2 %	123 ± 2 μm	0.51 ± 0.08	0.51 ± 0.08	1.03 ± 0.02	1.13
ShiftY005	44.88 %	90.2 %	122 ± 3 μm	0.58 ± 0.06	0.63 ± 0.07	1.02 ± 0.02	1.00
RotateY005	26.26 %	87.8 %	137 ± 6 μm	0.64 ± 0.07	0.72 ± 0.14	1.08 ± 0.03	1.29
RotateZ005	12.64 %	84.9 %	136 ± 5 μm	0.65 ± 0.08	0.86 ± 0.20	1.04 ± 0.04	0.89
Dip0005	44.92 %	90.2 %	118 ± 2 μm	0.55 ± 0.07	0.56 ± 0.08	1.03 ± 0.02	1.16
Ellips0005	44.90 %	90.2 %	120 ± 2 μm	0.55 ± 0.07	0.56 ± 0.08	1.03 ± 0.02	1.11
ExpandR0005	44.87 %	90.2 %	121 ± 2 μm	0.57 ± 0.06	0.62 ± 0.07	1.01 ± 0.02	1.06
ExpandZ0005	44.91 %	90.3 %	122 ± 3 μm	0.59 ± 0.06	0.64 ± 0.08	1.04 ± 0.02	0.72
TwistZ0005	22.76 %	84.7 %	133 ± 3 μm	0.67 ± 0.07	0.80 ± 0.15	1.09 ± 0.03	0.71
OuterShiftY	44.85 %	90.2 %	121 ± 2 μm	0.52 ± 0.08	0.52 ± 0.08	1.03 ± 0.02	1.30
OuterShiftZ	44.86 %	90.1 %	122 ± 2 μm	0.42 ± 0.07	0.58 ± 0.06	1.03 ± 0.02	0.97
Zero'			135 ± 3 μm	0.64 ± 0.03	0.93 ± 0.07	1.06 ± 0.02	1.35
LA101025 [3]			148 ± 3 μm	0.61 ± 0.04	0.92 ± 0.07	1.12 ± 0.02	1.10
LA202050			169 ± 3 μm	0.54 ± 0.06	0.82 ± 0.09	1.33 ± 0.03	1.11

Table 39: Reconstruction efficiencies and results of fits to the Δz residual and pull distributions for different reconstructions of the same events with different alignment sets. Two examples of the fits to pull distributions are shown in figure 90.

The Δz resolution and pull from $B^0 \to J/\Psi K_S^0$ MC for the three SVT LA sets were also fit to the double gaussian plus outlier gaussian model. The width of the outlier gaussian was fixed at 800 μm and 8 sigma for the resolution and pull respectively. The fit parameters are shown in Table 40. In Figure 91 comparisons are made between the probability of the χ^2 , error on Δz , and the number of tracks used in the tagside vertex for the different alignment sets. While the distributions look similar for the error on Δz and the number of tracks used in the fit, it seems clear that the probability of the χ^2 is affected by the misalignment. In Figure 92, comparisons are made between the probability of the χ^2 for the CP vertex and the error on this vertex for the different alignment sets. There don't appear to be meaningful discrepencies between these distributions given the statistics.

[3]These two were done with an old release and should be repeated. The conclusions are not expected to change.

Δz reso	f_1	σ_1	μ_1	f_{out}	$\frac{\sigma_2}{\sigma_1}$	$\mu_2 - \mu_1$	RMS μm	RMS(3g) μm	μ
Zero	71.5	101. $\pm$ 5. μm	-19.$\pm$ 3. μm	2.83	2.28$\pm$ 0.14	-44.$\pm$ 13. μm	147.$\pm$ 5. μm	198.$\pm$ 8. μm	-30. μm
LA101025	65.4	99. $\pm$ 4. μm	-20.$\pm$ 3. μm	2.62	2.21$\pm$ 0.08	-37.$\pm$ 8. μm	149. $\pm$ 4. μm	196.$\pm$ 5. μm	-31. μm
LA202050	64.3	102. $\pm$ 3. μm	-20.$\pm$ 2. μm	2.78	2.21$\pm$ 0.06	-41.$\pm$ 7. μm	156. $\pm$ 3. μm	203.$\pm$ 4. μm	-33. μm
Dip0005	60.0	242. $\pm$ 27. μm	-33.$\pm$ 9. μm	0.00	2.38$\pm$ 0.33	24.$\pm$ 26. μm	409.$\pm$ 46. μm	409.$\pm$ 58. μm	-23. μm
Ellips0005	59.2	239. $\pm$ 27. μm	-32.$\pm$ 8. μm	0.00	2.39$\pm$ 0.31	18.$\pm$ 24. μm	410.$\pm$ 46. μm	410.$\pm$ 60. μm	-25. μm
ExpandR0005	61.1	246. $\pm$ 26. μm	-31.$\pm$ 8. μm	0.00	2.36$\pm$ 0.33	15.$\pm$ 24. μm	410.$\pm$ 47. μm	410.$\pm$ 61. μm	-25. μm
ExpandZ0005	58.3	238. $\pm$ 28. μm	-32.$\pm$ 8. μm	0.00	2.39$\pm$ 0.30	21.$\pm$ 23. μm	409.$\pm$ 45. μm	409.$\pm$ 59. μm	-24. μm
TwistZ0005	57.9	250. $\pm$ 31. μm	-32.$\pm$ 9. μm	0.00	2.40$\pm$ 0.30	6.$\pm$ 23. μm	435.$\pm$ 54. μm	435.$\pm$ 72. μm	-30. μm
outerShiftY005	59.4	243. $\pm$ 27. μm	-33.$\pm$ 9. μm	0.00	2.34$\pm$ 0.31	21.$\pm$ 28. μm	408.$\pm$ 45. μm	408.$\pm$ 58. μm	-25. μm
outerShiftZ005	59.9	242. $\pm$ 26. μm	-38.$\pm$ 8. μm	0.00	2.36$\pm$ 0.32	17.$\pm$ 26. μm	408.$\pm$ 46. μm	408.$\pm$ 61. μm	-32. μm
rotateY005	60.2	254. $\pm$ 26. μm	-32.$\pm$ 9. μm	0.00	2.42$\pm$ 0.31	37.$\pm$ 24. μm	434.$\pm$ 51. μm	434.$\pm$ 73. μm	-17. μm
rotateZ005	55.4	244. $\pm$ 29. μm	-39.$\pm$ 10. μm	0.00	2.46$\pm$ 0.32	38.$\pm$ 23. μm	440.$\pm$ 56. μm	440.$\pm$ 75. μm	-22. μm
shiftY005	61.0	248. $\pm$ 24. μm	-28.$\pm$ 9. μm	0.00	2.33$\pm$ 0.33	18.$\pm$ 28. μm	410.$\pm$ 47. μm	410.$\pm$ 63. μm	-21. μm
Δz pull	f_1	σ_1	μ_1	f_{out}	$\frac{\sigma_2}{\sigma_1}$	$\mu_2 - \mu_1$	RMS	RMS(3g)	μ
Zero	83.1	1.06 $\pm$ 0.04	-0.19$\pm$ 0.03	1.91	1.82$\pm$ 0.18	-0.58$\pm$ 0.25 μm	1.23$\pm$ 0.05	1.65$\pm$ 0.09	-0.28
LA101025	84.5	1.10 $\pm$ 0.03	-0.22$\pm$ 0.02	1.67	1.83$\pm$ 0.14	-0.57$\pm$ 0.19 μm	1.27$\pm$ 0.04	1.63$\pm$ 0.07	-0.29
LA202050	86.4	1.16 $\pm$ 0.03	-0.24$\pm$ 0.02	1.63	1.91$\pm$ 0.17	-0.64$\pm$ 0.20 μm	1.34$\pm$ 0.04	1.67$\pm$ 0.06	-0.31
Dip0005	39.4	1.70 $\pm$ 0.16	-0.33$\pm$ 0.08	15.78	2.34$\pm$ 0.22	0.12$\pm$ 0.21 μm	3.12$\pm$ 0.30	4.28$\pm$ 0.37	-0.22
Ellips0005	33.1	1.58 $\pm$ 0.18	-0.32$\pm$ 0.09	18.05	2.31$\pm$ 0.17	0.06$\pm$ 0.19 μm	2.98$\pm$ 0.29	4.34$\pm$ 0.27	-0.23
ExpandR0005	34.4	1.62 $\pm$ 0.18	-0.31$\pm$ 0.09	17.65	2.28$\pm$ 0.17	0.05$\pm$ 0.19 μm	3.00$\pm$ 0.29	4.33$\pm$ 0.28	-0.23
ExpandZ0005	29.8	1.51 $\pm$ 0.20	-0.30$\pm$ 0.09	20.13	2.29$\pm$ 0.18	0.01$\pm$ 0.19 μm	2.90$\pm$ 0.33	4.43$\pm$ 0.24	-0.23
TwistZ0005	26.7	1.55 $\pm$ 0.23	-0.23$\pm$ 0.13	17.08	2.21$\pm$ 0.22	-0.15$\pm$ 0.21 μm	2.96$\pm$ 0.40	4.26$\pm$ 0.27	-0.27
outerShiftY005	34.1	1.60 $\pm$ 0.17	-0.32$\pm$ 0.09	18.74	2.29$\pm$ 0.17	0.07$\pm$ 0.20 μm	2.98$\pm$ 0.27	4.38$\pm$ 0.26	-0.22
outerShiftZ005	28.8	1.47 $\pm$ 0.19	-0.36$\pm$ 0.09	19.41	2.35$\pm$ 0.18	0.02$\pm$ 0.19 μm	2.91$\pm$ 0.33	4.39$\pm$ 0.24	-0.28
rotateY005	18.2	1.26 $\pm$ 0.29	-0.27$\pm$ 0.13	23.36	2.53$\pm$ 0.41	-0.01$\pm$ 0.19 μm	2.85$\pm$ 0.69	4.60$\pm$ 0.32	-0.21
rotateZ005	32.1	1.59 $\pm$ 0.19	-0.30$\pm$ 0.10	17.01	2.39$\pm$ 0.20	0.00$\pm$ 0.21 μm	3.13$\pm$ 0.34	4.36$\pm$ 0.33	-0.25
shiftY005	31.0	1.53 $\pm$ 0.21	-0.22$\pm$ 0.09	18.68	2.34$\pm$ 0.18	-0.06$\pm$ 0.20 μm	2.97$\pm$ 0.34	4.38$\pm$ 0.29	-0.21

Table 40: Resolution function parameters for the different Svt local alignment sets

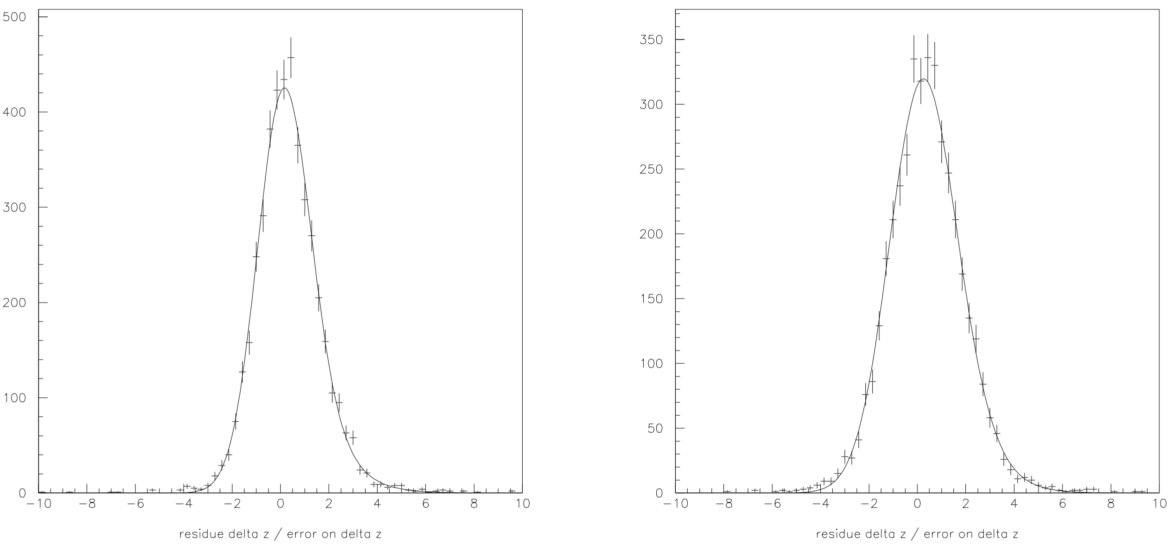

Figure 90: Δz pull for perfect alignment (Zero', left plot) and for poorly aligned SVT (LA202050, right plot).

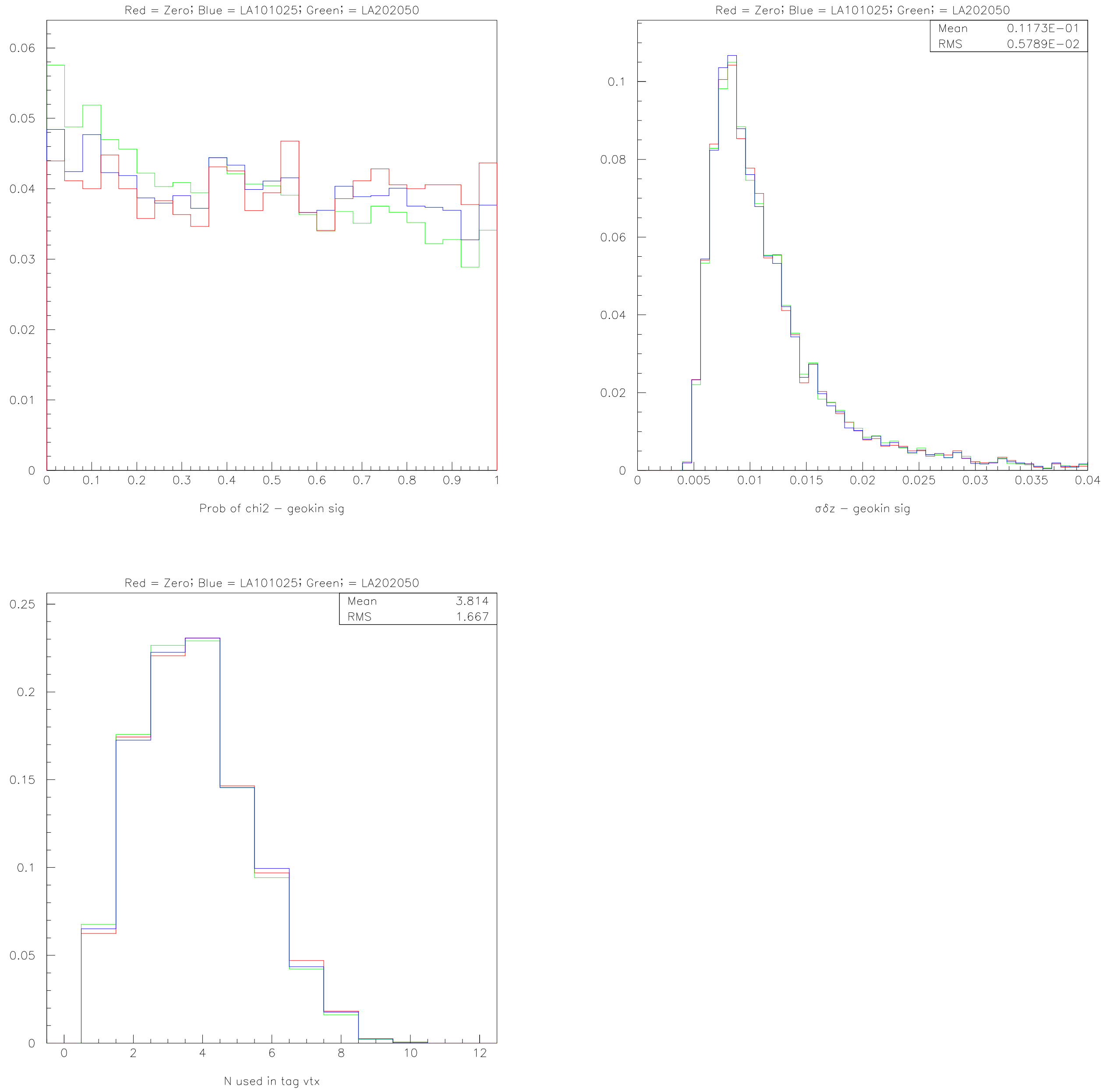

Figure 91: Comparison of the probability of the χ^2 error on Δz and the number of tracks used in the tagside vertex for the different local alignment sets (Red = Zero, Blue = LA101025, Green = LA202050)

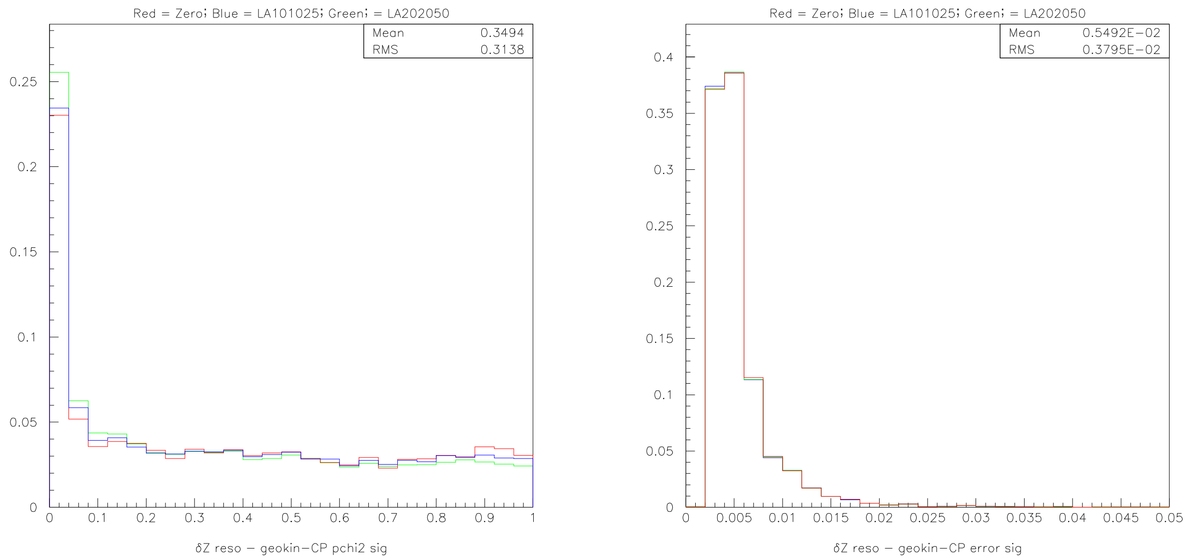

Figure 92: Comparison of the probability of the χ^2 for the CP vertex and the error on the CP vertex for the different local alignment sets (Red = Zero, Blue = LA101025, Green = LA202050) local alignment sets (Red = Zero, Blue = LA101025, Green = LA202050)

7 Further Δz vertexing studies

Here we are going to document all the new studies.

More checks were performed to determine the dependence of the mean and width of the Δz pull distribution on various quantities. This study was made with 10,000 $B^0 \to J/\psi K_S^0$ Monte Carlo events where both beam constraints (the beam spot and "psuedo-track") were used by `vtxTagBtaSelFit` in vertex determination. Figure 93 plots the average mean and width of the Δz pull distribution in bins of the measured Δz value. The first bin corresponds to a measured value of Δz being less than 500 μm and the last bin for a measured value of Δz being greater than 400 μm. For all plots shown the quantity being used to bin by increases from left to right. The correlation between the bias of the Δz pull distribution and the measured value of Δz is expected due to the charm bias which is not modelled by the pull. Figure 94 plots the average mean and width of the Δz pull distribution in bins of true $\Delta z\dot{\mathrm{N}}$o correlation is observed.

Figure 95 shows the average mean and width of the pull distribution in bins of the event-by-event Δz error. The first bin corresponds to an error less than 68 μm and the last bin corresponds to an error greater than 165 μm (recall that events with errors larger than 400 μm are not used). There is no obvious correlation in either plot. Finally, figure 96 shows the mean and width of the event-by-event error plotted in bins of Δz residual. It appears that the mean errors are worse for residuals far from zero as expected (and the error on the error grows in these cases as well).

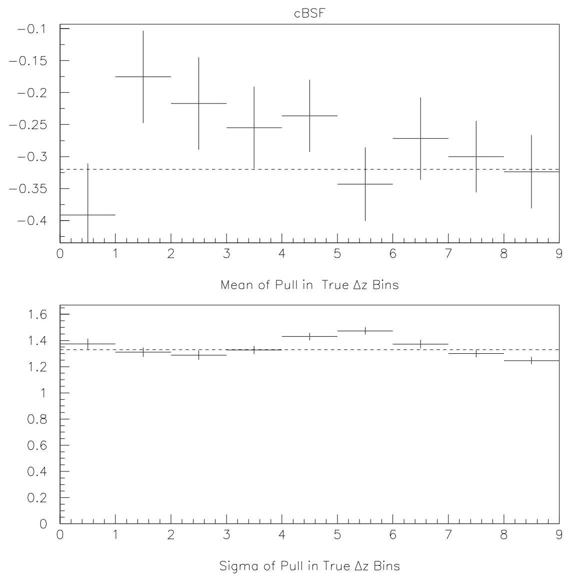

Figure 93: Average mean (top) and width (bottom) of Δz pull distribution in bins of Δz measured. The Δz measured bins increase from negative Δz measured to positive as one moves from left to right. The dashed lines in the top and bottom plots correspond respectively to the fitted mean and width of the Δz pull distribution.

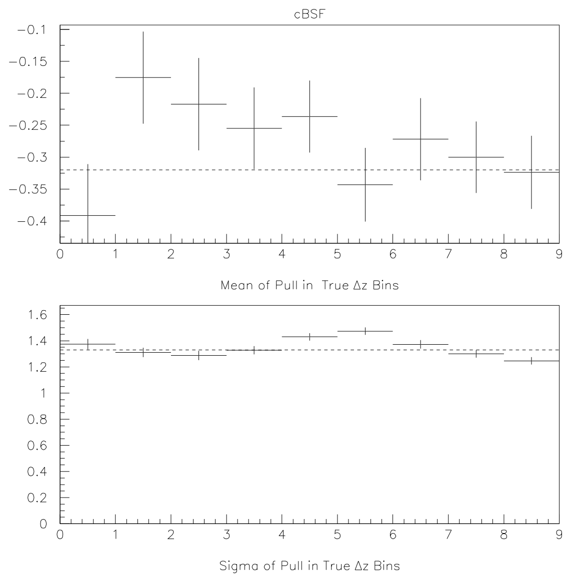

Figure 94: Average mean (top) and width (bottom) of Δz pull distribution in bins of Δz true. The Δz true bins increase from negative to positive as one moves from the left to the right. The dashed lines in the top and bottom plots correspond respectively to the fitted mean and width of the Δz pull distribution.

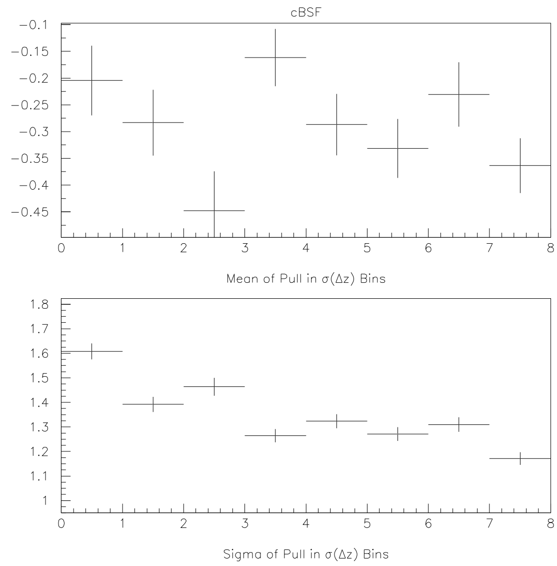

Figure 95: Average mean (top) and width (bottom) of Δz pull distribution in bins of the event-by-event error on ΔzThe event-by-event error bins increase from zero to more positive values as one moves from left to right.

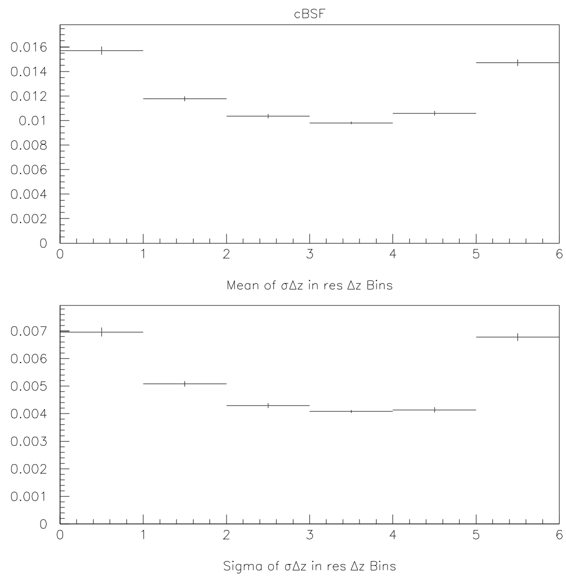

Figure 96: Average mean (top) and width (bottom) of the event-by-eventy error distribution in bins of Δz residual. The Δz residual bins increase from negative to positive values as one moves from left to right. Y-axis units are in cm.

References

[1] *BABAR* Analysis Document # 102, The *BABAR* Vertexing.

[2] *BABAR* Analysis Document # 183, Vertexing Control Samples.

[3] J. Smith, A. Soffer and R. Waldi, Recommendation for Exclusive B Reconstruction Analysis Variables", *BABAR* Note # 497 (1999).
W.T.Ford, Choice of Kinematic Variables in B Meson Reconstruction–Take 3, *BABAR* Analysis Document #53 (2000).

[4] *BABAR* Analysis Document # 113, Measurement of exclusive charmonium branching ratios using data from BaBar's first run.

[5] *BABAR* Analysis Document # 150, Exclusive B reconstruction to open charm final states.

[6] *BABAR* Analysis Document # 34, Selection of D^*-lepton Events for B Lifetime and Mixing Analyses.

[7] *BABAR* Analysis Document # 119, B Tagging in *BABAR*: Status for the Spring 2001 Conferences.

[8] *BABAR* Analysis Document # 14, Measuring the PEP-II Boost.

[9] Presentations at the Forum meeting on May 16^{th} (200),
http://www.slac.stanford.edu/BFROOT/www/Physics/Forum/forum/phonemeetings/forum_16may00/doc.html

[10] A. Gritsan, *SVT Local Alignment Diagnostics*,
http://www.slac.stanford.edu/g̃ritsan/svt/index.html

[11] J. Schieck, private communication.

[12] See their discussions in the "Tracking Reconstruction Software" HN forum, reference [10] and Jochen's page at http://www.slac.stanford.edu/s̃chieck/align/Welcome.html .

[13] G. Raven, $D^{*-} - D^0$ *vertexing in* $B^0 \to D^{*-}\ell\nu$ *events*, talk at $\sin 2\beta$ WorkShop, 3rd November, 2000,
http://www.slac.stanford.edu/BFROOT/www/Physics/CP/beta/Meetings/03Nov00/S2bWorkshop00.html

[14] *BABAR* Analysis Document # 18, A User's Guide to the RooFitTools Package for Unbinned Maximum Likelihood Fitting.

[15] *BABAR* Analysis Document # 144, Measurements of the charged and neutral B meson lifetimes using fully reconstructed B decays.

[16] A. Soffer, Beam parameters in data and Monte Carlo, talk at $\sin 2\beta$ WorkShop, 3rd November, 2000,
http://www.slac.stanford.edu/BFROOT/www/Physics/CP/beta/Meetings/03Nov00/S2bWorkshop00.html

[17] Chih-hsiang Cheng,

http://babar-hn.slac.stanford.edu:5090/HyperNews/get/pubboard01/25.html

http://babar-hn.slac.stanford.edu:5090/HyperNews/get/sin2beta/210.html